SOUTHWEST RESEARCH INSTITUTE
Post Office Drawer 28510, 6220 Culebra Road
San Antonio, Texas 78284

PIPELINE RESPONSE TO BURIED EXPLOSIVE DETONATIONS

VOLUME II - TECHNICAL REPORT

by
Edward D. Esparza
Peter S. Westine
Alex B. Wenzel

FINAL REPORT
A.G.A. Project PR-15-109
SwRI Project 02-5567

for
THE PIPELINE RESEARCH COMMITTEE
AMERICAN GAS ASSOCIATION

August 1981

Approved:

H. Norman Abramson, Vice President
Engineering Sciences

THIS PAGE IS INTENTIONALLY BLANK

SUMMARY

This report describes a blasting research program conducted to develop simple procedures for predicting the maximum stresses in steel pipelines induced by nearby, buried, explosive detonations. This extensive experimental and analytical study was funded by the Pipeline Research Committee of the American Gas Association and performed by Southwest Research Institute from 1975 to 1981.

In this program, the general problem of a buried explosive detonating near a pipeline was divided into two parts. In the first part, similitude theory, empirical analyses and test data were used to derive equations for estimating maximum ground displacement and particle velocity. The ground motions provided the forcing function imparted to a buried pipeline. In the second part, similitude theory, conservation of mass and momentum, and approximate energy methods were used to derive functional relationships for the maximum pipe strains and stresses. Experimental data from more than 60 tests, primarily in model scale, were then used to develop equations for estimating maximum pipe stresses induced by point and parallel line explosive sources buried in a homogeneous soil media. The large amount of data used and the wide range of these data make the solutions applicable to most soil blasting situations near pipelines.

Subsequently, the applicability of these prediction equations was extended to estimate pipe stresses from other more complex geometries. Test data were obtained from 38 model scale experiments using angled-line, parallel grid, and angled-grid explosive sources also buried in soil. These data were then used to develop empirical methods by which complex explosive geometries could be simplified into equivalent point or parallel line sources, depending on their proximity to the pipeline. Using the simplifying methods developed, the test data from the complex geometry source compared quite well with the point and parallel line source equations.

As part of the blasting research program, three other limited tasks were also performed. In the first, a correction factor to the point source solution was derived empirically for situations in which a pipeline is between a relatively near free surface and the explosive source. In this case, the lack of earth behind the pipe enhances the pipe stresses because of the lack of inertial resistance. In the second limited task, a literature study was conducted to determine the effects of barriers between an explosive source and a pipeline. Strain measurements from one specific set of field tests were used to develop an equation to predict the effects of a trench on strain levels on a pipe as a function of scaled distances. Because of the limited data base, this equation should be valid only within the range of the dimensionless parameters involved. Finally, four model experiments were also conducted in a study to determine the feasibility of simulating the problem of blasting in a rock mass adjacent to a pipeline buried in soil. The pipe stress and ground motion data from these experiments were used to develop an equation for computing an effective standoff distance so that the point source soil equations could be used to approximate the pipe response. Because no test data were obtained in rock/soil media, application of the effective standoff equation is tentative at this time.

This final engineering report was prepared in two volumes. Volume I is a summary of the prediction equations and methods developed. Definitions of parameters and symbols are included, as well as application information. Volume II is a complete technical report which describes in detail the background of this research effort, the experimental program and results, the development of the ground motion and pipe stress solutions, the use of some of these equations and methods in example problems, and the three smaller tasks performed. In addition, discussions are presented on assumptions and limitations of the solutions developed, the sensitivity of the point and parallel line stress equations, alternative forms for these equations, the total state of stress on a pipe and yield theories, factors of safety, and other procedures which are in some blasting codes and have been used to limit blasting near pipelines.

ACKNOWLEDGEMENTS

This program was sponsored by the Pipeline Research Committee of the American Gas Association and conducted by Southwest Research Institute. ‘Members of the Pipeline Research Committee at the time of publication of this report were:

W. T. Turner, Jr., Texas Gas Transmission Corporation
W. E. Almquist, Columbia Gas Transmission Corporation
J. W. Bledsoe, Southern Natural Gas Company
F. C. Boekell, Consolidated Gas Supply Corporation
R. C. Bonner, Consumers Power Company
A. H. Carameros, El Paso Natural Gas Company
W. F. Coates, Algonquin Gas Transmission Company
L. W. Emery, ARCO Oil and Gas Company
H. G. Gillit, Northwest Pipeline Corporation
E. H. Gilman, Colorado Interstate Gas Company
A. W. Guinee, N. V. Nederlandse Gasunie
A. R. Hagedorn, Exxon Production Research Company
L. E. Hanna, Panhandle Eastern Pipe Line Company
J. E. Hansford, Florida Gas Transmission Company
J. M. Hassoldt, Western Slope Gas Company
N. L. Hawes, Southern California Gas Company
V. L. Hayes, Phillips Petroleum Company
T. J. Hirt, Northern Natural Gas Company
H. W. Hodge, Texas Eastern Gas Pipeline Company
G. M. Hugh, TransCanada PipeLines, Ltd.
R. C. Jackson, Cities Service Gas Company
R. J. Judah, Transcontinental Gas Pipe Line Corporation
E. H. Kamphaus, Oklahoma Natural Gas Company
R. W. Lindgren, Natural Gas Pipeline Company of America
E. A. Milz, Shell Development Company
H. P. Prudhomme, Pacific Gas Transmission Company
C. D. Richards, NOVA, An Alberta Corporation
R. J. Simmons, Jr., United Gas Pipe Line Company
A. W. Stanzel, Michigan Wisconsin Pipe Line Company
W. Such, Tennessee Gas Pipeline Company
F. R. Schollhammer, American Gas Association
J. M. Holden, American Gas Association

Guidance and direction for the two research projects, PR-15-76 and PR-15-109, were provided by the Blasting Research Supervisory Committee. The membership of the Supervisory Committee had a number of changes throughout the program. The chairmen of this committee were as follows:

Mr. H. R. Wortman, Chairman, 1975-1976, Consumers Power Company
Mr. O. Lucas, Chairman, 1976-1978, Columbia Gas Transmission Corporation
Mr. J. S. Taylor, Chairman, 1978-1981, Consumers Power Company

Members of the Supervisory Committee listed in alphabetical order with the years in which they served were as follows:

Mr. J. M. Barron, 1979-1981, Southern Natural Gas Company
Mr. G, J. Bart, 1977-1981, Texas Gas Transmission Corporation
Mr. L. R. Butler, 1979-1981, United Gas Pipe Line Company
Mr. C. P. Hendrickson, 1976-1978, Northern Illinois Gas Company
Mr. J. M. Holden, 1975-1981, American Gas Association
Mr. O. Lucas, 1975-1978, Columbia Gas Transmission Corporation
Mr. J. D. McNorgan, 1975-1981, Southern California Gas Company
Ms. J. K. Means, 1979-1981, Michigan Wisconsin Pipe Line Company
Mr. O. Medina, 1979-1981, El Paso Natural Gas Company
Mr. R. L. Penning, 1976-1981, Panhandle Eastern Pipe Line Company
Mr. H. E. Russell, 1976-1981, Transcontinental Gas Pipe Line Corporation
Mr. B. P . Schrader , 1979- 1981, Consolidated Gas Supply Corporation
Mr. J . T. Sickman, 1976 - 1981, Texas Eastern Transmission Corporation
Mr. R. W. Skinner, 1975, Transcontinental Gas Pipe Line Corporation
Mr. J. S. Taylor, 1976-1981, Consumers Power Company
Mr. W. C. Thompson, 1979-1981, NOVA, An Alberta Corporation
Mr. H. R. Wortman, 1975-1977, Consumers Power Company
Mr. B. H. Young, 1975-1977, Texas Eastern Transmission Corporation

The authors thank the members of the Supervisory Committee for their cooperation, suggestions and comments during the performance of this research program.

In addition, the authors are very grateful for the support, assistance and cooperation provided by, Panhandle Eastern Pipe Line Company, and the Texas Gas Transmission Corporation in conducting the field experiments at the Kansas and Kentucky remote test sites, respectively. Furthermore, Texas Gas Transmission Corporation provided partial funding for Southwest Research Institute to conduct the field experiments at the Kentucky test site.

The authors also acknowledge the following organizations which provided other test data in the course of this program:

Dow Chemical Company
Michigan Wisconsin Pipe Line Company
VME-Nitro Consult, Inc.
American Natural Service Company Laboratory
Explosive Engineers Services, Inc.
Don Lind Custom Drilling and Blasting

The successful completion of this extensive research program was due to the contribution of many individuals at Southwest Research Institute. The authors would especially like to acknowledge the following personnel who assisted in the performance of the various technical and clerical tasks:

Field Testing:
Mr. E. R. Garcia, Jr., 1976-1979
Mr. A. C. Garcia, 1976-1980
Mr. R. A. Cervantes, 1976-1980
Mr. M. R. Burgamy, 1979-1980
Mr. M. R. Castle, 1979-1980
Mr. F. T. Castillo, 1979-1980
Mr. J. J. Kulesz, 1976-1977

Technical Consultation:
Dr. W. E. Baker, 1975-1978

Data Reduction Codes and Curve Fits:
Mr. J. C. Hokanson, 1976-1980
Mr. J. J. Kulesz, 1976-1977
Ms. N. R. Sandoval, 1980-1981

Data Processing and Graphing:
Mrs. P. A. Hugg, 1976
Ms. P. K. Moseley, 1976-1977
Ms. Y. R. Martinez, 1977
Ms. N. R. Sandoval, 1979-1981
Ms. D. K. Wauters, 1979

Final Drawing of Illustrations:
Mr. V. J. Hernandez, 1975-1981

Typing of Previous Reports:
Mrs. C. W. Dean, 1975-1976
Mrs. E. M. Hernandez, 1977
Mrs. J. B. Cooke, 1978
Mrs. J. H. Newman, 1979
Mrs. S. L. Carroll, 1979-1980
Ms. J. L. Decker, 1980

Typing and Processing 1981 Final Report:
Ms. J. L. Decker
Mrs. L. F. Ramon

Technical Proofreading:
Mr. L. M. Vargas, 1980-1981
Ms. N. R. Sandoval, 1980-1981

Editing and Proofing Reports:
Ms. D. J. Stowitts, 1978-1981

Printing Final Reports:
SwRI Print Shop, 1975-1981

THIS PAGE IS INTENTIONALLY BLANK

TABLE OF CONTENTS

TABLE OF CONTENTS (CONT'D)

LIST OF ILLUSTRATIONS

LIST OF ILLUSTRATIONS (CONT'D)

LIST OF ILLUSTRATIONS (CONT'D)

LIST OF ILLUSTRATIONS (CONT'D)

LIST OF TABLES

LIST OF EXAMPLE PROBLEMS

I. INTRODUCTION

This technical report is Volume II of the final engineering report which describes an extensive research program conducted to develop equations and methods for predicting the stresses in buried steel pipelines caused by nearby buried detonations. This research program was performed during the period 1975 through 1980 by Southwest Research Institute (SwRI) for the Pipeline Research Committee (PRCI) of the American Gas Association (A.G.A.).

Prior to 1975, no approach existed for estimating pipeline stresses caused by nearby buried explosive detonations within 100 ft. Many states had, and still have a ground motion criteria which limits maximum ground particle velocity to either 1.0 or 2.0 inches/second at the surface. This soil particle velocity criteria evolved from work published by Crandell (1949) for the effects of ground shock on buildings. More recent experimental work investigating the effects of buried charges on buildings such as that of Dovak (1962) in Czechoslovakia and Nicholls, et al. (1971) using data obtained by Thoenen and Windes (l942), Langefors, et al. (1958), and Edwards and Northwood (1960) basically show that threshold soil particle velocity criteria are reasonable when applied to above-ground structures. However, a pipeline is not a building. A steel pipe is a strong structure relative to a building, and when buried, also has a large mass of earth providing additional inertial resistance to any ground shock from a buried detonation. These soil particle velocity criteria have been applied to buried pipelines because: 1) they are simple (even if incorrect), and 2) nothing else existed except for the Battelle equations.

The Battelle equations, McClure, et al. (1964), were developed at the Battelle Memorial Institute under contract for the PRCI. These equations are theoretical elasticity solutions based upon Morris' equation (1950) for ground motion, and the assumptions that: 1) a pipeline movement equals exactly that of the surrounding soil, and 2) no diffraction of shock fronts occurs. No experimental data were available to compare to the Battelle equations when they were developed. The method was recommended for use only for explosive-to-pipe distances greater than 100 feet. However, they have been misapplied by many for closer distances. Now that test data exist at these closer distances, the Battelle circumferential stress equation can be demonstrated to give nonconservative results in certain instances at distances less than 100 feet.

Because of the limitations on surface ground motion criteria and the Battelle equations, a better method was needed to handle blasting near pipelines. As the energy crisis has become more severe, the use of explosives near gas pipelines has increased. More pipelines are being constructed, including parallel pipelines adjacent to earlier ones. More strip miners are blasting near pipelines to remove overburden. Also, other common usage of explosives, such as for highway construction, artificial lake construction, and utility line construction in the expanding suburbs has increased blasting activities near natural gas pipelines.

In 1975, the Pipeline Research Committee initiated a blasting research program with Southwest Research Institute for the purpose of developing procedures for predicting pipeline stresses induced by nearby buried explosive detonations, particularly those within 100 feet of a natural gas pipeline. The Blasting Research Supervisory Committee was formed by the PRCI to guide and monitor SwRI in this research. Two consecutive projects were funded by the PRCI. In the first project, Project No. PR-15-76, SwRI performed the following tasks:

- Reviewed the literature on ground shock propagation and the effects of blast-induced waves on buried pipe-like structures.
- Developed an analytical approach and test program for predicting blast-induced pipe stresses.
- Conducted model experiments using point and parallel line ,explosive sources buried in a homogeneous media to obtain ground motion and pipe response data.
- Quantified the procedures for estimating the radial soil ground motions and maximum dynamic circumferential and longitudinal pipe stresses using the experimental data.
- Conducted full-scale experiments to generate additional point source data and validate the ground motion and pipe stress solutions.
- Developed different methods of presenting the pipe stress solutions for easy pipeline industry use.
- Prepared and published a final engineering report and a summary videotape report. A seminar on the results of this project was also presented.

In 1979, the second project, PR-15-109, was initiated to expand the application of the solutions developed in the first project to other explosive geometries and field situations. This second project included tasks to:

- Conduct additional model experiments using point sources buried in soil to the same depth and deeper than the pipe.
- Revise the point source solutions for predicting ground motions and biaxial pipe stresses to include the additional test data.
- Conduct a limited number of parallel line, angled-line, parallel grid, and angled-grid explosive source tests.
- Develop empirical methods for simplifying these complex explosive geometries into equivalent point and parallel line sources.
- Perform an analytical and experimental study to determine the feasibility of using a concrete/soil model to simulate blasting in a rock mass adjacent to a pipeline buried in soil.
- Conduct a literature study concerning the use of trenches to reduce blasting stresses.

Present the results of the entire blasting research program in this final engineering report, in a videotape summary report, and in a seminar. In the-second project the prediction equations were improved and their application extended to other situations that were not studied in the first project. Therefore, these reports replace those available after the first research project and ail other interim reports published under this blasting research program.

The resulting prediction equations and methods interrelate the explosive type, explosive weight, standoff distance, pipe size, pipe modulus, explosive configurations, and the resultant circumferential and longitudinal pipe stresses caused by blasting. In order to create these solutions, the general problem was divided into two separate parts. The first part estimated maximum radial soil particle velocity and soil displacement at various distances from either single detonations (point sources) or multiple detonations from a line of charges (parallel line sources). The second problem was, then, to estimate both circumferential and longitudinal maximum pipe stresses caused by the previously determined ground motions. This division of the general problem into these two separate parts is apparent throughout this report until such time as the solutions can be combined to give a final interrelationship for point and parallel line sources. This solution is in an explicit closed form which can be solved by direct computation using calculators, tables or graphs. To develop the stress solution, similitude theory was combined with theoretical approaches using energy procedures, conservation of mass and momentum principles for shock fronts, and empiricism.

Subsequent experimental and analytical efforts were undertaken to develop methods for approximating angled-line, parallel line, and angled-grid explosive sources by equivalent parallel line or equivalent point source. In this way, the prediction equations could be applied to these more complex explosive geometries. In all, ground motion and pipe strain data were obtained in more than 100 tests from the detonations of point, line, and grid explosive sources at three different test sites. Five different size pipes were used to obtain circumferential and longitudinal strain data. These data were used in the development of the solutions and to demonstrate their validity.

Two smaller tasks were also performed as part of the PRCI blasting research program. One task consisted of a literature study concerning the effects of using trenches for shielding a pipeline to reduce blast-induced stresses. This study included a literature search for experimental and theoretical information, an analysis and evaluation of the data found, and recommendations as to, the effectiveness of this approach' to reduce blast effects on pipelines. Because no test data are available for blasting in rock adjacent to a pipeline buried in soil, the second of the two smaller tasks consisted of investigating the feasibility of using a concrete/soil model to simulate such a field problem. *Although this task was primarily a feasibility study, some experimental data were obtained which provide clues on how to use the soil solutions in rock/soil blasting situations.

In this Volume II of the final engineering report, the entire analytical and experimental effort performed as part of the PRCI blasting research program is documented. This volume is organized into 14 sections. Section II presents the analytical approach taken and describes briefly the pi theorem used to model the ground motion and pipe response to buried explosive detonations. The derivations of the general functions for ground motions and pipe stresses are then detailed. A replica modeling law which provided the basis for the experimental effort is then presented. This section shows why model tests could be used in place of full-scale experiments to accumulate the majority of the data.

Section III summarizes the entire experimental effort performed in a homogeneous soil media. Descriptions of the three test sites and five pipes tested are included in this section. Detailed descriptions of the different test layouts are provided and typical model and full-scale test procedures are illustrated. Finally, the transducers used to sense the various measurands are described in considerable detail and the entire measurement system is discussed.

In Section IV, a general discussion is presented on how the ground motion and pipe strain data are grouped. In addition, an explanation is included on how the circumferential and longitudinal strain data were combined to obtain the maximum pipe stresses. The soil particle velocity, peak soil displacement, pipe strain, and pipe stress data are compiled by explosive geometry, test series and test number together with all of the pertinent test setup information. Examples of ground motion and pipe strain records for each explosive geometry are also included.

In Section V, general ground motion equations for point sources are developed empirically using the test data summarized in Section IV plus other data from the literature. Some discussion of equations developed by other investigators is also included. The general point source equations are then simplified over the range of the SwRI data for ease in application. Similar log-linear equations for parallel line sources are presented in this section. The displacement equations for point and parallel line sources are then approximated to simplify the form of the function loading the pipes. Finally, two example problems are included to demons&rate the use of the log-linear ground motion prediction equations.

Section VI contains the analytical procedures used to develop the functional relationships of the pipe response. Expressions for the impulse imparted to the pipe by the explosively generated seismic wave and the elastic reaction of a buried pipe are derived. This section then proceeds to show how the pipe strain functions were developed and how the test data are used to complete the stress prediction equations empirically for point and parallel line explosive sources buried in soil. Also included are two illustrations on the application of these equations.

Section VII covers several alternative forms of presenting and applying the point and parallel line source solutions developed in Section VI for predicting pipe stresses in the field. This section is presented to suggest possible field procedures which pipeline companies might consider as better methods for use by their field crews. A simple example problem is used to show how each method presented would be applied and to point out its advantages and disadvantages.

In Section VIII, simple empirical methods for estimating pipe stresses from angled-line, parallel grid, and angled-grid explosive sources are delineated. The approach followed was that of using equivalent parallel line and point sources for these more complex explosive geometries. The test data are then used to confirm that the simplifying methods do provide reasonable predictions of pipe stress.

Section IX discusses some exceptions to the general procedures used in simplifying the angled-line, parallel grid and angled-grid explosive sources into equivalent parallel line or point sources. These methods and the equations for the two simpler sources are then summarized via a logic diagram or flow chart. This diagram provides a step-by-step outline to follow in estimating pipe stresses from point, line, and grid explosive sources. Two example problems are included at the end of this section to assist the reader in using the logic diagram, either manually or coded into a program, to estimate stresses from point, line or grid explosive sources buried in soil.

In Section X, the description and results of three other more limited tasks accomplished in this research program are covered in detail. The first of these studies concerned the response of pipelines relatively near a free surface, such as in the case of very deep point charges. The second limited study addressed the effects of a trench between the charge and a pipeline: The third task was a feasibility study on the use of concrete/soil tests to model the effects of placing the charge in a harder medium, e.g., rock, than that surrounding the pipe;

Section XI discusses in greater depth how pipe stresses are affected by each parameter in the prediction equations for point and parallel line explosive sources. A sensitivity analysis is used to show the variation in the blasting pipe stresses as another parameter in the equations is changed. To properly protect a pipe, stresses other than the blasting stresses must also be considered. These other stresses caused by internal pipe pressurization, thermal expansion, overburden, etc., must be superimposed on the blasting stresses to determine the correct state of stress. In addition, some yield theory must be chosen to decide when yielding begins as a result of the combined biaxial stresses acting on the pipe. We do not specify which theory should be selected, but five theories are mentioned. The two yield theories in most common use are emphasized. Also found in Section XI is a short discussion of safety factors and how they should be chosen. Finally, the section ends with a discussion of present procedures based on other research work and regulatory codes based on limiting peak particle velocities.

In Section XII, the major findings of this blasting research program are summarized together with the main limitations of the prediction equations and methods derived in this effort. In addition, recommendations are presented in this section for future research work.

Finally, a list of references is provided in Section XIII and a list of definitions of the parameters and symbols used in this report is given in Section XIV.

II. MODEL ANALYSIS

General

The objective of this study was to develop an accurate analysis procedure for predicting maximum longitudinal and circumferential stresses in a pipe caused by nearby buried explosive detonations. Although subsequent results arrived at after several years of study infer that soil properties such as density and seismic propagation velocity are relatively unimportant, this observation could not be made initially. At first it was thought that the soil problem should be approached using either 1) a finite difference or finite element computer code, or 2) an empirical approach. The analytical computer program was rapidly ruled out for two reasons, First, no generally accepted equation-of-state exists for various soils exposed to ground shock from nearby detonations. Any equation used would be subject to criticism and, in general, might compromise the study. Secondly, a computer program which had to be exercised every time a new problem was encountered would not be used by field crews and engineers concerned with day-to-day pipeline operations. This line of reasoning rapidly indicated that an empirical approach was more attractive.

An empirical method was used; however, it was supplemented with approximate analysis procedures. Experimental testing to obtain data on actual pipelines would have been very expensive. Hence, the approach became a compromise in which most tests were model experiments conducted on 3-, 6-, and 16-inch diameter pipes using small charges buried at shallow depths as *a* simulation of full scale pipeline conditions. A large amount of data was accumulated using models. A limited number of full scale or prototype experiments were conducted at two other test sites on a 24-inch diameter pipeline and on a 30-inch diameter pipeline to demonstrate that replica model experiments will predict the response of the full-scale conditions.

Because model tests and the associated similitude theory are an important part of the ground shock and pipe stress solutions, this section of the report provides at least a minimal modeling background so that the test program is properly understood and put in the proper perspective.

Pi Theorem and Its Significance

One of the best statements of the pi theorem is a mathematical one made by Bridgman (1931). His statement says if an equation

$$f(q_1, q_2, \ldots\ldots, q_N) = 0 \tag{1}$$

is complete, the solution has the form

$$f(\pi_1, \pi_2, \ldots\ldots, \pi_{N-K}) = 0 \tag{2}$$

where the π terms are independent products of the parameters q_1 , q_2, etc., and are dimensionless. The number of pi terms equals the number of parameters N minus the number of fundamental units of measure K.

The importance of the pi theorem is that only the dimensionless ratios (pi terms) have to be the same for the two systems to be equivalent. The individual parameters, the q's, do not have to be the same.

In addition, if a problem can be defined by six parameters as it was for ground shock propagation, then only three dimensionless pi terms follow which can be plotted using experimental data to develop an entire solution empirically. This approach was exactly the procedure used to obtain what would otherwise be a very difficult to derive ground motion solution.

The other main advantage to using models is an economic one. Many less expensive experiments can be performed on a 3-inch pipe than on a 24-inch pipeline. Smaller charges can be used, test sites can be local rather than remote, and the cratered hole is a much smaller one to be backfilled. These considerations mean that less money is spent on each test data point when models are used.

The most important limitation of the pi theorem is that, by itself, the resulting model law cannot determine the actual functional form for interdependence between one dimensionless-group and another. Any interrelationship is only obtained from either: 1) experimental test data, or 2) mathematical analysis (including, but not limited to, numerical computer solutions). Only by using one or both of these methods can an actual solution be determined.

In this program, the reader will be presented examples in which we took full advantage of modeling techniques and approximate approaches to obtain a general solution to a very complicated problem. For additional reading to supplement this short modeling discussion, we recommend W. E. Baker, P. S. Westine, and F. T. Dodge (1973).

Modeling of Ground Shock Propagation

For a single concentrated explosive source, assume that a buried energy release W_e is instantaneously detonated. At some standoff distance R from the explosive source we wish to know the peak radial velocity U and the maximum radial soil displacement X. The soil is assumed to be a semi-infinite, homogeneous, isotropic medium of mass density p_s and seismic P-wave propagation velocity c. These two parameters account for both inertial and compressibility effects in the soil. Finally, later observation inferred that perhaps atmospheric pressure p_o or some other pressure quantity also influences ground motions. This definition of the problem leads to a six-parameter space of dimensional variables which, in functional format, can be written as:

$$U = f_U(R, W_e, \rho_s, c, p_o) \tag{3}$$

$$X = f_X(R, W_e, \rho_s, c, p_o) \tag{4}$$

Our task for attempting to interrelate all six parameters experimentally in the above solution is simplified by conducting a similitude analysis.

We begin this analysis by writing an equation of dimensional homogeneity with an engineer's system for fundamental units of measure of force F, length L, and time T. The exponents a_1 , a_2, a_3 , a_4, a_5 , and a_6 in this equation of dimensional homogeneity are as yet undetermined integers.

$$U^{\alpha_1} \; R^{\alpha_2} \; W_e^{\alpha_3} \; \rho_s^{\alpha_4} \; c^{\alpha_5} \; p_o^{\alpha_6} \stackrel{d}{=} F^0 L^0 T^0 \tag{5}$$

The symbol $\stackrel{d}{=}$ means "dimensionally equal to" . This equation of dimensional homogeneity states that, if all parameters are listed so that the problem is completely defined, various products of these parameters exist that will be nondimensional. The next step is to substitute the fundamental units of measure for each parameter in Equation (5).

$$\left(\frac{L}{T}\right)^{\alpha_1} (L)^{\alpha_2} (FL)^{\alpha_3} \left(\frac{FT^2}{L^4}\right)^{\alpha_4} \left(\frac{L}{T}\right)^{\alpha_5} \left(\frac{F}{L^2}\right)^{\alpha_6} \stackrel{d}{=} F^0 L^0 T^0 \tag{6}$$

Then collect exponents for each of the fundamental units of measure to obtain:

$$(L)^{\alpha_1+\alpha_2+\alpha_3-4\alpha_4+\alpha_5-2\alpha_6} \; (F)^{\alpha_3+\alpha_4+\alpha_6} \; (T)^{-\alpha_1+2\alpha_4-\alpha_5} \stackrel{d}{=} F^0 L^0 T^0 \tag{7}$$

Equating exponents on the left- and right-hand sides of Equation (7) then yields three equations interrelating the five coefficients:

$$L: a_1, + a_2, + a_3, - 4a_4, + a_5 - 2a_6, = 0 \tag{8-a}$$

$$F: a_3, + a_4, + a_6, = 0 \tag{8-b}$$

$$T: \ -a_1 \ +2a_4, \ -a_5 \ = 0 \tag{8-c}$$

Solving for a_2 and a_4, and a_5 in terms of the other two coefficients yields:

$$a_2 = - \ 3a_3 \tag{9-a}$$

$$a_4 = - a_3, - a_6 \tag{9-b}$$

$$a_5 = - a_1 - 2a_3, \ -2a_6, \tag{9-c}$$

Substituting Equations (9) into the original equation of dimensional homogeneity, Equation (5), then gives:

$$\mathbf{U}^{\alpha_1} \ \mathbf{R}^{-3\alpha_3} \ \mathbf{W}_e^{\alpha_3} \ \rho_s^{-(\alpha_3+\alpha_6)} \ \mathbf{c}^{-(\alpha_1+2\alpha_3+2\alpha_6)} \ \mathbf{p}_o^{\alpha_6} \ \stackrel{\mathbf{d}}{=} \ \mathbf{F}^0\mathbf{L}^0\mathbf{T}^0 \tag{10}$$

Finally, collecting parameters with similar exponents yields:

$$\left(\frac{\mathbf{U}}{\mathbf{c}}\right)^{\alpha_1}\left(\frac{\mathbf{W}_e}{\rho_s\mathbf{c}^2\mathbf{R}^3}\right)^{\alpha_3}\left(\frac{\mathbf{p}_o}{\rho_s\mathbf{c}^2}\right)^{\alpha_6} \stackrel{\mathbf{d}}{=} \mathbf{F}^0\mathbf{L}^0\mathbf{T}^0 \tag{11}$$

Because the products and quotients inside parentheses in Equation (11) are nondimensional, the a_1 , a_3, and a_6 exponents are undetermined and can conceptually take on any value. These three nondimensional ratios in Equation (11) are called pi terms. Equation (11) restates the more complex Equation (3) as:

$$\frac{U}{c} = f_U\left[\frac{W_e}{\rho_s c^2 R^3}, \frac{p_o}{\rho_s c^2}\right] \qquad \text{[point source]} \tag{12}$$

The functional format for Equation (12) cannot be explicitly written until either experimental test data or theoretical analyses furnish additional information. The major advantage in conducting this model analysis was that the six-parameter space given by Equation (3) has been reduced to a three-parameter space of nondimensional terms.

The same procedure can next be applied to Equation (4) for maximum radial soil displacement, Algebraic procedures are not repeated as these are almost the same as those followed in Equations (5) through (11). The nondimensional equation which results from this application of similitude theory to Equation (4) is:

$$\frac{X}{R} = f_X\left[\frac{W_e}{\rho_s c^2 R^3}, \frac{p_o}{\rho_s c^2}\right] \qquad \text{[point source]} \tag{13}$$

To complete the shock propagation efforts, relationships for particle velocity and soil displacement when line sources generate the shock were needed. Precisely the same procedure was used as described earlier for a point source, except now the source is characterized by the energy release per unit length W_e/L rather than by the total energy release W_e . In this case, L is the total length of the explosive source. The line charge counterparts to the point source dimensional Equations (3) and (4) are:

$$U = f_U(R, W_e/L, \rho_s, c, p_o) \tag{14}$$

$$X = f_X(R, W_e/L, \rho_s, c, p_o) \tag{15}$$

A similitude analysis applied to Equations (14) and (15) yields the following two nondimensional equations for shock wave propagation from a line source.

$$\frac{U}{c} = f_U\left[\frac{W_e/L}{\rho_s c^2 R^2}, \frac{p_o}{\rho_s c^2}\right] \qquad \text{[line source]} \tag{16}$$

$$\frac{X}{R} = f_X\left[\frac{W_e/L}{\rho_s c^2 R^2}, \frac{p_o}{\rho_s c^2}\right] \qquad \text{[line source]} \tag{17}$$

The derivations of Equations (12), (13), (16) and (17) do not give final prediction equations. This was done in Section V by applying experimental test data on explosive sources ranging from 0.03 lb to 19.2 kilotons (nuclear blast equivalency). The experimental data for explosive sources ranging from 0.03 lb to 15 lb were obtained by SwRI through experiments conducted under this program. Data for charge weights up to 19.2 kilotons were obtained from published literature by the Atomic Energy Commission (AEC) and the Bureau of Mines. The data used to define the final functional format of the above equations covered nine orders of magnitude in scaled charge weight ($W_e/p_s c^2 R^3$). A more detailed description of the SwRI experiments as well as the derivation of the equations for soil particle velocity and displacement is given in Sections III, IV, and V of this report. These nondimensional equations empirically derived became the forcing function for the pipe structural response solution.

Modeling Stresses in Pipes

Similitude theory was also applied to determine the state of stress in buried pipes resulting from underground detonations. Tests were conducted primarily on smaller models rather than large pipes because more information could be accumulated for a given outlay of money. On the other hand, any financial advantage would only be meaningful provided the experiments on smaller test systems were indeed representative of structural response conditions in large prototype gas pipelines. To demonstrate that small structural response models could represent large-scale conditions and provide data, the following model analysis was conducted.

Assume that, as shown in Figure 1, an infinitely long circular pipe of radius r, wall thickness h, mass density ρ_p, and modulus of elasticity E is exposed to ground shock motions of particle velocity U and displacement X from either line or point explosive sources. The explosive source is located at a standoff distance R in a soil with a mass density ρ_s and a seismic P-wave propagation velocity c. The response of interest is the maximum elastic change in circumferential and longitudinal stresses σ_{max} caused by the passage of this shock over the buried pipe. No need exists for simulating the state of stress in the pipe from internal pipe gas pressures, as these elastic stresses can be superimposed on those caused by the seismic wave loading. This definition of the problem accounts for the load imparted to the pipe, inertial plus compressibility effects in both pipe as well as soil, the geometry of all major items in this problem, and for any effective mass of earth that might vibrate with a deforming pipe segment. All of the parameters used later in a theoretical pipe response calculation are included in this definition of the problem. In functional format, the stress in the pipe would be given by.

$$\sigma_{max} = f_\sigma(R, h, r, E, \rho_p, \rho_s, c, U, X) \tag{18}$$

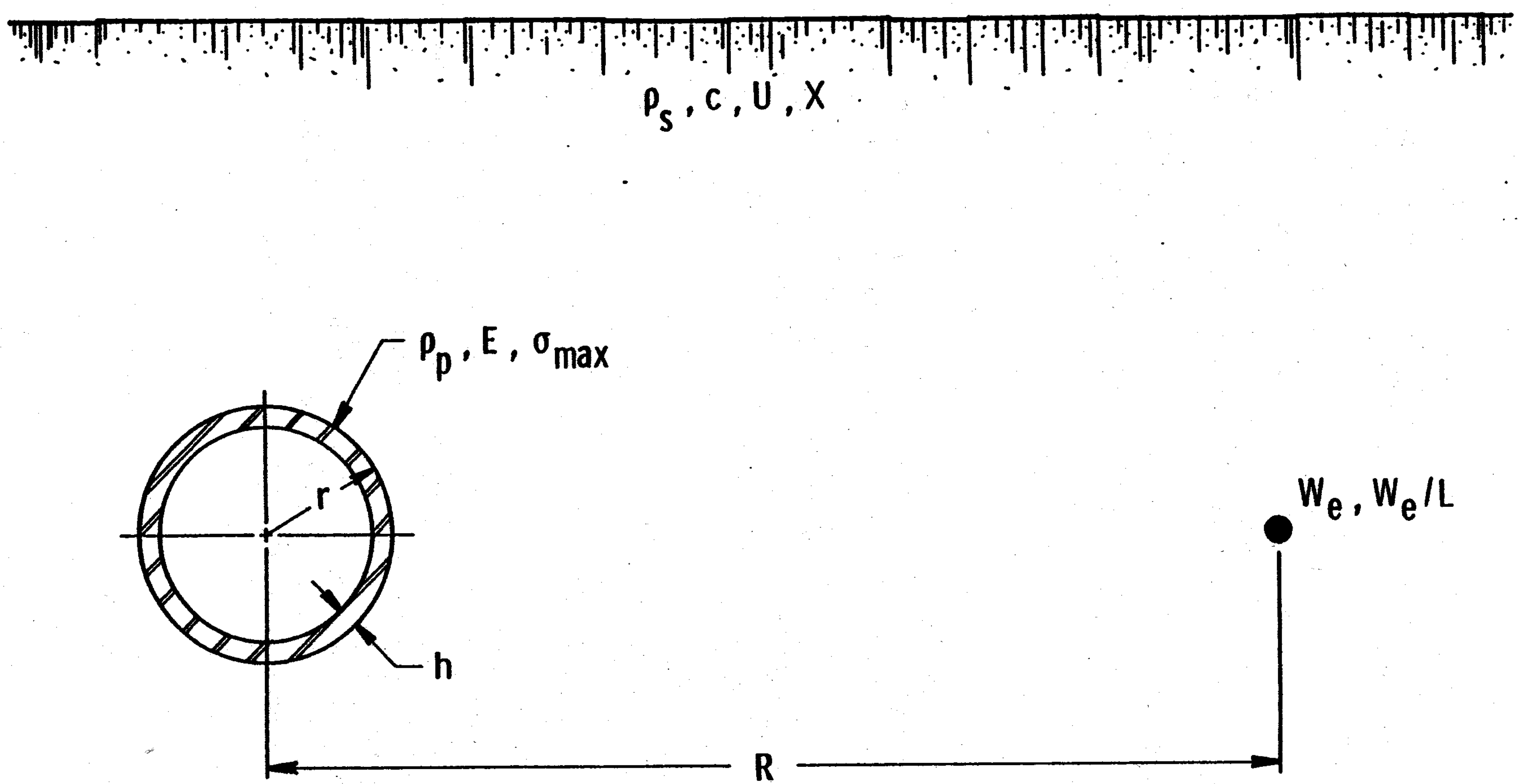

Figure 1. Definition of Pipe Response Problem

Writing a statement of dimensional homogeneity gives the equation:

$$\sigma_{max}^{\alpha_1}\ R^{\alpha_2}\ h^{\alpha_3}\ r^{\alpha_4}\ E^{\alpha_5}\ \rho_p^{\rho_6}\ \rho_s^{\alpha_7}\ c^{\alpha_8}\ U^{\alpha_9}\ X^{\alpha_{10}} \stackrel{d}{=} F^0L^0T^0 \qquad (19)$$

Substituting the fundamental units of measure gives:

$$\left(\frac{F}{L^2}\right)^{\alpha_1}(L)^{\alpha_2}(L)^{\alpha_3}(L)^{\alpha_4}\left(\frac{F}{L^2}\right)^{\alpha_5}\left(\frac{FT^2}{L^4}\right)^{\alpha_6}\left(\frac{FT^2}{L^4}\right)^{\alpha_7}\left(\frac{L}{T}\right)^{\alpha_8}\left(\frac{L}{T}\right)^{\alpha_9}(L)^{\alpha_{10}} \stackrel{d}{=} F^0L^0T^0 \qquad (20)$$

Collecting exponents for each of the fundamental units of measure gives the result:

$$(L)^{-2\alpha_1+\alpha_2+\alpha_3+\alpha_4-2\alpha_5-4\alpha_6-4\alpha_7+\alpha_8+\alpha_9+\alpha_{10}}(F)^{\alpha_1+\alpha_5+\alpha_6+\alpha_7}\ (T)^{2\alpha_6+2\alpha_7-\alpha_8-\alpha_9} \stackrel{d}{=} F^0L^0T^0 \qquad (21)$$

Equating exponents on the left and right sides of Equation (21) yields:

$$\text{L:}\ -2\alpha_1+\alpha_2+\alpha_3+\alpha_4-2\alpha_5-4\alpha_6-4\alpha_7+\alpha_8+\alpha_9+\alpha_{10}=0 \qquad \text{(22-a)}$$

$$\text{F:}\ \alpha_1+\alpha_5+\alpha_6+\alpha_7=0 \qquad \text{(22-b)}$$

$$\text{T:}\ 2\alpha_6+2\alpha_7-\alpha_8-\alpha_9=0 \qquad \text{(22-c)}$$

Solving for a_2, a_7, and a_8 in terms of the other seven coefficients in Equations (22) gives:

$$\alpha_2 = -\alpha_3-\alpha_4+\alpha_{10} \qquad \text{(23-a)}$$

$$\alpha_7 = -\alpha_1 - \alpha_5 - \alpha_6 \tag{23-b}$$

$$\alpha_8 = -2\alpha_1 - 2\alpha_5 - \alpha_9 \tag{23-c}$$

Substituting Equations (23) into Equation (19) then gives:

$$\sigma_{max}^{\alpha_1} R^{-\alpha_3-\alpha_4+\alpha_{10}} h^{\alpha_3} r^{\alpha_4} E^{\alpha_5} \rho_p^{\alpha_6} \rho_s^{-\alpha_1-\alpha_5-\alpha_6} c^{-2\alpha_1-2\alpha_5-\alpha_9} U^{\alpha_9} X^{\alpha_{10}} \stackrel{d}{=} F^0 L^0 T^0$$

Finally, gathering terms with like coefficients gives the seven pi terms:

$$\left(\frac{\sigma_{max}}{\rho_s c^2}\right)^{\alpha_1} \left(\frac{h}{R}\right)^{\alpha_3} \left(\frac{r}{R}\right)^{\alpha_4} \left(\frac{E}{\rho_s c^2}\right)^{\alpha_5} \left(\frac{\rho_p}{\rho_s}\right)^{\alpha_6} \left(\frac{U}{c}\right)^{\alpha_9} \left(\frac{X}{R}\right)^{\alpha_{10}} \stackrel{d}{=} F^0 L^0 T^0 \tag{25}$$

In nondimensional format, Equation (25) permits us to rewrite Equation (18) as:

$$\left(\frac{\sigma_{max}}{\rho_s c^2}\right) = f_{(\sigma_{max}/\rho_s c^2)} \left(\frac{h}{R}, \frac{r}{R}, \frac{E}{\rho_s c^2}, \frac{\rho_p}{\rho_s}, \frac{U}{c}, \frac{X}{R}\right) \tag{26}$$

As was the case in ground motion analysis, the functional format of Equation (26) cannot be written explicitly until test data are generated to measure the maximum circumferential stress and the maximum longitudinal stress in the pipe from the ground motions associated with a buried detonation.

Design of Experiments

For design of point source experiments, Equation (12) for U/c and Equation (13) for X/R were substituted into Equation (26). This substitution means that:

$$\left(\frac{\sigma_{max}}{\rho_s c^2}\right) = f_{(\sigma_{max}/\rho_s c^2)} \left[\frac{h}{R}, \frac{r}{R}, \frac{E}{\rho_s c^2}, \frac{\rho_p}{\rho_s}, \frac{p_o}{\rho_s c^2}, \frac{W_e}{\rho_s c^2 R^3}\right] \tag{27}$$

Tests were conducted on several different sizes of pipe including diameters of 3-, 6-, and 16-inches and eventually 24- and 30-inches. Equation (27) can be the same for a 3-inch diameter pipe as for a 30-inch diameter pipe, if the parameters are scaled correctly. A replica model in particular makes model and prototype systems equivalent by scaling all geometries h, R, and r by a geometric scale factor λ and all soil and pipe properties remain the same or have a scale factor of 1.0. The pi term ($W_e/p_s c^2 R^3$) indicates that the energy release W_e, (i.e. the size of the charge) must be scaled as λ^3 if this pi term is to be invariant, and the term $\sigma_{max}/\rho_s c^2$ indicates that the measured stresses will be the same in both model and prototype systems. Table 1 summarizes the scale factors which can satisfy Equation (27) for stress or, in a similar manner, Equations (12) and (13) for ground motion.

Table 1. Scale Factors for a Replica Modeling Law

Symbols	Parameters	Scale Factor
h, R, r, X	Geometric lengths or distances	λ
ρ_s, ρ_p	Mass density	1.0
E	Modulus of elasticity	1.0
P_O	Atmospheric pressure	I..O
c,U	Velocity	1.0
W_e	Explosive energy release	λ^3

Equation (27) is shown to be invariant by substituting the scale factors from Table 1 for a model system. A bar over each symbol indicates that Equation (27) is being written for a second system. This substitution gives:

$$\left[\frac{1\bar{\sigma}_{max}}{1\bar{\rho}_s(1\bar{c})^2}\right] = f_{(\sigma_{max}/\rho_s c^2)}\left[\frac{\lambda\bar{h}}{\lambda\bar{R}}, \frac{\lambda\bar{r}}{\lambda\bar{R}}, \frac{1\bar{E}}{1\bar{\rho}_s(1\bar{c})^2}, \frac{1\bar{\rho}_p}{1\bar{\rho}_s}, \frac{1\bar{p}_o}{1\bar{\rho}_s(1\bar{c})^2}, \frac{\lambda^3\bar{W}_e}{1\bar{\rho}_s(1\bar{c})^2(\lambda\bar{R})^3}\right] \qquad \textbf{(28)}$$

or, after factoring out the X's which are constants and canceling:

$$\left(\frac{\bar{\sigma}_{max}}{\bar{\rho}_s\bar{c}^2}\right) = f_{(\sigma_{max}/\rho_s c^2)}\left[\frac{\bar{h}}{\bar{R}}, \frac{\bar{r}}{\bar{R}}, \frac{\bar{E}}{\bar{\rho}_s\bar{c}^2}, \frac{\bar{\rho}_p}{\bar{\rho}_s}, \frac{\bar{p}_o}{\bar{\rho}_s\bar{c}^2}, \frac{\bar{W}_e}{\bar{\rho}_s\bar{c}^2\bar{R}^3}\right] \qquad (29)$$

Note that Equation (29) for the second system with bars over the symbols is exactly the same as Equation (27). This observation means that the systems are equivalent; they have the same equation, provided properties are scaled as in Table 1.

To illustrate, a 3-inch diameter steel pipe with a wall thickness of 0.060 inch buried 6 inches and loaded with a single explosive charge weighing 0.05 lb located 3.0 ft away could be used to correspond to some prototype 30-inch diameter pipe. The prototype would also be made of steel, have a 0.60-inch wall thickness, be buried 60 inches (5 ft) deep, and would be loaded with a SO-lb charge located 30 ft away. The maximum circumferential and longitudinal stresses in both of these pipes would be the same. In addition, ground motions also scale according to the replica model law in Table 1. At the pipe or other scaled location, the soil particle velocity would be the same and the peak displacements would scale as the geometric scale factor λ. Both ground motions and pipe strains were recorded in experiments so information would be obtained for studying and generating both the ground motion and the pipe stress solutions.

Actually, any one model test simulates a variety of different prototype conditions. A test on a 3-inch diameter pipe models a certain set of conditions on a 24-inch, 36-inch, or any other size pipe at the same time that it is simulating a 30-inch pipe. This type of generalized thinking emphasizes that a whole spectrum of conditions is being studied in every model experiment provided the results of a test are interpreted properly. The final variations for charge weights, standoff distances, etc., were selected to give several orders of magnitude variation in any given prototype condition. Different sizes of pipe were tested to emphasize that indeed the solutions are general ones. In particular, as results are studied in Section V for ground motion and Section VI for pipe stress, the reader will become aware that the scaled standoff distances are closer to the charge than in other earlier ground motion and pipe stress studies. The reader will realize that a buried pipe is a strong structure capable of withstanding more severe buried blasting conditions than have generally been accepted in the past. Furthermore, the results given in Section IV and analyzed in Sections V, VI, and VIII clearly demonstrate that the approach selected and the solutions obtained are valid for various ranges of the scaled parameters which define the ground motions and pipe stresses.

III. EXPERIMENTAL PROGRAM

Scope

To achieve the objectives of the blasting research program funded by the Pipeline Research Committee (PRCI) of the American Gas Association (A.G.A.), Southwest Research Institute (SwRI) conducted an extensive experimental program. These experiments were performed in several series throughout the period of 1975 through 1980. Each series of tests provided the necessary data to analyze a number of blasting situations and develop equations and methods for predicting pipeline stresses from nearby buried explosive detonations.

Summary of Tests

A total of 113 experiments were accomplished in this blasting research program. The majority of the tests were executed as model scale experiments. The rest of the tests were conducted on full scale pipelines. All but four of the experiments were conducted with both the explosive source and pipe buried in a homogeneous soil media. Ground motion and pipe strain measurements were made for use in generating and validating the prediction equations and methods presented in other sections of this report. Several blasting situations were studied experimentally. In general terms, the situations modeled were as follows:

- A point explosive source buried near a pipeline.
- An equally spaced line of equal size explosive charges buried parallel to a pipeline.
- A similar explosive line buried at an angle to a pipeline.
- A rectangular grid of equal size explosive charges equally spaced and buried parallel to a pipeline.
- A similar grid of explosives buried at an angle to a pipeline.

In addition to these experimental studies, four of the total number of tests were performed to determine the feasibility of blasting in a concrete block to simulate detonations in a rock media adjacent to a model pipe buried in soil. Details and results of these last tests are discussed in depth in Section X. No additional comments about them will be made in this part of the report.

The homogeneous soil experiments were conducted at various test sites, in different tasks of the program, and at different time frames. In order to summarize the tests, they have been arranged chronologically by explosive geometry and grouped together if they were executed during the same time frame and at the same test site. This summary is presented in Table 2. All of the tests conducted at SwRI were in model scale on unpressurized pipes. Those performed in Kansas and Kentucky were the only full-scale experiments. Serveral of these experiments used pressurized pipes.

Table 2. Summary of Experimental Program

Test Series	Year Performed	Test Site	Explosive Source	Number of Experiments
1	1976	SwRI	Point	20
			Parallel Line	11
2	1977	Kansas	Point	8
3	1977	Kentucky	Point	4
4	1979	SwRI	Point	12
			Angled-Line	10
			Parallel Grid	11
			Angled-Grid	9
5	1980	SwRI	Point	12
			Parallel Line	4
			Parallel Grid	4
			Angled-Grid	4

Test Facilities and Test Pipes

All of the model tests listed in Table 2 were conducted on the campus of SwRI at the Explosives and Ballistics Range shown in Figure 2. The Range is approximately one mile from the center of the Institute complex. The site consists of a relatively homogeneous field of sandy loam. At the beginning of the research program, cores were taken down to 6 ft in depth to ensure that the soil was, in fact, homogeneous and to obtain a good measure of the soil density, one of the parameters used in the model analysis to characterize the soil. The average density measured from the survey cores was 102 lb_m/ft^3. Small sample density measurements were made during the test series and, in general, did not vary much from this average value. From these soil samples, the water content of the soil at the surface and at the depth of the charge was also measured during the tests. In most cases, water content was in the range of 8 to 10 percent. In a few tests, the water content of the soil was as low as 3 percent and as high as 14 percent at the surface during a dry spell and after some heavy rains, respectively.

Three different size model pipes were tested at the SwRI test site. These pipes were nominally 3-inch diameter by 24 ft long, 6-inch diameter by 45 ft long, and 16-inch diameter

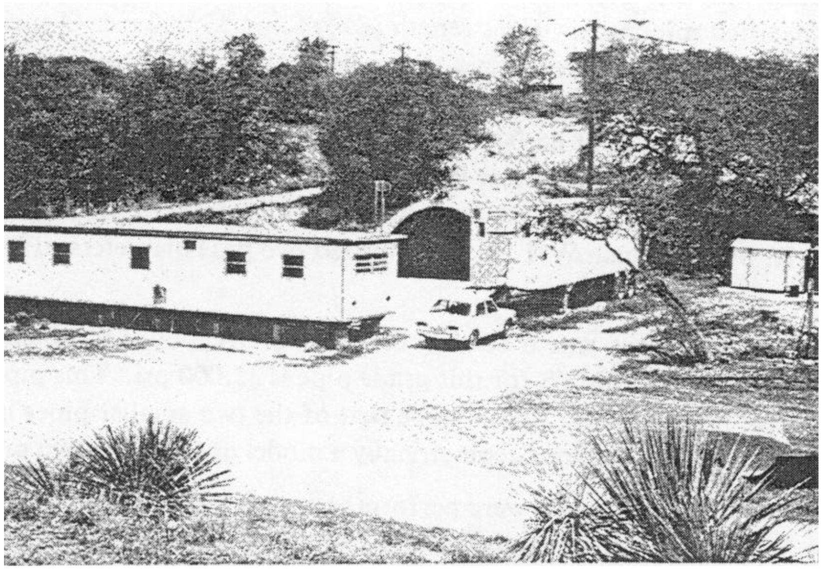

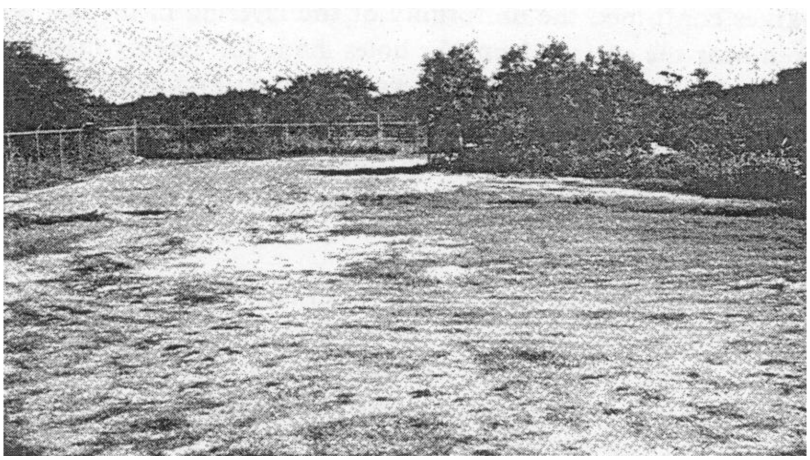

Figure 2. Explosives and Ballistics Range at Southwest Research Institute

by 7 ft long. The two smaller diameter pipes were actually sections of drawn-over-mandrel, 1020 carbon steel tubing with a manufacturer-specified minimum ultimate tensile strength of 65,000 psi and a specified minimum yield strength (SMYS) of 55,000 psi. Tensile tests performed at SwRI on coupons from these pipes showed the ultimate strength to be about 80,000 psi. Assuming the yield strength to be 85 percent of the ultimate strength, the yield strength of these pipes would be about 68,000 psi. These pipes had been ground prior to testing making them 2.95 inch outside diameter (O.D.) by 0.059 inch wall thickness (W.T.), and 5.95 inch O.D. by 0.093 inch W.T. These two pipes were approximate I:8 and 1:4 scale models of a 24 inch O.D. by 0.375 inch W.T. pipeline buried two pipe diameters to its center line.

The largest of the model pipes was a section of 16-inch O.D. by 0.515-inch W.T., ASTM A53, Grade "B" pipe. The SMYS for this grade pipe is 35,000 psi. This pipe had a wall thickness-to-diameter ratio that was about twice that of the two smaller pipes in order to obtain data on a model pipe that was not geometrically a model of the other two pipes.

The 12 full-scale tests listed in Table 2 were performed at two different test sites. Eight of these experiments were done at a test site in the state of Kansas near Kansas City, Missouri, during the summer of 1977. A 98-ft section of Panhandle Eastern Pipe Line Company (PEPLC) pipeline, which had recently been taken out of service due to new highway construction, was made available by PEPLC for these tests. The 24-inch 0.D. by 0.312 W.T., API-5L, Grade "B" section of pipe with an SMYS of 35,000 psi was buried approximately 5 ft to the centerline of the pipe.

The location of the test pipe was surveyed and soil samples taken by PEPLC. The section tested was adjacent and parallel to a small creek. Figure 3 shows pictures of the test area. The soil samples taken from two test holes indicated a 2-ft upper layer of black loam, followed by 6 ft of sandy clay, and clay mixed with, small sandstone for the bottom 3 ft of the test holes. Subsequent digging around the pipe, and augering of holes for soil instrumentation and charges confirmed the uniformity of the layering in the test area soil. Small soil samples taken near the surface from the holes made for placing the charge and velocity transducers on each test were checked for water content and density. The water content was measured to be between I0 and 12 percent on all the Kansas City tests and the density averaged close to 100 $_{m}/ft^3$. Because of the larger scale of these tests versus those conducted at SwRI, an auger andbackhoe were required to instrument these tests and bury the charges. This support was provided by PEPLC.

The last four full-scale experiments were conducted in late fall of 1977 on an operational pipeline belonging to the Texas Gas Transmission Company (TGTC). In this joint effort, between TGTC, the A.G.A., and SwRI, a 30-inch O.D. by 0.344 W.T., API-5LX-60 pipeline with an SMYS of 60,000 psi was instrumented and tested. The test site, near Madisonville, Kentucky, was located on the TGTC right-of-way on the edge of a cornfield and adjacent to a soybean field.. Figure 4 shows two photographs of the test site. The last mile to the site was accessible most of the time only by foot or tracked vehicles because snow and rain made the soft ground extremely muddy. The pipe at the test site is buried approx-

(a) View Looking West from Across Bend of Creek

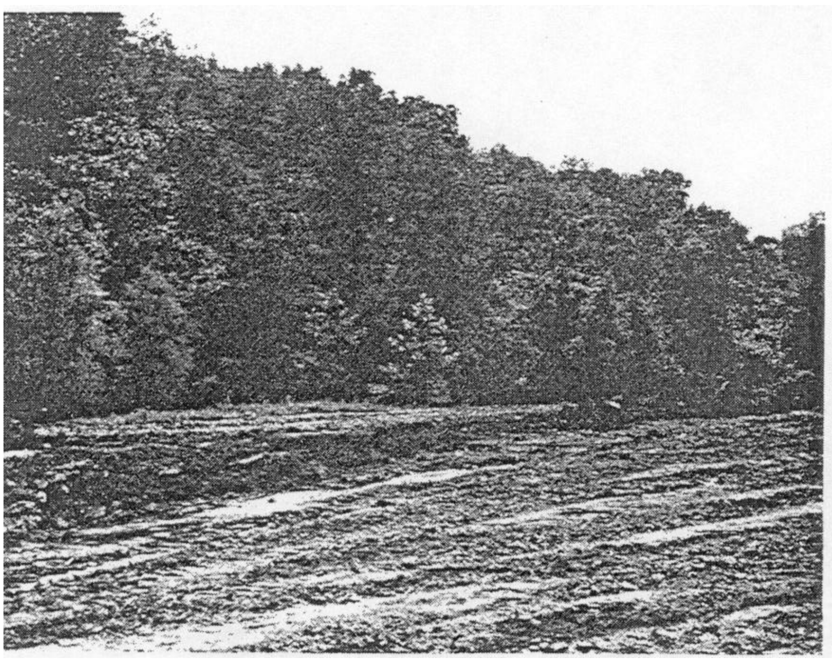

(b) View Looking South from Record Van Location

Figure 3. Kansas City Test Site

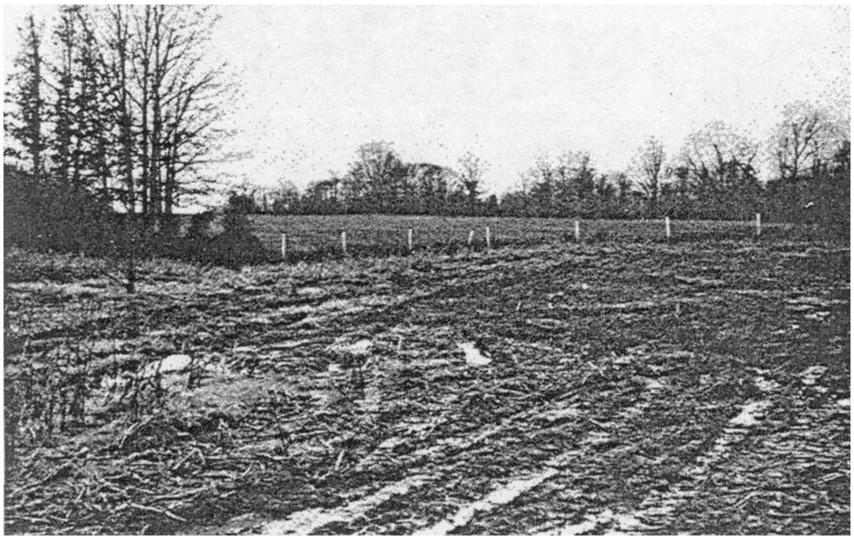

(a) View Looking Northwest from Corn Field

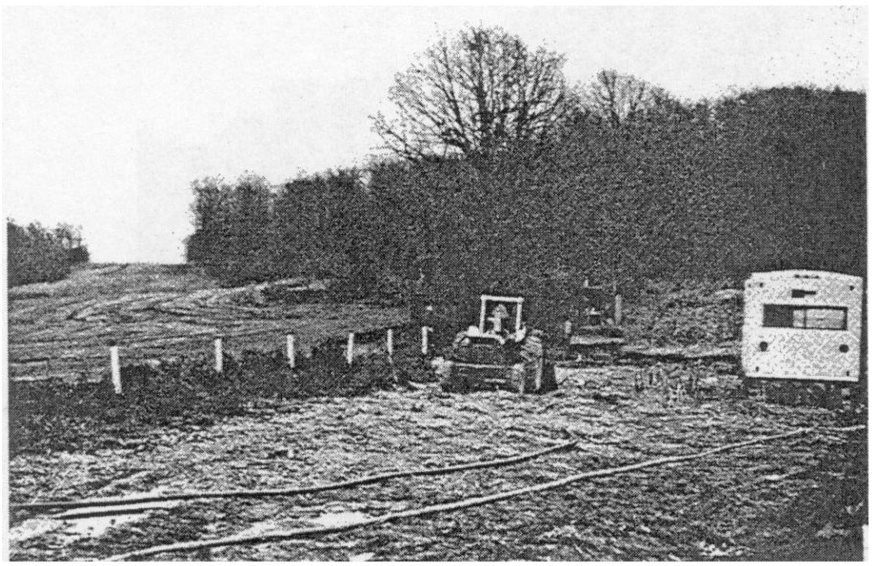

(b) View Looking East Toward Entrance to Site

Figure 4. Kentucky Test Site

imately 5.5 ft to its centerline. The excavation around the test pipe indicated a very uniform layer of soft, reddish clay down to at least 7.5 ft in depth. Field support for uncovering the pipe, burying the transducers, and preparing the ground after each test was provided by TGTC. During the test series, water content in the soil measured near the surface ranged from 14 to 16 percent. The high water content made it difficult to make the holes for the charges and velocity transducers. The average soil density obtained from the small soil samples taken during each test averaged 101 lb_m/ft^3.

During these tests, the pipeline was operated at a reduced pressure of 400 psig. Although four tests were fired, five were actually set up. Test No. 5 resulted in a misfire in the booster used which precluded detonation of the explosive charge. A subsequent rain made conditions in the field impossible for setting up the test again the following day. An ensuing snowstorm and extremely cold weather forecast for the week, plus the necessity of placing the 30-inch line back in normal service prompted TGTC to cancel a try for a fifth test and declare this test series complete.

Description of Experiments

As mentioned earlier in this section, test data were obtained from three different explosive geometries configured into five different explosive sources. The three geometries are labeled throughout this report as point, line, or grid explosive sources. The line and grid sources were oriented either parallel or at an angle to the pipe being tested.

In the first part of the blasting research program, the majority of the tests were point source tests with some parallel line tests also, being conducted. After first phase prediction equations were developed on these simpler explosive geometries using model test data, full-scale point source experiments were planned and performed to validate the results. In all of these tests, the charges were buried to the same depth as' the centerline of the pipe.

Two types of experiments were fired at the Kansas site using single charges buried to the same depth as the pipe: one set without any internal pressure and the other with an air pressure of 300 psig. The section of test pipe was capped at both ends and connections welded for air pressurization; High pressure air cylinders were used to pressurize the pipe. Two sizes of charges were used in these tests; 5 and 15 lb of ammonium nitrate-fuel oil (ANFO) explosive. The original test plan called for conducting only five tests. However, conditions in the field indicated that some revisions to the test plan would provide additional data which would increase the confidence level of the field measurements. This included a test to determine if a difference in strain levels could be detected on measurements made near a coupled joint in the pipe. As had originally been planned, the final test was designed to yield the pipe from the higher loading of a closer charge. The test plan for the Kentucky site, as originally outlined, called for five point source experiments with the charge (5 lb) buried to the same depth as the pipe on three of them, and with the charge buried much deeper on the other two. However, the plan was slightly modified in the field. The charge weights used were decreased on some tests so that-a test at the closer standoff distance could be conducted without exceeding the stress limit set by TGTC for the combined blast and internal pressure stresses. Also, because of the extremely muddy conditions and very soft soil in the test area, the holes for the explosive charges had to be dug using a post hole digger. Consequently, a maximum charge depth of only 7.5 ft could be obtained. Therefore, only one deeper charge test was attempted. Unfortunately, Test No. 5 had a misfire.

After the full-scale experiments, a model test series was conducted at SwRI which included point charges buried at varying depths such that the charge-to-pipe centerline Was at a 45° angle to the horizontal. The data indicated that using the slant distance in the prediction equations produced a good comparison with the previously derived solutions. In this test series, experiments using angled-line, parallel grid, and angled-grid explosive sources were executed for the first time in this program. Data from these complex explosive source experiments were used to develop the first empirical methods for simplifying these explosive geometries into equivalent parallel line or point sources. With these equivalent sources, the prediction equations could then be used to obtain pipe stress estimates within the limitations of the data base available.

In the final test series, data were obtained from point, parallel line, and grid explosive sources. With the much expanded data base, new point and parallel line prediction equations were derived for estimating uniaxial pipe stresses and radial ground motions. In addition, revised methods for simplifying the more complex explosive geometries into equivalent parallel line or point sources were developed. Not only were all of these new equations and methods more accurate and simpler to use than the earlier results, they were also applicable over a broader parameter variation.

All of, the model experiments performed at SwRI used unpressurized pipes, The small spherical charges used in single or multiple configurations were made from C-4, a plastic explosive. Explosive bridgewire (EBW) detonators were used to explode the C-4 charge. A Reynolds Model FS-10 Portable Firing System was used to power the Reynolds RP-83 EBW's and provide a time-zero reference pulse for use in the data processing.

Five of the Kansas full-scale tests were performed with the pipe section pressurized to 300 psig with air. All four of the Kentucky tests used a pipeline with a pressure of 400 psig, half of the normal operating pressure. All of the full-scale tests used charges of ammonium nitrate-fuel oil (ANFO) explosive. These charges were primed with a two component explosive manufactured by Atlas Powder Company called Kinestik, The two components are nonexplosive when not mixed. Once the materials are mixed, they become a, cap-sensitive, high-energy explosive., Electrical blasting caps and a capacitor discharge firing system were used to, initiate each charge.

The point experiments, regardless of whether they were model or full-scale, were set up much the same way. With the exception of the one set of tests in which the charge was buried. deeper, all point sources were buried at about the same depth as the centerline of the pipe opposite a location on the pipe that had been strain-gaged. On the other side of the charge, several ground motion transducers at different standoff distances were buried to the same depth as the pipe, and oriented to sense horizontal radial ground motions. A typical layout for a point source experiment is shown in Figure 5. To measure the response of the tested pipes, strain gages were epoxy-bonded at a minimum of three and a maximum of five different stations along the upper half-circumference of each pipe. Two-element strain gage rosettes were used to sense both hoop and axial strains at each station.

For the group of experiments in which data were obtained from point charges deeper than the pipe, one set of strain gages included rosettes installed on the front (side nearer the charge), top and back of the pipe. A second set of strain gages was located 45 ° around from the first and was the primary set used to measure the pipe response from the point charges buried deeper than the pipe. Figure 6 shows a typical elevation view of the field layout for these tests. As shown in this figure, the ground motion transducers were at the same depth as the center of the pipe, but oriented along their slant distance from the charge.

The pipe and explosive charge information for all the 56 point source tests performed are summarized in Table 3. In this table, each test is identified by test series and test number. The pipe description includes the outside diameter, length, depth to pipe center, line pressure if any, and wall thickness (h). Except for nine experiments, the depth of the pipe is the same as the depth of the charge. For these nine tests, the charge was located at a 45° angle to the pipe. Other charge information in this table includes the equivalent energy release constant (n), the charge weight (W), and the standoff distance (R) measured from the center of the charge to the center of the pipe.

To simulate an explosive line source, several charges of the same weight were placed in a straight line equally spaced and detonated simultaneously. The length of the explosive line is defined as the number of charges multiplied by the spacing between the charges. The line of charges are treated as a continuous explosive charge distributed along the line and having a uniform explosive density. The explosive density equals to the weight of one charge divided by the spacing between two charges. This is equivalent to the total charge weight available divided by the total length of the explosive line.

Fifteen of the experiments used parallel explosive lines as the blasting source while ten used explosive lines oriented at 15°, 30°, and 45° angles to the pipe. All of these explosive line tests were executed in model scale and were set up in a similar fashion as the point source tests. All of the individual charges ‘were buried to the same depth as the longitudinal centerline of the pipe. Pipe strains were again measured by orthogonal sets of strain gages at a location along. the pipe in line with the geometric center of the explosive line. At this primary strain gage location, circumferential and longitudinal strains were measured primarily on the front (side, nearer the charge), top, and back of the pipe. In some cases, measurements were also made in between these three sensing points at 45° from the horizontal. In addition, some strain measurements were made at other locations along the pipe between the center and one end of the array to insure as much as possible that the maximum strains were being recorded.

Ground motion transducers far the explosive line tests were again positioned on the opposite side of the charge as the pipeline. Figure 7 shows a typical plan view layout for a parallel line experiment. For the angled-line tests, ground motion measurements were made

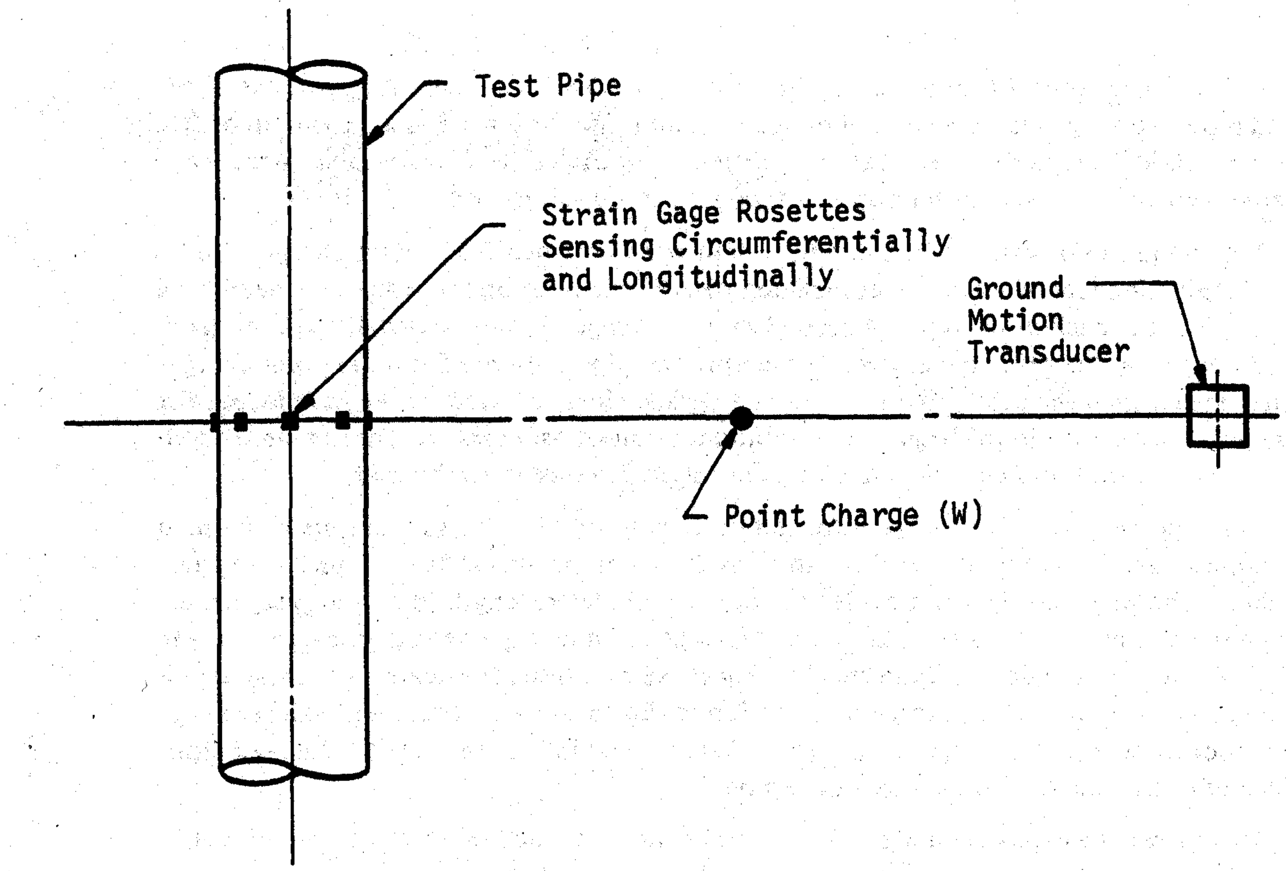

<u>**Plan View**</u>

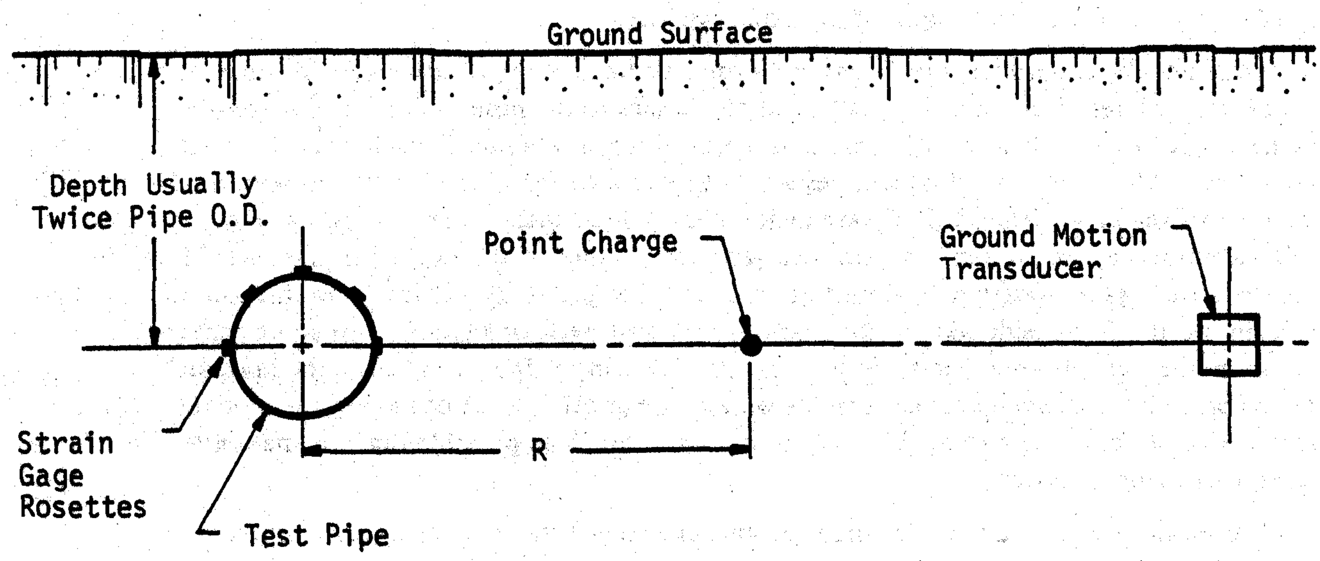

<u>Elevation View</u>

Figure 5. Typical Experimental Layout for Point Source Test

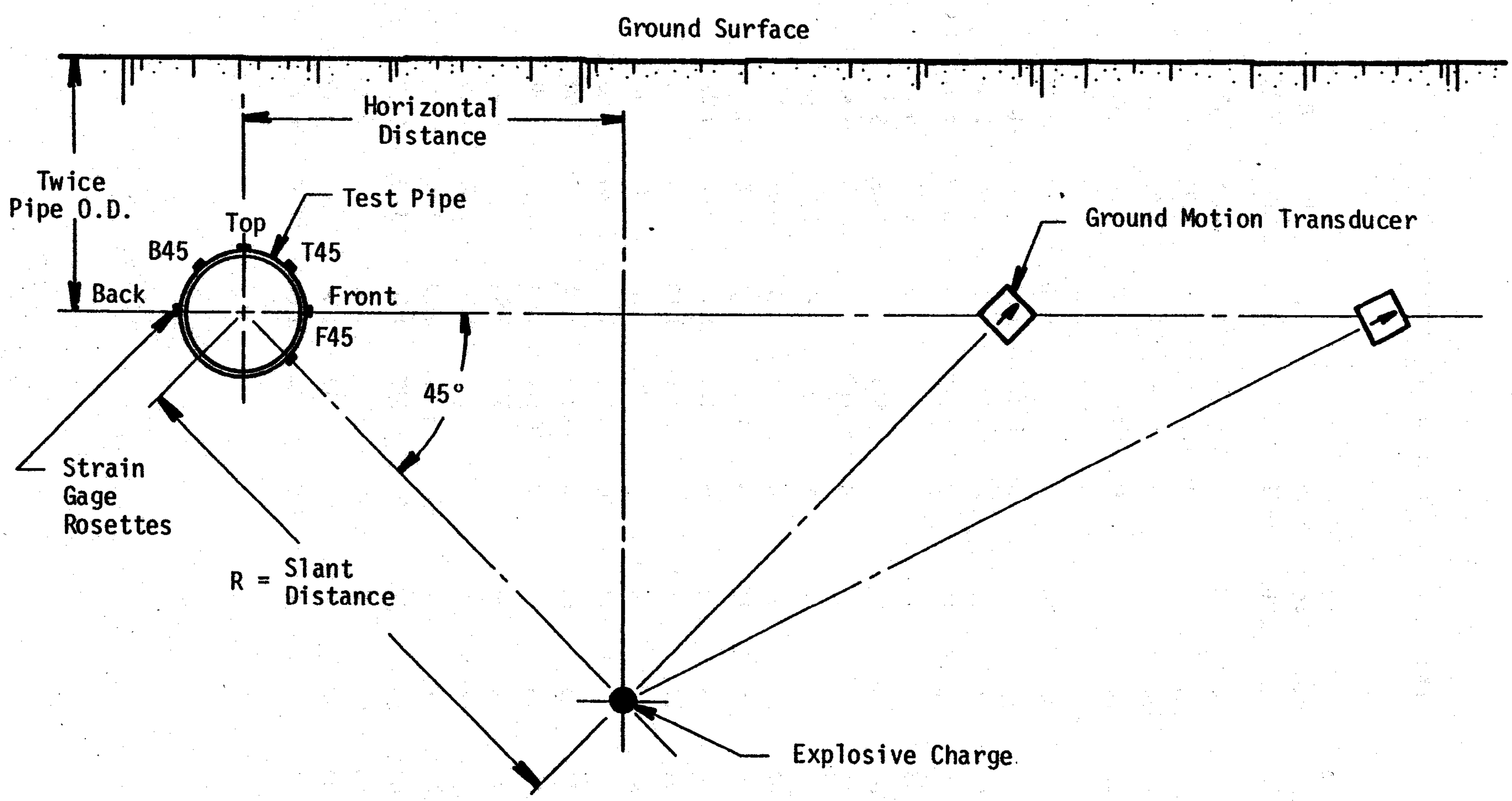

Figure 6. Typical Layout for Deeper Charge Test

Table 3. Description of Point Source Experiments

Test Series	Test No.	Pipe O.D. (in.)	Pipe Lgth (ft)	Pipe Depth (in.)	Line Press. (psig)	(in.)	n	W (lb)	R (ft)
1	1	2.95	24	6	0	0.059	1.12	0.05	1.50
1	2	2.95	24	6	0	0.059	1.12	0.05	1.50
1	3	2.95	24	6	0	0.059	1.12	0.05	1.50
1	4	2.95	24	6	0	0.059	1.12	1.00	11.00
1	5	5.95	45	12	0	0.093	1.12	0.40	3.00
1	6	5.95	45	12	0	0.093	1.12	0.40	3.00
1	7	5.95	45	12	0	0.093	1.12	1.00	11.00
1	8	5.95	45	12	0	0.093	1.12	0.03	2.00
1	9	5.95	45	12	0	0.093	1.12	0.03	1.00
1	10	2.95	24	6	0	0,059	1.12	0.03	0.75
1	20	16.00	7	32	0	0.515	1.12	0.03	3.00
1	21	16.00	7	32	0	0.515	1.12	0.03	1.50
1	22	16.00	7	32	0	0.515	1.12	0.03	1.00
1	23	16.00	7	32	0	0.515	1.12	0.03	1.00
1	24	16.00	7	32	0	0.515	1.12	0.06	1.50
1	25	16.00	7	32	0	0.515	1.12	0.06	1.25
1	28	2.95	24	6	0	0.059	1.12	0.05	1.50
1	29	2.95	24	6	0	0.059	1.12	0.05	1.50
1	30	5.95	45	12	0	0.093	1.12	0.40	3.00
1	31	5.95	45	12	0	0.093	1.12	0.40	3.00
2	1	24.00	98	60	0	0.312	1.00	15.00	9.40
2	2	24.00	98	60	0	0.312	1.00	5.00	6.00
2	3	24.00	98	60	0	0.312	1.00	5.00	6.00
2	4	24.00	98	60	300	0.312	1.00	15.00	13.00
2	5	24.00	98	60	300	0.312	1.00	5.00	9.00
2	6	24.00	98	60	300	0.312	1.00	15.00	13.00
2	7	24.00	98	60	300	0.312	1.00	15.00	13.00
2	8	24.00	98	60	300	0.312	100	15.00	6.00

Table 3. Description of Point Source Experiments (Cont'd)

Test Series	Test No.	Pipe O.D. (in.)	Pipe Lgth (ft)	Pipe Depth (in.)	Line Press. (psig)	h (in.)	n	W (lb)	R (ft)
3	1	30.00	∞	66	400	0.344	1.00	5.00	15.00
3	2	30.00	∞	66	400	0.344	1.00	4.00	15.00
3	3	30.00	∞	66	400	0.344	1.00	3.00	9.00
3	4	30.00	∞	66	400	0.344	1.00	3.00	15.00
4	1	5.95	45	12	0	0.093	1.12	0.40	3.00
4	2	5.95	45	12	0	0.093	1.12	0.10	1.50
4	3*	5.95	45	12	0	0.093	1.12	0.40	4.24
4	4*	5.95	45	12	0	0.093	1.12	0.40	4.24
4	5*	5.95	45	12	0	0.093	1.12	0.20	4.24
4	6*	5.95	45	12	0	0.093	1.12	0.20	4.24
4	7*	5.95	45	12	0	0.093	1.12	0.10	2.12
4	8*	5.95	45	12	0	0.093	1.12	0.10	2.12
4	9*	5.95	45	12	0	0.093	1.12	0.20	2.12
4	10*	5.95	45	12	0	0.093	1.12	0.20	2.12
4	11*	5.95	45	12	0	0.093	1.12	0.40	4.28
4	38	5.95	45	12	0	0.093	1.12	3.60	22.50
5	1	5.95	45	12	0	0.093	1.12	0.40	8.00
5	2	5.95	45	12	0	0.093	1.12	0.40	11.00
5	3	5.95	45	12	0	0.093	1.12	0.40	15.00
5	4	5.95	45	12	0	0.093	1.12	0.25	8.00
5	5	5.95	45	12	0	0.093	1.12	0.08	4.00
5	6	5.95	45	12	0	0.093	1.12	0.12	11.00
5	7	5.95	45	12	0	0.093	1.12	0.08	11.00
5	8	5.95	45	12	0	0.093	1.12	0.08	7.00
5	9	5.95	45	12	0	0.093	1.12	0.20	5.00
5	10	5.95	45	12	0	0.093	1.12	0.08	2.50
5	11	5.95	45	12	0	0.093	1.12	0.40	5.00
5	12	5.95	45	12	0	0.093	1.12	0.40	3.00

*In these tests the charge was buried deeper than the pipe as shown in Figure 6.

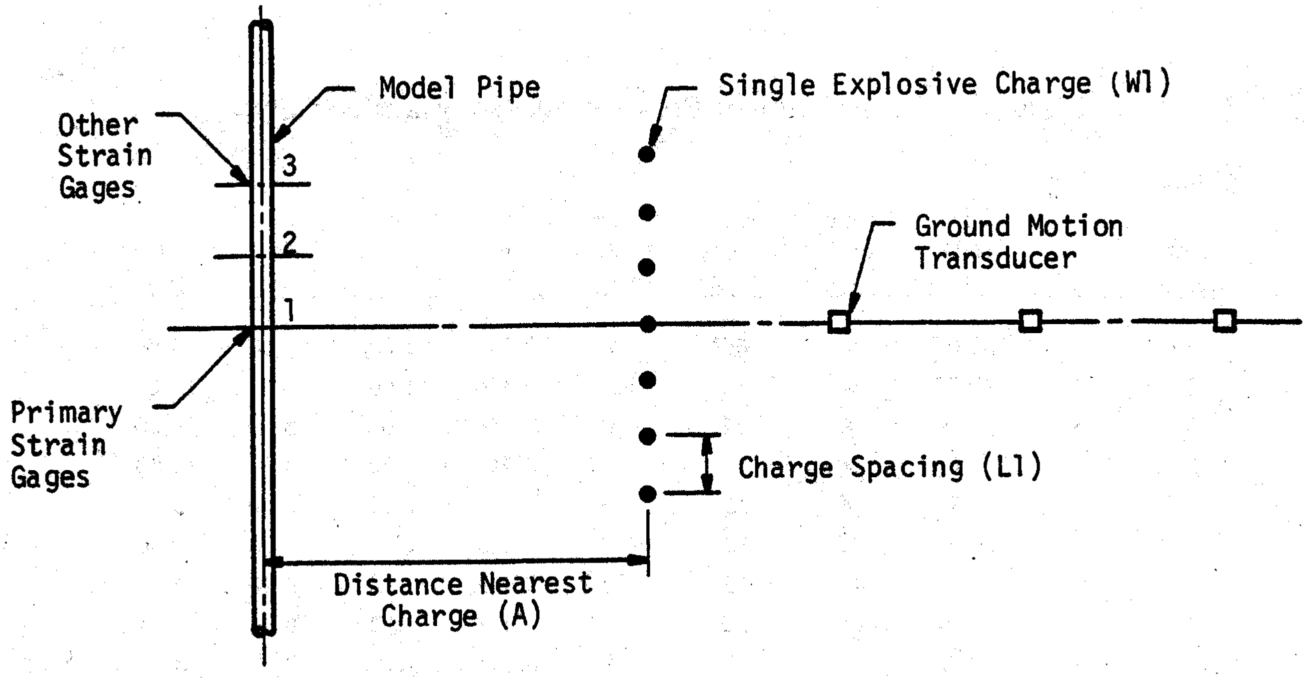

Figure 7. Typical Plan View of Parallel Line Test

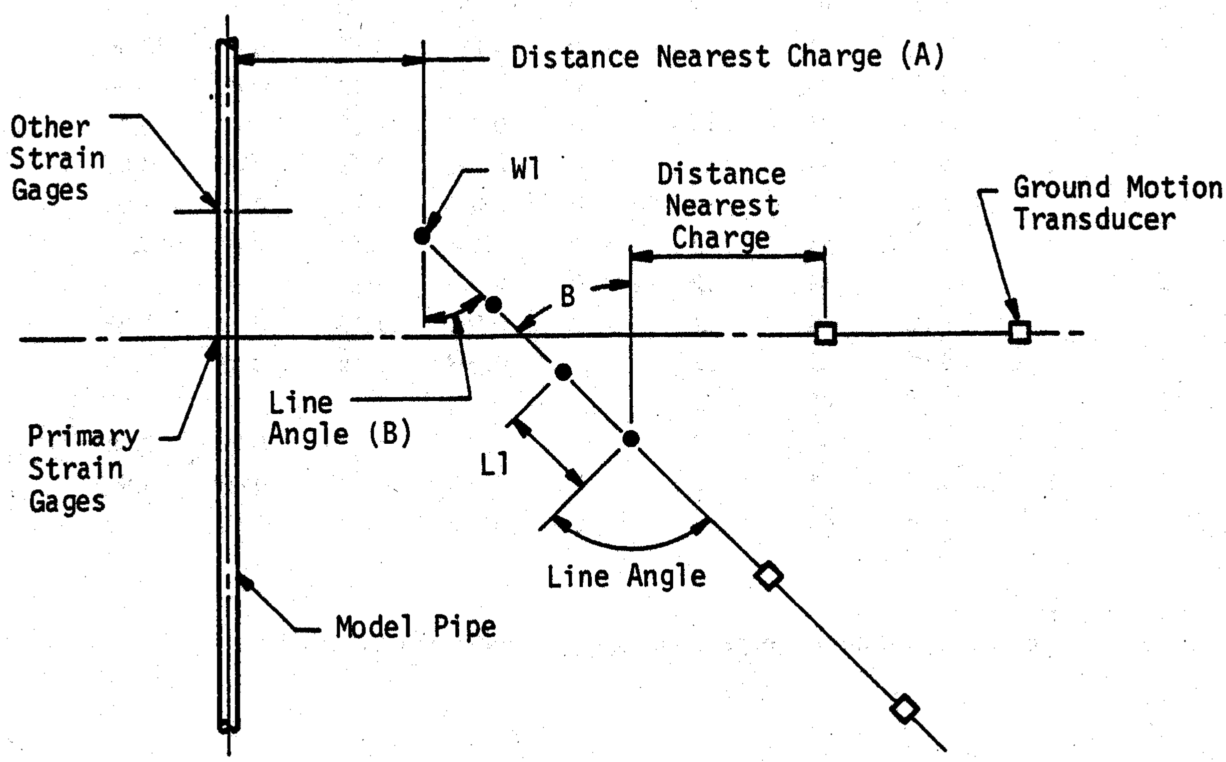

Figure 8. Typical Plan View of Angled-Line Test

at the same three angles as the pipe and at three other angles (60°, 75°, and 90°) to obtain as much data as possible from the limited number of experiments. Figure 8 depicts the plan view of a typical layout for an angled-explosive line experiment.

The pipe and explosive charge information for the 25 explosive line source tests are summarized in Table 4. Each test is identified by the test series and test number. The same kind of pipe description given for the point source tests is provided for the line sources. The charge information in this table includes the equivalent energy release (n), the number of equally spaced charges in the line (Nl), the spacing of these charges (Ll), the weight of each charge (Wl), the angle, between the explosive line and the pipeline (B), and the distance between the pipe center line and the nearest charge in the explosive line (A).

The third and final explosive geometry used in this program was a rectangular array or grid of equally spaced charges of the same weight oriented either parallel or at an angle to the instrumented pipe. Of the 28 grid tests performed in this program, 15 had the grid oriented parallel to the pipe and 13 at an angle. All of these experiments were conducted using one of the model pipes. In the majority of these tests, the charges in the grids were detonated simultaneously. In six tests, time delays between rows were used in an effort to enhance the strength of the seismic wave propagating in the soil. The delay time, either 3 or 6 milliseconds, was selected to be about the same as the approximate time required for the wave to travel the distance separating the explosive rows. Initiation was always on the explosive row farthest from the pipe. The strains measured on these delayed grid tests were of similar magnitude (within the scatter of the data) as obtained from the simultaneous detonations. Therefore, no enhancement was detected on the pipe response. Likewise, no reduction on the pipe maximum strains was apparent indicating that the delay times were sufficiently short relative to the response time of the buried pipe that they could be considered simultaneous. Consequently, no differentiation was made in analyzing the data from these grid tests with delays nor in presenting the results in this report.

To record the response of the pipe to the grid charges, strain measurements were made at a location along the pipe in line with the geometric center of the grid. In addition, some' measurements were made at other locations along the pipe. Ground motion transducers for these tests were again positioned on the other side of the grid opposite the pipe. Figure 9 shows the typical plan view layout for the parallel grid experiments. For the angled-grid tests, the ground motion transducers were oriented to sense at a similar angle as the model pipe, as well as perpendicular to the grid as shown in Figure 10. For all the, grid experiments, the individual charges making up the explosive array and the velocity transducers were buried to the same depth as the longitudinal centerline of the model.

The test parameters for the 28 grid experiments are listed in Table 5. The tests are identified by test series and number. Like all the other tests in this research program, description of the pipe tested is provided in this table. The explosive grid sources are defined by the equivalent energy release (n), the number of equally spaced charges on the front row of the grid (Nl), the spacing of charges in the front row (Ll), the weight of an individual charge in the grid (Wl), the angle between the grid and the pipeline (B), the distance between the

Table 4. Description of Line Source Experiments

Test Series	Test No.	Pipe O.D. (in.)	Pipe Lgth (ft)	Pipe Depth (in.)	Line Press. (psig)	h (in.)	n	N1	L1 (ft)	W1 (lb)	B (deg)	A (ft)
1	11	5.95	45	12	0	0.093	1.12	7	1.50	0.05	0	5.00
1	12	5.95	45	12	0	0.093	1.12	7	2.40	0.40	0	8.00
1	13	5.95	45	12	0	0.093	1.12	7	1.50	0.40	0	5.00
1	14	5.95	45	12	0	0.093	1.12	7	1.50	0.40	0	5.00
1	15	2.95	24	6	0	0.059	1.12	7	0.75	0.05	0	2.50
1	16	2.95	24	6	0	0.059	1.12	7	0.75	0.05	0	2.50
1	17	2.95	24	6	0	0.059	1.12	7	1.50	0.03	0	5.00
1	18	2.95	24	6	0	0.059	1.12	7	0.90	0.40	0	3.00
1	19	5.95	45	12	0	0.093	1.12	7	0.46	0.03	0	1.50
1	26	2.95	24	6	0	0.059	1.12	7	3.30	0.05	0	8.00
1	27	2.95	24	6	0	0.059	1.12	7	3.30	0.05	0	8.00
5	21	5.95	45	12	0	0.093	1.12	4	1.50	0.40	0	15.00
5	22	5.95	45	12	0	0.093	1.12	7	1.50	0.40	0	15.00
5	23	5.95	45	12	0	0.093	1.12	7	1.50	0.40	0	10.00
5	24	5.95	45	12	0	0.093	1.12	7	1.50	0.05	0	10.00
4	31	5.95	45	12	0	0.093	1.12	4	2.50	0.10	15	5.00
4	32	5.95	45	12	0	0.093	1.12	4	2.50	0.10	15	5.00
4	33	5.95	45	12	0	0.093	1.12	4	2.50	0.10	30	5.00
4	34	5.95	45	12	0	0.093	1.12	4	2.50	0.10	30	5.00
4	35	5.95	45	12	0	0.093	1.12	4	2.50	0.10	45	5.00
4	36	5.95	45	12	0	0.093	1.12	4	2.50	0.10	45	5.00
4	39	5.95	45	12	0	0.093	1.12	6	2.50	0.20	30	10.00
4	40	5.95	45	12	0	0.093	1.12	6	2.50	0.20	30	10.00
4	41	5.95	45	12	0	0.093	1.12	6	2.50	0.40	30	10.00
4	42	5.95	45	12	0	0.093	1.12	6	2.50	0.40	30	10.00

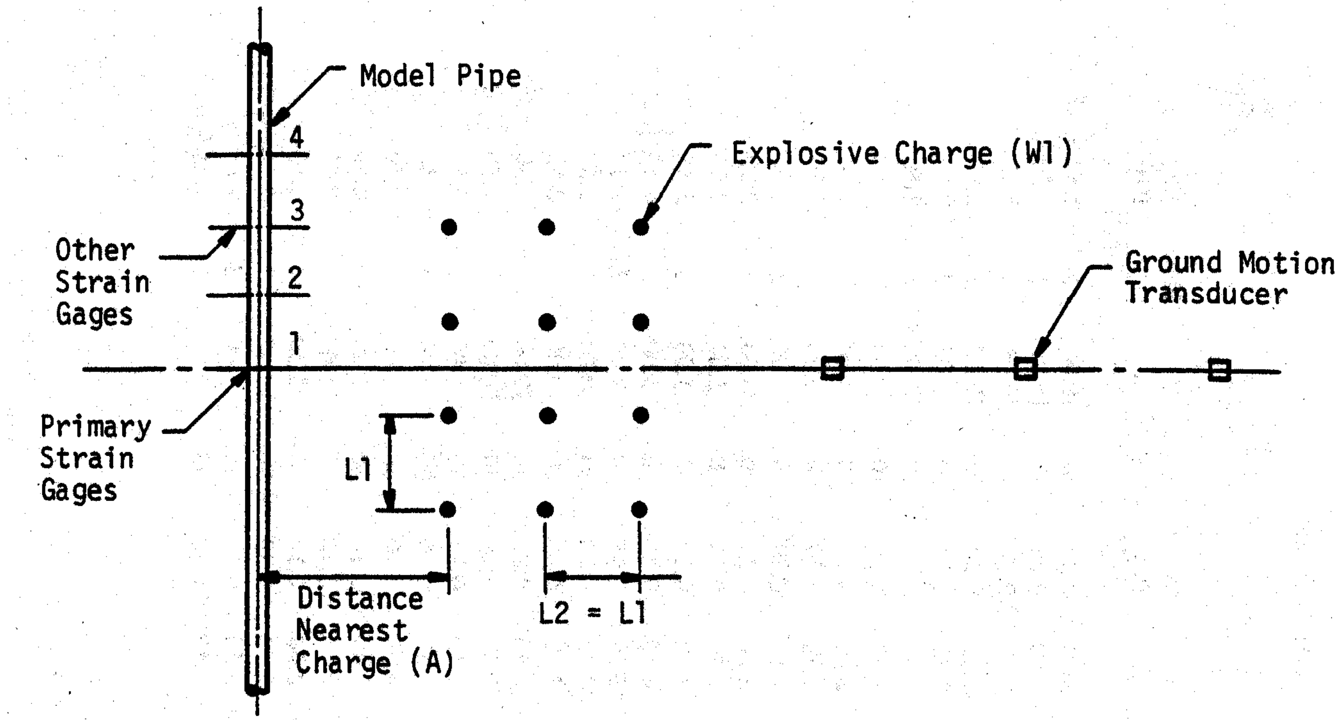

Figure 9. Typical Plan View of Parallel Grid Test

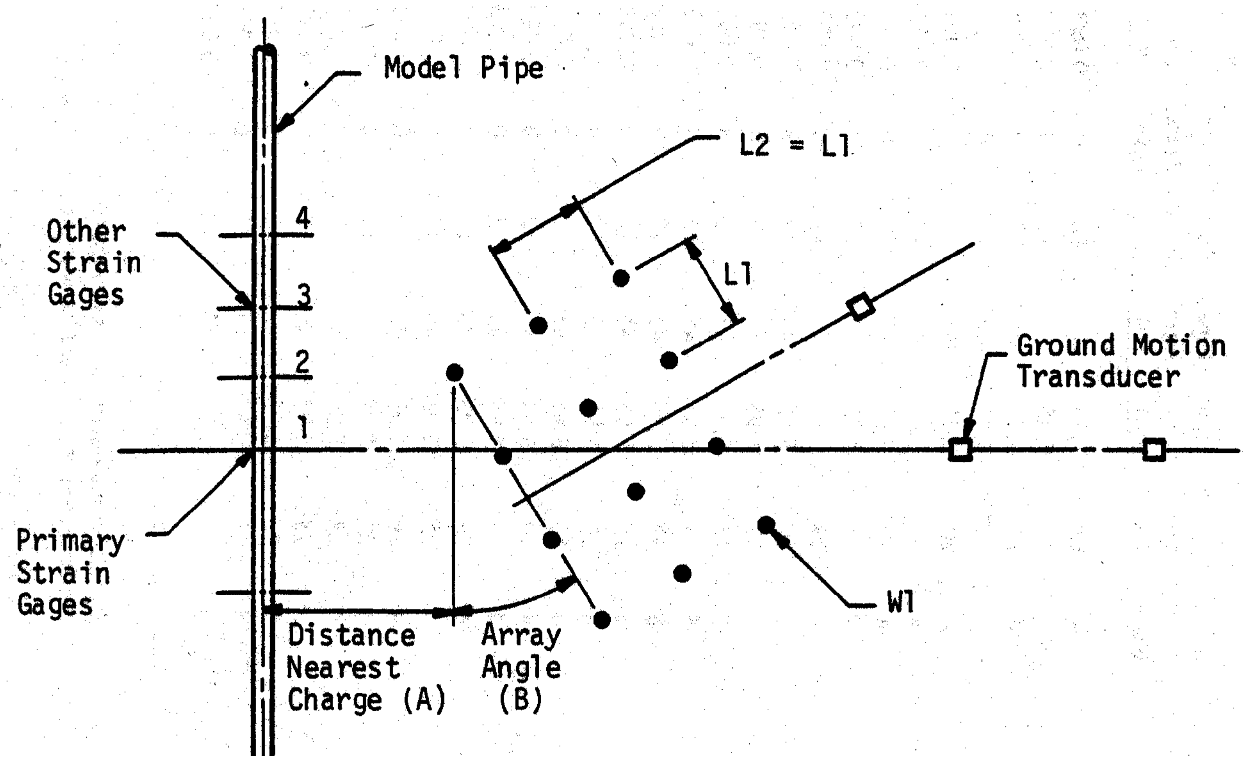

Figure 10. Typical Plan View of Angled-Grid Test

Table 5. Description of Grid Source Experiments

Test Series	Test No.	Pipe O.D. (in.)	Pipe Lgth (ft)	Pipe Depth (in.)	Line Press. (psig)	h (in.)	n	N1	L1 (ft)	W1 (lb)	B (deg)	A (ft)	N2	L2 (ft)
4	12	5.95	45	12	0	0.093	1.12	4	2.50	0.20	0	10.00	3	2.50
4	13	5.95	45	12	0	0.093	1.12	4	2.50	0.20	0	10.00	3	2.50
4	14**	5.95	45	12	0	0.093	1.12	4	2.50	0.20	0	10.00	3	2.50
4	15*	5.95	45	12	0	0.093	1.12	4	2.50	0.20	0	10.00	3	2.50
4	20	5.95	45	12	0	0.093	1.12	4	2.50	0.10	0	5.00	3	2.50
4	21	5.95	45	12	0	0.093	1.12	4	2.50	0.10	0	5.00	3	2.50
4	22*	5.95	45	12	0	0.093	1.12	4	2.50	0.10	0	5.00	3	2.50
4	23	5.95	45	12	0	0.093	1.12	4	2.50	0.10	0	3.00	3	2.50
4	29	5.95	45	12	0	0.093	1.12	4	2.50	0.30	0	20.00	3	2.50
4	30	5.95	45	12	0	0.093	1.12	4	2.50	0.30	0	20.00	3	2.50
4	37	5.95	45	12	0	0.093	1.12	4	2.50	0.30	0	20.00	3	2.50
5	13	5.95	45	12	0	0.093	1.12	4	2.50	0.15	0	5.00	3	2.50
5	14	5.95	45	12	0	0.093	1.12	4	2.50	0.30	0	5.00	3	2.50
5	17	5.95	45	12	0	0.093	1.12	4	4.00	0.20	0	8.00	3	4.00
5	18	5.95	45	12	0	0.093	1.12	4	1.50	0.05	0	4.00	3	1.50
4	16	5.95	45	12	0	0.093	1.12	4	2.50	0.20	30	10.00	3	2.50
4	17	5.95	45	12	0	0.093	1.12	4	2.50	0.20	30	10.00	3	2.50
4	18	5.95	45	12	0	0.093	1.12	4	2.50	0.20	30	10.00	3	2.50
4	19*	5.95	45	12	0	0.093	1.12	4	2.50	0.20	30	10.00	3	2.50
4	24	5.95	45	12	0	0.093	1.12	4	2.50	0.10	30	5.00	3	2.50
4	25	5.95	45	12	0	0.093	1.12	4	2.50	0.10	30	5.00	3	2.50
4	26*	5.95	45	12	0	0.093	1.12	4	2.50	0.10	30	5.00	3	2.50
4	27	5.95	45	12	0	0.093	1.12	4	2.50	0.10	30	5.00	3	2.50
4	28*	5.95	45	12	0	0.093	1.12	4	2.50	0.10	30	5.00	3	2.50
5	15	5.95	45	12	0	0.093	1.12	4	2.50	0.15	30	3.50	3	2.50
5	16	5.95	45	12	0	0.093	1.12	4	2.50	0.30	30	3.50	3	2.50
5	19	5.95	45	12	0	0.093	1.12	4	2.50	0.10	15	5.00	3	2.50
5	20	5.95	45	12	0	0.093	1.12	4	2.50	0.10	45	5.00	3	2.50

* 6 millisecond delays used between rows
** 3 millisecond delays used between rows

centerline of the pipe and the nearest charge in the explosive grid (A), the number of equally spaced rows making up the grid (N2), and the spacing of these rows (L2).

Typical Test Procedures

All of the experiments in this program followed a similar test procedure regardless of when they were performed or what charge geometry was used. However, the charge geometry and scale factor (pipe size) had a direct bearing on the time and personnel required to set up a test, and the type of equipment necessary. In this section of the report, two typical procedures will be described, one for the model tests and one for the full-scale tests. Although similar, each had its own unique requirements and problems.

For the model tests, the pipe sections were first instrumented at the primary and secondary strain gage locations. Redundant strain rosettes were installed on these pipes in case any gages malfunctioned or were damaged during testing.. In this way, a working set of gages could be substituted without having to unearth the pipe and mount the new gages.

After the model pipes were instrumented, a trench of the proper size and depth was then excavated at the SwRI test site. Each pipe was then placed in the trench and carefully backfilled by hand with soil. The soil was tamped to approximately the original compactness. In all ‘test series, about a month elapsed between the time a pipe section was buried and testing was begun. This allowed the soil around the pipe to return further to its “in situ” condition.

Once the model pipe was in the ground, the instrumentation hardware was set up, cables installed, and the strain gages connected to the measurement system. After all channels were determined to be operational and within the required specifications, the first explosive charge was prepared and the explosive firing system set up and checked.

Ground motion transducer locations were selected for each given charge weight, charge geometry, and standoff distance from the pipe. One of these transducers was normally placed at the same standoff distance as the pipe or two of them bracketed this distance. The rest of the transducers were normally buried at farther distances. With the location of the pipe and ground motion transducers known for a particular test, estimates of the peak ground motions and pipe strains were then made. In the early part of the program, the ground motion estimates were made from other data in the literature while the strain estimates were strictly conservative engineering guesses since no other data existed, Later, all the estimates were based on the data obtained previously on this program and the latest prediction equations derived from them. From these amplitude estimates, amplifier gains and record levels were computed and set to provide a reasonably conservative full-scale record range which would still allow good resolution.

The holes necessary for the charge and ground motion transducers were then dug and the transducers connected to the rest of the system. Figure 11 shows the charge holes making up a grid. Once each ground motion measurement channel was completely wired end-to-end and checked for proper operation, the transducer was buried by hand to its proper

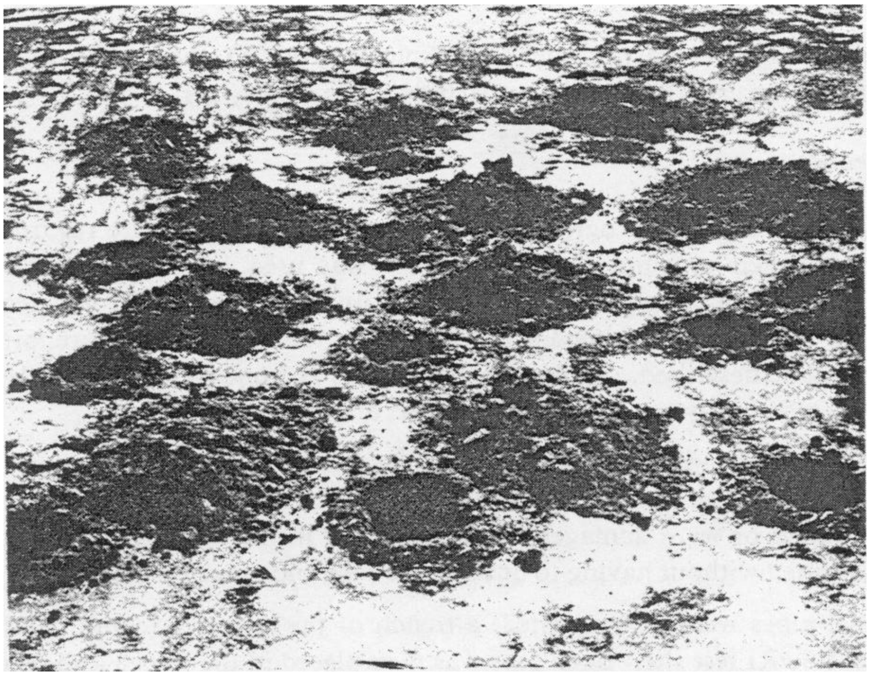

Figure 11. Array of Holes for Explosive Grid Test

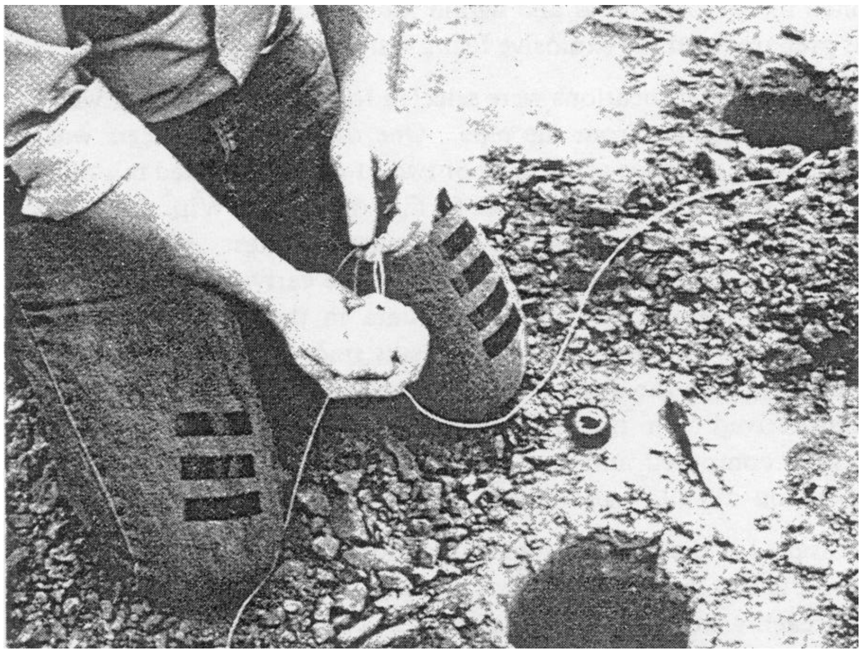

Figure 12. Model Charge Ready for Placement

depth. The holes were backfilled and the soil tamped to approximately the original compactness. Density and water content in the soil were checked prior to testing. An electrical calibration was then recorded to facilitate playback and data reduction, and then a countdown sequence was recorded on the voice channel of the tape recorder.

The explosive charge or charges were then placed downhole as shown in Figure 12. The charges were buried, the hole or holes backfilled, and the soil tamped by hand. To provide maximum confinement, steel plates were placed on the ground centered on the charge and weighed down with sandbags. Figure 13 shows a grid test ready for firing. After the test site was secured, the firing system was armed. Then, the tape recorder was started and the charge fired at the end of the prerecorded countdown sequence. Figure 14 shows the condition of the ground after a grid test has been fired,

The data were played back into an oscillograph recorder for quick-look analysis of the traces before resetting the whole system for the following test. The area around the hole made by the charge in the soil was dug, backfilled and tamped before making a new hole for the test that followed. For a single small point charge, it was possible to do this operation manually; a backhoe was used for the larger charges and other geometries.

For the full-scale tests conducted at the Kansas and Kentucky test sites, the pipe was first uncovered around the section to be strain gaged as shown in Figure 15. The holes were excavated large enough to allow working room for sanding and cleaning the pipe surface and installing the strain gages. Each hole turned out to be deep and large enough to keep the seeping water level from rising too rapidly. As a result, during the strain gaging of the pipe, any water in the hole only had to be pumped out every three or four hours. Figure 15b shows the exposed test pipe with a standing water level as was typically found prior to pumping.

Once the pipe was exposed, the outer coating was removed and the pipe surface was then finished with emery cloth of decreasing coarseness until the surface needed for the strain gages was free of rust, scale, oxides and surface irregularities. The area was then thoroughly degreased and washed with solvent just prior to spot welding the strain gages. The gages were then mounted, lead wires connected and the entire installation heavily coated for environmental and physical protection. The lead wires for each set of gages were routed up through rubber hosing to an adjacent junction-box (J-box) for connecting to the long cable lines going back to the electronic instrumentation housed in a mobile office trailer. Figure 16a shows the connecting of the strain gage lead wires to the long lines. Each strain channel was then tested forproper connections and operation; After every channel checked out, the exposed pipe was very carefully backfilled. Figure 16b shows the beginning of this operation. All the backfill near the pipe was placed and tamped by hand to preclude any damage to the strain gages and their cable. Once the pipe was well covered, the rest of the hole was filled and tamped in layers by machine until the ground was level. Part of this procedure is shown in Figure 17.

Once the pipe strain gage operation was completed, the holes for the velocity transducers and the explosive charge to be used on the first test were made using an auger as

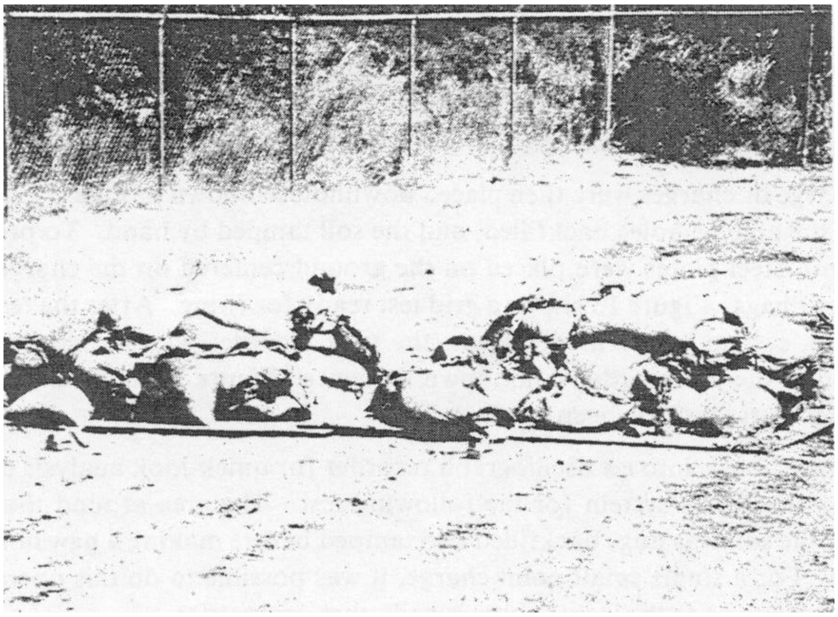

Figure 13. Model Grid Test Ready for Firing

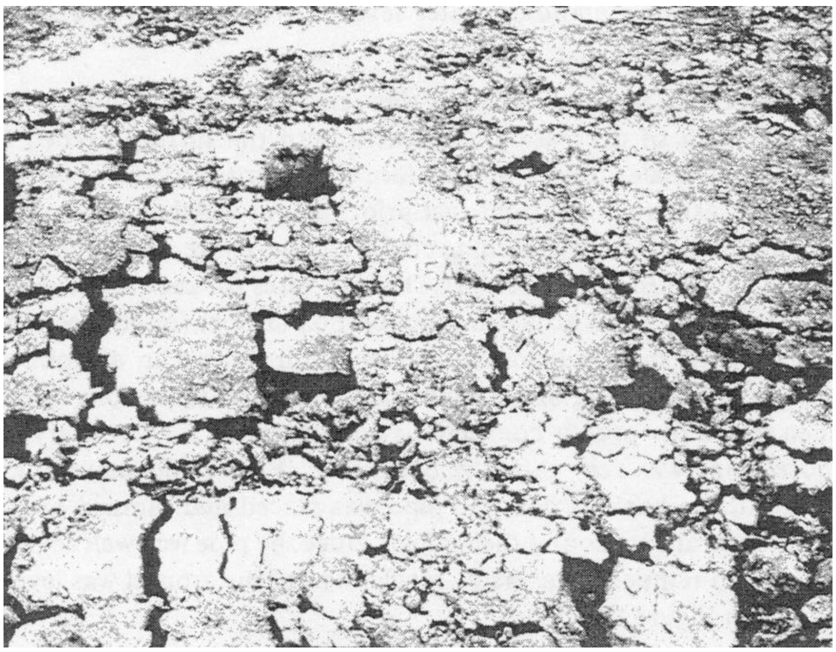

Figure 14. View of Ground After Grid Test

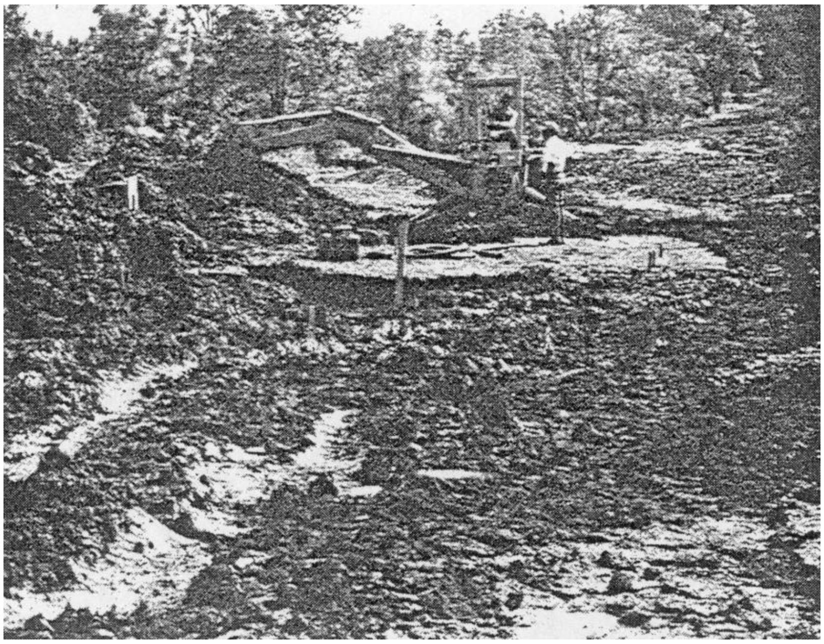

(a) Excavation Around Test Pipe

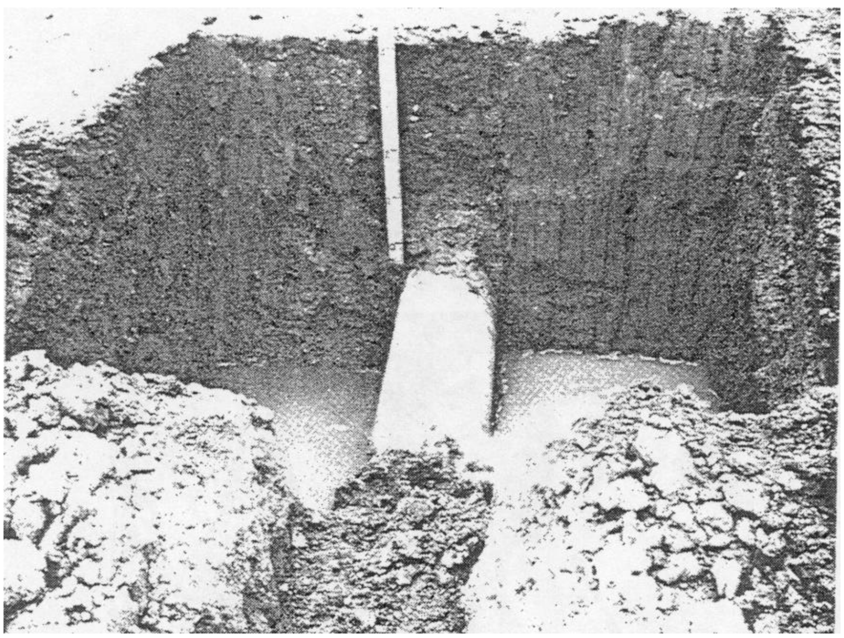

(b) Exposed 24-inch Pipeline

Figure 15. Uncovering of Pipeline for Strain Gaging

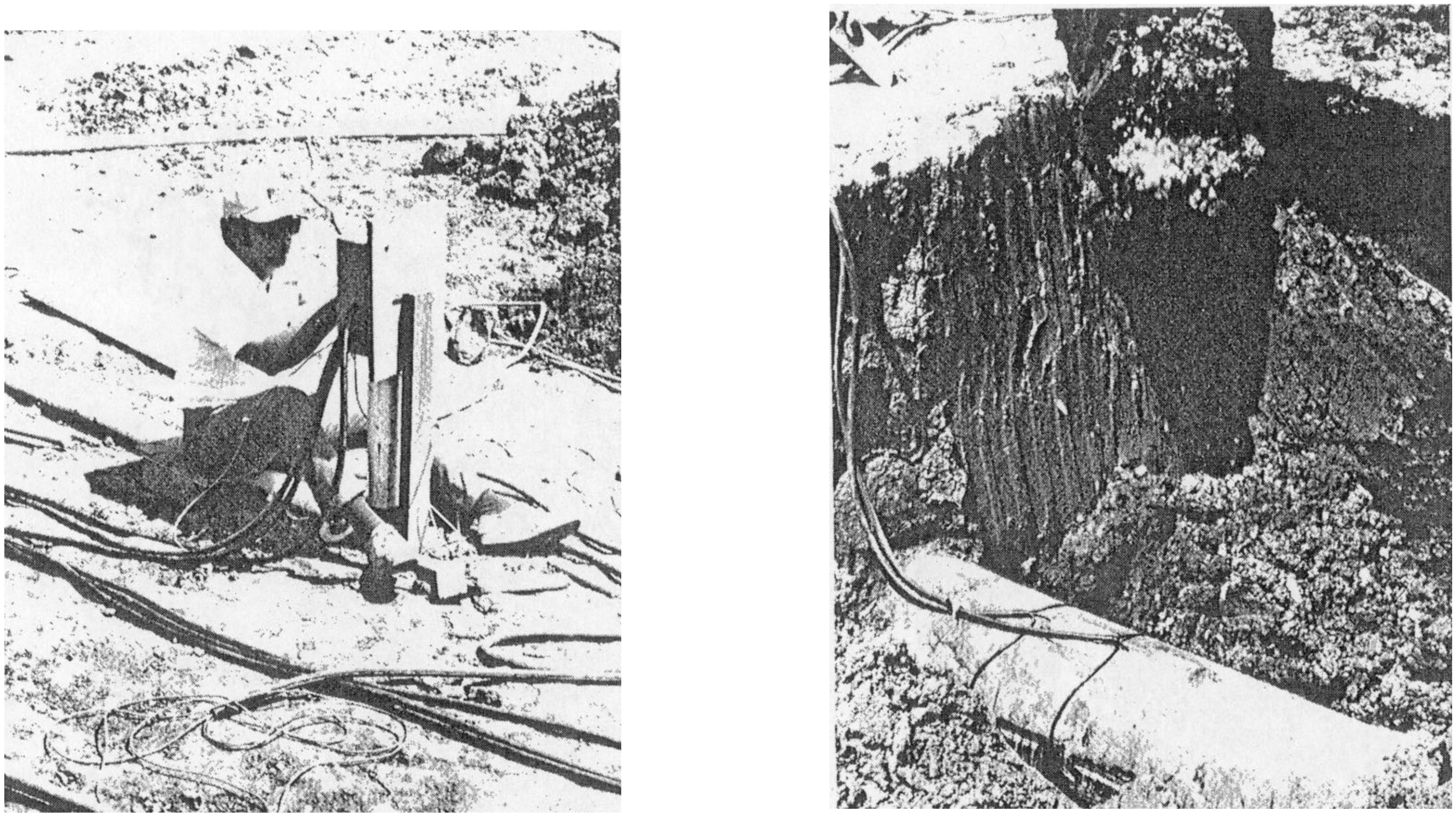

(a) (b)

Figure 16. Connection and Check-Out of Strain Channels

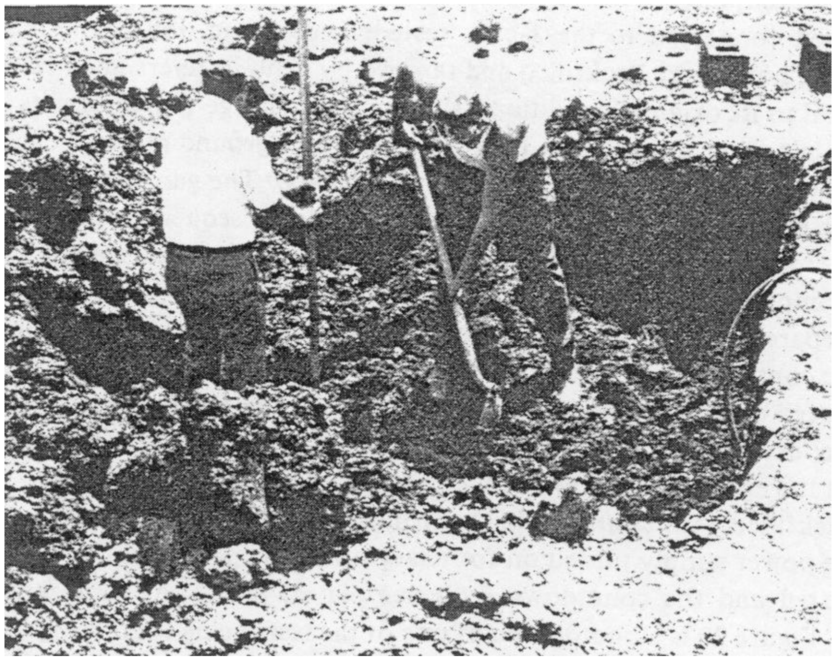

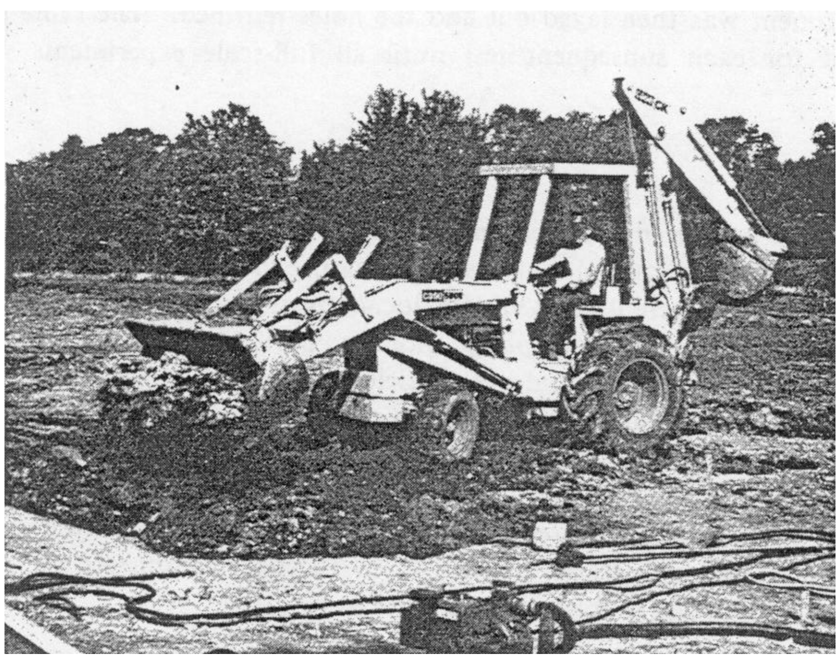

Figure 17. Backfilling of Hole Around Pipe

shown in Figure 18. The completed array of holes is also pictured in this figure. The velocity transducers were then connected to the J-box, tested, and placed down-hole in their respective locations. The holes were backfilled and tamped by hand in layers in an effort to restore the disturbed soil to its original condition, knowing the charge weight and its location with respect to the pipe and transducers, the pipe strains and ground motions expected were estimated using the result of the earlier model experiments. The gains and recording levels were then set for each measurement channel. A countdown sequence and 'electrical calibration voltages were recorded for each measurement channel on the magnetic tape recorder. Once the complete measurement system Was ready for testing, the ANFO explosive charge was prepared by placing the cap, booster and the required amount of explosive in a thin blastic container to protect from any water or moisture. The plastic bag was then sealed and placed down-hole as shown in Figure 19. At the same time, the site was cleared of ail personnel except, for the ordnance technician, and danger signs and audible flashers were placed at the entrance road to the site to warn any unexpected visitors. Once the charge hole was backfilled with tamped soil, the firing circuit was checked one last time for continuity, and the power supply turned on for charging the firing capacitor. The tape recorder was then started and the countdownsequence played back, At time-zero, the charge was detonated. Figure 20 is a photograph of *one* of the tests being fired using a 15-lb explosive charge. The following two photographs, Figure 21, show the craters made by a 15-lb charge and a 5-lb charge. After each test, the area around the crater was excavated about 2 ft past visible cracks in the soil and down 2 ft below the location of the charge. The hole was then refilled in layers and tamped in an effort to restore the ground back to its undisturbed condition. Velocity transducers which required moving to a new location were dug up and the holes refilled and tamped. The velocity transducer and explosive hole pattern for the next experiment was then layed out and the holes redrilled. The same procedures were followed for each subsequent test until all full-scale experiments were completed.

Measurement Systems

Two types of transient measurement were made in the blasting research experiments performed, namely pipe strain and ground motions, To measure the response of the model and full-scale pipes, strain gages were used at various locations on the outer surface of the pipe. The preliminary analysis for predicting pipe response to buried explosive detonations indicated that the maximum horizontal radial soil particle velocity and displacement were required to determine the forcing function, To measure these two parameters, motion transducers were required to be placed at the location of interests in both the model and full-scale experiments. Because this program was primarily designed for conducting tests using available technology for making required measurements, no efforts were undertaken to develop new measurement methods or hardware. Existing transducers and techniques were modified for application in this program,

Two primary techniques for mounting strain gages on steel structures are available: adhesive bonding and spot welding. For most applications, adhesive bonding of strain

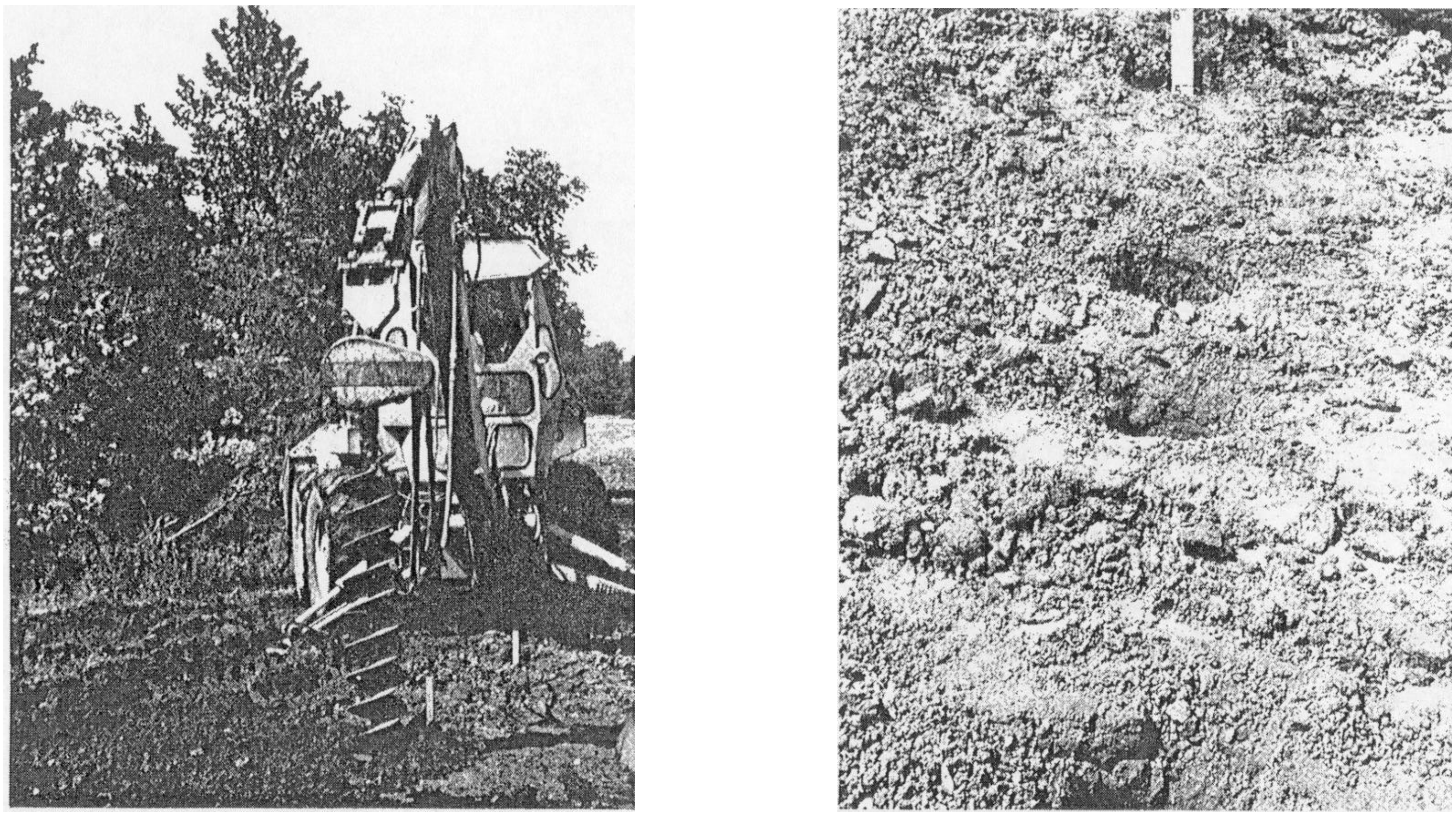

Figure 18. Drilling of Ground Motion Transducer and Charge Holes

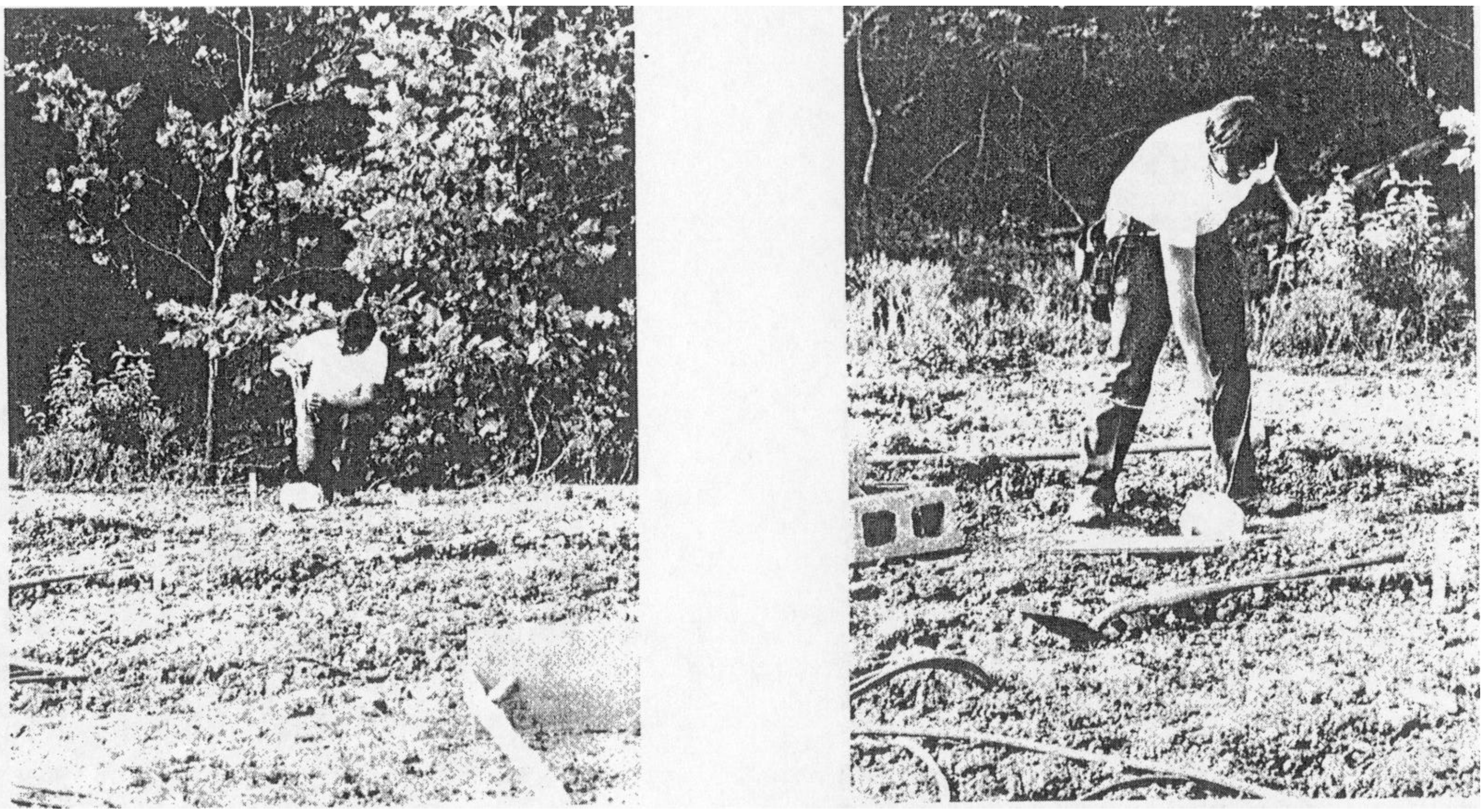

Figure 19. Preparation and Placement of Explosive Charge

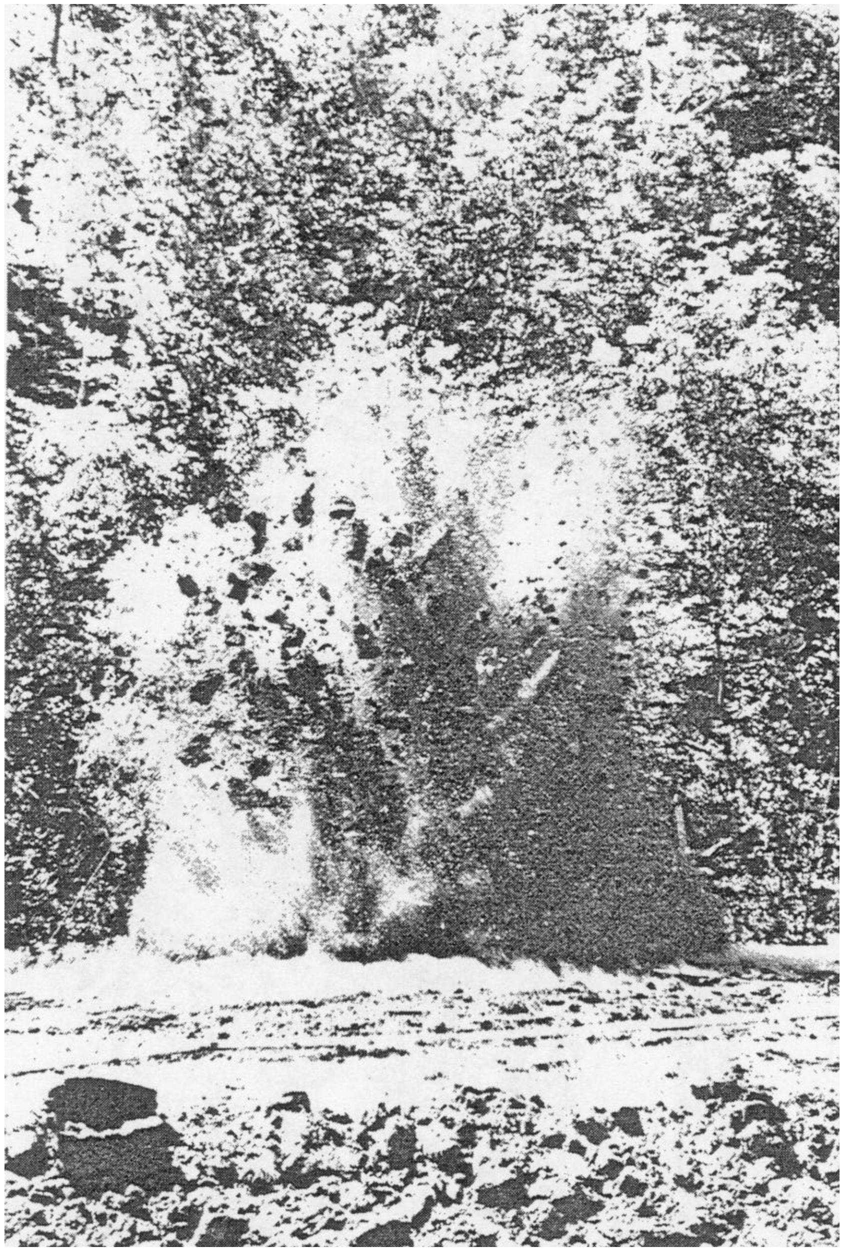

Figure 20. Detonation of Buried 15-lb Explosive Charge

(a) 15-lb Charge

(b) 5-lb Charge

Figure 21. Craters Made by Buried Detonations

gages is the common technique used, particularly if the size of the structure or component is such that it can be indoors during the installation. On the three pipes used in the model scale experiments, Micro-Measurements Type CEA-06-125UT-350, two element, 90° strain gage rosettes were bonded with M-BOND AE-10 epoxy adhesive after proper surface preparation. Because all the strain measurements required were in the longitudinal or circumferential direction, an orthogonal rosette was chosen instead of two single gages to decrease installation time. The rosettes consisted of two self-temperature-compensated strain elements with a resistance of 350 ohms. These types of rosettes are polyimide encapsulated with constantan alloy gage elements featuring large integral copper-coated terminals for ease in soldering leadwires directly to the strain elements. Each strain element was connected to a shielded cable using a three-wire lead system. Figure 22 shows a set of rosettes installed and wired on the 6-inch model pipe. After the rosette installation was completed, it was electronically tested for proper operation by measuring insulation resistance and shift in gage resistance due to installation procedures. Insulation resistances measured on all strain elements exceeded 5,000 megohms and shifts in gage resistance after installation were less than 0.5 percent.

For the two full-scale pipes tested in Kansas and Kentucky, weldable strain gages were chosen because conditions in the field would have made adhesive bonding of gages a very difficult and time consuming operation. The weldable gages selected are also made by Micro-Measurements. They are precision foil strain gages carefully bonded by the manufacturer to a metal carrier, Series 17 stainless steel, for spot welding to structures by the user. Spot welding in the field is easily accomplished with a portable, hand-probe spot welder which is equipped to operate from either AC of internal DC power. Surface preparation is not as critical for the weldable gage, further simplifying their installation. The 24-inch pipe tested in Kansas City used Type CEA-06-W250C-120 weldable strain gage rosettes. These two-elqment, 90° rosettes simplified installation of orthogonal gages at each location. For the 30-inch pipe tested in Kentucky, however, weldable rosettes were not available from the manufacturer for delivery within the time required. Therefore, TYPE CEA-06-W25OA-120 single gages were purchased and installed in orthogonal pairs at each sensing location to measure the longitudinal and circumferential strains. These two types of strain gages have a resistance of 120 ohms (350 ohm gages were not yet available at the time).

Installation of the weldable strain gages used on the two full-scale pipes was begun by removing the coating on the pipe and grinding the metal to remove any rust, scale and surface irregularities. This procedure was completed by handgrinding with silicon-carbide paper until the surface was smooth. The smooth surface area was then thoroughly degreased and washed with solvent to remove all residue. After the surface was properly prepared, a sample metal carrier supplied with each package of gages was used to determine the proper weld-energy setting for the welding unit and electrode force required to obtain a good Spot weld. A setting of approximately 10 watt-seconds with an electrode force of 4 lb will usually produce satisfactory welds. Once these settings were determined, the single gage or rosette was aligned on the pipe and held in place with a piece of drafting tape. The metal

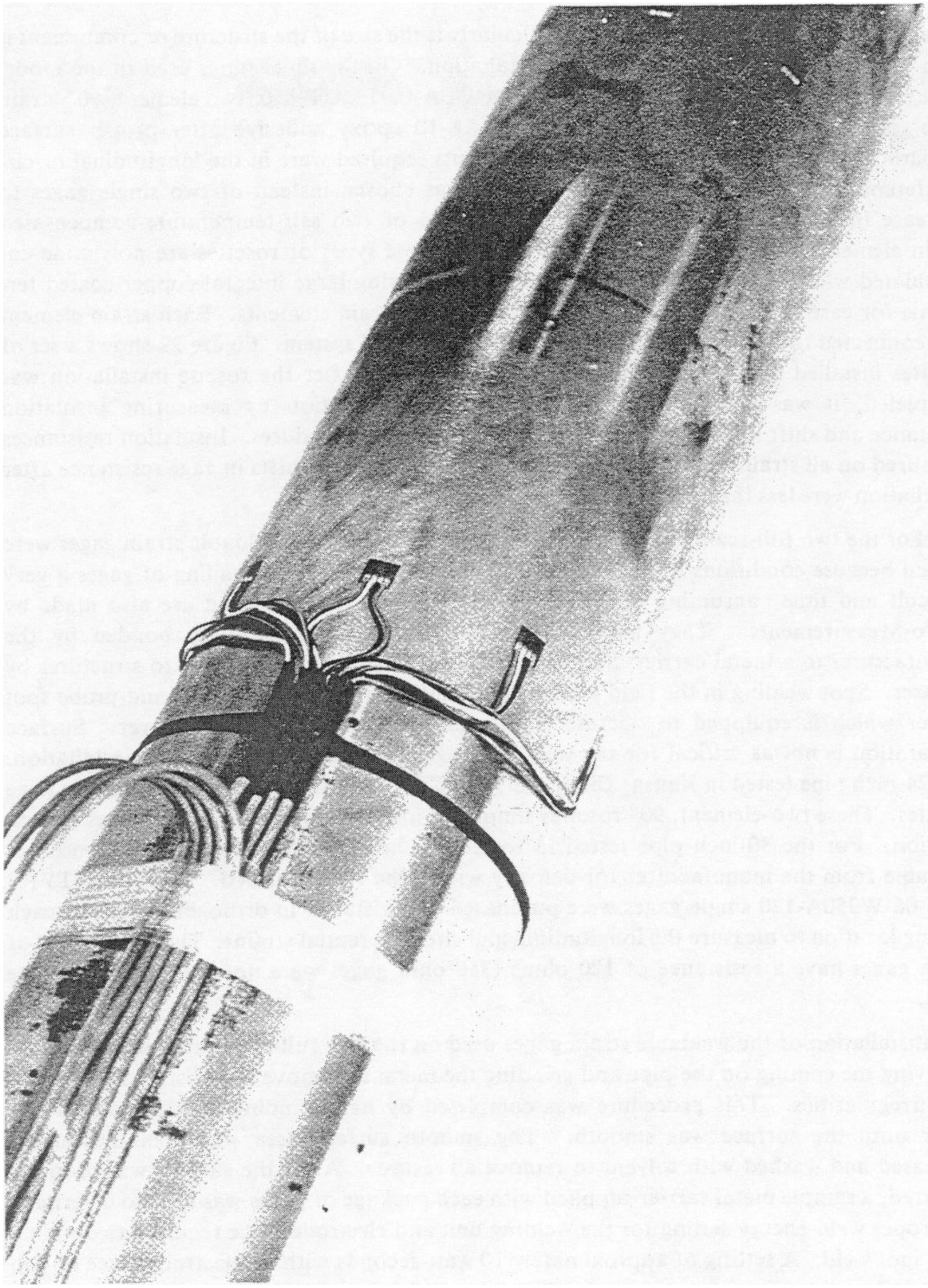

Figure 22. Strain Gaging of 6-inch Model Pipe

carrier was then tacked in place by single spot welds on each side and the tape removed. The gage was then spot welded all around by two rows of alternating spot welds. Figure 23 shows a rosette being spot welded in place on the 24-inch pipe. After each rosette was installed, cable leads were soldered to the strain gage elements and each element was electrically checked before the complete installation was covered with protective coating..

Both the bondable and weldable strain gage installations were protected against the environment using the same protective coatings. In addition to protecting the rosettes and lead wires from moisture, which causes most of the field installation failures in strain gages, mechanical protection was required to ensure the integrity of the installation during the backfilling operations. All leads were first primed with a solvent-thinned, nitrile rubber compound (Micro-Measurements M-COAT BT) for good adhesion between the vinyl insulation and subsequent coatings. After the required curing time, each rosette installation was degreased and warmed with a heat gun to remove any moisture present and immediately coated with a solvent-thinned RTV silicone rubber (M-COAT C). This noncorrosive coating provided a cover to the exposed solder connections as well as a good moisture and chemical barrier to the entire installation. After this thin coating layer was cured, each installation was further protected with M-COAT F, a protective coating well-suited for field applications. Application of this “coating” started with a layer of butyl-rubber to seal further against moisture. This operation is shown in Figure 24. For mechanical protection, a patch of neoprene rubber was placed over the butyl-rubber as shown in Figure 25. Next, aluminum tape was installed, as shown in Figure 26, over the entire installation and M-COAT BT was used around all the edges of the aluminum tape. Figure 27 shows the spot welding and installation of protection of the 30-inch pipe gages. Near the gage installation the outer jackets of all cables were completely sealed with butyl-rubber and eventually placed in a rubber hose for additional protection. This hose routed- the cables up to the ground and to a nearby junction box.

The strain gage elements-were again checked for pro& operation. In the case of the model pipes, each instrumented section was placed in the ground as shown in Figure 28 for the 3- and 6-inch pipes. Similarly, Figure 29 shows the strain gage installation completed on the 16-inch pipe section and the pipe being carefully buried so as not to damage the strain gages and their cables.

Regardless of whether bondable or weldable gages were being used, each strain element was connected as a single active arm three-wire hookup and remote electrical calibration connections as shown in Figure 30. B&F Model I-700 SG signal conditioner units provided bridge completion and balance, excitation voltage to the bridge, and a two-point electrical calibration. For each bridge, 14-15 VDC was’ used as the excitation voltage, making the bridge sensitivity about 7.5-8.0 microvolts/microinch/inch $(\mu V/\mu\epsilon)$ peak strains as low as 6 pinch/inch $(\mu\epsilon)$ were recorded for which the peak voltage prior to amplification was 0.045 millivolts.

The output of each bridge circuit was amplified with a B&F Model 702A-10D differential amplifier. This unit has a full power bandwidth of DC to 100 Hz (± 3 db) and in the dif-

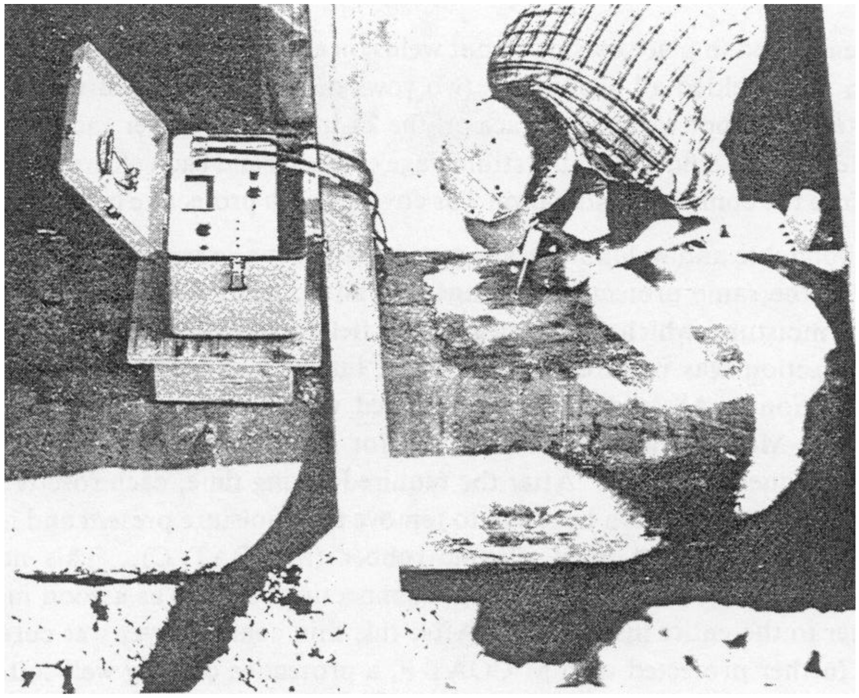

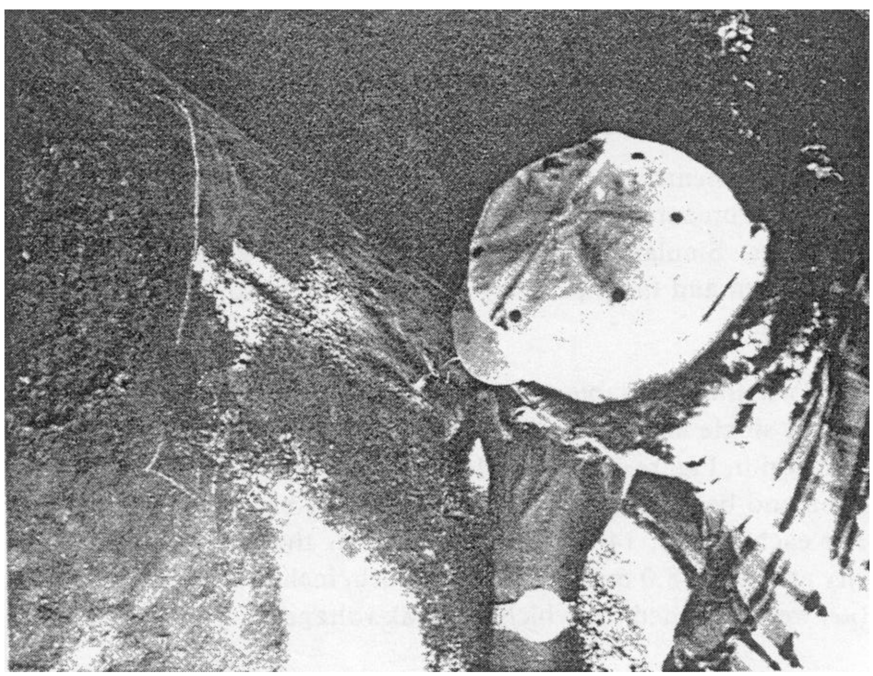

Figure 23. Spot Welding of Strain Gage Rosette on 24-inch Pipe

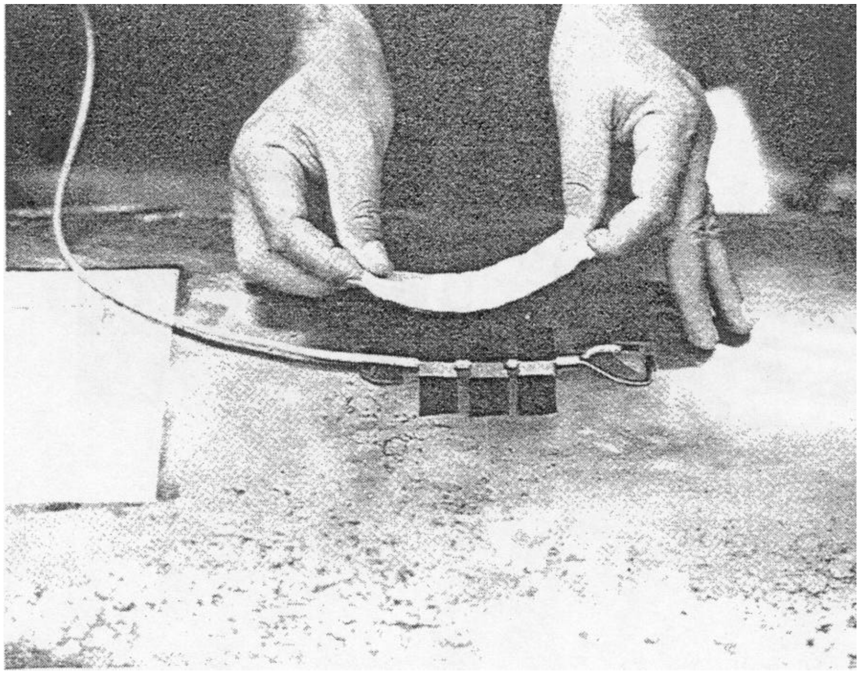

Figure 24. Application of Butyl-Rubber Coat Over Strain Gage Rosette and Lead Wires

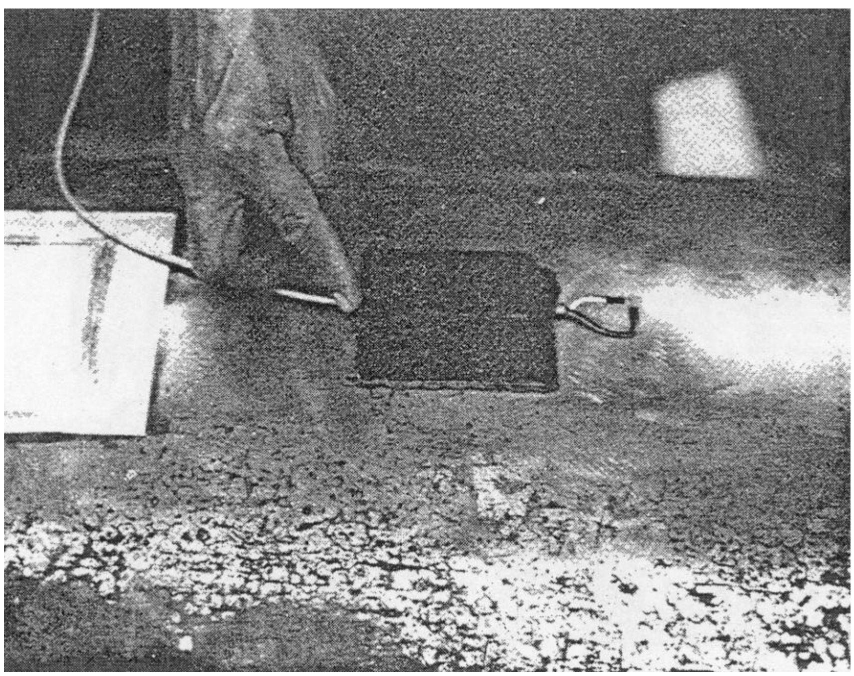

Figure 25. Neoprene in Place for Mechanical Protection of Rosette Installation

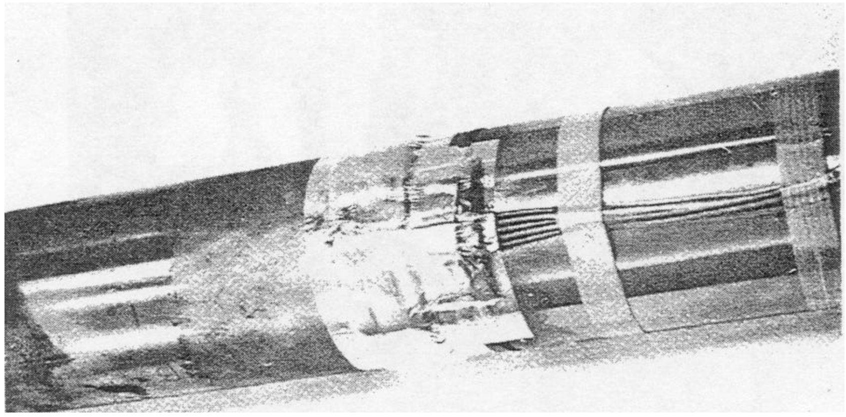

(a) 6-inch Diameter Pipe

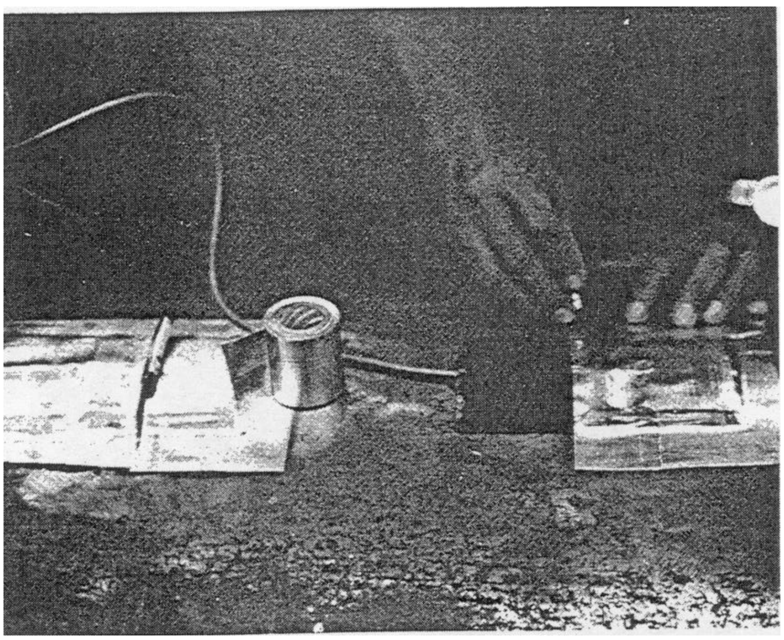

(b) 24-inch Diameter Pipe

Figure 26. Strain Gage Coatings Completed on Model and Full-Scale Pipes

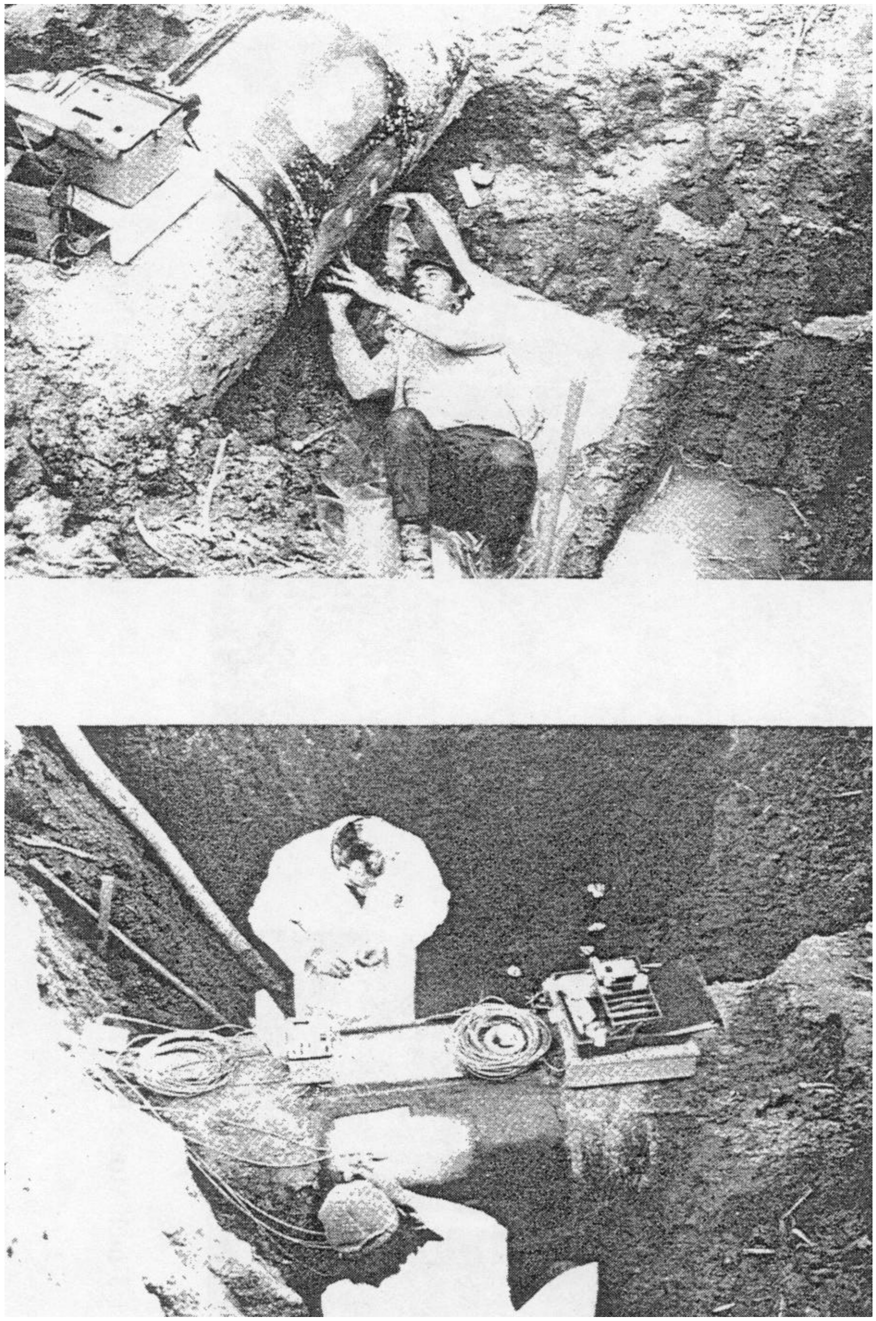

Figure 27. Installation of Strain Gages on 30-inch Pipe

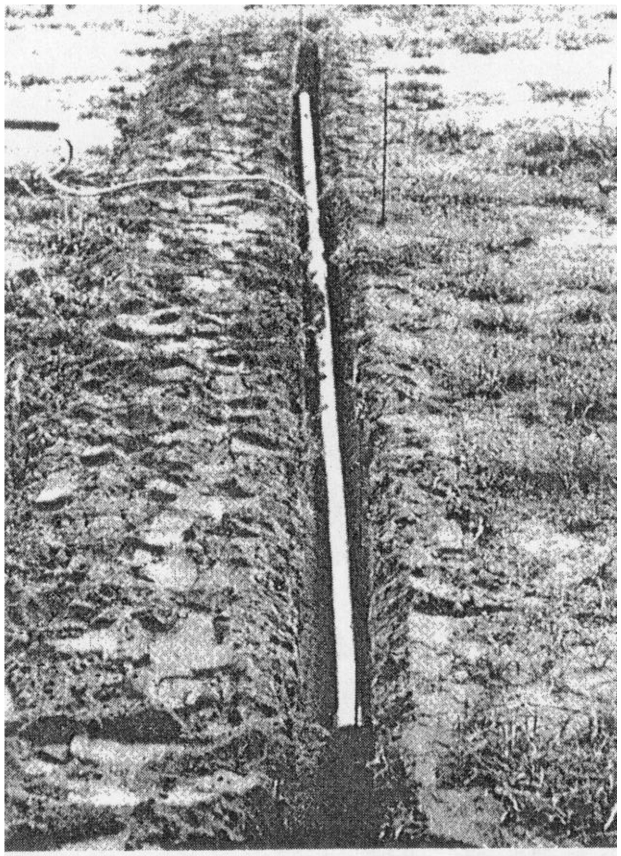

(a) 3-inch Model Pipe

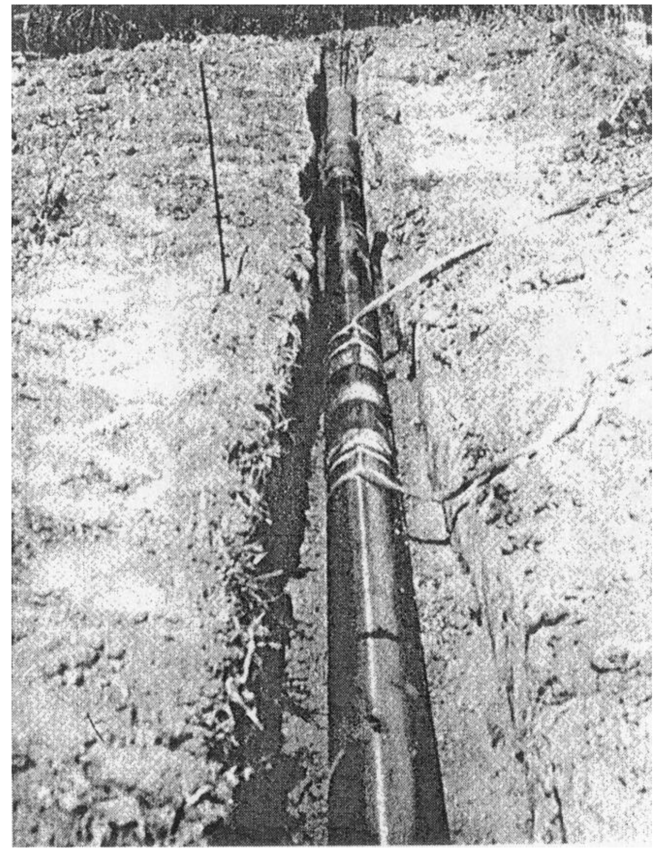

(b) 6-inch Model Pipe

Figure 28. Field Installation of 3- and 6-inch Pipes

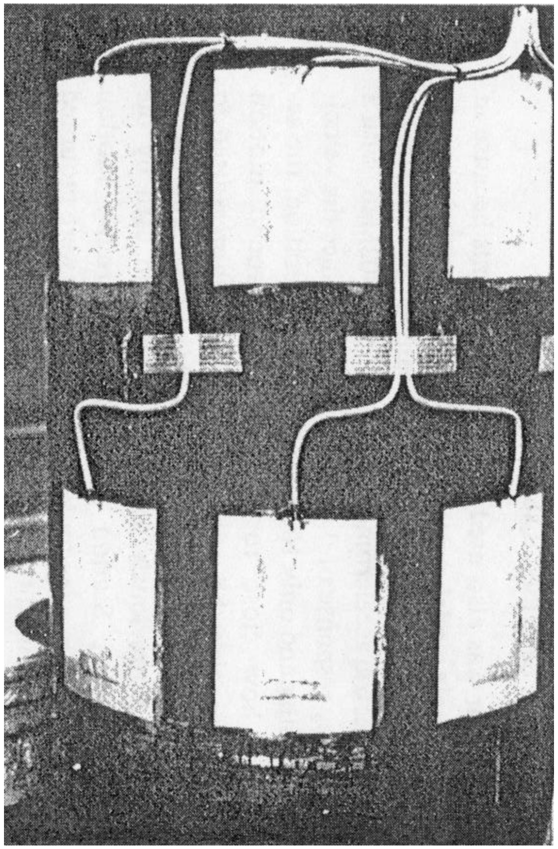

Figure 29. Strain Gage Installation Burial of 16-inch Model Pipe

ferential mode has a high common mode rejection ratio (120 db with a 1 kiloohm unbalance from DC to 60 Hz at a gain of 1000). Because the pipe response was expected to be damped considerably by the surrounding soil, the amplifier output was internally low pass filtered up to a frequency of 10 kHz. At this upper frequency, rise times in the order of 40 microseconds can be faithfully reproduced. Even for the model pipes, the data r&corded showed no rise times shorter than about 2 milliseconds; almost two orders of magnitude slower than the filter setting of the amplifier. Thus, the amplifier as used was not limiting the fidelity of the voltage signals being recorded. The accuracy of the strain data was estimated to be ± 3 percent of the full scale value or $\pm\mu\epsilon$, whichever was larger.

Bell & Howell Type 4-155 piezoelectric velocity transducers were used for the measurement of radial ground motions. Most commercially available transducers, including the one chosen, are not designed for the high external stress which is present in the vicinity of high-explosive underground detonations. Therefore, transducers were installed in protective canisters which simplified placement procedures, provided weatherproofing, and matched the assembly impedance to the soil. The Type 4-155 transducer is a small, rugged vibration transducer with a high natural frequency which allows a linear response over a wide frequency range. The transducer can withstand shock accelerations up to 100 g's peak without damage and is sealed 'water tight. The "high sensitivity makes it desirable for low-level velocity measurements which can be externally integrated to provide displacement signals. Each unit combines within its housing a piezoelectric accelerometer, an impedance matching source follower, and an integrating amplifier. The low electrical output impedance of the amplifier allows the use of long interconnecting cables between the sensor and the recording instrumentation. The usable velocity range of this type of sensor is 0.2 to 100 in./sec, with a dynamic frequency response of 1 to 2000 Hz. The transient velocity data were of short enough duration that the low frequency response of the transducer and its recording system would produce negligible undershoot in the recorded data. The upper frequency response of the velocity transducer was high enough to record rise times at least one order of magnitude shorter than that observed in the velocity data recorded. The circuit diagram of the velocity measurement system described is shown in Figure 31.

A second type of ground motion sensor was also used in these experiments because in. the early part of the program some of the scale model experiments required detonations very close to the pipes and measurement of ground motions were wanted at comparable distances. These transducers were piezoelectric accelerometers, PCB Model 302M46, with a full-scale range of 2500 g's and a frequency response of 0.05 to 10,000 Hz. Since the velocity transducers previously described can withstand only 100 g's of shock acceleration, the accelerometers were used to determine how close to the explosives ground motion measurements could be made without 'damaging the velocity gage. The canisters used to house the velocity gages were designed so that an accelerometer could also be mounted in them. The canisters were similar to some previously designed, tested, and used by the United States Army Waterways Experiment Station to make 'soil ground motion measurements. A sketch showing how a velocity gage and an accelerometer were mounted in a canister is shown in Figure 32. A hose was used to route the interconnecting cable from

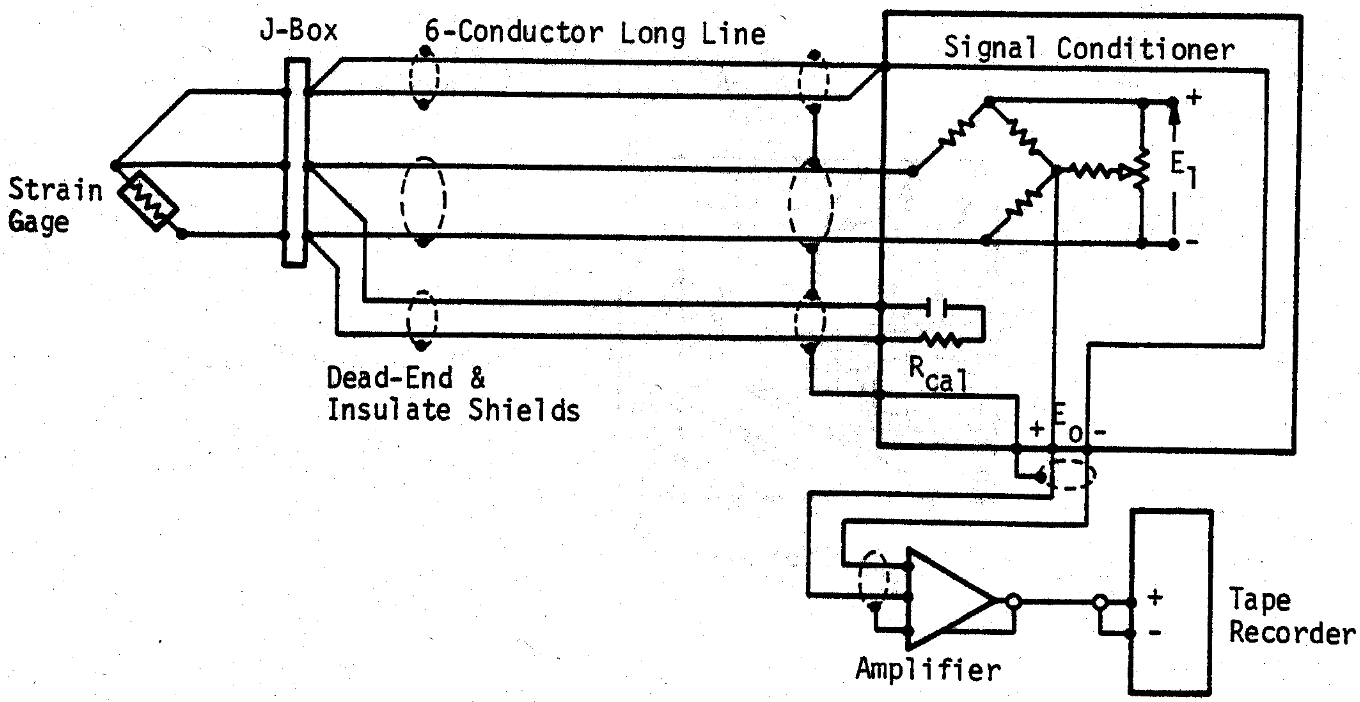

Figure 30. Circuit Diagram for Pipe Strain Gages

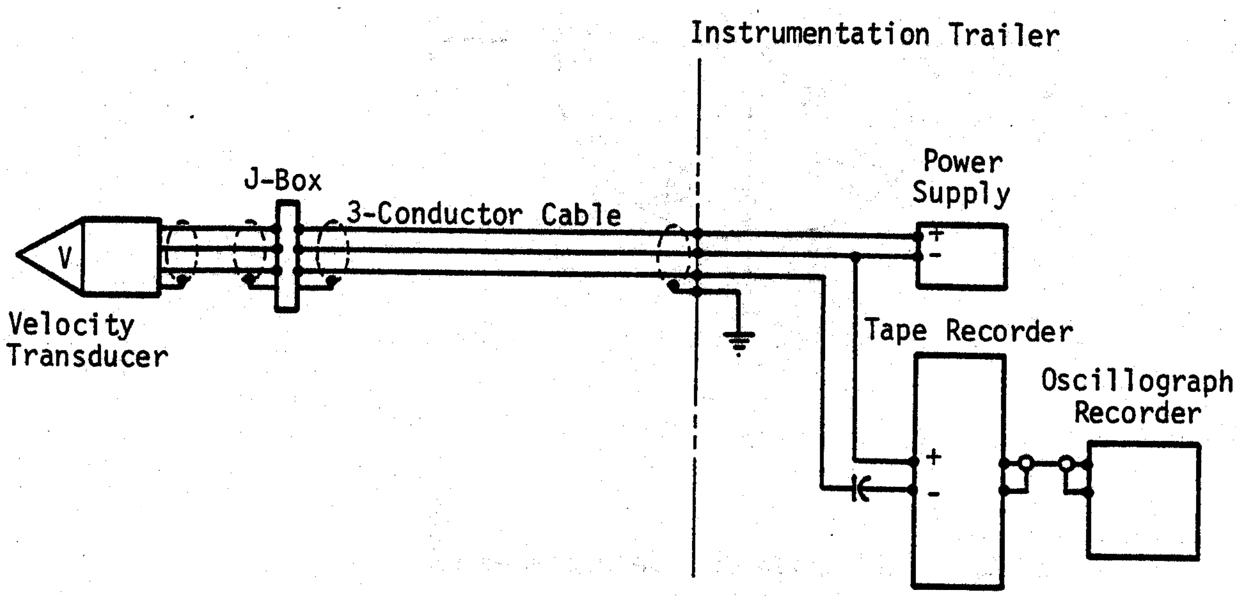

Figure 31. Circuit Diagram for Soil Velocity Transducer

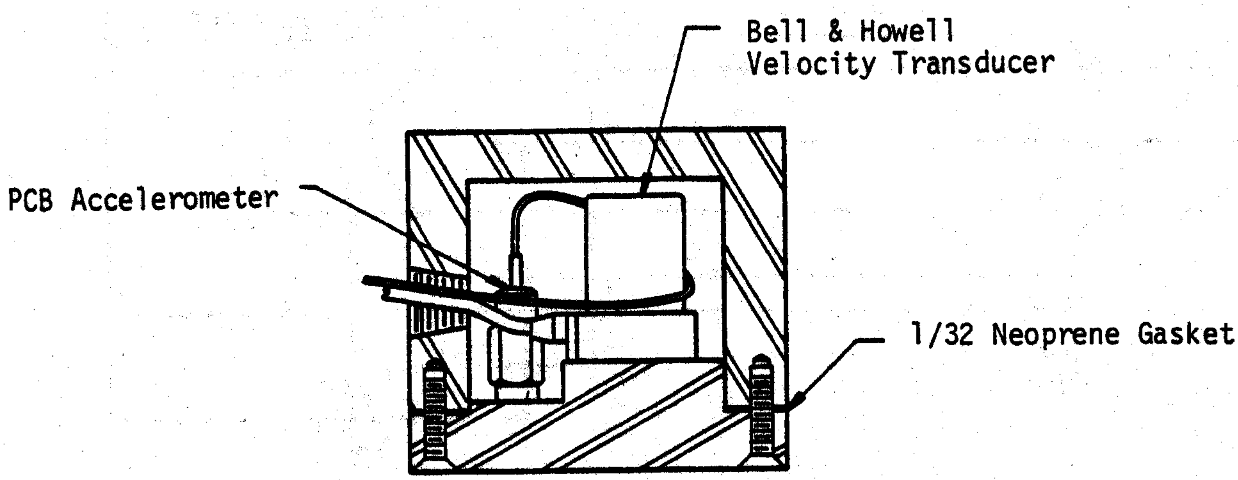

Section A-A

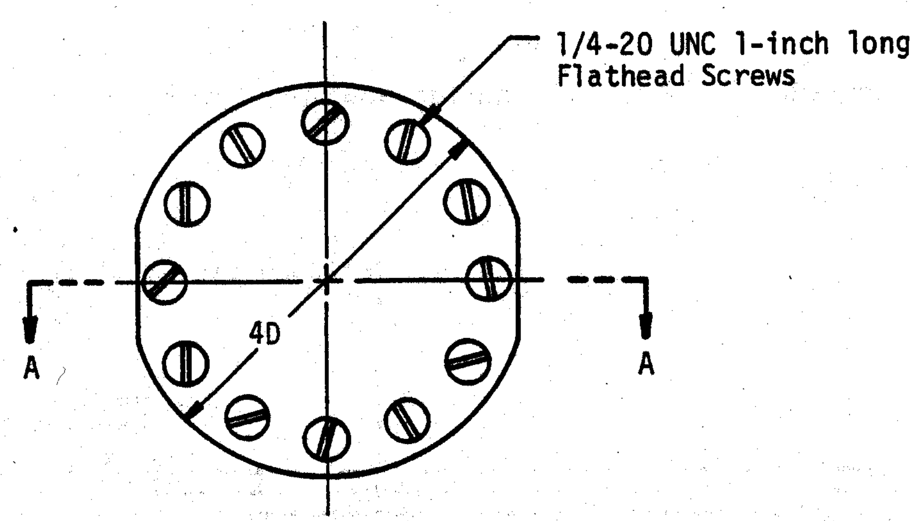

Scale: 1/2" = 1'

Figure 32. Ground Motion Canister Assembly

the canister to a junction-box above ground. The hose provided physical and environmental protection to the cable.

The placement of the motion transducers in the field experiments required the digging of holes of the proper depth and slightly larger than the canister used. Each velocity transducer and accelerometer was first inspected when received from the manufacturer by checking the factory calibration over a frequency range of 20 to 400 Hz using a shake table at SwRI. Then it was placed in a canister and the whole assembly mounted on the shake table again to insure that. the sensitivity remained constant. Then it was taken to the field for use in the experiments. On the full-scale experiments, the holes made were up to 6 ft in depth.

All of the data signals were recorded on magnetic tape along with fiducial and time-base reference signals. The data for the. scale-model experiments were recorded on an Ampex FR-1900 tape recorder. The field data taken in the Kansas City and Kentucky tests were recorded on a Honeywell Model 5600C system. All data were recorded using FM electronics at a recording speed to obtain a minimum bandwidth of 10 kHz. The recorded data were played back into a Bell & Howell Model 5-164 oscillograph system for quick-look data analysis and subsequent data reduction. The data signals were time extended on playback by a factor of 16 and inputted into galvonometers having a 1 kHz upper frequency response, Thus, the data were pot attenuated below an effective frequency of 16 kHz on playback.

The oscillograph records were subsequently digitized at SwRI, manipulated, scaled and plotted using a Hewlett-Packard Model 9830 microcomputer system, From the digitized data, the Peak soil particle velocity, the computer soil displacement, and the pipe strains were obtained for use in the analyses. The accelerometer data were also played back onto oscillograph paper, then digitized and integrated to obtain velocity data to compare to that of the velocity transducer housed in the same canister., In some tests, an accelerometer was used by itself close-in to the explosive charge. In these cases, a similar, though smaller, canister was used since no velocity transducer was included. Because most of the acceleration measurements and their integrated velocities were made to determine whether the velocity gage could be used at a given close-in standoff distance, the data were not used in the analysis. Instead, the direct velocity measurements, which are more accurate, and their integrated displacements were used. In the case of the displacements, which turned out to be the controlling parameter in the analysis for most detonations near gas pipelines, a double integration would have been required on the acceleration data, thus increasing errors and inaccuracies. Consequently, no double integrations were attempted.

In the next section, all of the pipe strain and ground motion data are presented.

IV. EXPERIMENTAL RESULTS

General

The experimental data obtained by Southwest Research Institute (SwRI) for the American Gas Association (A.G.A.) from the 109 pipe and explosive in soil tests will be presented in this section. The. data were obtained from point, line, and grid explosive sources and will be grouped together by these explosive geometries. In the analyses that follow this section, the ground motion data are first used to determine the nature of the forcing function which causes the buried pipelines to be stressed. Subsequently, the pipe strain and stress data are used to complete the derivation of the prediction equations and methods. Therefore, for each charge geometry, the ground motion data will be presented separately from the pipe response data to parallel this order of solution development.

Radial soil motion measurements were made throughout the blasting research program. The recorded peak soil particle velocities and the corresponding computed peak soil displacements from each velocity-time trace are presented in this section of the report. a Examples of time histories are also included.* From the soil particle velocity traces recorded on each test, the time-of-arrival of the stress wave at each transducer location was determined and used to compute an average seismic velocity for each test. These data are also included in the ground motion data tables in this section.

Typically two to four velocity transducers were used in all the tests,. The transducers were usually located opposite the test pipe at different standoff distances from the charge. The first ground motion canister was in most cases buried at the same distance from the charge (or charge line) as the pipe being tested. If not, the first two canisters would be located such that the distance of the pipe was between them. (See Figures 5 through 10.)

A number of strain measurements were made to determine the pipe response far each test. As many as ten strain-time histories were recorded with the mininnun number usually being six. Measurements were made at various points around the pipe at a location along the pipe opposite the explosive source. The principal measurements were usually on the front, top, and back of the pipe as shown in Figure 5. However, in same tests other measurements were made at points rotated 45° from the principal locations (set Figure 6). Also, on some of the later test series, additional strain measurements were made at other sensing locations along the length of the pipe to insure the maximum strains were recorded and to obtain a better feel of how the pipe responds to the different blast loads.

*A separate data report consisting of all the data traces recorded in this program has been compiled by SwRI. For those interested in purchasing a copy of this data report, contact the A.G.A.

In the early part of the blasting research program, the pipe response was characterized by the maximum strains measured in the circumferential and longitudinal direction. Because it was desired that the prediction equations be as easy as possible to understand and apply, the strain prediction equations were approximately converted to stress equations. The uniaxial strain to stress relation was used because of its simplicity in combining time-varying strain data. For orthogonal gage pairs in which the strain magnitude from one gage was low while the other was peaking and vice-versa, and considering the scatter of the data, the uniaxial stress conversion provided. a reasonable approximation. However, for those instances in which the peak values for an orthogonal pair of gages occurred at about the same time and, in addition, the strains were of the same polarity (both tensile or compressive), the uniaxial stress approximation would significantly underpredict the biaxial stress. For this reason, towards the end of the program SwRI and the supervisory committee decided that the steel pipe strains be converted to stresses using the plane stress (biaxial) formulae which are as follows:

$$\sigma_{cir} = \frac{E}{1-\nu^2}(\epsilon_{cir} + \nu\epsilon_{long}) \tag{30}$$

$$\sigma_{long} = \frac{E}{1-\nu^2}(\epsilon_{long} + \nu\epsilon_{cir}) \tag{31}$$

where E = **modulus of elasticity (29.5 × 10^6 lb/in.^{2})**
ν = **Poisson's ratio (0.3)**
ϵ_{cir} = **measured circumferential strain (in./in.)**
ϵ_{long} = **measured longitudinal strain (in./in.)**

Strictly speaking, the stresses computed with these equations are the surface biaxial stresses at the location on which the strain gages are mounted. The algebraic signs of the strains are taken into account, as is the time phase for dynamic or transient strains.

To convert over 900 strain-time records into stress-time records, with corresponding strain records (hoop and axial) correctly phased in time would have been a monumental and expensive task. Because it is not possible to measure strain at every point on a pipe being tested, one would not be absolutely sure that the maximum biaxial stresses were, in fact, obtamed in each test. For this reason, this alternative for biaxial conversion was not pursued.

Instead, if one assumes that (regardless of gage location) the peak hoop and axial strains measured can occur at the same point on the pipe, in addition to being of the same polarity and peaking at the same time, then Equations (30) and (31) can be used to compute the biaxial stresses. This was the approach followed to obtain the stresses which are presented in this section. Because of the conservative assumptionsmade to determine these biaxial stresses, they will always be larger than the approximate uniaxial stresses. Consequently, more conservative prediction equations and methods should result using these biaxial stresses. Furthermore, since the total state of stress on an operational pipeline is what is of interest, after obtaining direct estimates of the blast-induced biaxial stresses, the total state of stress can be determined by superimposing the other stresses loading the pipe.

Since only the maximum, absolute values of circumferential and longitudinal strain from each test are required to compute the corresponding maximum stresses, only these maximum strains and stresses are tabulated in this section of the report. However; examples of strain-time histories at the various sensing locations are included for representative tests. *

Point Source Test Data

The majority of the tests performed in the blasting research program used point explosive sources. In most of the model tests of the first test series, four velocity transducers were used to obtain the ground motion data. In some tests, accelerometers were used with the velocity transducers to insure that the shock at the close-in ground motion sensing locations would not damage the velocity transducers. As mentioned before, the location of the ‘velocity transducers varied for different test conditions. However, the first canister was usually buried at the same standoff distance from the charge as the pipe being tested. A typical set of data traces from the first point source test series is shown in Figure 33. The horizontal radial velocity and displacement records shown in this figure are for a 0.4-lb charge located a distance of 4 ft from the transducer. In this figure, as well as in all other ground motion figures, positive values denote motion away from the charge. The velocity-time plot was obtained by digitizing the oscillograph record, scaling the graph with the microcomputer, and drawing the results with its plotter.

In the eight full-scale tests conducted at the Kansas test site, three velocity transducers were placed in the ground at the same depth as the charge and the center of the pipe. An ex--ample of ground motion data from this test series, in which a 15-lb charge was used, is shown in Figure 34. Note that as expected,’ the time durations in these traces are longer than for the model test because of the larger scale of these experiments. The soil particle velocity and displacement data recorded in the four full-scale tests performed at the Kentucky site were of similar nature as those obtained in Kansas. In this case, at least two measurements were attempted on each test.

*A separate data report consisting of all the data traces recorded in this program has been. compiled by SwRI. For those interested in purchasing a copy of this data report, contact the A.G.A.

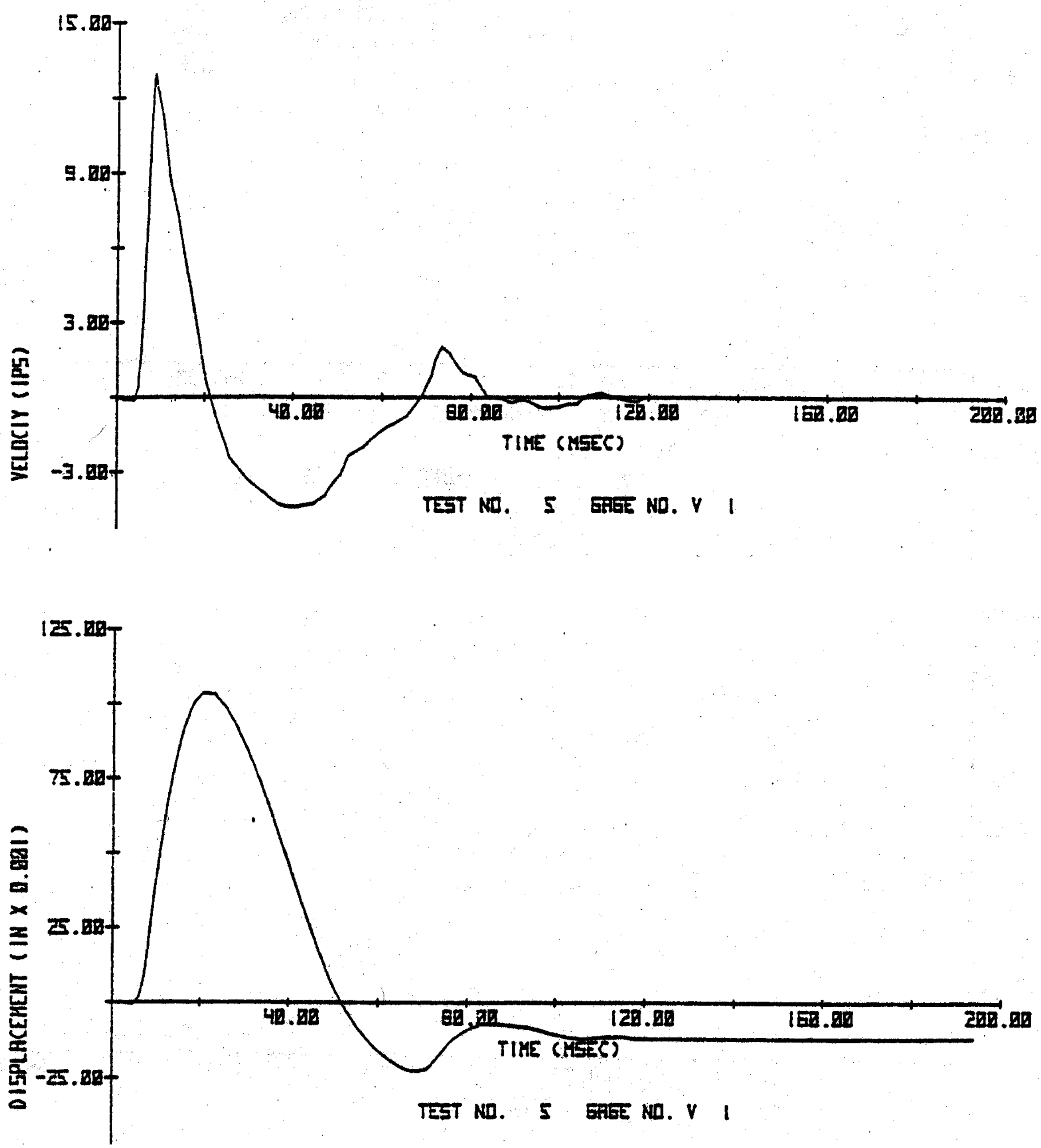

Figure 33. Ground Motions from 0.4-lb Charge at a Radial Distance of 4 ft

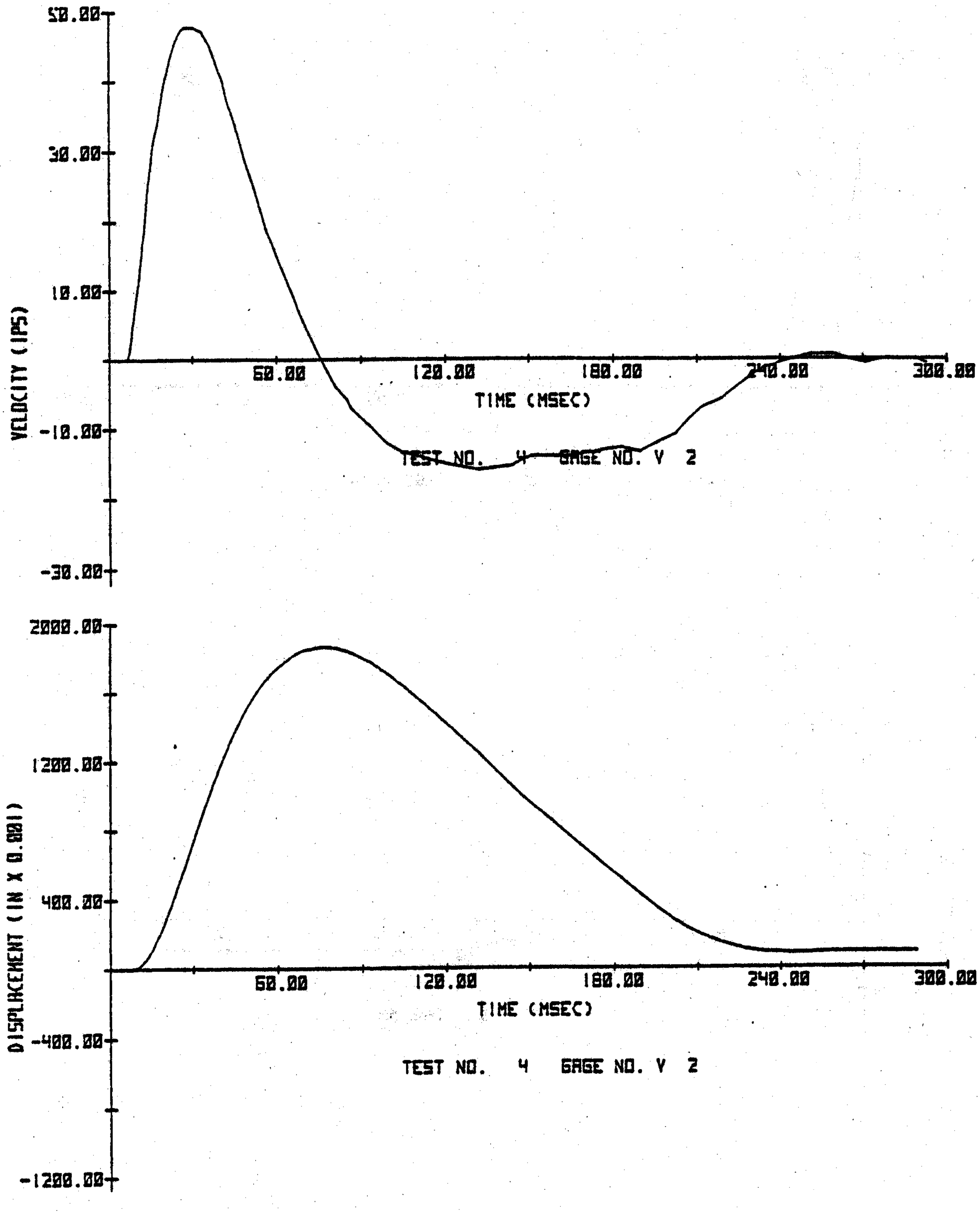

Figure 34. Radial Ground Motions at 12ft from 15-lb Charge

Two particle velocity transducers were used in the deeper point source tests that followed the full-scale tests. The ground motion data from these model experiments repeated well and appeared similar to that of the earlier model tests. Figure 35 shows an example from a velocity transducer located at a slant distance of 4.2 ft from a 0.2-lb charge. In the final series of point source experiments, three velocity transducers were normally used to obtain ground motion data. These ground motion records were also similar to those from the earlier model tests.

All of the velocity transducer data from point sources are listed in Table 6. This table identifies each experiment by test series and number. Also listed in the table for each test is the average seismic velocity c obtained from the arrival time recorded for each transducer and its distance from the charge. In addition; the equivalent energy release n, the charge weight W, and the standoff distance R for each transducer is provided. The last. two columns list the peak radial velocity and displacement from each of the buried velocity transducers. These ground motion data are used in the next section of the report to develop the point source ground motion prediction equations.

Strain measurements were made on both the model and full scale experiments to determine quantitatively the response of pipelines to nearby underground detonations. As previously mentioned, two-element strain gage rosettes were used to obtain circumferential and longitudinal pipe strain measurements. Because the pipe response was not known, the first series of model tests used the five gage locations shown in Figure 5. The testing program was begun by recording the five circumferential strains since it was felt that these would be the larger strains. Also, the mode of the pipe response in this direction needed to be determined so that those gages recording significantly lower peak strains could be dropped and longitudinal gages substituted.

From the first fivemodel tests, it was determined that the pipe was ovalling and that the significant circumferential strains were at the front, top, and back locations on the pipe. Figure 36 shows the five circumferential strains measured in Test Series No. 1, Test No. 2 using the 3-inch pipe. Therefore, after these early tests, longitudinal strain gages were recorded instead of the two circumferential gages located at 45° between the top and side locations. The first few longitudinal strain measurements indicated that the pipe was also bending significantly away and upward from the charge. Therefore, for the majority of the remaining model experiments, as well as all of the full-scale tests, longitudinal strains were measured and recorded at the same locations as the circumferential ones: on the front, top and back side of each pipe. Figures 37 and 38 are examples of the strains measured in the hoop and axial directions, respectively, on the 6-inch pipe used in the early test series. For comparison, a similar set of strain data from one of the full-scale tests is shown in Figures 39 and 40. For all the strain traces presented in this report, positive values of strain denote compression.

For the test series in which the point source was buried deeper than the pipe, the primary strain measurements were made at three locations rotated 45º from the front, top, and back of the pipe (see Figure 6). Although it was believed that, the maximum strains

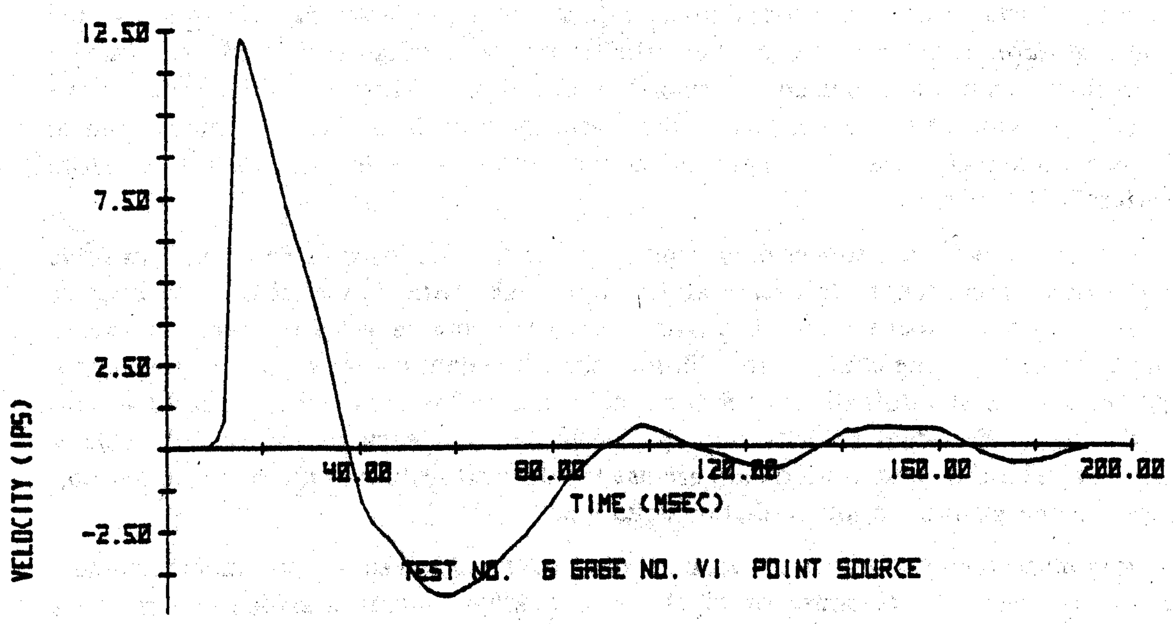

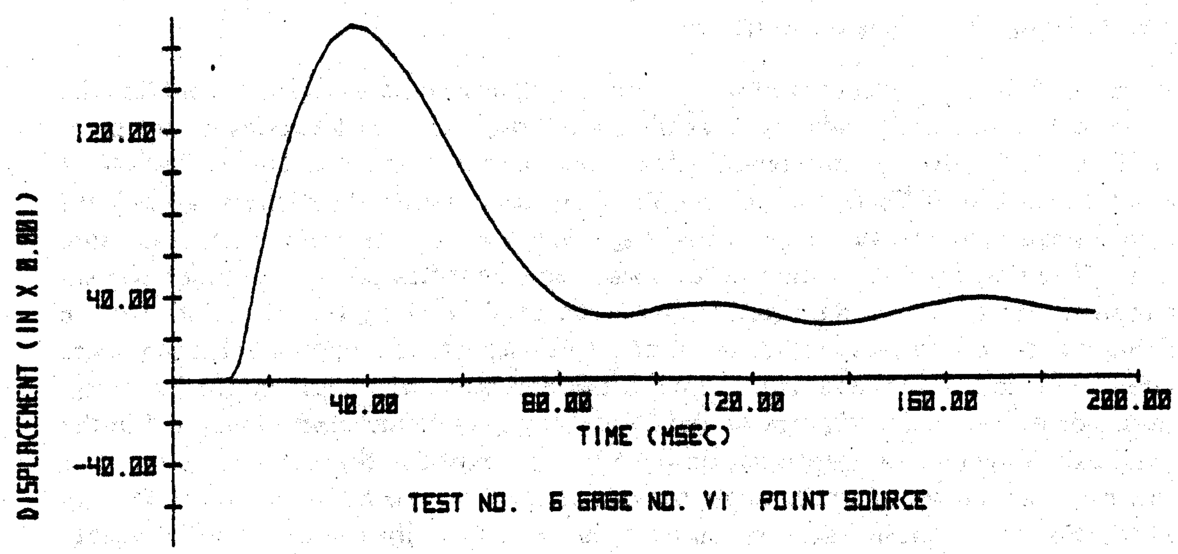

Figure 35. Ground Motions from Deeper 0.2-lb Charge at a Slant Distance of 4.2 ft

Table 6. Ground Motion Data From Point Source Tests

Test Series	Test No.	c (fps)	n	W (lb)	R (ft)	U (ips)	X (in.)
1	2	958	1.12	0.05	3.00	12.4	0.042
1	2	958	1.12	0.05	4.50	3.0	0.012
1	2	958	1.12	0.05	6.00	2.3	0.013
1	4	922	1.12	1.00	7.00	23.0	0.234
1	4	922	1.12	1.00	11.00	5.8	0.056
1	4	922	1.12	1.00	15.00	2.5	0.030
1	5	929	1.12	0.40	4.00	13.0	0.105
1	5	929	1.12	0.40	8.00	5.8	0.050
1	5	929	1.12	0.40	12.00	2.1	0.016
1	6	895	1.12	0.40	4.00	24.2	0.150
1	6	895	1.12	0.40	8.00	8.9	0.066
1	6	895	1.12	0.40	12.00	3.0	0.022
1	7	1038	1.12	1.00	7.00	15.4	0.160
1	7	1038	1.12	1.00	11.00	10.3	0.118
1	7	1038	1.12	1.00	15.00	2.7	0.038
1	8	958	1.12	0.03	2.00	10.9	0.053
1	8	958	1.12	0.03	4.00	2.3	0.018
1	8	958	1.12	0.03	6.00	0.8	0.005
1	9	751	1.12	0.03	2.00	7.4	0.031
1	9	751	1.12	0.03	4.00	1.7	0.011
1	9	751	1.12	0.03	6.00	0.9	0.006
1	10	1014	1.12	0.03	1.00	33.4	0.050
1	10	1014	1.12	0.03	3.00	4.3	0.019
1	10	1014	1.12	0.03	5.00	1.6	0.007
1	20	1138	1.12	0.03	1.50	14.0	0.029
1	20	1138	1.12	0.03	3.00	4.7	0.011
1	20	1138	1.12	0.03	4.00	2.1	0.005
1	20	1138	1.12	0.03	5.00	1.3	0.003
1	21	964	1.12	0.03	1.50	10.4	0.039
1	21	964	1.12	0.03	3.00	3.0	0.011
1	21	964	1.12	0.03	4.50	1.5	0.005
1	21	964	1.12	0.03	6.00	0.8	0.003
1	22	1100	1.12	0.03	1.00	57.4	0.185
1	22	1100	1.12	0.03	2.50	2.2	0.010
1	22	1100	1.12	0.03	4.00	1.5	0.004
1	22	1100	1.12	0.03	5.50	0.6	0.001
1	23	975	1.12	0.03	1.00	44.2	0.113

Table 6. Ground Motion Data From Point Source Tests (Cont'd)

Test Series	Test No.	c (fps)	n	W (lb)	R (ft)	U (ips)	X (in.)
1	23	975	1.12	0.03	2.50	3.3	0.015
1	23	975	1.12	0.03	4.00	1.4	0.006
1	23	975	1.12	0.03	5.50	0.7	0.003
1	24	866	1.12	0.06	1.50	57.7	0.390
1	24	866	1.12	0.06	3.00	5.5	0.030
1	24	866	1.12	0.06	4.50	3.1	0.002
1	24	866	1.12	0.06	6.00	1.3	0.006
1	25	675	1.12	0.06	1.75	40.5	0.187
1	25	675	1.12	0.06	3.20	5.1	0.029
1	25	675	1.12	0.06	4.75	3.0	0.019
1	25	675	1.12	0.06	6.20	1.1	0.007
1	28	568	1.12	0.05	1.50	44.2	0.270
1	28	568	1.12	0.05	3.00	9.0	0.085
1	28	568	1.12	0.05	4.50	3.9	0.040
1	28	568	1.12	0.05	6.00	2.0	0.021
1	29	612	1.12	0.05	1.50	46.0	0.230
1	29	612	1.12	0.05	3.00	12.2	0.110
1	29	612	1.12	0.05	4.50	5.3	0.056
1	29	612	1.12	0.05	6.00	2.9	0.028
1	30	592	1.12	0.40	3.00	60.0	0.670
1	30	592	1.12	0.40	6.00	8.6	0.179
1	30	592	1.12	0.40	12.00	1.0	0.017
1	30	592	1.12	0.40	18.00	0.7	0.009
1	31	447	1.12	0.40	3.00	52.0	0.480
1	31	447	1.12	0.40	6.00	8.2	0.180
2	1	900	1.00	15.00	7.00	55.4	0.920
2	1	900	1.00	15.00	10.00	14.3	0.280
2	1	900	1.00	15.00	15.00	3.6	0.057
2	2	573	1.00	5.00	5.00	159.7	2.620
2	2	573	1.00	5.00	8.00	80.0	2.180
2	3	519	1.00	5.00	6.00	88.0	2.170
2	3	519	1.00	5.00	12.00	8.7	0.330
2	3	519	1.00	5.00	15.00	3.0	0.700
2	4	1232	1.00	15.00	6.00	118.8	1.960
2	4	1232	1.00	15.00	12.00	47.7	1.860
2	4	1232	1.00	15.00	14.00	36.0	1.210
2	5	582	1.00	5.00	6.00	82.4	2.040

Table 6. Ground Motion Rata From Point Source Tests (Cont'd)

Test Series	Test No.	c (fps)	n	W (lb)	R (ft)	U (ips)	X (in.)
2	5	582	1.00	5.00	12.00	10.4	0.350
2	5	582	1.00	5.00	14.00	3.4	0.110
2	6	735	1.00	15.00	10.00	76.3	2.350
2	6	735	1.00	15.00	14.00	13.0	0.510
2	6	735	1.00	15.00	23.50	2.5	0.032
2	7	792	1.00	15.00	8.00	98.6	5.500
2	7	792	1.00	15.00	16.00	8.2	0.250
2	7	792	1.00	15.00	24.00	3.6	0.110
2	8	622	1.00	15.00	8.00	138.0	4.780
2	8	622	1.00	15.00	16.00	6.2	0.340
2	8	622	1.00	15.00	24.00	1.2	0.049
3	1	1230	1.00	5.00	12.00	22.0	0.290
3	3	974	1.00	3.00	6.00	72.5	0.790
3	3	974	1.00	3.00	12.00	14.1	0.330
3	3	974	1.00	3.00	18.00	2.1	0.036
3	4	980	1.00	3.00	6.00	93.0	1.570
3	4	980	1.00	3.00	12.00	18.8	0.250
4	1	650	1.12	0.40	3.00	46.0	0.530
4	1	650	1.12	0.40	9.00	6.1	0.084
4	2	711	1.12	0.10	1.50	88.0	--
4	2	711	1.12	0.10	4.50	8.4	0.094
4	3	556	1.12	0.40	4.20	15.0	0.330
4	3	556	1.12	0.40	9.50	3.2	0.055
4	4	519	1.12	0.40	4.20	17.0	0.300
4	4	519	1.12	0.40	9.50	4.3	0.073
4	5	465	1.12	0.20	4.20	10.0	0.150
4	5	465	1.12	0.20	9.50	2.1	0.031
4	6	513	1.12	0.20	4.20	12.0	0.170
4	6	513	1.12	0.20	9.50	2.0	0.032
4	8	568	1.12	0.10	2.10	38.0	0.520
4	8	568	1.12	0.10	3.40	7.6	0.088
4	9	755	1.12	0.20	2.10	87.0	--
4	10	652	1.12	0.20	2.10	98.0	--
4	10	652	1.12	0.20	3.40	23.0	0.450
4	11	616	1.12	0.40	4.40	12.0	0.340
4	11	616	1.12	0.40	9.90	3.9	0.071
4	38	577	1.12	3.60	12.50	12.2	0.128

Table 6, Ground Motion Data From Point Source Tests (Cont'd)

Test Series	Test No.	c (fps)	n	W (lb)	R (ft)	U (ips)	X (in.)
4	38	577	1.12	3.60	22.50	3.1	0.039
5	1	859	1.12	0.40	4.00	20.2	0.230
5	1	859	1.12	0.40	8.00	5.8	0.068
5	2	642	1.12	0.40	5.00	14.2	0.149
5	2	642	1.12	0.40	8.00	8.0	0.095
5	2	642	1.12	0.40	11.00	3.2	0.040
5	3	716	1.12	0.40	4.00	25.4	0.289
5	3	716	1.12	0.40	7.00	9.1	0.091
5	3	716	1.12	0.40	15.00	2.2	0.024
5	4	715	1.12	0.25	4.00	10.1	0.133
5	4	715	1.12	0.25	4.00	9.9	0.138
5	4	715	1.12	0.25	8.00	5.0	0.050
5	5	676	1.12	0.08	2.00	24.4	0.246
5	5	676	1.12	0.08	4.00	7.4	0.060
5	5	676	1.12	0.08	8.00	2.1	0.019
5	6	729	1.12	0.12	3.00	14.5	0.173
5	6	729	1.12	0.12	7.00	2.8	0.020
5	6	729	1.12	0.12	11.00	1.2	0.012
5	7	718	1.12	0.08	3.00	8.8	0.086
5	7	718	1.12	0.08	7.00	1.9	0.014
5	7	718	1.12	0.08	11.00	0.8	0.005
5	8	668	1.12	0.08	3.00	9.8	0.078
5	8	668	1.12	0.08	7.00	3.0	0.023
5	8	668	1.12	0.08	11.00	1.2	0.011
5	9	684	1.12	0.20	5.00	9.1	0.097
5	9	684	1.12	0.20	9.00	2.7	0.028
5	9	684	1.12	0.20	13.00	1.4	0.016
5	10	672	1.12	0.08	2.50	10.3	0.101
5	10	672	1.12	0.08	3.00	10.0	0.098
5	10	672	1.12	0.08	7.00	1.7	0.017
5	11	804	1.12	0.40	5.00	12.6	0.131
5	11	804	1.12	0.40	8.00	8.3	0.083
5	11	804	1.12	0.40	11.00	3.8	0.043
5	12	713	1.12	0.40	3.00	45.5	0.364
5	12	713	1.12	0.40	7.00	5.4	0.063
5	12	713	1.12	0.40	13.00	1.9	0.022

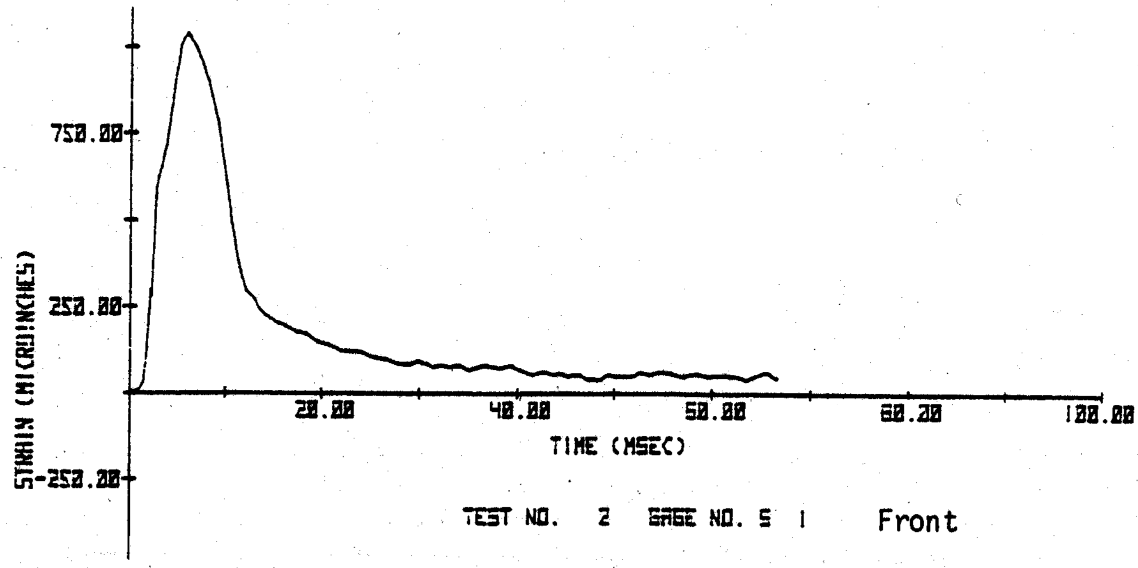

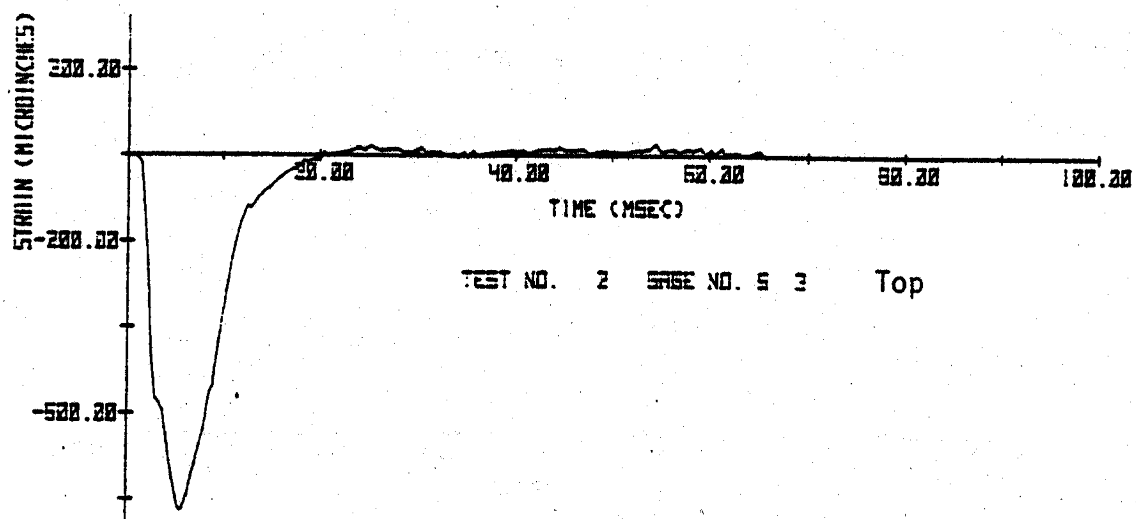

(Positive Strains Denote Compression)

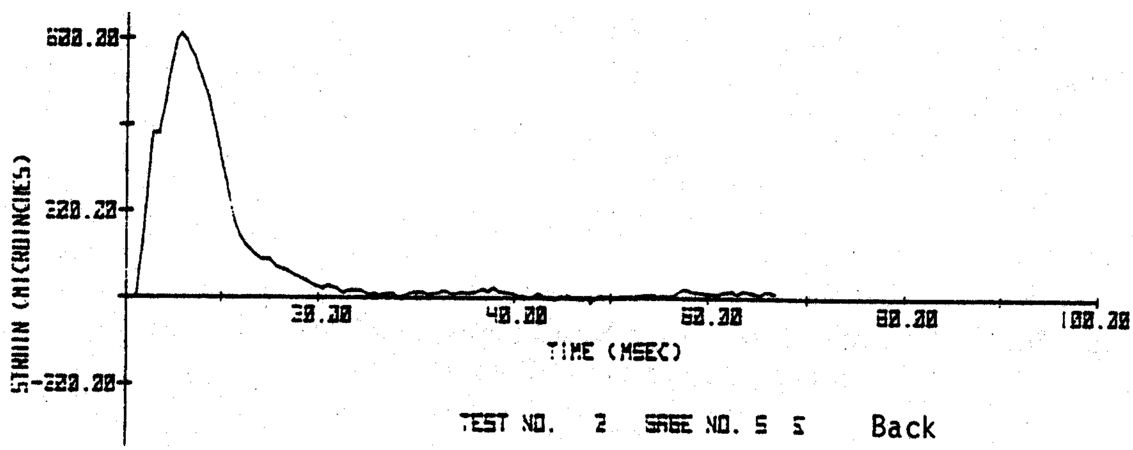

Figure 36. Circumferential Strain Measurements on 3-inch Diameter Pipe From a Point Source

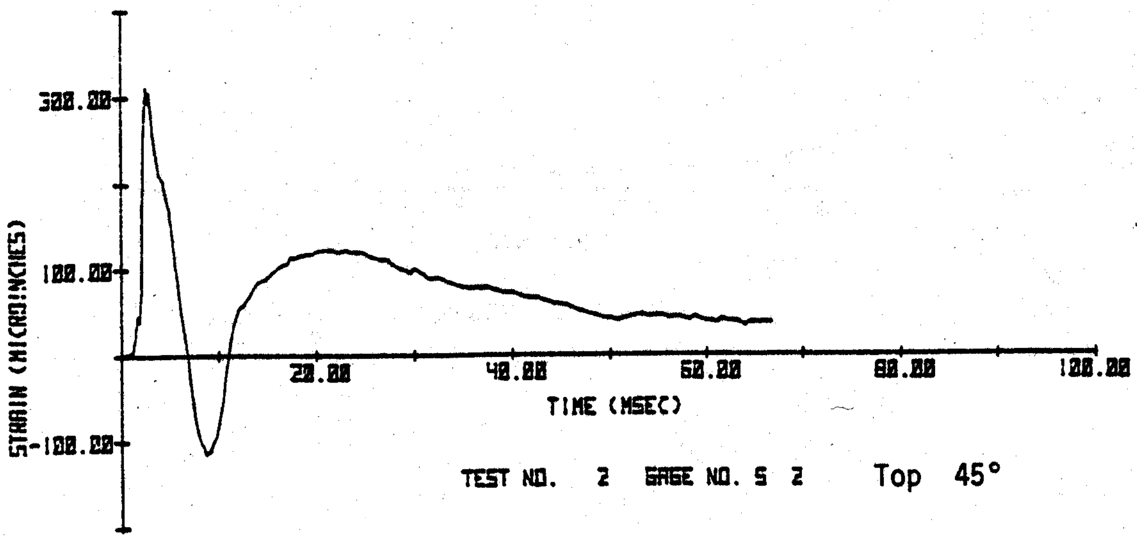

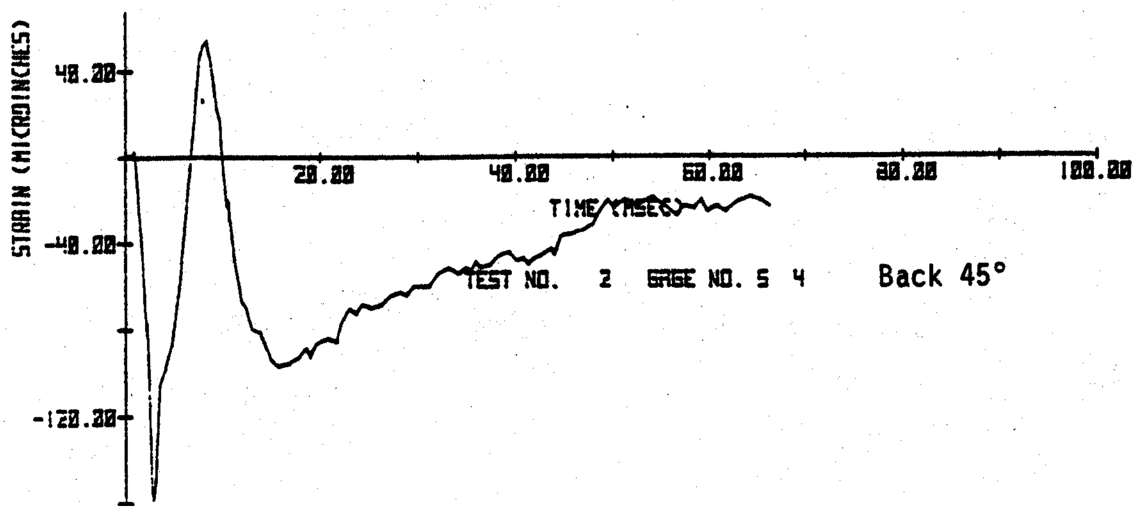

Figure 36. Circumferential Strain Measurements on 3-inch Diameter Pipe From a Point Source (Cont'd)

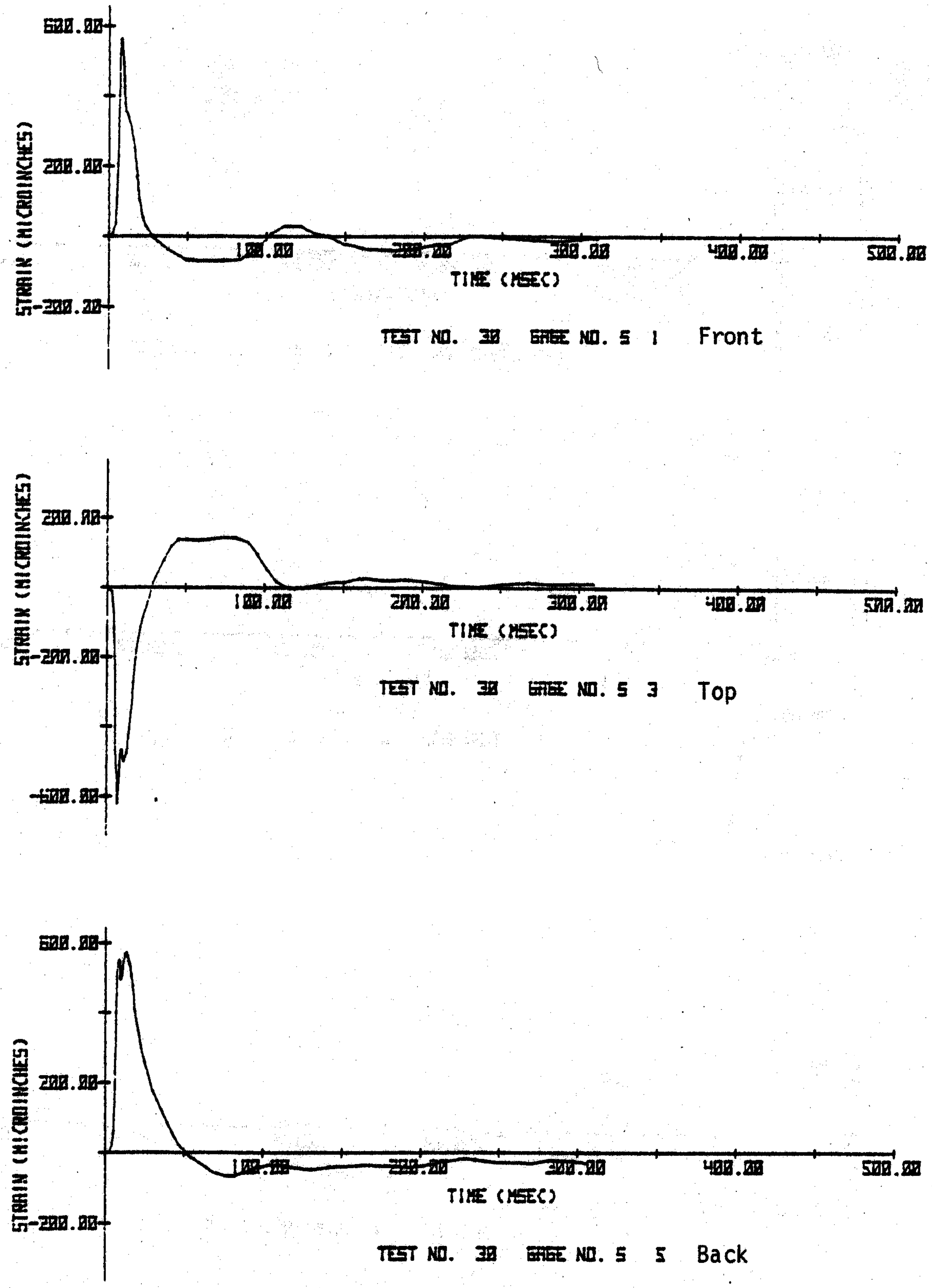

Figure 37. Circumferential Strain Measurements for 6-inch Pipe From a Point Source

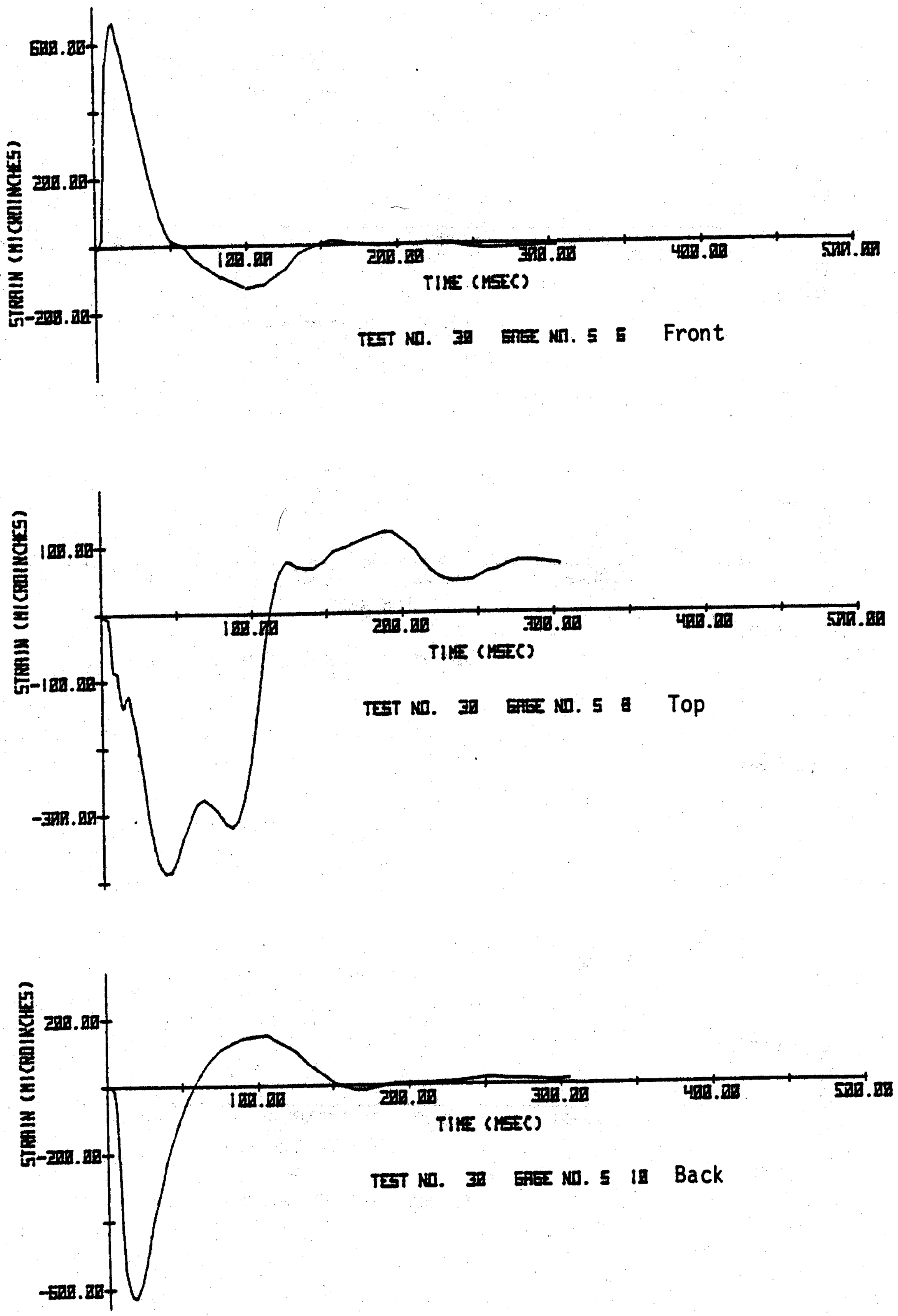

Figure 38. Longitudinal Strain Measurements for 6-inch Pipe From a Point Source

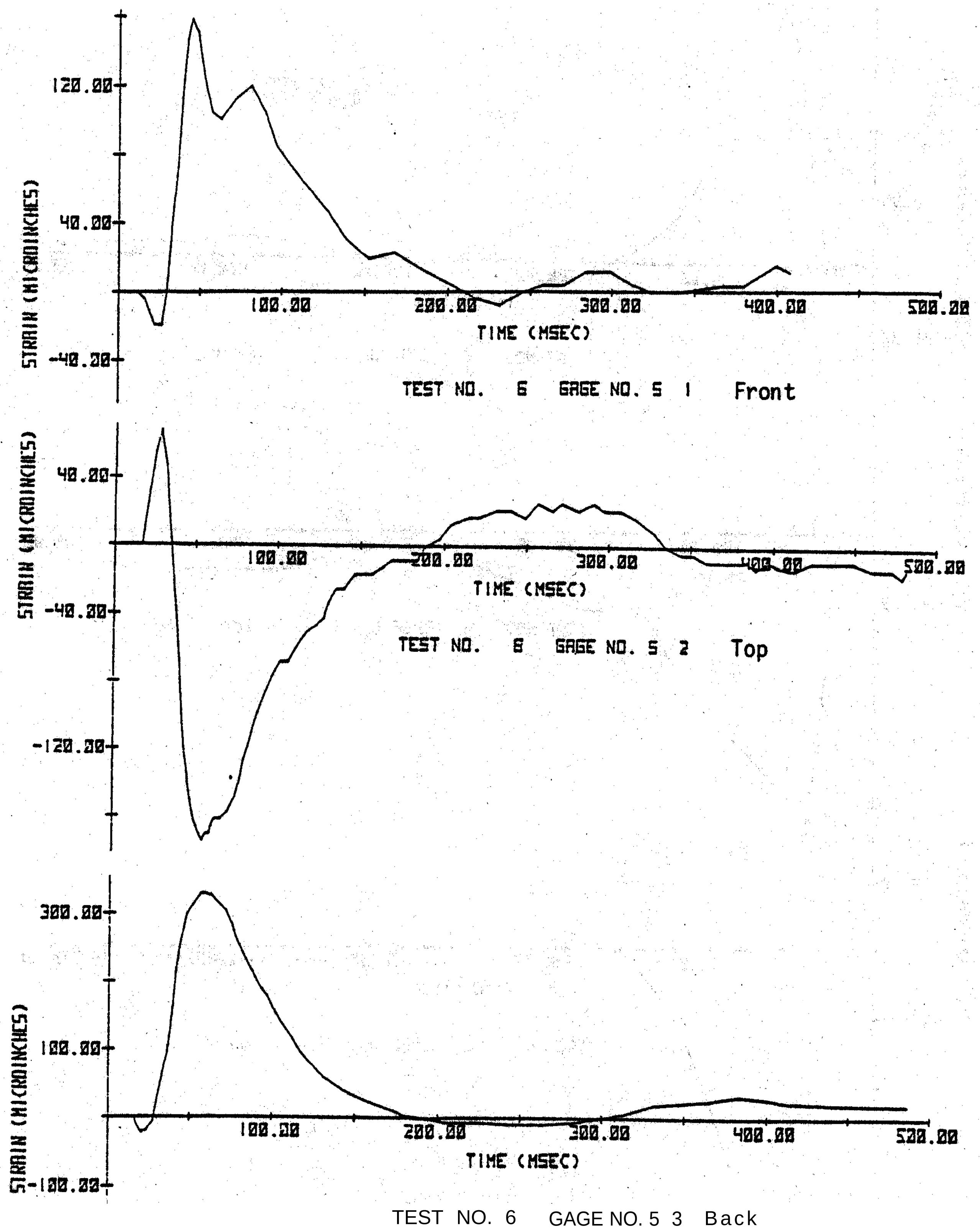

Figure 39. Circumferential Strains on 24-inch Pipe From a Point Source

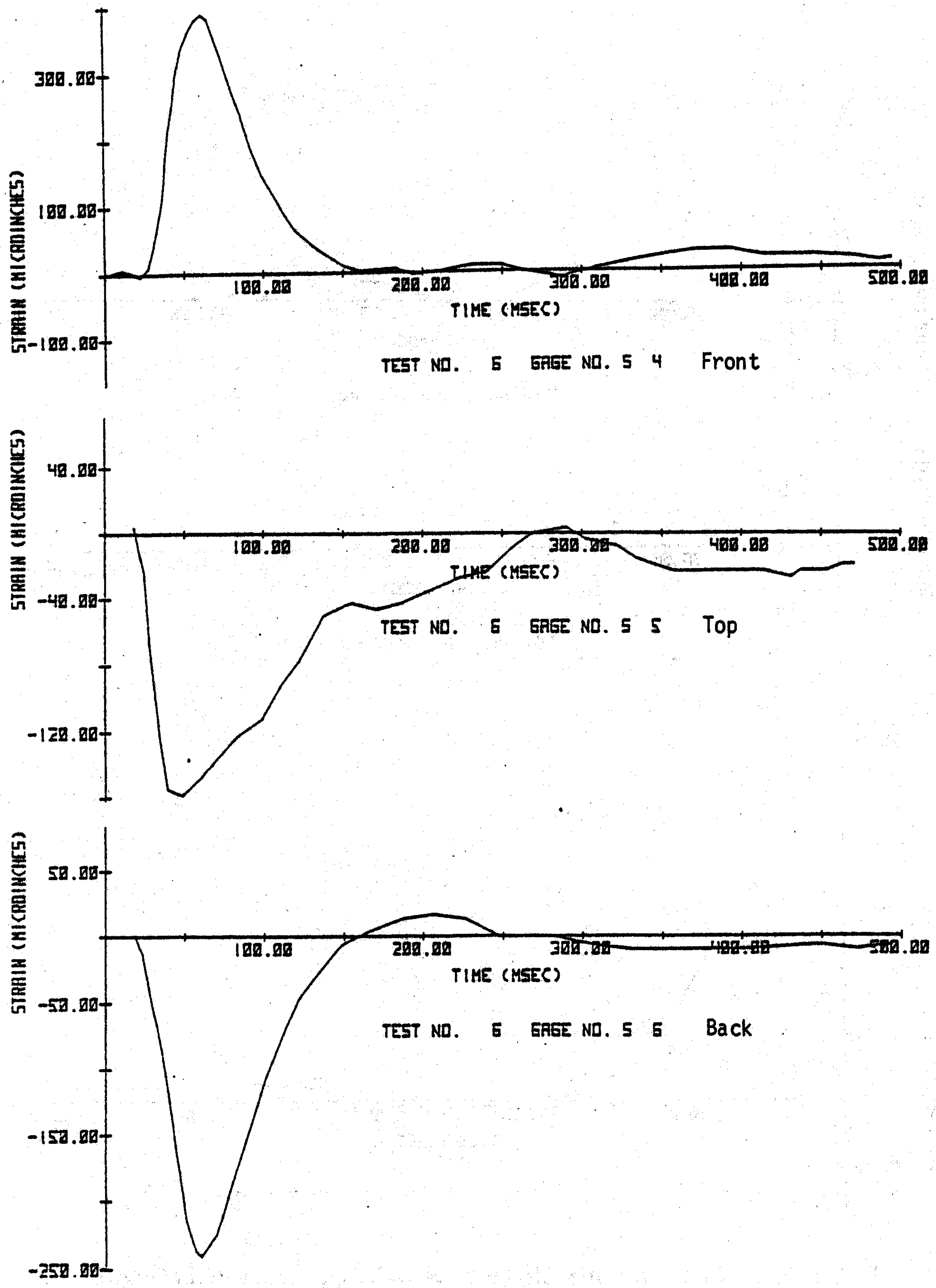

Figure 40. Longitudinal Strains on 24-inch Pipe From a Point Source

would normally occur at one of these locations, strain data were also recorded as much as possible from the front, top and back strain gages. Figures 41 and 42 are examples of the strain data from the 45° locations recorded on one of the deeper charge experiments. As can be observed, these traces are quite similar to the rest of the point source traces. For this same experiment, circumferential strain data were also obtained on the front and back locations on the pipe and are included in Figure 43. Furthermore, for the top and back strain locations, longitudinal data were obtained as shown in Figure 44.

Most of the model test data examples presented so far show peak strains in the order of 300 to 1,000 microinches/inch (µin./in.). In the last series of tests, charge weights and standoff distances were selected such that most of the pipe response data would be at the lower end of the stress prediction curves. The majority of the peak strains were less than 100 &,/in. The primary measurements were made as before: on the front, top, and back of the pipe. Examples of these low amplitude measurements are provided in Figures 45 and 46.

The maximum stresses for each point source test are listed in Table 7. In this table, some of the test pipe description is also provided with the charge information. The absolute value in µin./in. of the maximum circumferential and longitudinal strains measured, from which the stresses were computed, are also included in this table, Together with Table 3 in Section II, this table provides a complete description of each test, the measured maximum strains, and the corresponding stresses. These data are plotted in Section VII and compared with the point and parallelline strain and stress prediction curves.

Line Source Test Data

Twenty-five explosive line experiments were conducted in this program. Of these, 15 used an explosive line parallel to the pipeline. The remaining 10 tests used an explosive line at an angle to the pipeline. The explosive lines were made up of several charges of identical weight spaced equally apart. In these tests, three or four velocity transducers were used to obtain soil particle velocity and' displacement data. For the parallel line tests, all of the velocity transducers were positioned to sense radial horizontal ground motions perpendicular to the line explosive sources. For the angled-line experiments, ground motion data were obtained not only at the same angle as the corresponding pipe strain data, but also at another angle (see Figures 7 and 8).

Examples of radial velocity and displacement records from a parallel line explosive source are presented in Figure 47. An example of the data recorded on an angled-line test is shown in Figure 48. In this case the transducer location corresponded to a field situation in which the explosive line, was at a 30° to the pipe. These velocity and displacement traces are quite similar to those from point sources.

The peak soil radial particle velocity and displacement for each explosive line experiment are shown in Table 8. In this table, the parallel line data are grouped together. and then the angled-line data are listed. The average seismic velocity c is provided for each test along with the equivalent energy release n. Also listed in this table are the weight (mass) W1

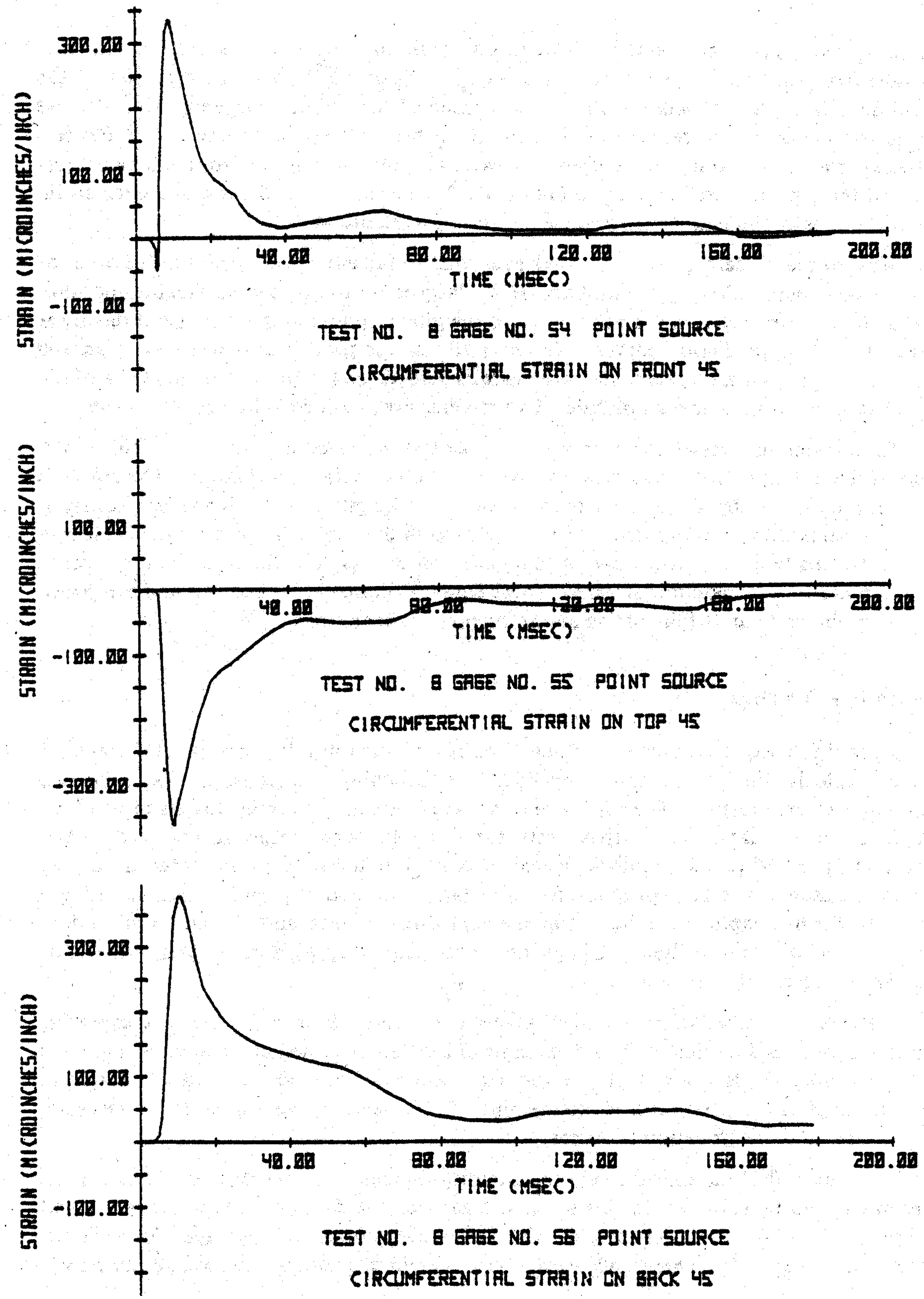

Figure 41. Circumferential Strains from Deeper Point Source

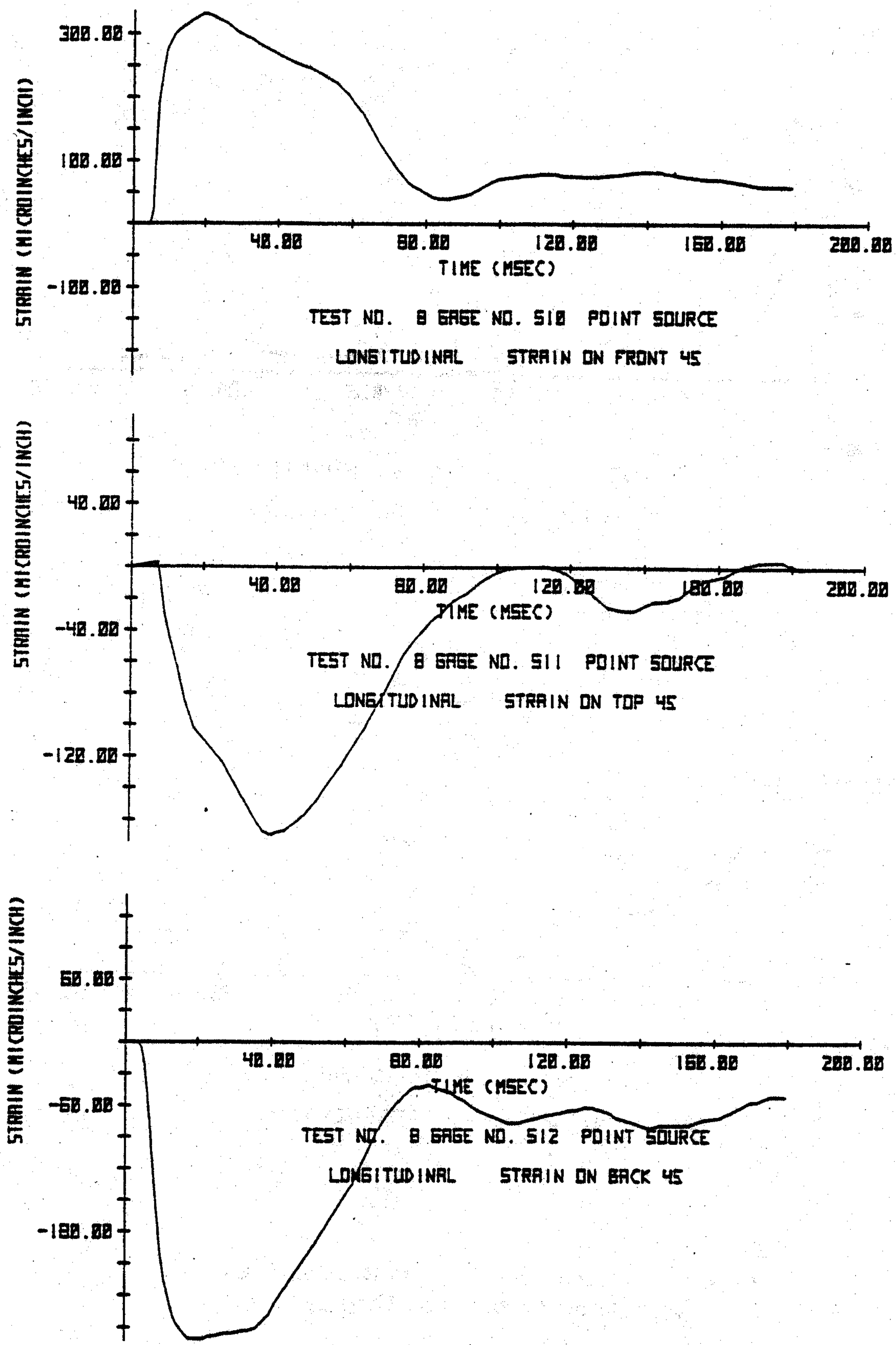

Figure 42. Longitudinal Strains from Deeper Point Source

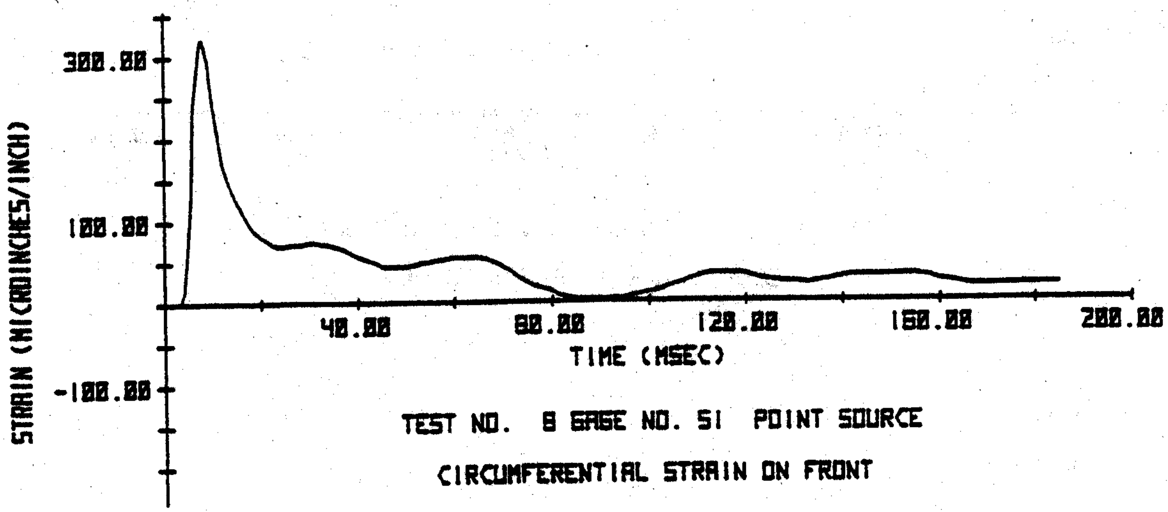

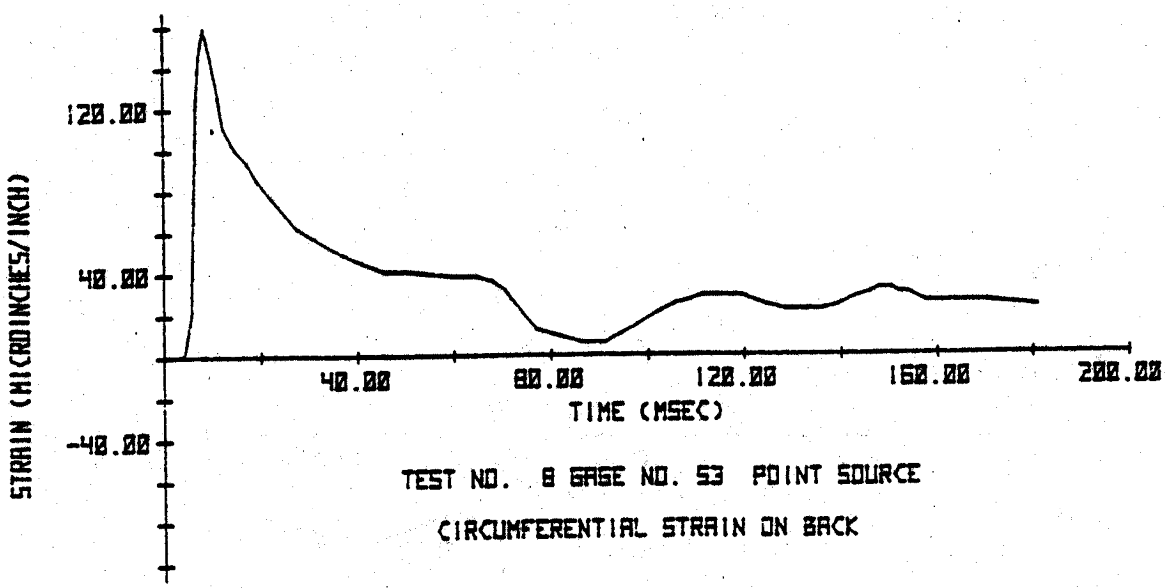

Figure 43. Additional Circumferential Strains. from Deeper Point Source Experiment

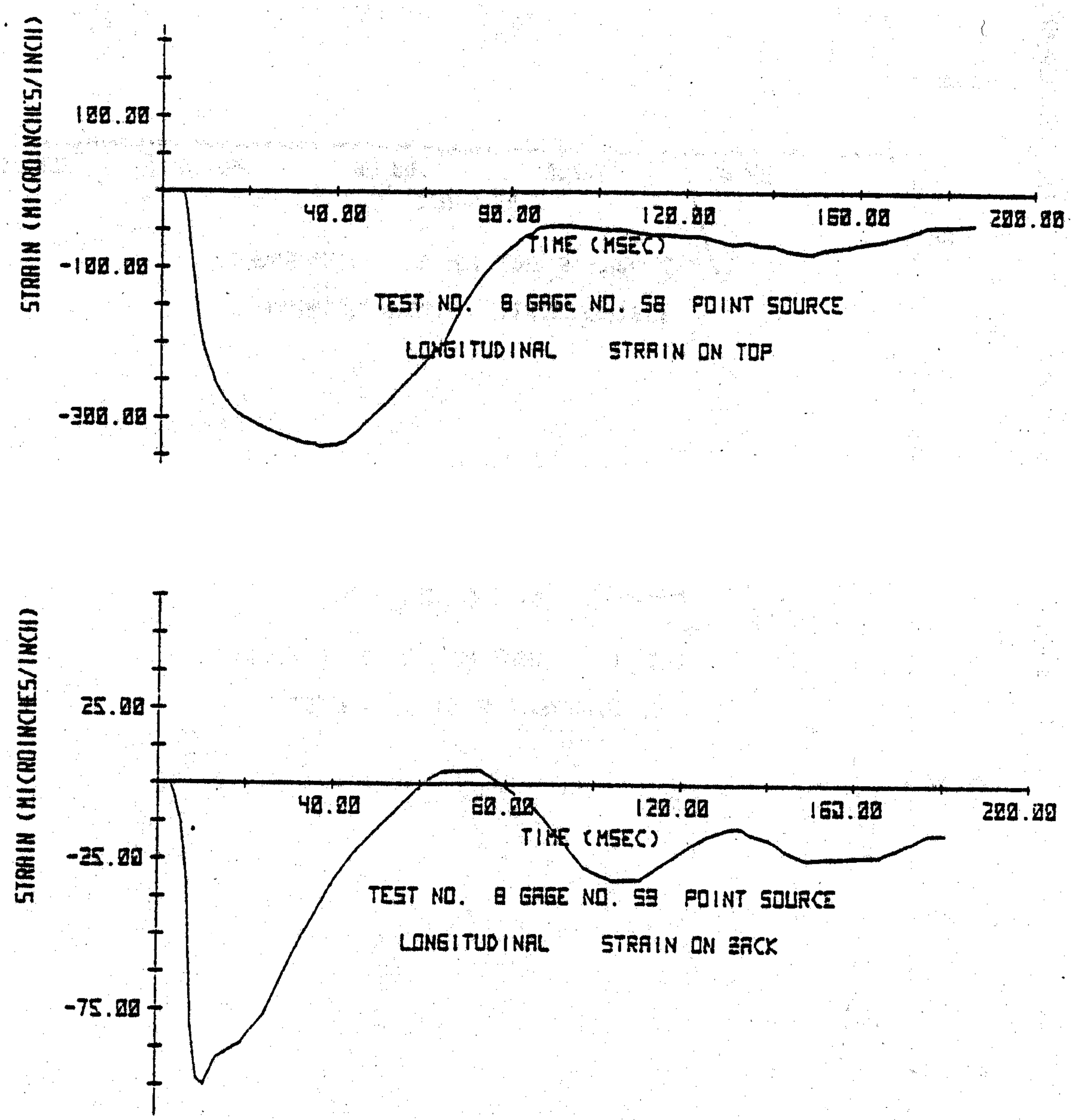

Figure 44. Additional Longitudinal Strains from Deeper Point Source Experiment

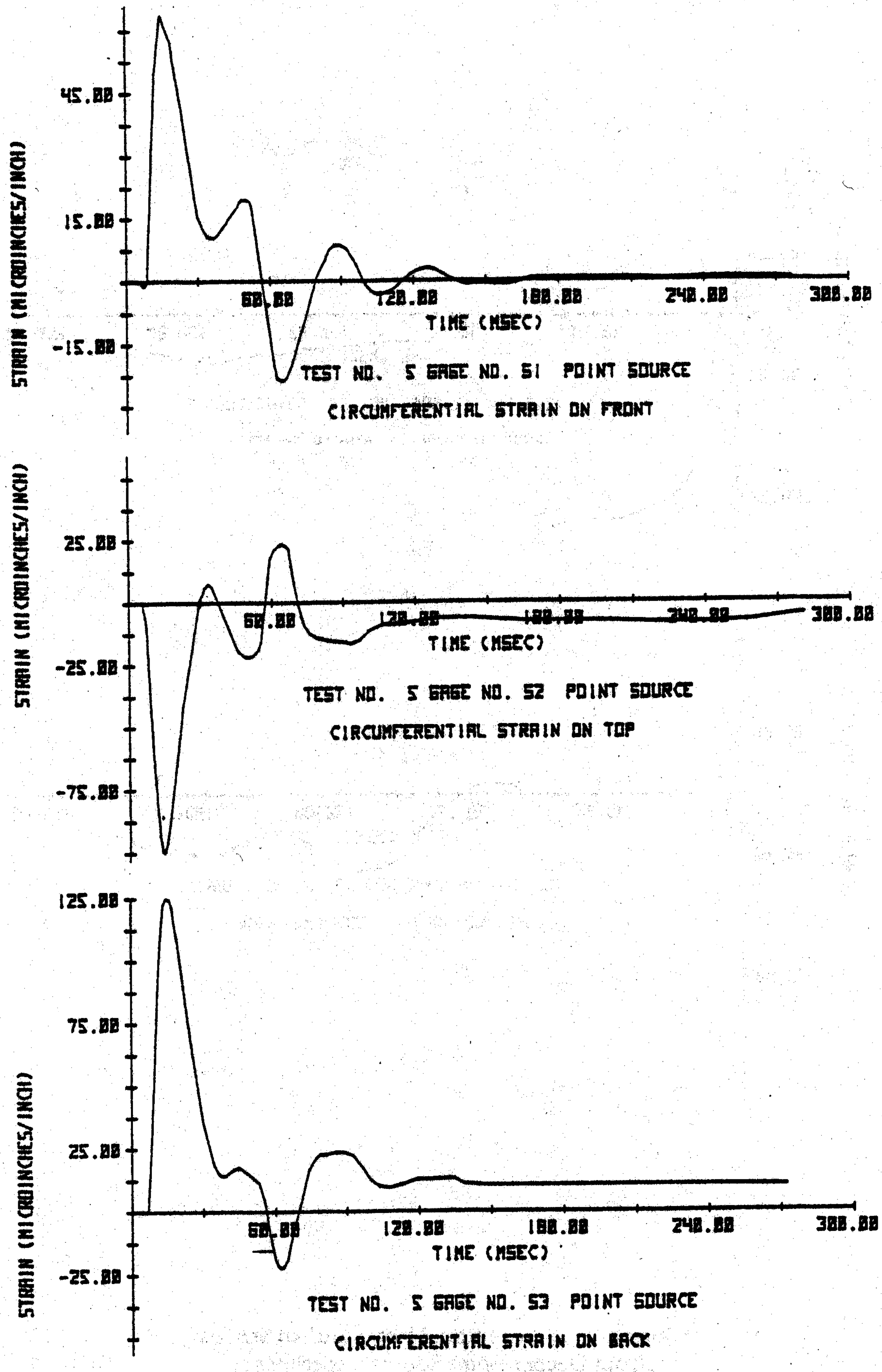

Figure 45. Circumferential Strains from 0.08-lb Point Explosive Source

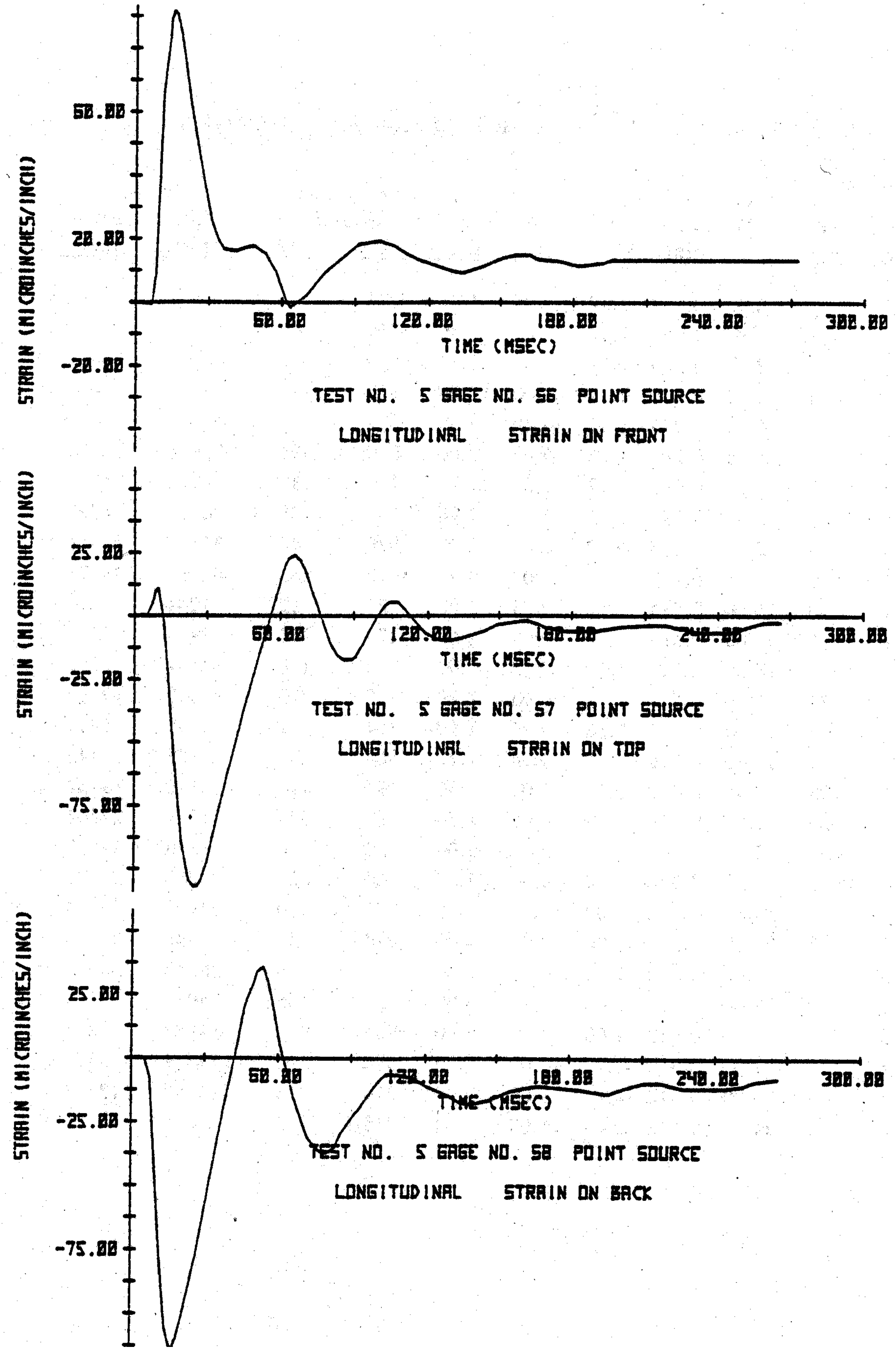

Figure 46. Longitudinal Strains from 0.08-lb Point Explosive Source

Table 7. Pipe Response Data From Point Source Tests

Test Series	Test No.	Pipe O.D. (in.)	h (in.)	n	W (lb)	R (ft)	Maximum Strains Cir	Maximum Strains Long	Stresses Cir (psi)	Stresses Long (psi)
1	1	2.95	0.059	1.12	0.05	1.50	474	--	--	--
1	2	2.95	0.059	1.12	0.05	1.50	1039	--	--	--
1	3	2.95	0.059	1.12	0.05	1.50	875	--	--	--
1	4	2.95	0.059	1.12	1.00	11.00	112	--	--	--
1	5	5.95	0.093	1.12	0.40	3.00	608	--	--	--
1	6	5.95	0.093	1.12	0.40	3.00	930	592	35906	28236
1	7	5.95	0.093	1.12	1.00	11.00	120	137	5222	5608
1	8	5.95	0.093	1.12	0.03	2.00	156	169	6701	6996
1	9	5.95	0.093	1.12	0.03	1.00	996	548	37617	27451
1	10	2.95	0.059	1.12	0.03	0.75	1217	868	47894	39974
1	20	16.00	0.515	1.12	0.03	3.00	27	17	1041	814
1	21	16.00	0.515	1.12	0.03	1.50	477	205	17457	11285
1	22	16.00	0.515	1.12	0.03	1.00	312	158	11651	8156
1	23	16.00	0.515	1.12	0.03	1.00	865	270	30667	17165
1	24	16.00	0.515	1.12	0.06	1.50	214	119	8095	5939
1	25	16.00	0.515	1.12	0.06	1.25	564	298	21182	15145
1	28	2.95	0.059	1.12	0.05	1.50	337	490	15690	19162
1	29	2.95	0.059	1.12	0.05	1.50	463	620	21039	24602
1	30	5.95	0.093	1.12	0.40	3.00	620	666	26576	27620
1	31	5.95	0.093	1.12	0.40	3.00	560	627	24252	25772
2	1	24.00	0.312	1.00	15.00	9.40	352	360	14912	15094
2	2	24.00	0.312	1.00	5.00	6.00	974	933	40648	39718
2	3	24.00	0.312	1.00	5.00	6.00	917	854	38032	36603
2	4	24.00	0.312	1.00	15.00	13.00	537	786	25052	30703
2	5	24.00	0.312	1.00	5.00	9.00	404	492	17882	19878
2	6	24.00	0.312	1.00	15.00	13.00	330	390	14491	15852
2	7	24.00	0.312	1.00	15.00	13.00	274	336	12150	13557
2	8	24.00	0.312	1.00	15.00	6.00	3815	6783	--	--

Table 7. Pipe Response Data From Point Source Tests (Cont'd)

Test Series	Test No.	Pipe O.D. (in.)	h (in.)	n	W (lb)	R (ft)	Maximum Strains Cir	Maximum Strains Long	Stresses Cir (psi)	Stresses Long (psi)
3	1	30.00	0.344	1.00	5.00	15.00	101	166	4889	6364
3	2	30.00	0.344	1.00	4.00	15.00	40	80	2075	2982
3	3	30.00	0.344	1.00	3.00	9.00	251	389	11920	15051
3	4	30.00	0.344	1.00	3.00	15.00	39	123	2460	4367
4	1	5.95	0.093	1.12	0.40	3.00	578	601	24582	25104
4	2	5.95	0.093	1.12	0.10	1.50	783	689	32084	29951
4	3	5.95	0.093	1.12	0.40	4.24	211	389	10623	14662
4	4	5.95	0.093	1.12	0.40	4.24	240	504	12682	18673
4	5	5.95	0.093	1.12	0.20	4.24	79	172	4234	6344
4	6	5.95	0.093	1.12	0.20	4.24	115	189	5566	7245
4	7	5.95	0.093	1.12	0.10	2.12	557	345	21412	16601
4	8	5.95	0.093	1.12	0.10	2.12	378	339	15551	14666
4	9	5.95	0.093	1.12	0.20	2.12	1147	987	46782	43151
4	10	5.95	0.093	1.12	0.20	2.12	1537	1191	61409	53557
4	11	5.95	0.093	1.12	0.40	4.28	265	594	14367	21833
4	38	5.95	0.093	1.12	3.60	22.50	73	58	2931	2590
5	1	5.95	0.093	1.12	0.40	8.00	150	122	6049	5414
5	2	5.95	0.093	1.12	0.40	11.00	78	70	3209	3028
5	3	5.95	0.093	1.12	0.40	15.00	36	40	1556	1647
5	4	5.95	0.093	1.12	0.25	8.00	90	79	3686	3436
5	5	5.95	0.093	1.12	0.08	4.00	125	114	5161	4911
5	6	5.95	0.093	1.12	0.12	11.00	24	23	1002	979
5	7	5.95	0.093	1.12	0.08	11.00	18	13	710	596
5	8	5.95	0.093	1.12	0.08	7.00	55	47	2240	2059
5	9	5.95	0.093	1.12	0.20	5.00	169	201	7433	8160
5	10	5.95	0.093	1.12	0.08	2.50	235	226	9816	9612
5	11	5.95	0.093	1.12	0.40	5.00	188	226	8292	9155
5	12	5.95	0.093	1.12	0.40	3.00	616	501	24842	22232

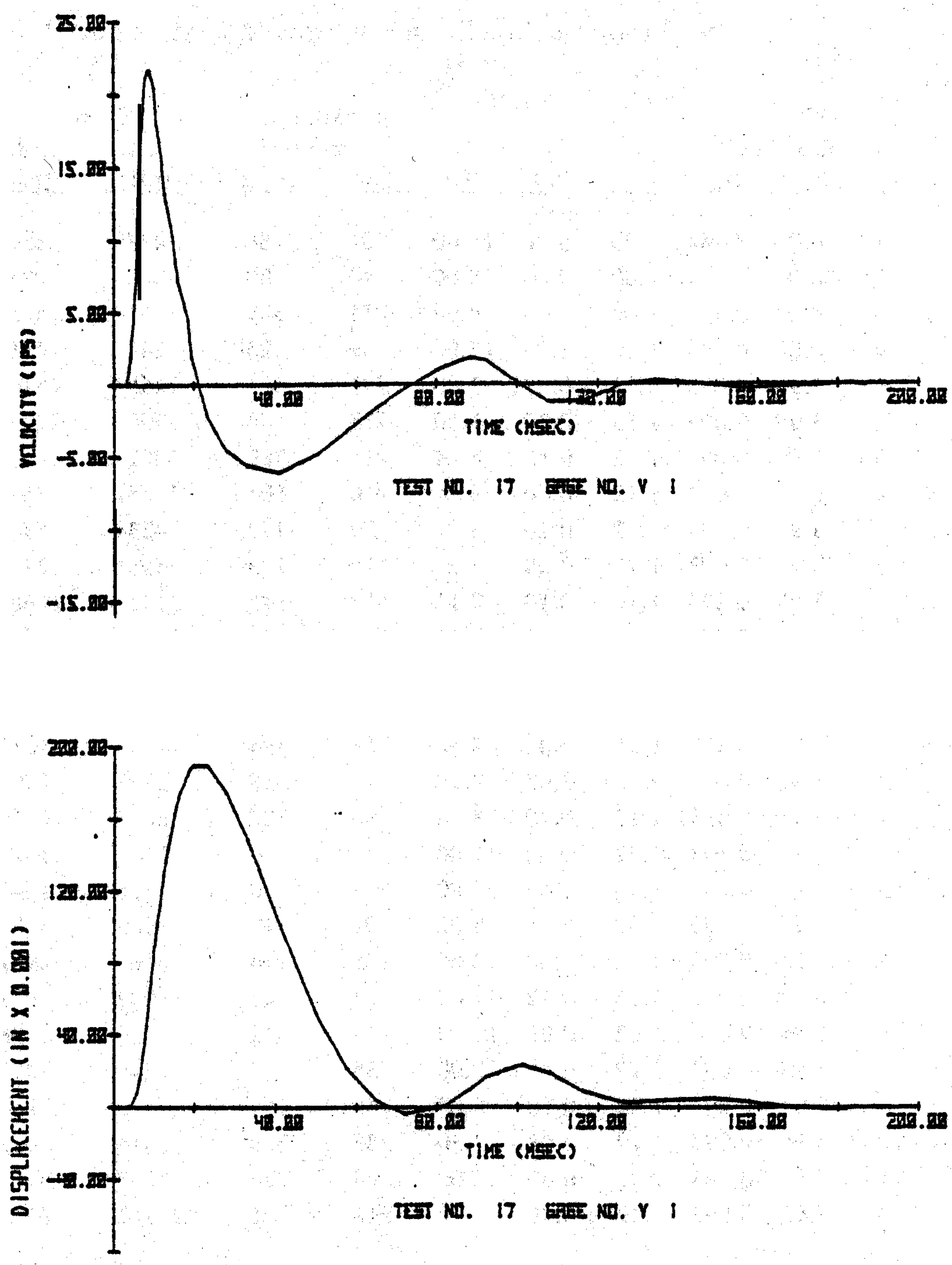

Figure 47. Ground Motions from Parallel Line Source

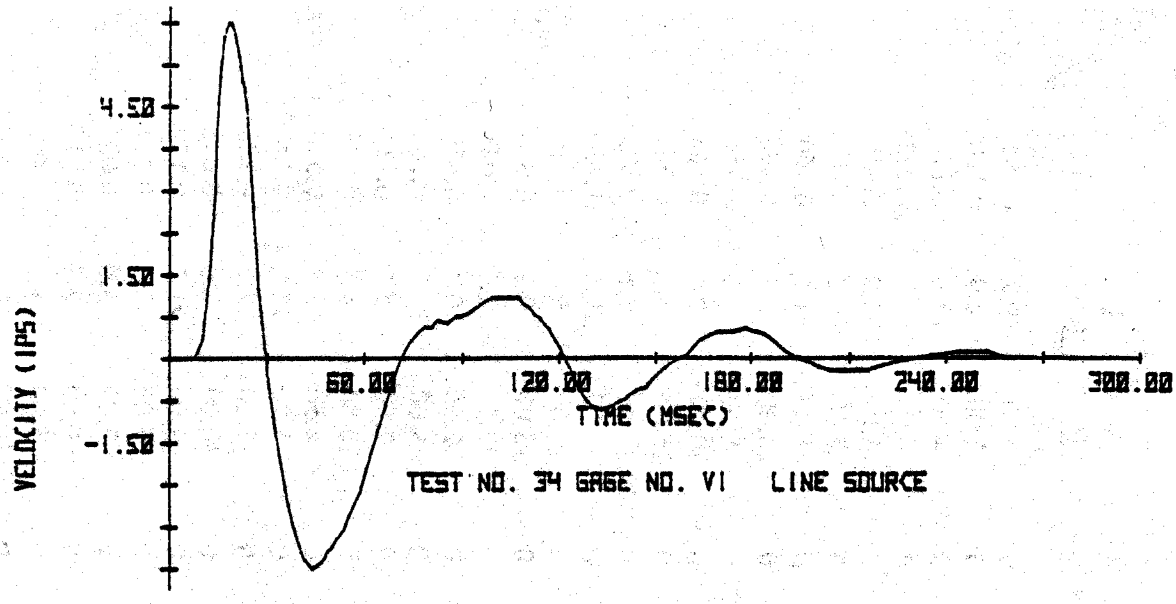

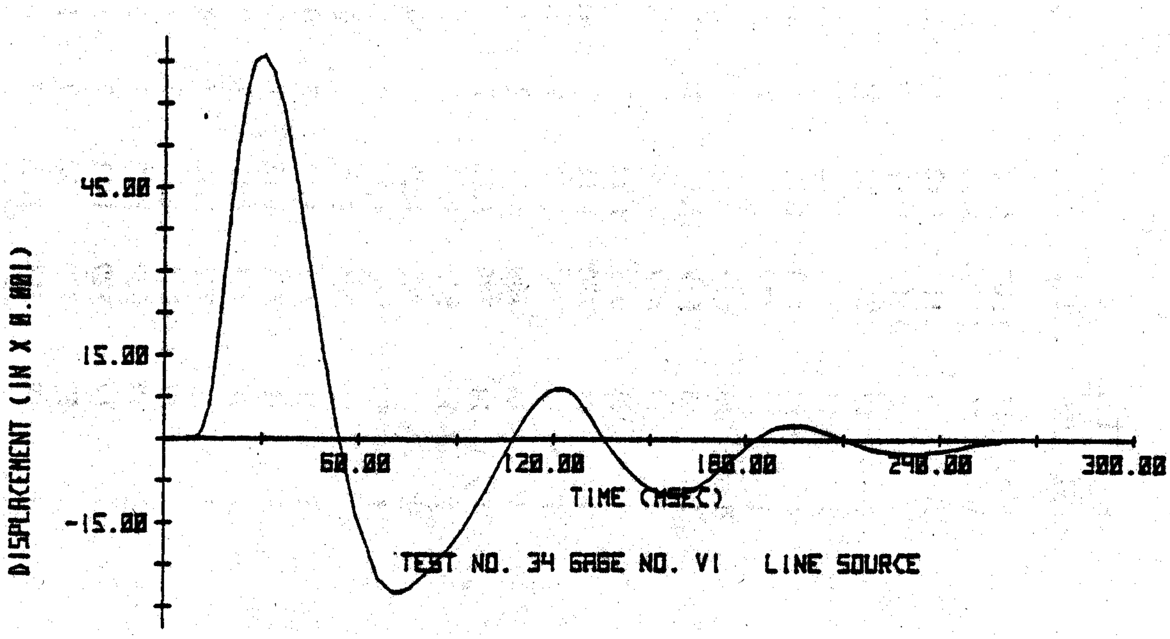

Figure 48. Ground Motions from a 30° Angled-Line Source

Table 8. Ground Motion Data From Line Source Tests

Test Series	Test No.	c (fps)	n	N1	L1 (ft)	W1 (lb)	B (deg)	A (ft)	U (ips)	X (in.)
1	11	1110	1.12	7	1.50	0.05	0	2.00	19.2	0.195
1	11	1110	1.12	7	1.50	0.05	0	2.00	18.9	0.130
1	11	1110	1.12	7	1.50	0.05	0	4.00	13.0	0.170
1	11	1110	1.12	7	1.50	0.05	0	6.00	6.4	0.073
1	12	738	1.12	7	2.40	0.40	0	5.00	25.9	0.410
1	12	738	1.12	7	2.40	0.40	0	8.00	12.3	0.195
1	12	738	1.12	7	2.40	0.40	0	11.00	11.5	0.160
1	12	738	1.12	7	2.40	0.40	0	14.00	5.8	0.094
1	13	679	1.12	7	1.50	0.40	0	5.00	36.3	1.350
1	13	679	1.12	7	1.50	0.40	0	10.00	9.1	0.166
1	13	679	1.12	7	1.50	0.40	0	15.00	3.2	0.065
1	13	679	1.12	7	1.50	0.40	0	20.00	1.6	0.025
1	14	780	1.12	7	1.50	0.40	0	5.00	39.6	1.460
1	14	780	1.12	7	1.50	0.40	0	10.00	9.1	0.136
1	14	780	1.12	7	1.50	0.40	0	15.00	2.2	0.044
1	14	780	1.12	7	1.50	0.40	0	20.00	1.6	0.023
1	15	945	1.12	7	0.75	0.05	0	2.50	50.1	0.480
1	15	945	1.12	7	0.75	0.05	0	5.00	14.1	0.200
1	15	945	1.12	7	0.75	0.05	0	7.50	5.8	0.082
1	15	945	1.12	7	0.75	0.05	0	10.00	1.5	0.023
1	16	771	1.12	7	0.75	0.05	0	2.50	72.8	0.550
1	16	771	1.12	7	0.75	0.05	0	5.00	17.2	0.240
1	16	771	1.12	7	0.75	0.05	0	7.50	7.9	0.108
1	16	771	1.12	7	0.75	0.05	0	10.00	2.0	0.031
1	17	829	1.12	7	1.50	0.03	0	3.00	21.7	0.190
1	17	829	1.12	7	1.50	0.03	0	5.00	8.1	0.114
1	17	829	1.12	7	1.50	0.03	0	7.00	5.0	0.051
1	17	829	1.12	7	1.50	0.03	0	10.00	2.3	0.017
1	18	734	1.12	7	0.90	0.40	0	5.00	51.5	1.490
1	18	734	1.12	7	0.90	0.40	0	10.00	6.8	0.130
1	18	734	1.12	7	0.90	0.40	0	15.00	4.6	0.075

Table 8. Ground Motion Data From Line Source Tests (Cont'd)

Test Series	Test No.	c (fps)	n	N1	L1 (ft)	W1 (lb)	B (deg)	A (ft)	U (ips)	X (in.)
1	18	734	1.12	7	0.90	0.40	0	20.00	3.0	0.043
1	19	564	1.12	7	0.46	0.03	0	1.50	66.5	0.520
1	19	564	1.12	7	0.46	0.03	0	3.00	19.8	0.270
1	19	564	1.12	7.	0.46	0.03	0	6.00	6.1	0.120
1	19	564	1.12	7	0.46	0.03	0	9.00	1.8	0.035
1	26	701	1.12	7	3.30	0.05	0	5.00	4.5	0.042
1	26	701	1.12	7	3.30	0.05	0	8.00	2.5	0.021
1	26	701	1.12	7	3.30	0.05	0	11.00	2.0	0.014
1	26	701	1.12	7	3.30	0.05	0	14.00	1.8	0.011
1	27	645	1.12	7	3.30	0.05	0	5.00	4.7	0.041
1	27	645	1.12	7	3.30	0.05	0	8.00	3.0	0.023
1	27	645	1.12	7	3.30	0.05	0	11.00	2.5	0.018
1	27	645	1.12	7	3.30	0.05	0	14.00	2.0	0.013
5	21	908	1.12	4	1.50	0.40	0	5.00	55.3	0.520
5	21	908	1.12	4	1.50	0.40	0	10.00	17.4	0.229
5	21	908	1.12	4	1.50	0.40	0	15.00	7.5	0.071
5	22	747	1.12	7	1.50	0.40	0	10.00	22.1	0.330
5	22	747	1.12	7	1.50	0.40	0	15.00	9.9	0.114
5	22	747	1.12	7	1.50	0.40	0	20.00	6.0	0.071
5	23	888	1.12	7	1.50	0.40	0	5.00	39.7	0.820
5	23	888	1.12	7	1.50	0.40	0	10.00	11.1	0.281
5	23	888	1.12	7	1.50	0.40	0	15.00	6.4	0.137
5	24	784	1.12	7	1.50	0.05	0	5.00	7.0	0.111
5	24	784	1.12	7	1.50	0.05	0	10.00	2.1	0.031
5	24	784	1.12	7	1.50	0.05	0	15.00	0.9	0.013
4	31	815	1.12	4	2.50	0.10	15	10.00	2.6	0.039
4	31	815	1.12	4	2.50	0.10	60	5.00	4.7	0.050
4	31	815	1.12	4	2.50	0.10	60	10.00	1.5	0.020
4	32	704	1.12	4	2.50	0.10	15	5.00	8.0	0.086
4	32	704	1.12	4	2.50	0.10	15	10.00	2.0	0.029
4	32	704	1.12	4	2.50	0.10	60	5.00	4.0	0.041

Table 8. Ground Motion Data From Line Source Tests (Cont'd)

Test Series	Test No.	c (fps)	n	N1	L1 (ft)	W1 (lb)	B (deg)	A (ft)	U (ips)	X (in.)
4	32	704	1.12	4	2.50	0.10	60	10.00	0.7	0.008
4	33	740	1.12	4	2.50	0.10	30	5.00	6.6	0.077
4	33	740	1.12	4	2.50	0.10	30	10.00	1.7	0.026
4	33	740	1.12	4	2.50	0.10	75	5.00	4.3	0.038
4	33	740	1.12	4	2.50	0.10	75	10.00	1.6	0.015
4	34	706	1.12	4	2.50	0.10	30	5.00	6.0	0.069
4	34	706	1.12	4	2.50	0.10	75	5.00	4.7	0.037
4	34	706	1.12	4	2.50	0.10	75	10.00	1.4	0.013
4	35	707	1.12	4	2.50	0.10	45	10.00	2.3	0.028
4	35	707	1.12	4	2.50	0.10	90	10.00	1.5	0.014
4	36	749	1.12	4	2.50	0.10	45	5.00	6.8	0.056
4	36	749	1.12	4	2.50	0.10	45	10.00	1.9	0.020
4	36	749	1.12	4	2.50	0.10	90	5.00	5.2	0.049
4	36	749	1.12	4	2.50	0.10	90	10.00	1.5	0.013
4	39	644	1.12	6	2.50	0.20	30	10.00	3.9	0.075
4	39	644	1.12	6	2.50	0.20	30	15.00	2.1	0.038
4	39	644	1.12	6	2.50	0.20	90	10.00	2.7	0.021
4	39	644	1.12	6	2.50	0.20	90	15.00	1.2	0.012
4	40	782	1.12	6	2.50	0.20	30	10.00	3.3	0.053
4	40	782	1.12	6	2.50	0.20	30	15.00	2.0	0.026
4	40	782	1.12	6	2.50	0.20	45	10.00	3.6	0.041
4	40	782	1.12	6	2.50	0.20	45	15.00	1.1	0.011
4	41	771	1.12	6	2.50	0.40	30	10.00	5.8	0.108
4	41	771	1.12	6	2.50	0.40	30	15.00	3.7	0.057
4	41	771	1.12	6	2.50	0.40	45	10.00	5.1	0.070
4	41	771	1.12	6	2.50	0.40	45	15.00	1.9	0.022
4	42	672	1.12	6	2.50	0.40	30	10.00	5.7	0.112
4	42	672	1.12	6	2.50	0.40	30	15.00	3.8	0.058
4	42	672	1.12	6	2.50	0.40	90	10.00	5.2	0.034
4	42	672	1.12	6	2.50	0.40	90	15.00	2.2	0.019

of each individual charge making up the explosive line, the charge spacing L1, the angle B between the pipeline and the explosive line, and the distance A between each transducer and the nearest point charge.

The strain data from the explosive line experiments were obtained primarily at a location on the pipe opposite the geometric center of the explosive source. As was the case with the point sources, measurements were made mostly on the front, top, and back of the pipe since the explosive lines were also buried to the same depth as the model pipe. Examples of strain-time data at the primary sensing locations are shown in Figures 49 and 50 for a parallel line source. Examples of strain traces from similar sensing locations for an angled-line source are shown in Figures 51 and 52. Measurements made approximately at a pipe location opposite the nearest point of the explosive line arc presented in Figures 53 and 54 for the same test as the preceding two figures. Note that the explosive line data appear to be more complex than the point source data, especially in the longitudinal direction. This implies that the forcing function produced by explosive line sources excited the model pipe system into other modes which complicated the character of the strain records.

The stresses calculated from the absolute value of the maximum measured strains are listed in Table 9. In addition, this table contains some of the test pipe information and charge description. The absolute value of the maximum measured strains are also included. Together with Table 3 in Section Ii, this table provides a complete description of each explosive line test and the corresponding stress data.

Grid Explosive Source Data

Twenty-eight experiments were performed using explosive grid sources. In 15 tests, the grid was parallel to the test pipe and in the other 13 tests, the grid was oriented at an angle to the pipe. All of the grids were made up of 12 equal weight point charges arranged in a 4 x 3 pattern. The spacing of all the charges in both directions was the same for each grid.

As was the case in all experimentation on this project, ground motion measurements were made on each grid test. Normally, three or four velocity transducers were used to obtain the soil particle velocity and displacement data. In some instances, the transducers were oriented at a similar angle as the test pipe. In others, some of the transducers were oriented at a different angle. An example of ground motion data from one of the grid tests is presented in Figure 55. Note that these grid traces are slightly different than the point and parallel line data. They show a distinct and significant negative velocity and displacement, and more distinct oscillations.

The measured peak radial soil velocity and computed peak displacement data are presented in Table 10 for each test by series and number. Also listed on this table are the weight W1 of each individual charge making up the grid, the equal spacings L1 and L2 between charges, the average seismic velocity c, the array angle B, and the distance A between each transducer and the grid, These ground motion data are used in Section VIII of the report to complement the stress data in developing prediction methods for parallel grid and angled-grid explosive sources.

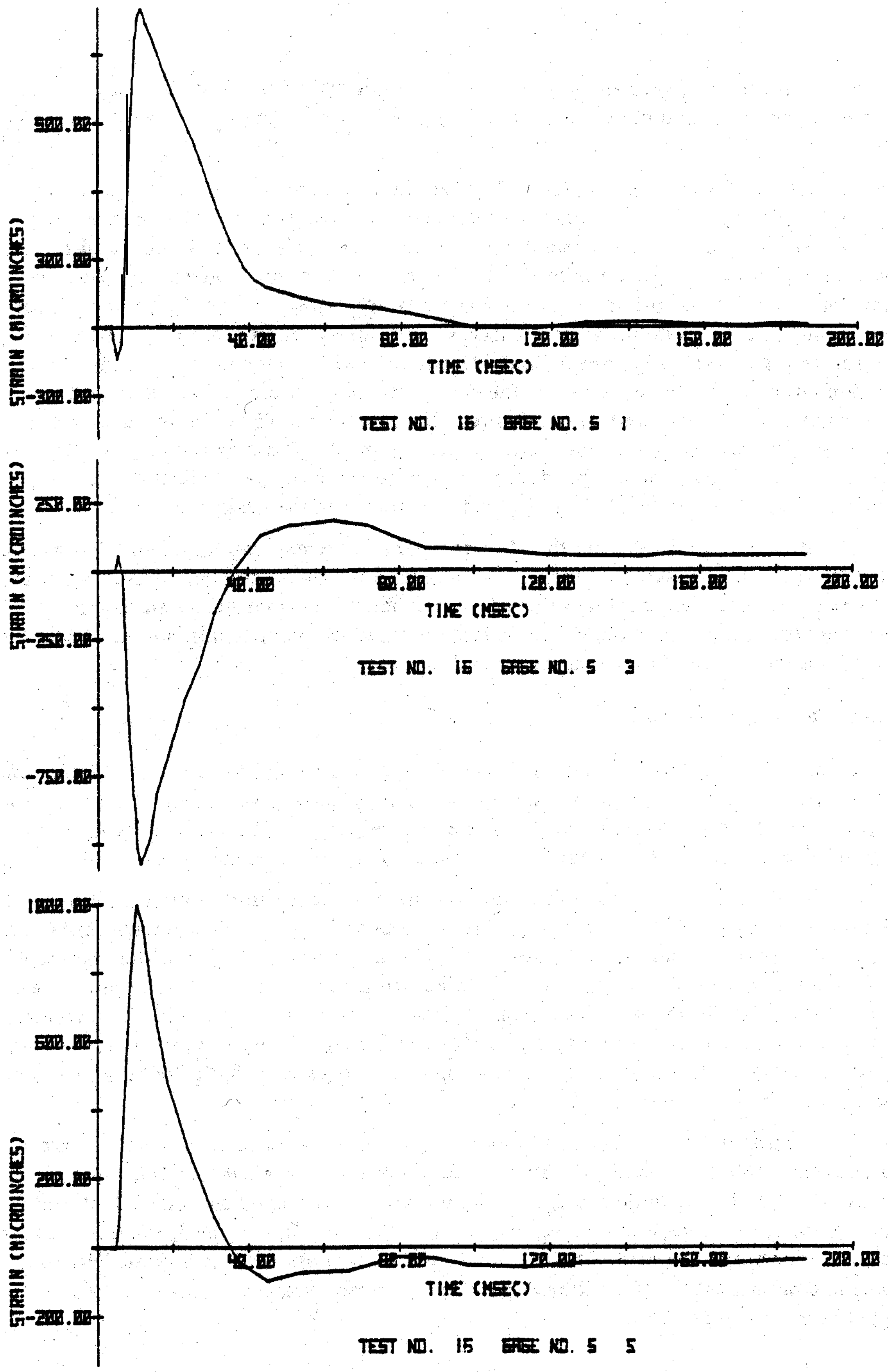

Circumferential Strains from Parallel Line Source

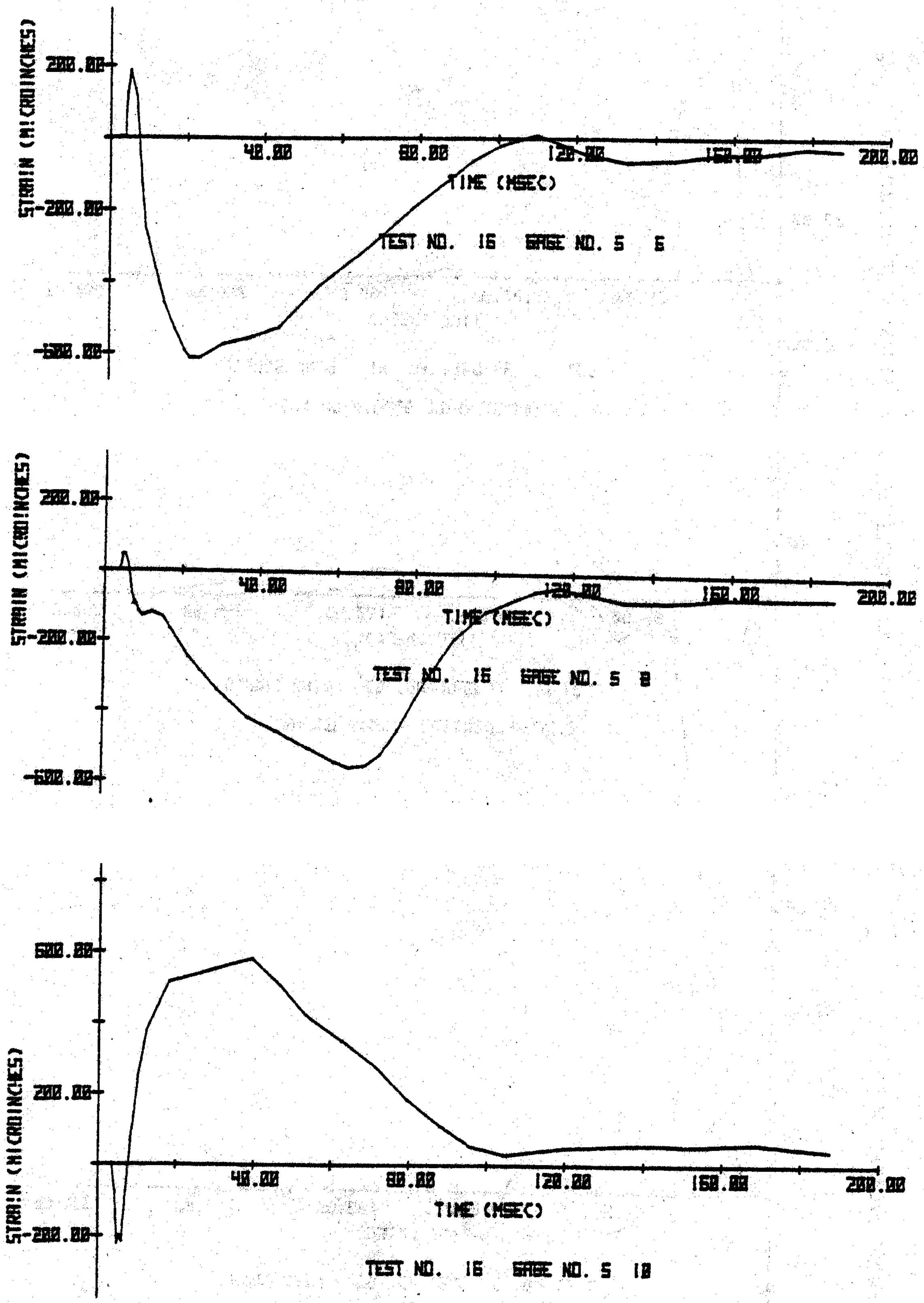

Figure 50. Longitudinal Strains from Parallel Line Source

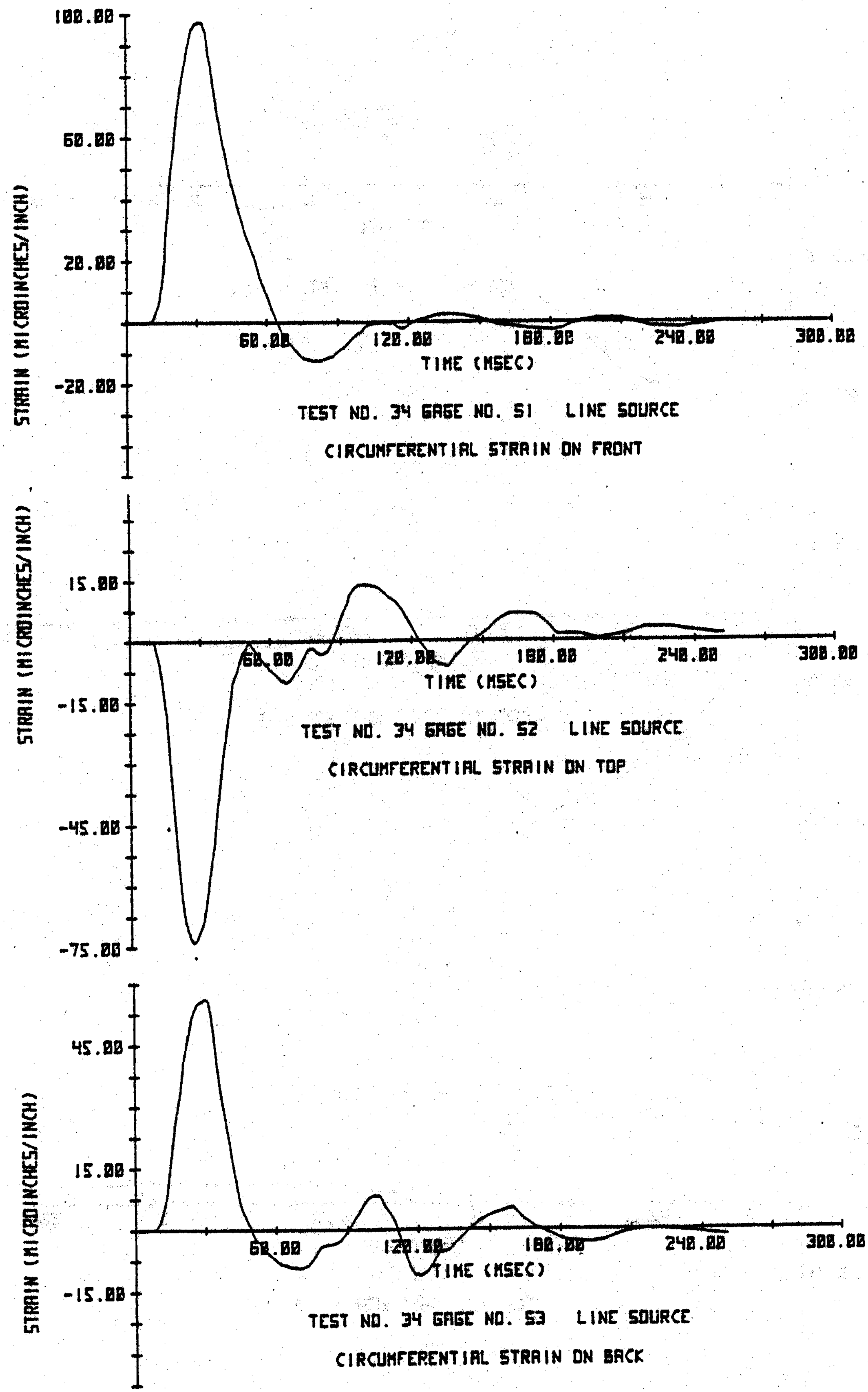

Figure 51. Circumferential Strains from Angled-Line Source

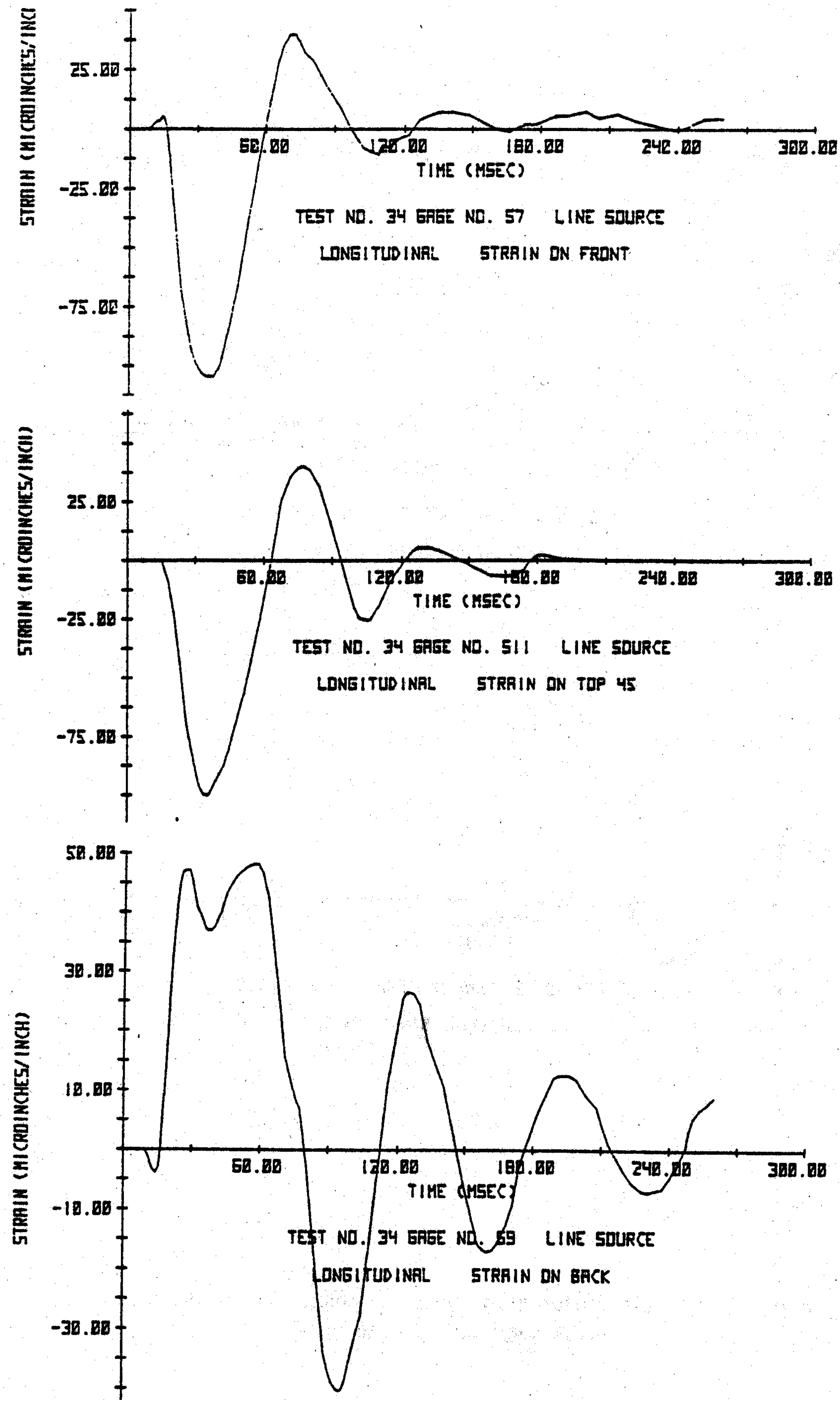

Figure 52. Longitudinal Strains from Angled-Line Source

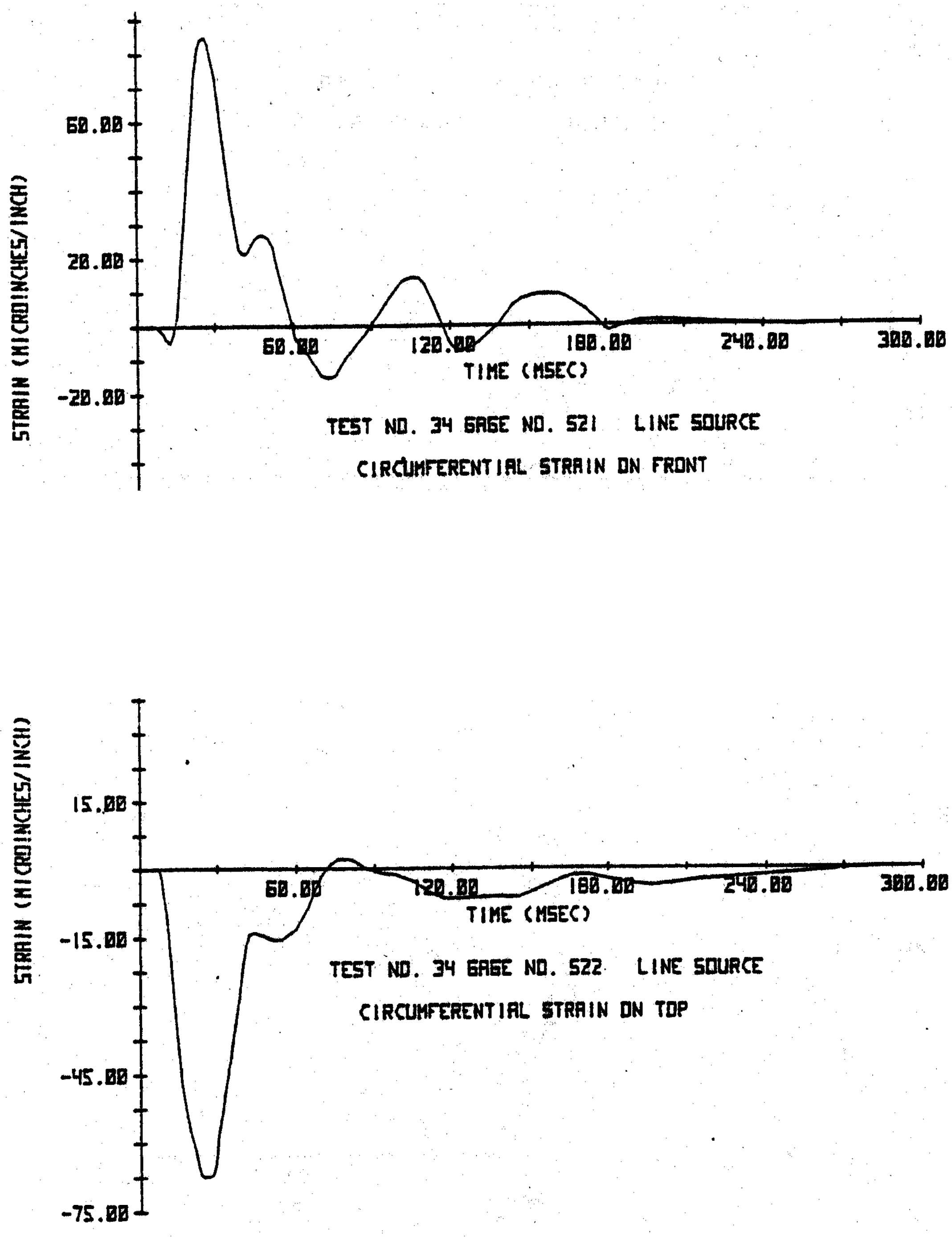

Figure 53. Circumferential Strains Opposite Nearest Point of Angled-Line Source

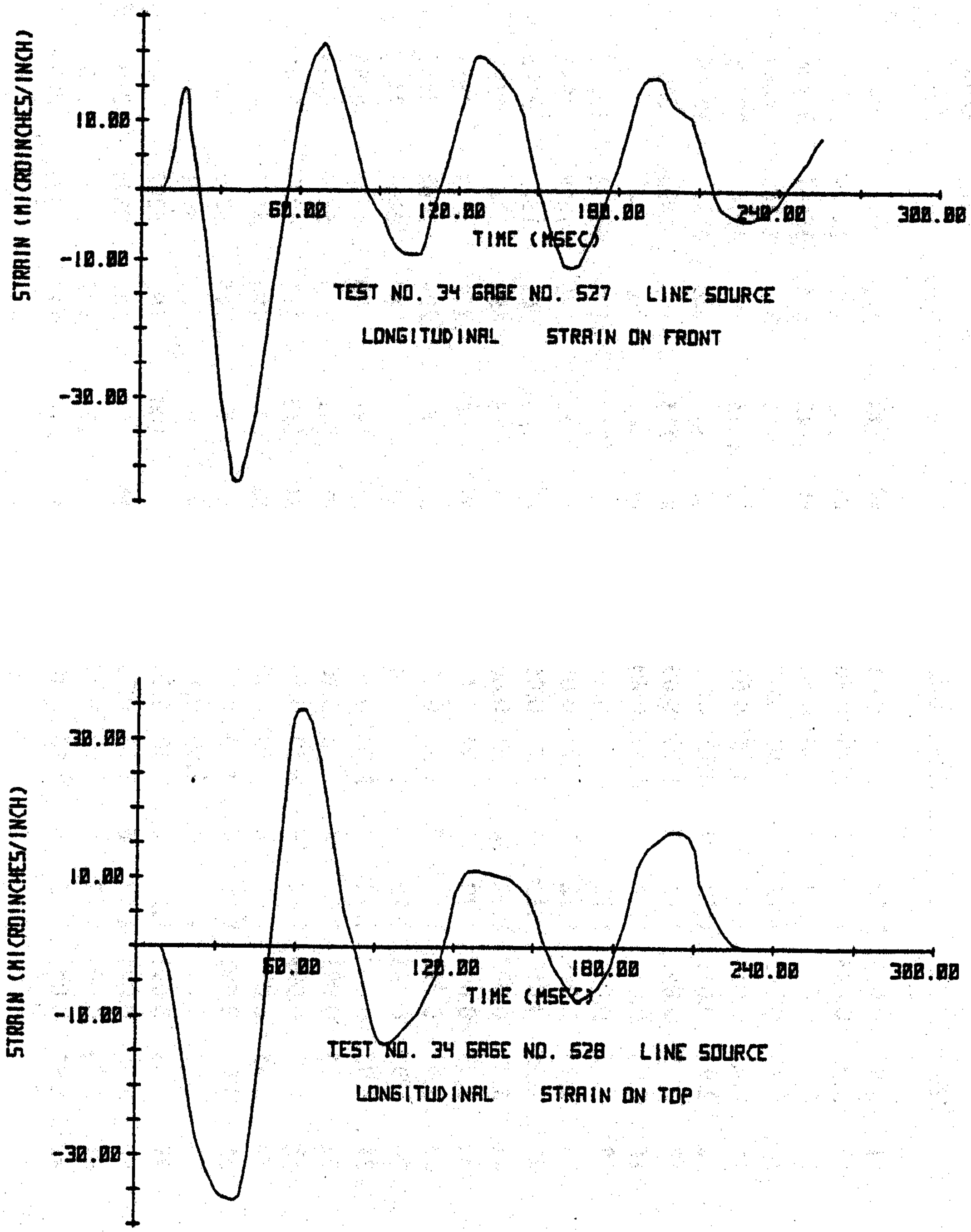

Figure 54. Longitudinal Strains Opposite Nearest Point of Angled-Line Source

Table 9. Pipe Response Data From Line Source Tests

Test Series	Test No.	Pipe O.D. (in.)	h (in.)	n	N1	L1 (ft)	W1 (lb)	B (deg)	A (ft)	Maximum Strains Cir	Maximum Strains Long	Stresses Cir (psi)	Stresses Long (psi)
1	11	5.95	0.093	1.12	7	1.50	0.05	0	5.00	230	239	9780	9985
1	12	5.95	0.093	1.12	7	2.40	0.40	0	8.00	360	285	14442	12740
1	13	5.95	0.093	1.12	7	1.50	0.40	0	5.00	942	825	38561	35906
1	14	5.95	0.093	1.12	7	1.50	0.40	0	5.00	713	850	31380	34489
1	15	2.95	0.059	1.12	7	0.75	0.05	0	2.50	1355	600	49761	32628
1	16	2.95	0.059	1.12	7	0.75	0.05	0	2.50	1395	620	51252	33666
1	17	2.95	0.059	1.12	7	1.50	0.03	0	5.00	115	140	5090	5657
1	18	2.95	0.059	1.12	7	0.90	0.40	0	3.00	--	1780	--	--
1	19	5.95	0.093	1.12	7	0.46	0.03	0	1.50	1750	1304	69413	59292
1	26	2.95	0.059	1.12	7	3.30	0.05	0	8.00	42	48	1828	1965
1	27	2.95	0.059	1.12	7	3.30	0.05	0	8.00	43	61	1987	2396
5	21	5.95	0.093	1.12	4	1.50	0.40	0	15.00	66	83	2947	3333
5	22	5.95	0.093	1.12	7	1.50	0.40	0	15.00	96	121	4289	4856
5	23	5.95	0.093	1.12	7	1.50	0.40	0	10.00	217	209	9067	8886
5	24	5.95	0.093	1.12	7	1.50	0.05	0	10.00	47	60	2107	2402
4	31	5.95	0.093	1.12	4	2.50	0.10	15	5.00	131	170	5900	6785
4	32	5.95	0.093	1.12	4	2.50	0.10	15	5.00	131	165	5851	6623
4	33	5.95	0.093	1.12	4	2.50	0.10	30	5.00	113	131	4937	5346
4	34	5.95	0.093	1.12	4	2.50	0.10	30	5.00	97	104	4156	4315
4	35	5.95	0.093	1.12	4	2.50	0.10	45	5.00	77	76	3235	3213
4	36	5.95	0.093	1.12	4	2.50	0.10	45	5.00	97	85	3971	3699
4	39	5.95	0.093	1.12	6	2.50	0.20	30	10.00	100	107	4282	4441
4	40	5.95	0.093	1.12	6	2.50	0.20	30	10.00	54	61	2344	2503
4	41	5.95	0.093	1.12	6	2.50	0.40	30	10.00	121	122	5109	5132
4	42	5.95	0.093	1.12	6	2.50	0.40	30	10.00	114	114	4804	4804

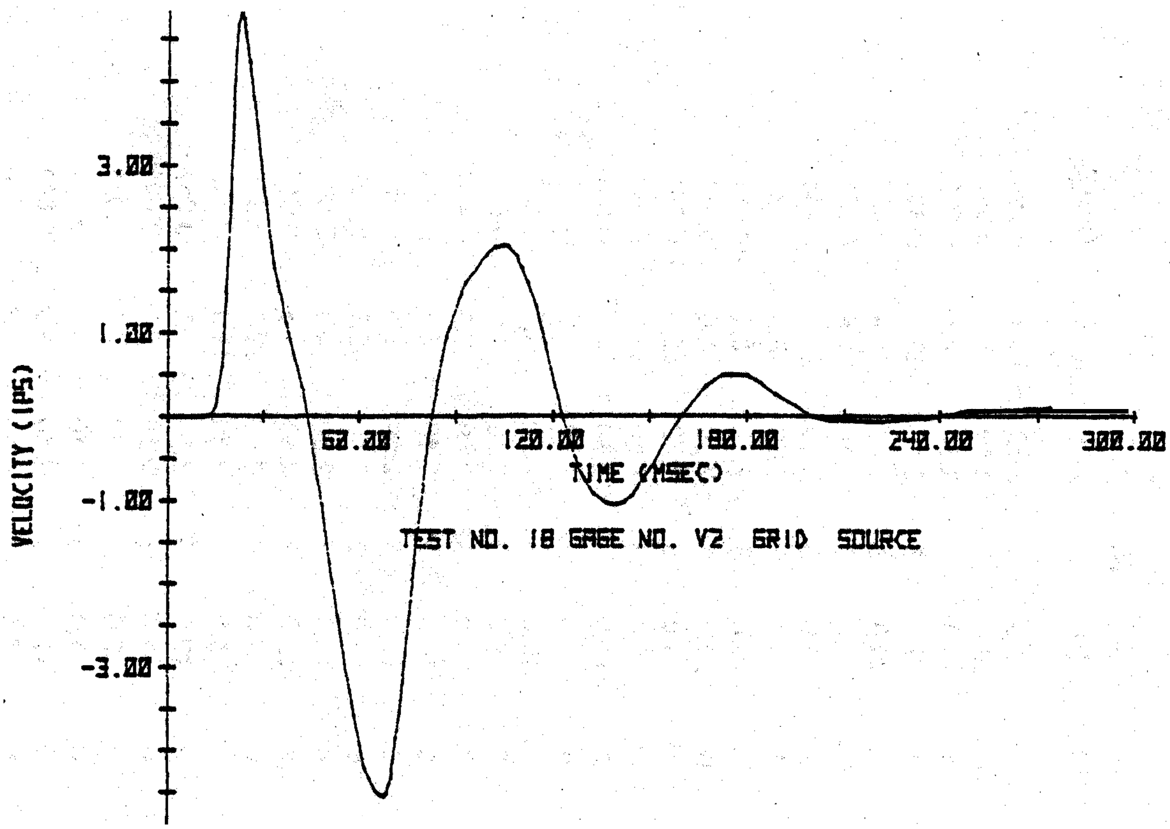

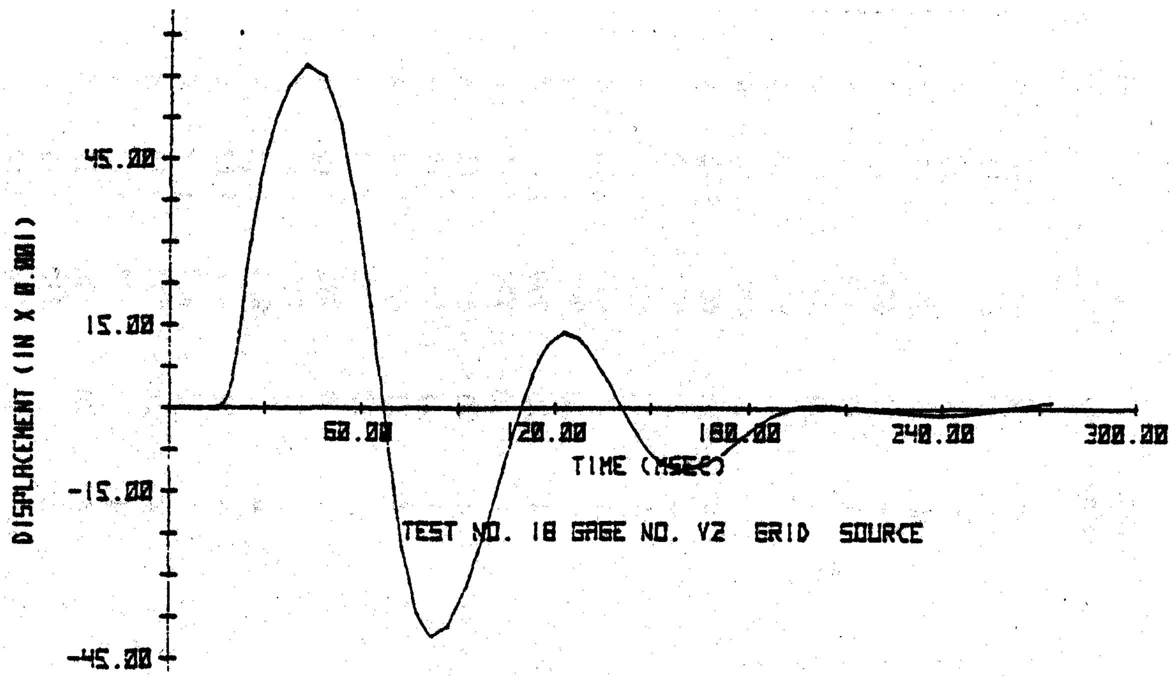

Figure 55. Ground Motions from Grid-Explosive Source

Table 10. Ground Motion Data From Grid Tests

Test Series	Test No.	c (fps)	n	N1	L1 (ft)	W1 (lb)	B (deg)	A (ft)	N2	L2 (ft)	U (ips)	X (in.)
4	12	851	1.12	4	2.50	0.20	0	5.0	3	2.50	15.3	0.299
4	12	851	1.12	4	2.50	0.20	0	10.0	3	2.50	5.0	0.068
4	12	851	1.12	4	2.50	0.20	0	20.0	3	2.50	1.5	0.019
4	13	676	1.12	4	2.50	0.20	0	5.0	3	2.50	20.2	0.332
4	13	676	1.12	4	2.50	0.20	0	10.0	3	2.50	5.8	0.088
4	13	676	1.12	4	2.50	0.20	0	20.0	3	2.50	1.5	0.023
4	14	651	1.12	4	2.50	0.20	0	5.0	3	2.50	24.5	0.448
4	14	651	1.12	4	2.50	0.20	0	5.0	3	2.50	18.5	0.434
4	14	651	1.12	4	2.50	0.20	0	10.0	3	2.50	6.1	0.091
4	14	651	1.12	4	2.50	0.20	0	20.0	3	2.50	1.0	0.013
4	15	637	1.12	4	2.50	0.20	0	5.0	3	2.50	16.1	0.353
4	15	637	1.12	4	2.50	0.20	0	5.0	3	2.50	32.2	0.432
4	15	637	1.12	4	2.50	0.20	0	10.0	3	2.50	4.5	0.068
4	20	799	1.12	4	2.50	0.10	0	5.0	3	2.50	12.6	0.132
4	20	799	1.12	4	2.50	0.10	0	10.0	3	2.50	5.7	0.073
4	20	799	1.12	4	2.50	0.10	0	15.0	3	2.50	2.0	0.023
4	21	655	1.12	4	2.50	0.10	0	5.0	3	2.50	9.3	0.110
4	21	655	1.12	4	2.50	0.10	0	10.0	3	2.50	4.0	0.056
4	21	655	1.12	4	2.50	0.10	0	15.0	3	2.50	1.5	0.020
4	22	712	1.12	4	2.50	0.10	0	5.0	3	2.50	8.7	0.107
4	22	712	1.12	4	2.50	0.10	0	10.0	3	2.50	4.4	0.057
4	22	712	1.12	4	2.50	0.10	0	15.0	3	2.50	1.5	0.016
4	23	808	1.12	4	2.50	0.10	0	3.0	3	2.50	17.1	0.217
4	23	808	1.12	4	2.50	0.10	0	5.0	3	2.50	11.1	0.146
4	23	808	1.12	4	2.50	0.10	0	10.0	3	2.50	3.8	0.052
4	24	773	1.12	4	2.50	0.10	0	5.0	3	2.50	7.7	0.095
4	24	773	1.12	4	2.50	0.10	0	10.0	3	2.50	4.7	0.058
4	25	738	1.12	4	2.50	0.10	0	5.0	3	2.50	4.2	0.041
4	25	738	1.12	4	2.50	0.10	0	10.0	3	2.50	3.2	0.032
4	26	598	1.12	4	2.50	0.10	0	7.5	3	2.50	5.4	0.060

Table 10. Ground Motion Data From Grid Test (Cont'd)

Test Series	Test No.	c (fps)	n	N1	L1 (ft)	W1 (lb)	B (deg)	A (ft)	N2	L2 (ft)	U (ips)	X (in.)
4	26	598	1.12	4	2.50	0.10	0	12.5	3	2.50	3.5	0.039
4	27	839	1.12	4	2.50	0.10	0	5.0	3	2.50	12.2	0.138
4	27	839	1.12	4	2.50	0.10	0	10.0	3	2.50	5.6	0.062
4	28	730	1.12	4	2.50	0.10	0	5.0	3	2.50	4.3	0.060
4	28	730	1.12	4	2.50	0.10	0	10.0	3	2.50	2.3	0.027
4	29	731	1.12	4	2.50	0.30	0	10.0	3	2.50	4.7	0.110
4	29	731	1.12	4	2.50	0.30	0	20.0	3	2.50	2.5	0.030
4	29	731	1.12	4	2.50	0.30	0	25.0	3	2.50	1.8	0.024
4	30	863	1.12	4	2.50	0.30	0	10.0	3	2.50	15.2	0.165
4	30	863	1.12	4	2.50	0.30	0	20.0	3	2.50	3.3	0.038
4	30	863	1.12	4	2.50	0.30	0	25.0	3	2.50	3.2	0.042
4	37	759	1.12	4	2.50	0.30	0	10.0	3	2.50	9.6	0.089
4	37	759	1.12	4	2.50	0.30	0	10.0	3	2.50	7.6	0.159
4	37	759	1.12	4	2.50	0.30	0	20.0	3	2.50	2.9	0.031
4	37	759	1.12	4	2.50	0.30	0	25.0	3	2.50	1.3	0.016
5	13	755	1.12	4	2.50	0.15	0	5.0	3	2.50	8.2	0.121
5	13	755	1.12	4	2.50	0.15	0	10.0	3	2.50	3.9	0.053
5	13	755	1.12	4	2.50	0.15	0	15.0	3	2.50	2.0	0.025
5	16	717	1.12	4	2.50	0.30	0	5.0	3	2.50	14.0	0.199
5	17	864	1.12	4	4.00	0.20	0	4.0	3	4.00	25.6	0.284
5	17	864	1.12	4	4.00	0.20	0	8.0	3	4.00	12.6	0.136
5	17	864	1.12	4	4.00	0.20	0	12.0	3	4.00	7.7	0.080
5	18	738	1.12	4	1.50	0.05	0	2.0	3	1.50	22.6	0.244
5	18	738	1.12	4	1.50	0.05	0	4.0	3	1.50	10.0	0.128
5	18	738	1.12	4	1.50	0.05	0	8.0	3	1.50	2.0	0.030
5	19	835	1.12	4	2.50	0.10	0	5.0	3	2.50	7.9	0.089
5	20	826	1.12	4	2.50	0.10	0	5.0	3	2.50	7.6	0.082
4	16	617	1.12	4	2.50	0.20	30	7.0	3	2.50	6.4	0.074
4	16	617	1.12	4	2.50	0.20	30	10.0	3	2.50	3.8	0.055
4	16	617	1.12	4	2.50	0.20	30	17.0	3	2.50	2.0	0.023

Table 10. Ground Motion Data From Grid Tests (Cont'd)

Test Series	Test No.	c (fps)	n	N1	L1 (ft)	W1 (lb)	B (deg)	A (ft)	N2	L2 (ft)	U (ips)	X (in.)
4	17	612	1.12	4	2.50	0.20	30	7.0	3	2.50	5.7	0.064
4	17	612	1.12	4	2.50	0.20	30	10.0	3	2.50	3.5	0.049
4	17	612	1.12	4	2.50	0.20	30	17.0	3	2.50	1.8	0.023
4	18	718	1.12	4	2.50	0.20	30	7.0	3	2.50	7.9	0.086
4	18	718	1.12	4	2.50	0.20	30	10.0	3	2.50	4.8	0.062
4	18	718	1.12	4	2.50	0.20	30	17.0	3	2.50	1.8	0.027
4	19	716	1.12	4	2.50	0.20	30	10.0	3	2.50	3.2	0.039
4	19	716	1.12	4	2.50	0.20	30	17.0	3	2.50	1.1	0.017
4	24	773	1.12	4	2.50	0.10	30	5.0	3	2.50	7.1	0.084
4	24	773	1.12	4	2.50	0.10	30	10.0	3	2.50	2.7	0.031
4	25	738	1.12	4	2.50	0.10	30	5.0	3	2.50	2.5	0.032
4	25	738	1.12	4	2.50	0.10	30	10.0	3	2.50	1.2	0.015
4	26	598	1.12	4	2.50	0.10	30	7.2	3	2.50	4.4	0.049
4	26	598	1.12	4	2.50	0.10	30	12.2	3	2.50	1.6	0.018
4	27	839	1.12	4	2.50	0.10	30	5.0	3	2.50	6.3	0.069
4	27	839	1.12	4	2.50	0.10	30	10.0	3	2.50	2.2	0.027
4	28	730	1.12	4	2.50	0.10	30	5.0	3	2.50	2.5	0.031
4	28	730	1.12	4	2.50	0.10	30	10.0	3	2.50	0.8	0.012
5	15	738	1.12	4	2.50	0.15	30	3.5	3	2.50	10.5	0.142
5	15	738	1.12	4	2.50	0.15	30	5.0	3	2.50	5.8	0.082
5	15	738	1.12	4	2.50	0.15	30	10.0	3	2.50	3.1	0.039
5	16	717	1.12	4	2.50	0.30	30	3.5	3	2.50	17.8	0.223
5	16	717	1.12	4	2.50	0.30	30	5.0	3	2.50	11.1	0.153
5	16	717	1.12	4	2.50	0.30	30	10.0	3	2.50	5.5	0.079
5	19	835	1.12	4	2.50	0.10	15	3.0	3	2.50	11.3	0.117
5	19	835	1.12	4	2.50	0.10	15	5.0	3	2.50	6.1	0.075
5	19	835	1.12	4	2.50	0.10	15	10.0	3	2.50	3.0	0.035
5	20	826	1.12	4	2.50	0.10	45	3.0	3	2.50	8.0	0.083
5	20	826	1.12	4	2.50	0.10	45	5.0	3	2.50	2.4	0.027
5	20	826	1.12	4	2.50	0.10	45	10.0	3	2.50	0.7	0.006

In these grid experiments, strain measurements were made around the pipe primarily at a location opposite the geometric center of the explosive grid as shown in Figures 9 and 10. At strain gage location No. 1, measurements were made mostly on the front, top, and back since the explosive grids were again buried to the same depth as the pipe. Additional strain measurements were made at other sensing locations in an effort to record the maximum circumferential and longitudinal strains. Examples of strain-time data measured at the primary sensing locations arc shown in Figures 56 and 57 for an explosive grid parallel to the model pipe. Note that as the explosive geometry gets more complex, the character of the strain data traces also increases in complexity, especially in the longitudinal direction. This implies that the forcing function produced by the parallel grid sources excited the model pipe into different modes as compared to the point and line sources. This is reflected by the character of the strain records.

For some of the parallel grid tests, strains recordings were also made at locations Nos. 2, 3, and 4 (see Figure 9) to determine how the longitudinal strain on the front of the pipe varied at other locations away from the primary one. Examples of the results are shown in Figure 58. Looking at these three traces along with the front trace from Figure 57, one can observe that at a time of 32 msec, the peak strain at location No. 1 is 196 µin./in. compressive. At the same time, the gage at location No. 2 registered 20 µin./in. tensile, the gage at location No. 3 registered 152 µin./in. tensile, and the gage at location No. 4 measured 160 µin./in. tensile. Similar amplitude and phase comparisons can be made at other time increments.

For an angled-grid test, examples of strain traces recorded from gages at the primary measurement location are presented in Figures 59 and 60. As was the case with the parallel grid experiments, the data traces from angled-grid tests are considerably more complex and less symmetric than those from point sources.

The maximum stresses computed from the measured peak strains for each of the grid tests are shown in Table 11. The table also lists some of the pipe information and description. Together with Table 3 in Section II, this table defines every grid test and tabulates the stress data. These grid stress data are used in Section VIII to develop the methodology for simplifying these complex geometries into an equivalent parallel line or point source such that the point and parallel line stress equations can be used to estimate pipe stresses for the complex explosive geometries.

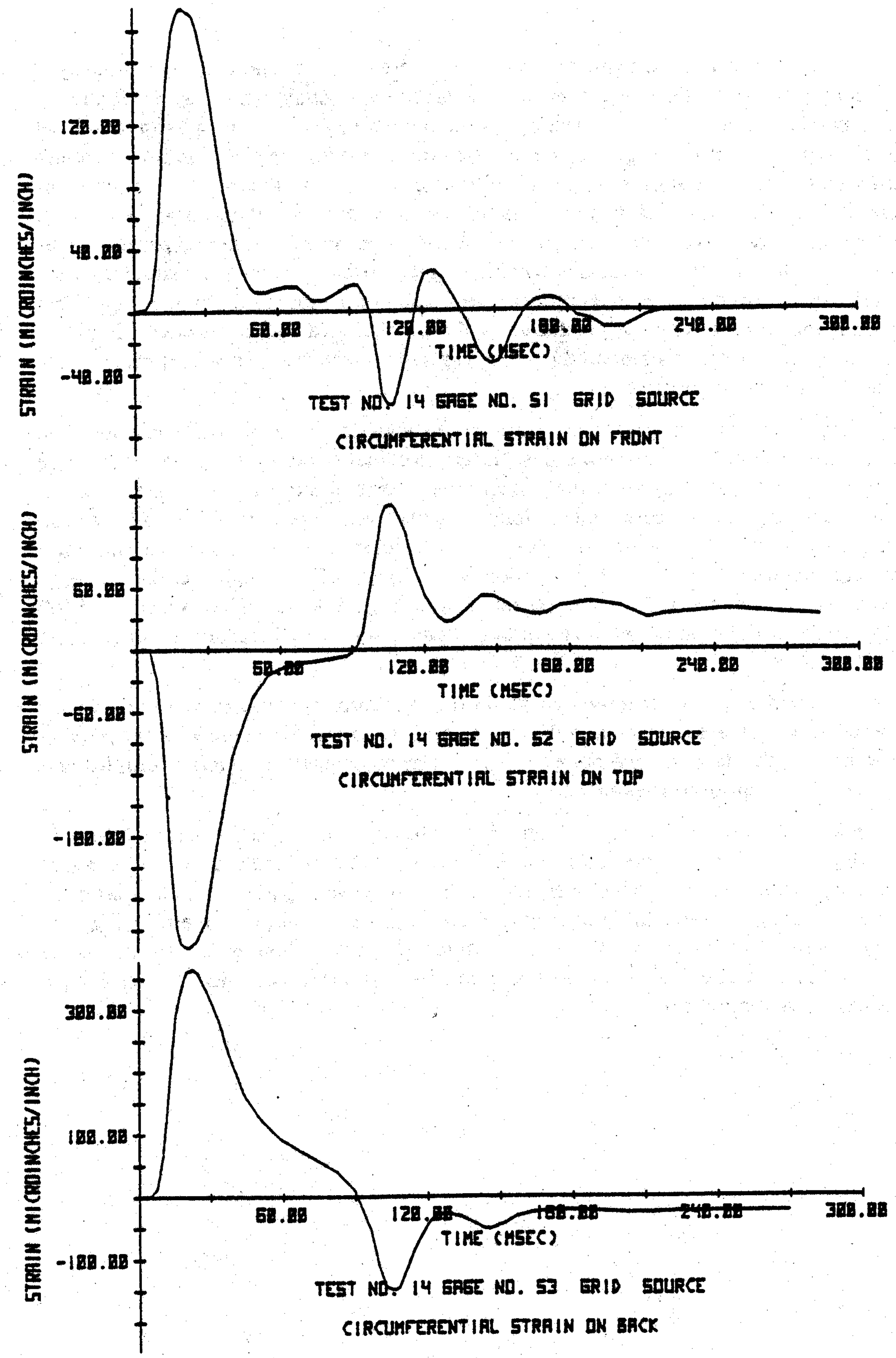

Figure 56. Primary Circumferential Strains from Parallel Grid Source

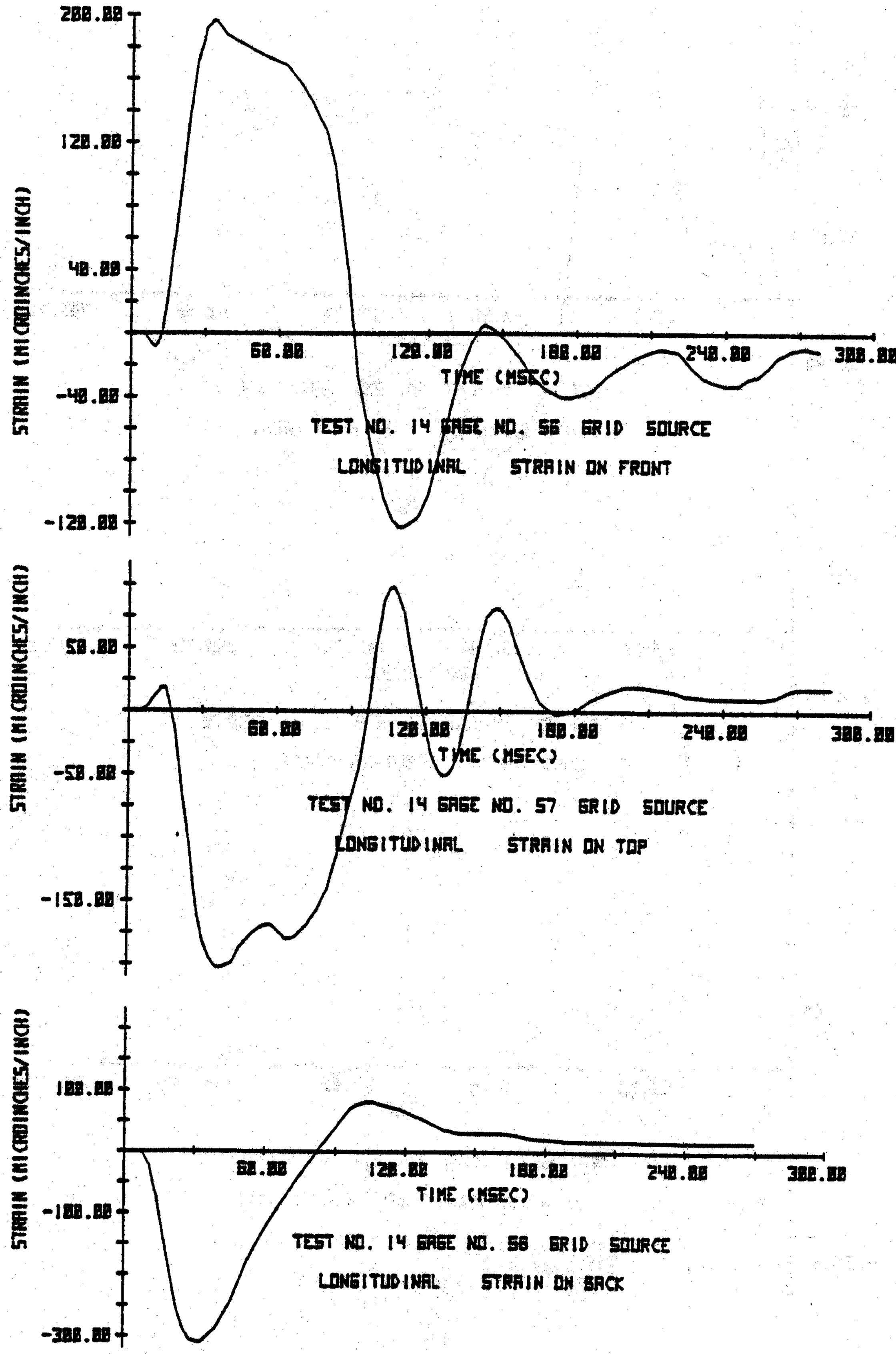

Figure 57. Primary Longitudinal Strains from Parallel Grid Source

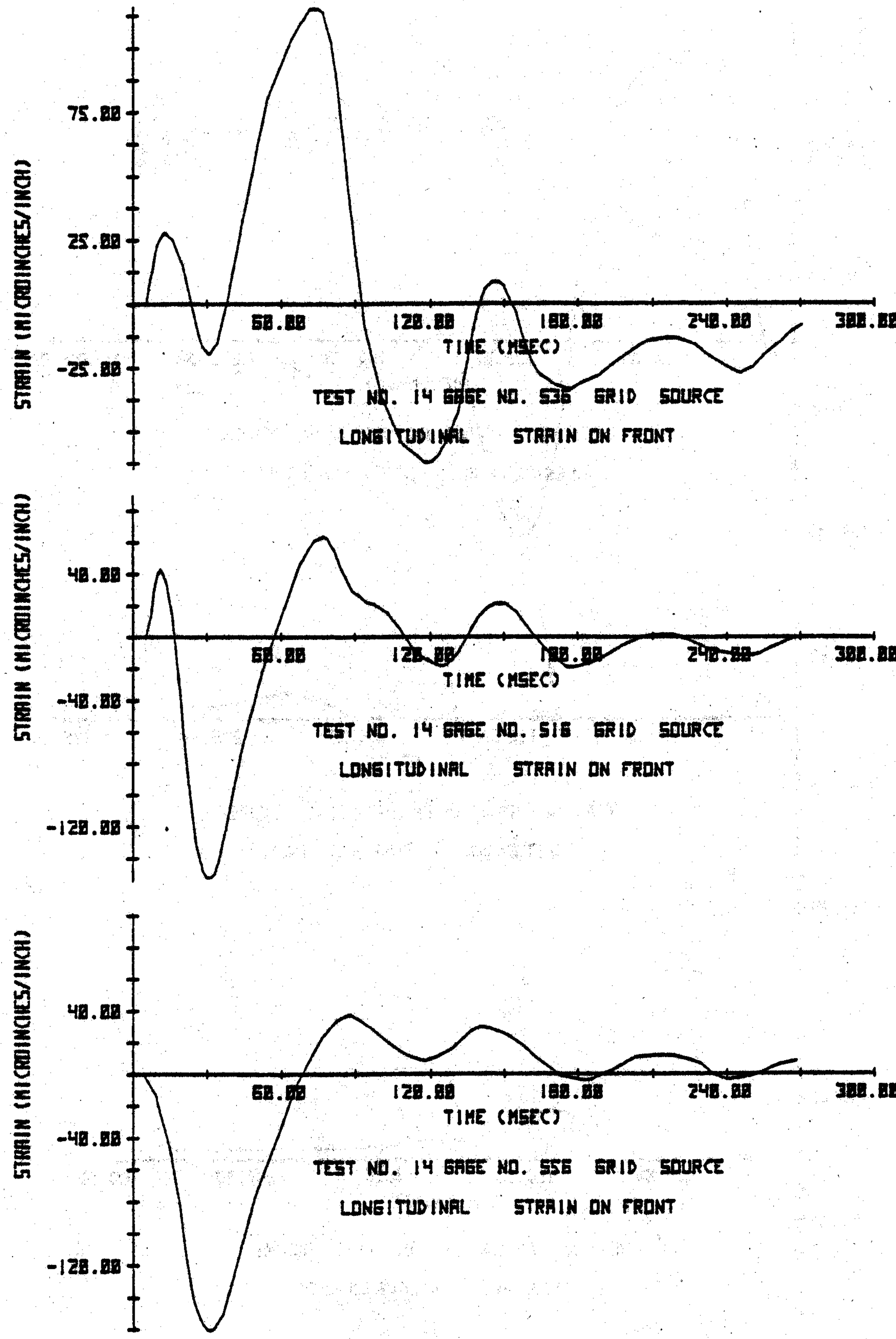

Figure 58. Longitudinal Strains on Front of Pipe at Other Strain Locations

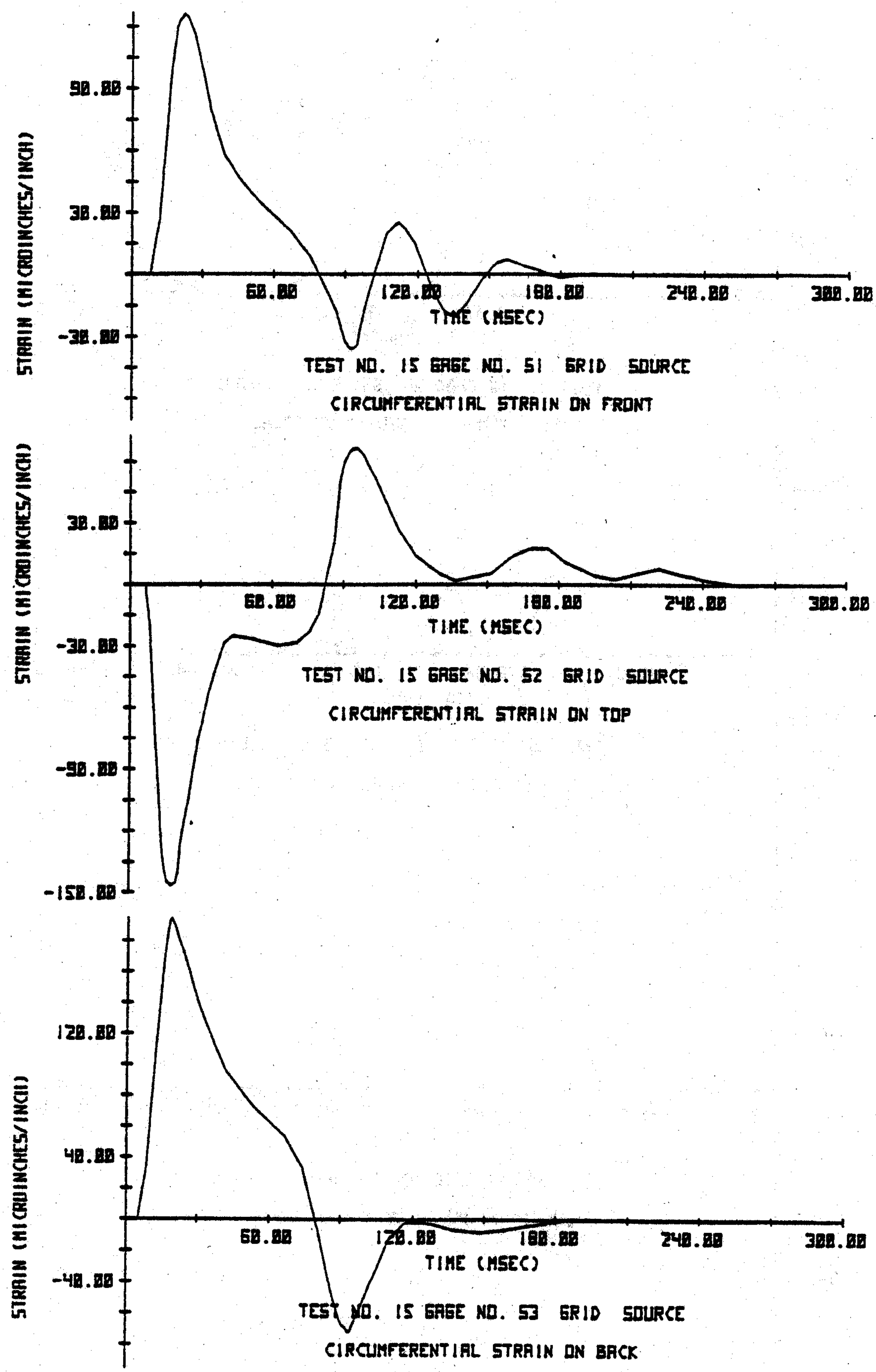

Figure 59. Primary Circumferential Strains from Angled-Grid Source

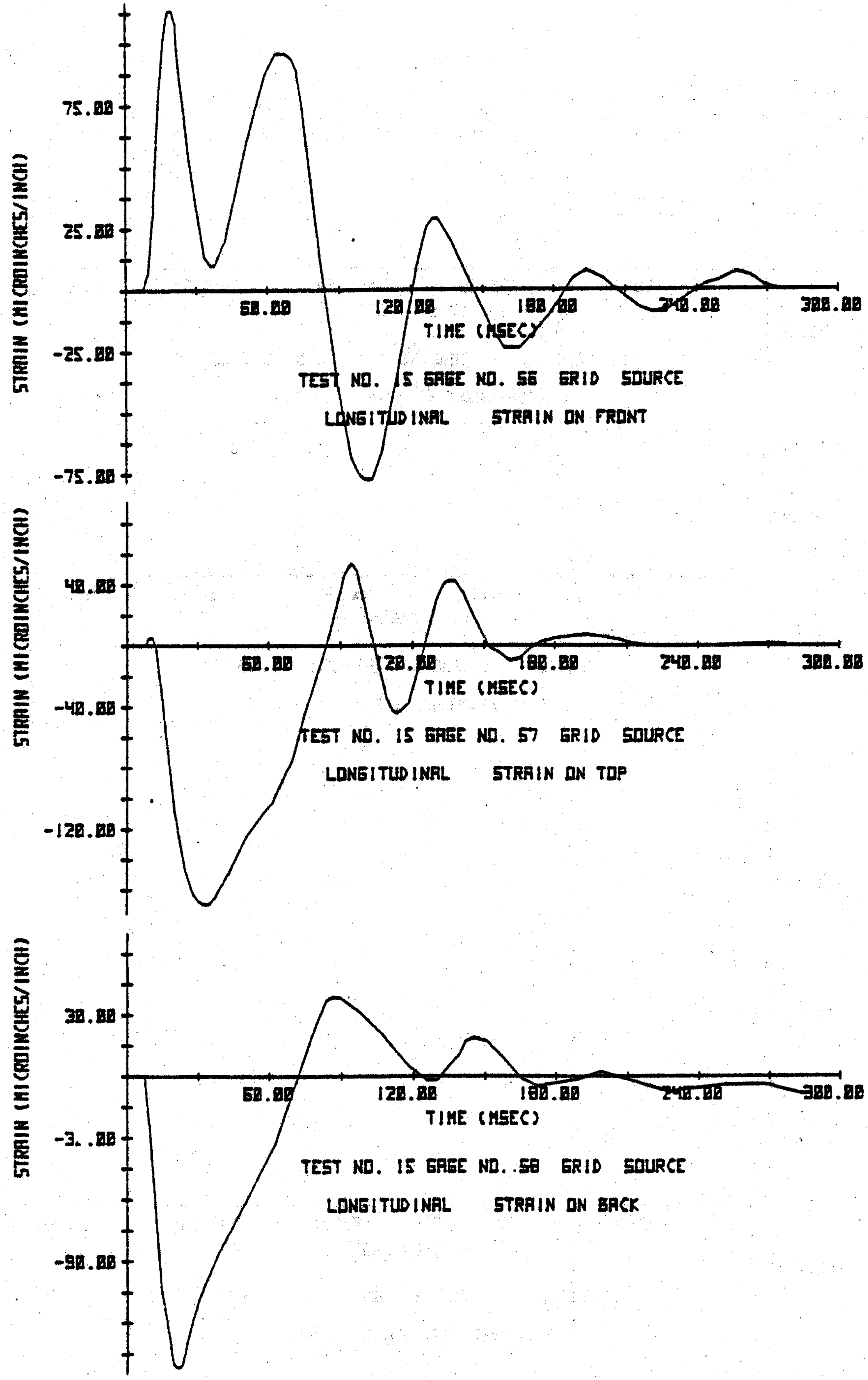

Figure 60. Primary Longitudinal Strains from Angled-Grid Source

Table 11. Pipe Response Data From Grid Source Tests

Test Series	Test No.	Pipe O.D. (in.)	h (in.)	n	N1	L1 (ft)	W1 (lb)	B (deg)	A (ft)	N2	L2 (ft)	Maximum Strains Cir	Maximum Strains Long	Stresses Cir (psi)	Stresses Long (psi)
4	12	5.95	0.093	1.12	4	2.50	0.20	0	10.00	3	2.50	98	108	4227	4454
4	13	5.95	0.093	1.12	4	2.50	0.20	0	10.00	3	2.50	128	120	5316	5135
4	14	5.59	0.093	1.12	4	2.50	0.20	0	10.00	3	2.50	124	110	5090	4772
4	15	5.95	0.093	1.12	4	2.50	0.20	0	10.00	3	2.50	133	148	5751	6091
4	20	5.95	0.093	1.12	4	2.50	0.10	0	5.00	3	2.50	265	183	10370	8510
4	21	5.95	0.093	1.12	4	2.50	0.10	0	5.00	3	2.50	265	178	10322	8348
4	22	5.95	0.093	1.12	4	2.50	0.10	0	5.00	3	2.50	263	163	10111	7842
4	23	5.95	0.093	1.12	4	2.50	0.10	0	3.00	3	2.50	387	248	14957	11803
4	29	5.95	0.093	1.12	4	2.50	0.30	0	20.00	3	2.50	79	68	3222	2973
4	30	5.95	0.093	1.12	4	2.50	0.30	0	20.00	3	2.50	57	41	2247	1883
4	37	5.95	0.093	1.12	4	2.50	0.30	0	20.00	3	2.50	53	51	2214	2169
5	13	5.95	0.093	1.12	4	2.50	0.15	0	5.00	3	2.50	221	227	9372	9508
5	14	5.95	0.093	1.12	4	2.50	0.30	0	5.00	3	2.50	365	311	14857	13632
5	17	5.95	0.093	1.12	4	4.00	0.20	0	8.00	3	4.00	102	87	4153	3812
5	18	5.95	0.093	1.12	4	1.50	0.05	0	4.00	3	1.50	178	158	7307	6853
4	16	5.95	0.093	1.12	4	2.50	0.20	30	10.00	3	2.50	74	76	3138	3183
4	17	5.95	0.093	1.12	4	2.50	0.20	30	10.00	3	2.50	75	83	3239	3420
4	18	5.95	0.093	1.12	4	2.50	0.20	30	10.00	3	2.50	77	56	3041	2564
4	19	5.95	0.093	1.12	4	2.50	0.20	30	10.00	3	2.50	51	59	2227	2409
4	24	5.95	0.093	1.12	4	2.50	0.10	30	5.00	3	2.50	112	80	4409	3683
4	25	5.95	0.093	1.12	4	2.50	0.10	30	5.00	3	2.50	98	69	3848	3190
4	26	5.95	0.093	1.12	4	2.50	0.10	30	5.00	3	2.50	128	79	4918	3806
4	27	5.95	0.093	1.12	4	2.50	0.10	30	5.00	3	2.50	105	59	3978	2934
4	28	5.95	0.093	1.12	4	2.50	0.10	30	5.00	3	2.50	115	119	4885	4976
5	15	5.95	0.093	1.12	4	2.50	0.15	30	3.50	3	2.50	194	170	7942	7398
5	16	5.95	0.093	1.12	4	2.50	0.30	30	3.50	3	2.50	324	264	13071	11709
5	19	5.95	0.093	1.12	4	2.50	0.10	15	5.00	3	2.50	91	87	3796	3705
5	20	5.95	0.093	1.12	4	2.50	0.10	45	5.00	3	2.50	52	65	2318	2613

V. GROUND MOTION RELATIONSHIPS

Introduction

New empirical relationships were developed for predicting maximum radial soil velocity and displacement when buried explosive charges are detonated in soil or rock. These relationships are needed because the ground motion defines the forcing function applied to a buried pipe from blasting. In addition, some state laws have at times limited blasting near pipelines based on a maximum particle velocity criteria.

The seismic wave propagation problem for point and parallel line sources was solved by creating the three pi terms derived in the model analysis of Section II, empirical observation to combine two of these pi terms, and a vast quantity of test data from the literature and tests conducted in this study to interrelate energy release and standoff distance to the resulting scaled ground motions.

General ground motion equations for point sources were developed using data from tests that used explosive sources ranging from 0.03 lb to 19.2 kiloton (nuclear blast equivalent). Over a more limited range suitable, for pipeline applications, simpler log-linear equations were also derived. For parallel, line sources, data were available primarily from this program and log-linear equations were fitted to the test data to define the functional relationships developed in the model analysis for line sources.

The pipe response equations were made less complex if one additional simplification was made to the displacement prediction equation as pointed out in the next section of this report. Therefore, the displacement solutions for point and parallel line explosive sources were approximated with log-linear relationships having an exponent of unity.

Historical Background

Two different ground shock propagation procedures have been used in the past for empirical relationships interrelating charge weight, standoff distance and ground motion. The first approach, generally used by statisticians, is to propose a propagation law of the form

$$G = CW^{\beta_1} R^{\beta_2} \tag{32}$$

where
- G = the peak amplitude for either velocity or displacement
- β's = constant exponents
- C = constant
- W = charge weight
- R = standoff distance

This format is popular because the logarithm can be taken of both sides to obtain:

$$[\ln G] = [\ln C] + \beta_1 [\ln W] + \beta_2 [\ln R] \tag{33}$$

Because this logarithm equation is linear, a least squares curve fit can be made to obtain the three coefficients 1n C, β_1, and β_2. Using the statistical approach, various investigators obtain different results dependent upon the amount and range of their data and the properties of the specific test site. Typical values of coefficient and exponents found in the literature [Carder and Cloud (1959), Crandell (1960), Habberjam and Whettan (1952), Hudson, et al. (1961), Ito (1953), Morris (1950), Ricker (1940), Teichmarm and Westwater (1957), Thoenen and Windes (1942), and Willis and Wilson (1960)] have a range for β_1 from 0.4 to 1.0 and for β_2 from -1 to -2 with G as particle displacement or velocity.

The weakness of this statistical approach is that this format is assumed regardless of what happens physically. The resulting equations are dimensionally illogical. A serious problem is the statistician's use of an incomplete expression. Other parameters enter the ground shock propagation problem, especially soil properties, which are ignored. Because these properties are ignored, the definition of the problem is incomplete, and the results do not represent a general solution.

The second procedure, used by other investigators, usually those associated with the Atomic Energy Commission, presents particle velocity U and displacement X in the format:

$$U \propto \left(\frac{W^{1/3}}{R}\right)^{\beta_U} \tag{34}$$

$$\left(\frac{X}{W^{1/3}}\right) \propto \left(\frac{W^{1/3}}{R}\right)^{\beta_X} \tag{35}$$

This approach is an extension of the scaling law for air blast waves [Hopkinson (1915) and Cranz (1926)], and is a dimensional version of a model analysis. If soil properties such as ρ and c are treated as constants and dropped from the resulting pi terms in a model analysis, the dimensional versions as presented in Equations (34) and (35) are obtained. An example of curve fits for velocity and displacement to Equations (34) and (35) is given by Murphey (1961).

$$\frac{U\ R^{1.65}}{W^{0.55}} = \text{constant} \tag{36}$$

$$\frac{X\ R^{1.5}}{W^{0.833}} = \text{constant} \tag{37}$$

Murphey's data were all obtained for chemical explosive detonations in Halite (salt domes) and cover scaled charge weight over three orders of magnitude. The authors certainly agree with Murphey and other AEC investigators on using modeling principles. Their curve fits were expanded in this research effort by including data obtained in this program to extend the range over nine orders of magnitude and by including an additional parameter.

Problems With the Conventional Modeling Approach

If the soil properties ρ and c are listed in a model analysis together with the explosive energy release W,, standoff distance R, and either of the response parameters U or X, then two dimensionless pi terms are obtained for either displacement or velocity as in the following functional relationships:

$$\frac{X}{R} = f_X\left(\frac{W_e}{\rho c^2 R^3}\right) \tag{38}$$

$$\frac{U}{c} = f_U\left(\frac{W_e}{\rho c^2 R^3}\right) \tag{39}$$

Experienced modelers can readily see that with ρ and c considered as invariant, these equations amount to Equations (36) and (37). No reason exists to presume that the general but unspecified functional format given by Equations (38) and (39) should be log linear. The functional format can be obtained by nondimensionalizing experimental test data and plotting the results provided the analysis is completely defined.

Figures 61 and 62 are plots of scaled displacement and scaled velocity using limited amounts of test data from chemical explosive detonations. The displacement data seen in Figure 61 come from only two sources, Murphey (1961) and the test results obtained in the first test series of this program at the SwRI test site. Murphey (1961) describes two types of Halite experiments. In one group of tests, the soil is in contact with the explosive charge. In another group of tests, 6 to 15 ft radius cavities placed an air gap between the soil and the explosive charge. These tests described by Murphey and called "Cowboy" used 200-, 500-, and 1000-lb charges. The tests conducted by SwRI were in silty clay soils with various moisture contents. The charges ranged from 0.03 to 1.00 lb of explosive. Although more data could be plotted in Figure 61, correlation will not occur. Obviously, some phenomena are present in Figure 61 which are not reflected in a solution as given by Equation (38).

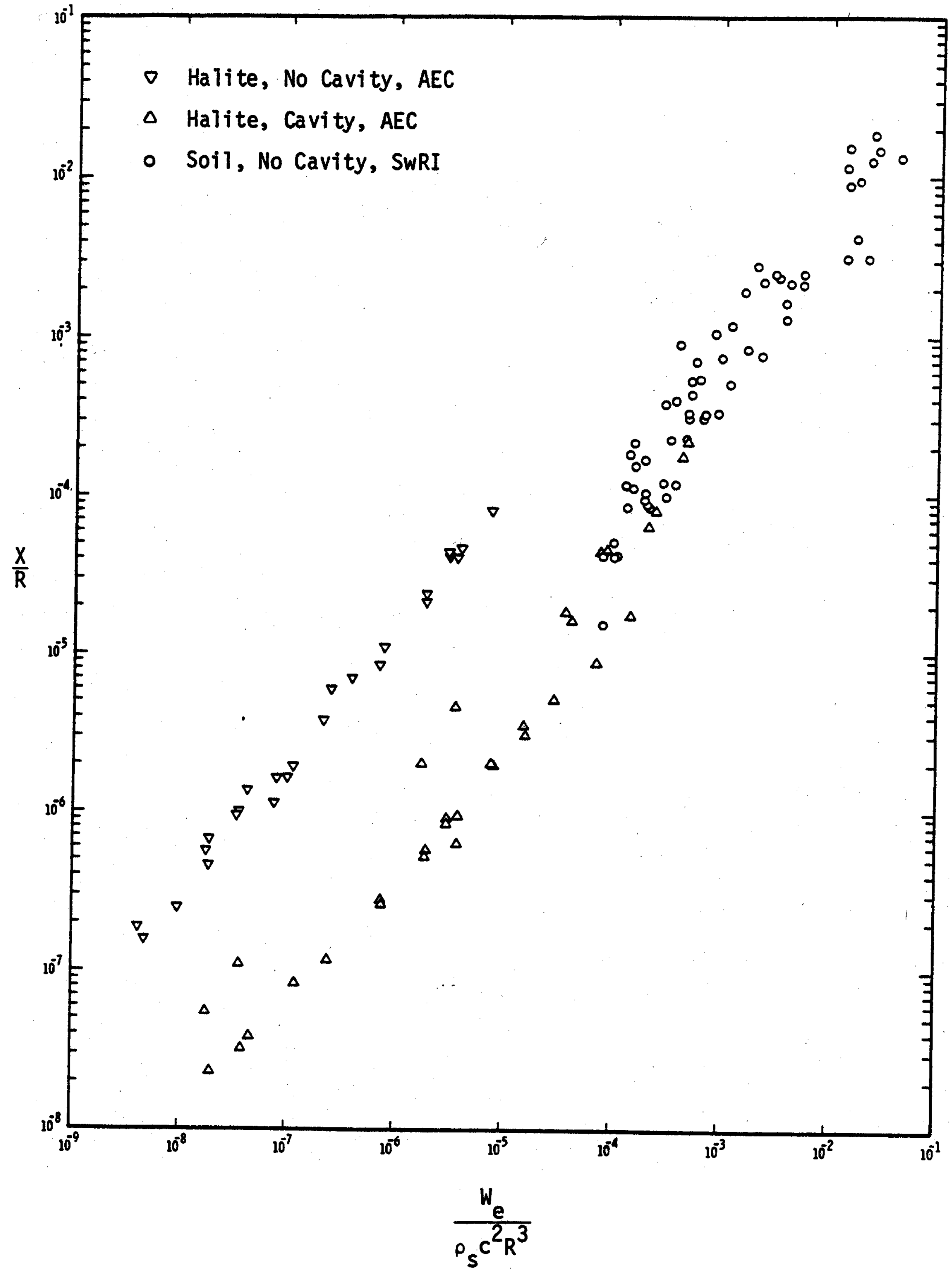

Figure 61. Ground Displacement in Rock and Soil No Coupling

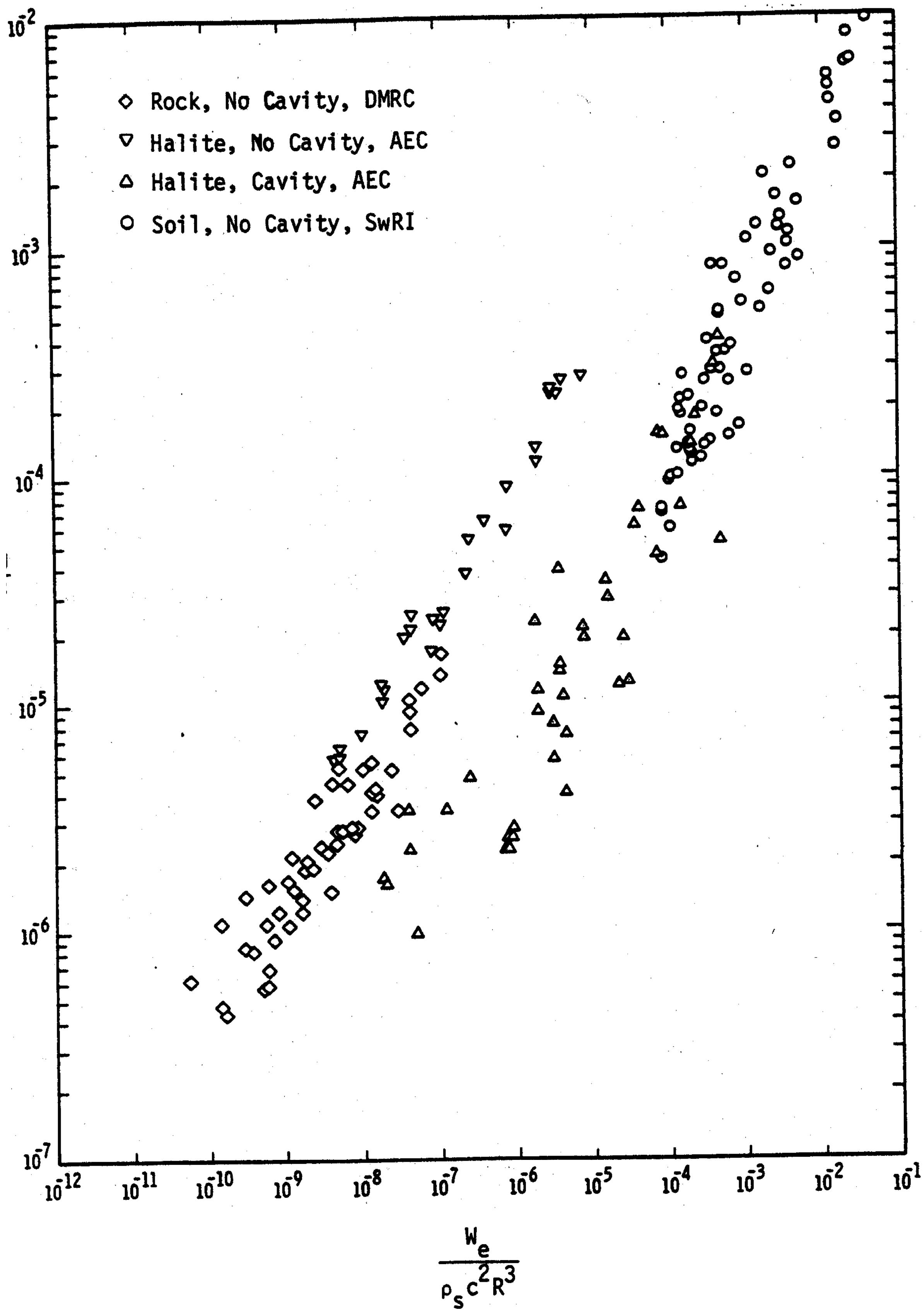

Figure 62. Particle Velocity 'in Rock and Soil No Coupling

The same lack of correlation which became apparent in Figure 61 for soil displacement is also apparent in Figure 62 for peak soil particle velocity. An additional compilation of data not contained in Figure 61 has been included in the Figure 62 velocity plot. Harry Nicholls, et al. (1971) summarize velocities obtained from blasting in stone quarries. If only the single explosive source detonations are used in this compilation, approximately 50 data points can be obtained for a variety of charge weights, site locations and standoff distances. In addition to these new data, the peak particle velocity data corresponding to halite, both with and without cavity, and SwRI soil test results are included in Figure 62.

Although the data in both Figures 61 and 62 fail to correlate, they do show some systematic tendencies. Increasing values of $(W_e/\rho c^2 R^3)$ result in increasing values of scaled ground motion, and the slopes associated with the various data points are almost identical. The figures infer that some phenomena not included in the analysis should be added. In particular, both figures indicate that a different coupling must exist between different soils or rock and the explosive source. Obviously, the poorest coupling exists when an air gap or cavity separates the transmitting media from the explosive source as in some of Murphey's halite experiments. Figures 61 and 62 show that the resulting ground motions are less for experiments with a cavity in halite. However, a weak rock, such as halite, should have a better coupling than soil when both are in contact with explosives. These figures also indicate that ground motions are greater for detonations in rock than for similar detonations in soil. These results definitely infer that a coupling term should be added to Equations (38) and (39) to achieve better correlation.

Addition of an Impedance Term

The term which was added to both the scaled displacement X/R and the scaled velocity U/c terms was the square root of the soil compressibility relative to a standard compressibility, the compressibility of air. This quantity $(\rho c^2/p_o)$ was divided into the non-dimensionalized ground motions to obtain the functional equations, (40) and (41).

$$\left(\frac{p_o}{\rho c^2}\right)^{0.5} = f_X\left(\frac{W_e}{\rho c^2 R^3}\right) \tag{40}$$

$$\frac{U}{c}\left(\frac{p_o}{\rho c^2}\right)^{0.5} = f_U\left(\frac{W_e}{\rho c^2 R^3}\right) \tag{41}$$

Creation of the terms (X/R) $(p_o/\rho c^2)^{0.5}$ and (U/c) $(p_o/\rho c^2)^{0.5}$ was based entirely on empirical observation. A functional format could also be created by plotting the dependent and independent variables in Equations (40) and (41). In addition to using the no cavity data presented in Figures 61 and 62, the ground motion data obtained in this program at the SwRI, Kansas and Kentucky test sites, and additional AEC data from buried nuclear detonations were plotted together using the format shown in Equations (40) and (41). The cavity test results in halite were not replotted because this empirical approach does not account for ground shock propagation when charges are placed in cavities.

The AEC data, which were added, come from Anon., Project Dribble Salmon (1965) and Adams, et al. (1961). Both soil displacement and maximum particle velocity were reported for Project Dribble Salmon, a nuclear blast yield of 5.3 kilotons; hence, these data will appear in both scaled velocity and displacement plots. Adams, et al. (1961) is a summary of displacement and acceleration, but not velocity, for numerous large AEC buried detonations. Maximum scaled displacement data are included for such projects as a 19.2-kiloton detonation named Blanca, a 77-ton detonation named Tamalpais, a 13.5-ton detonation named Mars, a 30-ton detonation named Evans, and a 5.0-kiloton detonation named Logan. For these nuclear shots, the writers are not clear as to whether they mean the radio-chemical yield or the equivalent blast yield. We have assumed that they quoted equivalent blast yields. Test results indicate that for buried nuclear detonations where all the energy can couple into the ground, the radio-chemical yield is more appropriate than the equivalent air blast yield. The radio-chemical yield is twice as great as the equivalent air blast yield, so all of the blast yields listed in this paragraph were doubled before plotting any data points. In addition, the energy W_e had to be converted to foot pounds of energy by multiplying each explosive weight by the appropriate conversion factor, so the quantity $(W_e/\rho c^2 R^3)$ would be nondimensional. The density is a bulk mass (not weight) density, a total density of the media, and c is the seismic P-wave propagation velocity. Other soil data might exist, but only results in which c was measured and reported could be used in this evaluation. Obviously, the gas industry has little interest in nuclear explosions; however, the inclusion of these data emphasizes the broad applicability of this analysis.

Figures 63 and 64, respectively, are plots of the nondimensionalized displacement and nondimensionalized velocity data in the form given by Equations (40) and (41). Because the data appear to collapse into a unique function, these results give a graphical solution. Scatter does exist; however, no experiments or test site appears to yield systematic errors. The range in any test condition is larger than ranges in any previous ground shock propagation reports. The scaled charge weight $(W_e/\rho c^2 R^3)$ ranges over almost ten orders of magnitude. The charge weight itself ranges from 0.03 lb of chemical explosive to the radio-chemical yield of 38.4 kilotons in Blanca, a factor of over two billion. The range in soil or rock densities is small because nature offers only a small variation, but the wave velocity c ranges from approximately 500 fps *to* 15,000 fps, a factor of 30. The soil data measured in this program are at much closer scaled distances to the charge than other results, but the transition does seem to be a continuous one.

The continuous curves in Figures 63 and 64 are approximate fits through the data. points. These radial displacement and radial particle velocity prediction curves for point explosive sources are defined by the following equations:

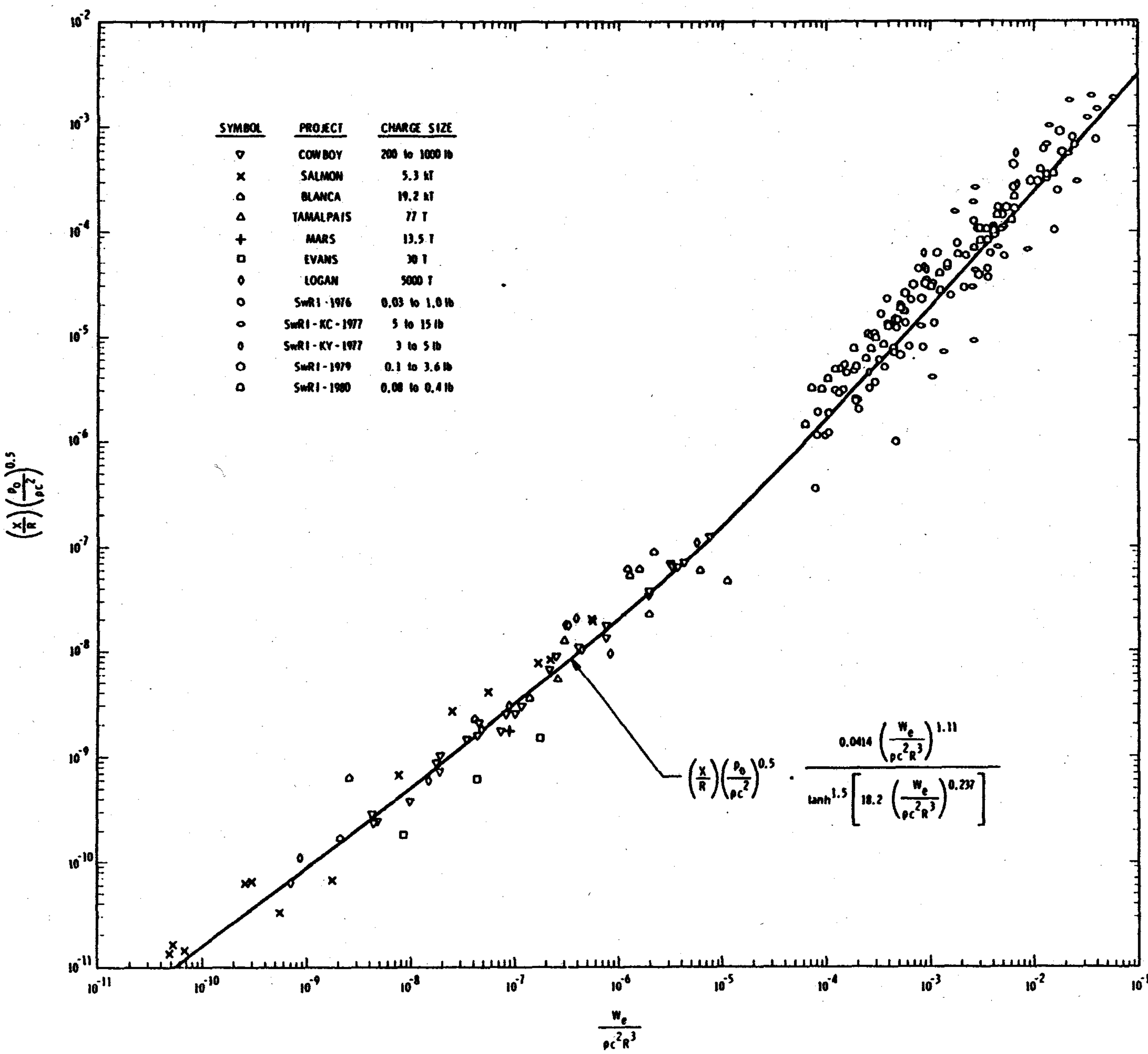

Figure 63. Coupled Radial Displacement in Rock and Soil

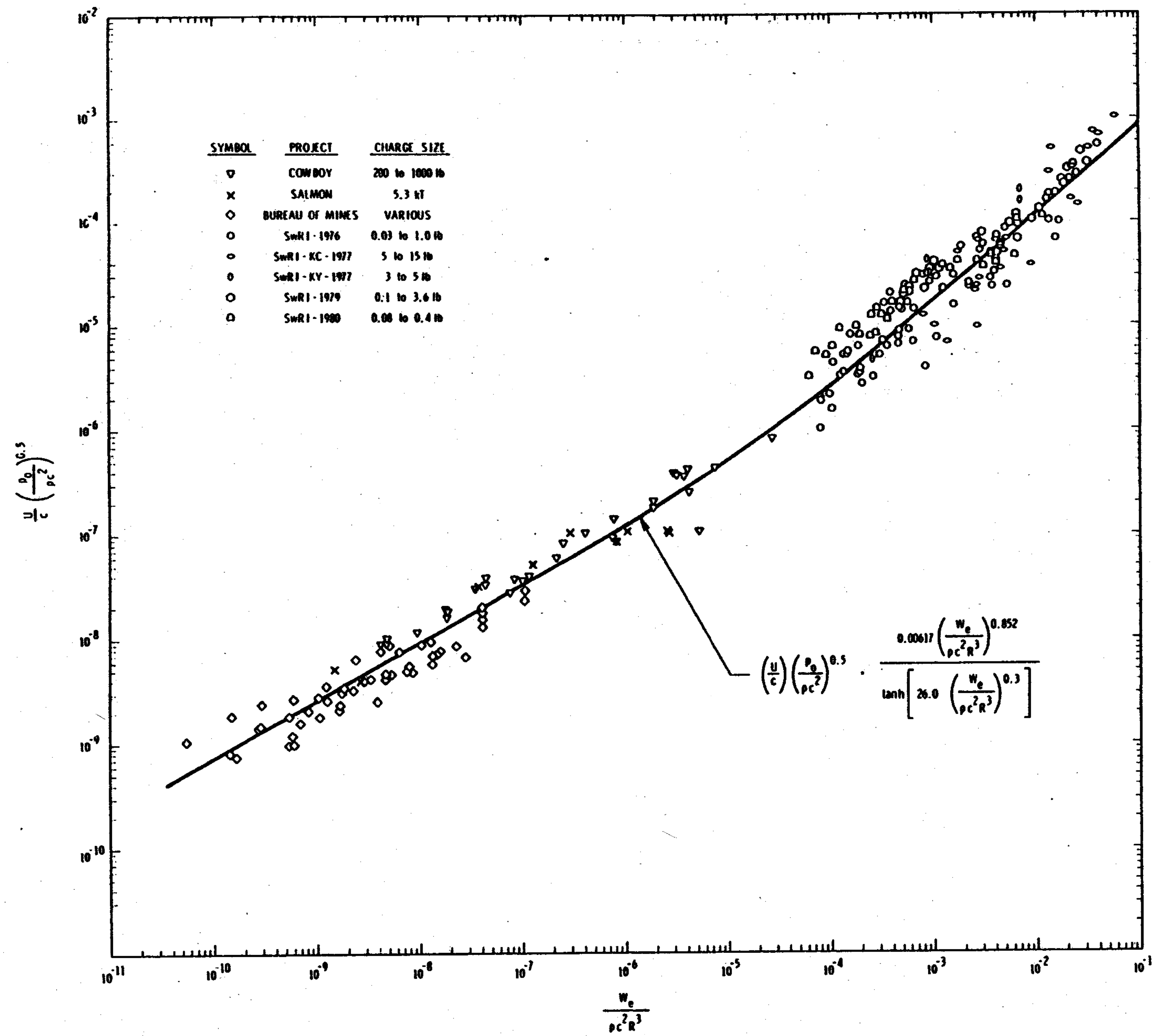

Figure 64. Coupled Radial Particle Velocity in Rock and Soil

$$\frac{X}{R}\left(\frac{p_o}{\rho c^2}\right)^{0.5} = \frac{0.0414\left(\frac{W_e}{\rho c^2 R^3}\right)^{1.11}}{\tanh^{1.5}\left[18.2\left(\frac{W_e}{\rho c^2 R^3}\right)^{0.237}\right]} \tag{42}$$

$$\frac{U}{c}\left(\frac{p_o}{\rho c^2}\right)^{0.5} = \frac{0.00617\left(\frac{W_e}{\rho c^2 R^3}\right)^{0.852}}{\tanh\left[26.0\left(\frac{W_e}{\rho c^2 R^3}\right)^{0.30}\right]} \tag{43}$$

in which

X = peak radial ground displacement (ft)
U = peak radial ground particle velocity (ft/sec)
R = standoff distance (ft)
W_e = explosive energy release (ft-lb)
ρ = mass density of the soil or rock (lb-sec^2/ft^4)
c = seismic P-wave velocity in the soil or rock (ft/sec)
p_o = atmospheric pressure (lb/ft^2)

Note that any consistent set of units can be used in these equations and that each term in these relationships is nondimensional. The estimate of the standard error S of the test data about the fitted curves is approximately ± 50 percent.

Major differences separate these empirical equations from others that predict ground motions. This new procedure is not log linear; test results cover more orders of magnitude, and a coupling term $(\rho c^2/p_o)^{0.5}$ is divided into the scaled displacement and velocity. The presence of atmospheric pressure in the prediction relationships does not mean atmospheric pressure is a physical phenomena influencing the results. The quantity pc^2 is a measure of the compressibility of the shock propagation media. Hence, the quantity p_o is a reference standard (compressibility of air) and introduces empirically relative compressibilities for different media such as soil and rock. Although straight lines can be curve fit to segments of the results in Figures 63 and 64, the rate of change for either X or U with respect to either W or R varies dependent upon the scaled charge weight. These variations are reasonably close to those given by others and discussed in the historical background presented earlier in this section. Closest to the charge where these slopes are greatest, are slightly larger exponents than those which were previously reported; however, the earlier observations did not include data obtained in this research program.

Discussion of Coupling Term

The term $(\rho c^2/p_o)^{0.5}$ which is divided into the scaled velocity term U/c and scaled displacement term X/R is a factor which empirically seems to work. The fact that the compressibility of the soil (ρc^2) is proportional to a modulus of elasticity (E), which in turn is related to the compressibility of air, does not mean that atmospheric pressure is actually a parameter physically entering this problem. If these ground shocks were to be propagated on the moon where essentially no atmosphere exists, the amplitudes of the response would not be infinite as inferred by this solution but rather of some finite amplitude. The atmospheric pressure p_o was just a convenient constant which nondimensionalized ρc^2.

Perhaps p_o enters pore pressure considerations and actually does belong in these calculations; however, this is doubtful. Other parameters which have the dimensions of pressure could be considered, but those parameters would essentially have to be constants in all soils. Examples of possible substitutes for p_o could include: (1) η(the density times the heat of fusion) if one believes significant amounts of energy are dissipated in phase changes, (2) $\rho c_p \theta$ (the heat capacity times an increase in temperature) if thermal heating is important, (3) the energy per unit volume (area under a stress-strain curve) in a hysteresis loop if material damping is important, and (4) others or combinations of all of these effects. No satisfactory explanation has been drawn. The point which makes all hypotheses difficult to accept is that p_o or its counterpart must be essentially constant in all soil and rock tests. A numerical value other than 14.7 psi does not invalidate this solution; a different constant only translates all curves.

Simplified Point Source Equations

The general point source equations derived in the preceding portions of this section are applicable over about ten orders of magnitude of the scaled charge weight $(W_e/\rho c^2 R^3)$. As can be seen in Figures 63 and 64, all of the data obtained by SwRI were for values of $(W_e/\rho c^2 R^3)$ greater than 6.4 x 10^{-5} or within the last four cycles of these two figures. In order to obtain simpler equations which are more applicable to the range of scaled charge weights encountered in blasting situations in the vicinity of pipelines, log-linear curves were fitted to all of the SwRI point source data. The resulting radial soil displacement and particle velocity equations applicable to point explosive sources are as follows:

$$\frac{X}{R}\left(\frac{p_o}{\rho c^2}\right)^{0.5} = 0.0373\left(\frac{W_e}{\rho c^2 R^3}\right)^{1.060} \tag{44}$$

$$\frac{U}{c}\left(\frac{p_o}{\rho c^2}\right)^{0.5} = 0.00489\left(\frac{W_e}{\rho c^2 R^3}\right)^{0.790} \tag{45}$$

for

$$6 \times 10^{-5} < \frac{W_e}{\rho c^2 R^3} < 6/10^{-2}$$

As was the case with the general equations, each parameter group is dimensionless and, therefore, any consistent set of units can be used in evaluating a particular problem. Note again that like the general solutions the simplified point source equations would predict the radial ground motions at a point below the ground surface which correspond to the depth of the center of the pipe being tested. In most tests, this depth was two pipe diameters. The equations should be applicable to a reasonable range of scaled depths up to almost the ground surface.

The prediction curves generated by the simplified equations are shown in Figure 65 together with all the SwRI point source data. The estimates of the standard error S of the data about the fitted curves were 0.67 and 0.54, respectively, for the peak soil displacements and peak particle velocities. In this figure, the curves generated from the simplified equations are also compared to the general prediction curves. This comparison shows quite clearly that both sets of equations 'would provide very close to the same predictions for radial ground motions. Therefore, because of their simpler form Equations (44) and (45) are recommended for estimating ground' motions whenever $W_e/\rho c^2 R^3$ lies between the limits given.

Ground Motions from Parallel Line Sources

When a number of equally spaced explosive charges of the same weight are strung along in line, as in explosive ditch digging, the ground motions must be predicted for a line rather than a point source. In Section II, the functional relationships derived from the similitude analysis for the soil displacement and velocity generated by an explosive line showed that $W_e/\rho c^2 R^3$ should be replaced with $W_e/L/\rho c^2 R^2$. If the same empirical explosive to soil coupling observations are made for the line source as for a point source, Equations (16) and (17) in Section II can be rewritten as follows:

$$\frac{X}{R}\left(\frac{p_o}{\rho c^2}\right)^{0.5} = f_X\left(\frac{W_e/L}{\rho c^2 R^2}\right) \tag{46}$$

$$\frac{U}{c}\left(\frac{p_o}{\rho c^2}\right)^{0.5} = f_U\left(\frac{W_e/L}{\rho c^2 R^2}\right) \tag{47}$$

In these functions L is the effective length of the line source and W_e/L is the energy release per unit length of explosive line.

To define the functions of these two equations, test data are required. Not every measurement made in the parallel line experiments was applicable because these functional relationships are for infinitely long lines. Therefore, only data from transducers located at a distance from the charge that was less than the length of the explosive line were selected.

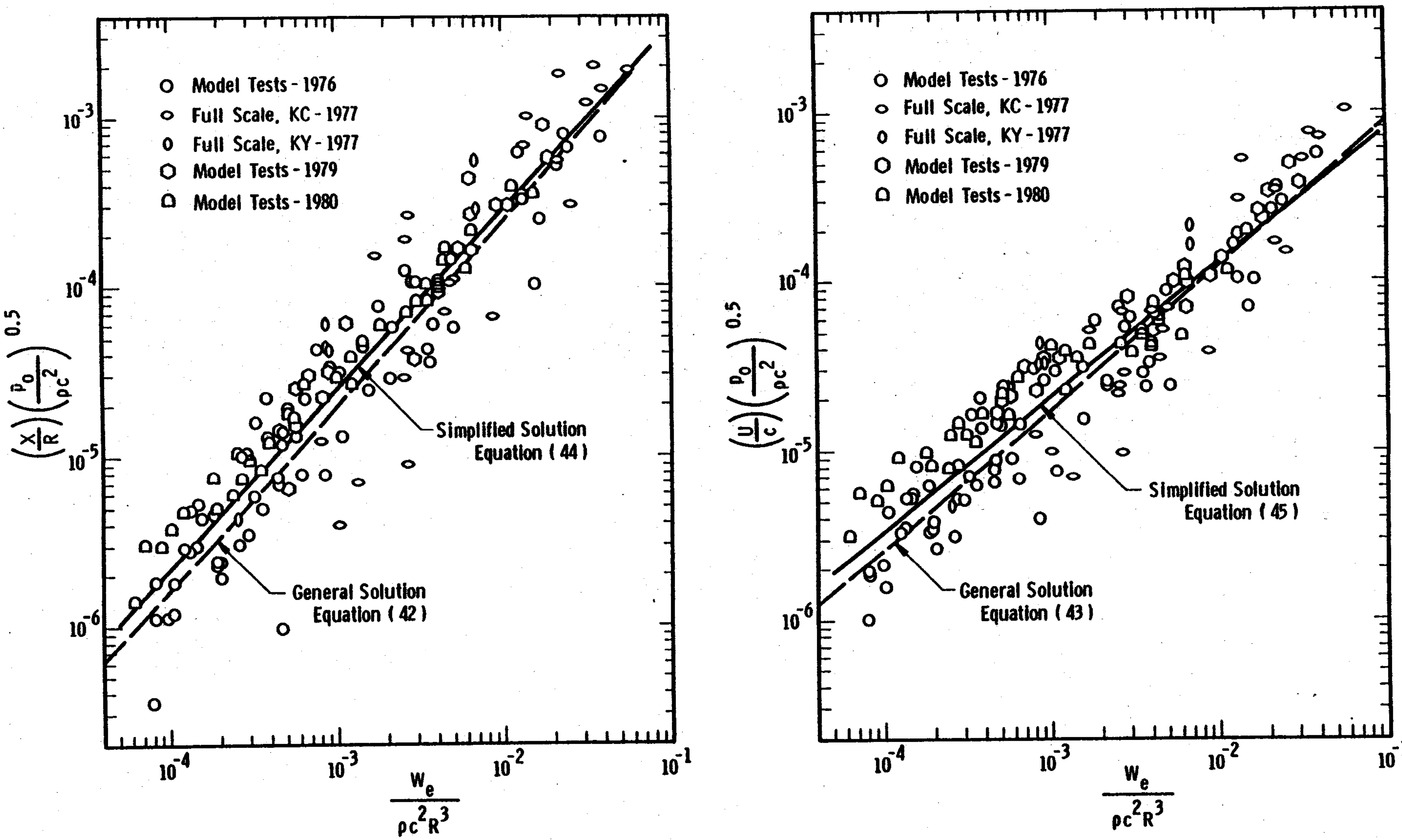

Figure 65. Simplified Radial Ground Motion Solutions and Comparison with Test Data

Furthermore, in all cases the standoff distance was larger than the spacing between successive charges to better approximate an infinitely long explosive line source rather than multiple individual charges. For all the SwRI data selected for defining the functions of Equations (46) and (47), the ratio of the standoff distance to explosive line length was smaller than 0.7 and the ratio of the standoff distance to charge spacing was no smaller than 1.33. Subsequent analysis of both ground motion and pipe stress data indicated that the parallel line solution could be used to obtain reasonable estimates up to a standoff distance R which was equal to or less than the length L of the explosive line. This analysis is presented in Section VIII.

In addition to the SwRI ground motion data, some velocity data at a different range of scaled distances reported by H. Nicholls, et al. (1971) were used to define the radial velocity equation for parallel line explosive sources. Some of the multiple detonation data from this reference, could not be used as being from a parallel line source because either successive charges were delayed or the standoff distances were much larger than the length of the explosive line. Using the applicable SwRI ground motion data and some of Nicholls' Bureau of Mines (BOM) particle velocity data, the functions for parallel line sources were curve fit and are as follows:

$$\frac{X}{R}\left(\frac{p_o}{\rho c^2}\right)^{0.5} = 0.0746\left(\frac{W_e/L}{\rho c^2 R^2}\right)^{1.073} \tag{48}$$

$$\frac{U}{c}\left(\frac{p_o}{\rho c^2}\right)^{0.5} = 0.00465\left(\frac{W_e/L}{\rho c^2 R^2}\right)^{0.734} \tag{49}$$

for

$$R/L \leq 1.0$$

The curves defined by these equations are graphed in Figure 66 along with the radial ground motion data. The estimates of the standard error were 0.47 and 0.35, respectively, for the soil displacement and soil particle velocity.

The range of the test parameters on which the data shown in Figure 66 are based is not as broad as that found in deriving the general point source equations. Ideally, more data over a wider range of scaled charge weights and from several test sites (different ground media) would increase the confidence of Equations (48) and (49). As general parallel line prediction relationships, these equations should be given only tentative acceptance and used with certain amount of engineering judgement. However, for field situations in a soil envi-.

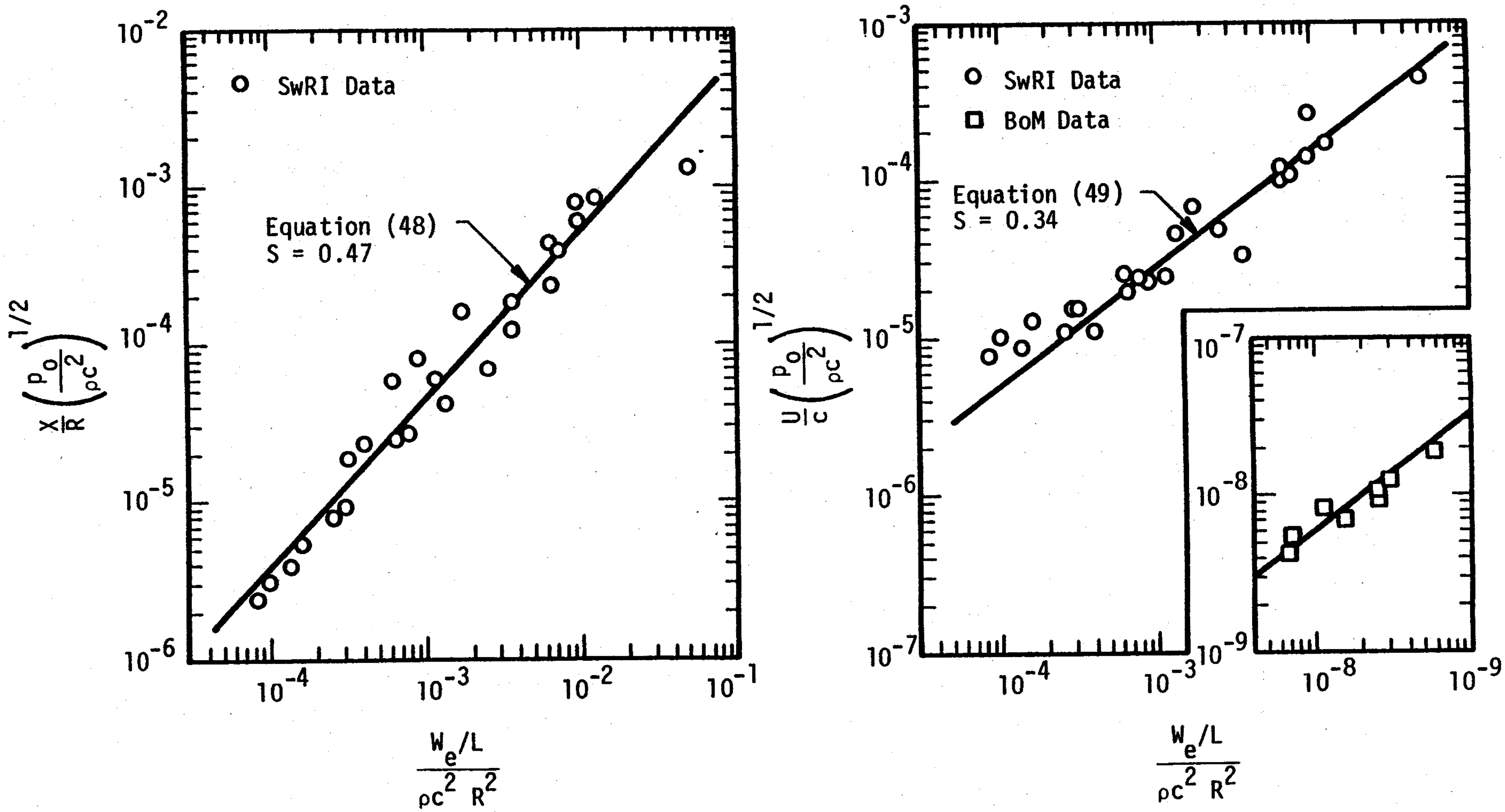

Figure 66. **Relationships for Predicting Radial Ground Motions for Parallel Explosive Line Sources**

ronment similar to those of the SwRI model tests, Equations (48) and (49) should provide reasonable ground motion predictions within the range of scaled charge weights of

$$10^{-4} < \frac{W_e/L}{\rho c^2 R^2} < 10^{-1}$$

Further Approximations for Displacement

The two log-linear equations for radial ground displacement from point and parallel line explosive sources presented in the preceding parts of this section are quite similar. In Equations (44) and (48), the dimensionless displacement, the left side of the equation, is almost a first power function of the right side of the equation. Thus, good simplified approximations of these equations with unity exponents are possible.

For a point source, Equation (44) can be approximated over the range of the data by the following simplified equation

$$\frac{X}{R}\left(\frac{p_o}{\rho c^2}\right)^{0.5} = 0.0262\left(\frac{W_e}{\rho c^2 R^3}\right) \tag{50}$$

In Figure 67, the curve defined by this equation is compared to that of Equation (44). One can observe that relative to the scatter of the experimental data, the approximation is quite good.

Similarly, for a parallel explosive line, Equation (48) can be approximated by the following unity exponent function

$$\frac{X}{R}\left(\frac{p_o}{\rho c^2}\right)^{0.5} = 0.0488\left(\frac{W_e/L}{\rho c^2 R^2}\right) \tag{51}$$

In the derivations of the pipe response equations, which are presented in the section that follows, Equations (50) and (51) are used as the expressions for the soil displacement. Use of these approximate relationships resulted in simplified final solutions for the pipe response.

Illustrative Examples

The log-linear equations for estimating ground motions from point and parallel line sources are quite similar. To apply these equations directly to field situations requires some

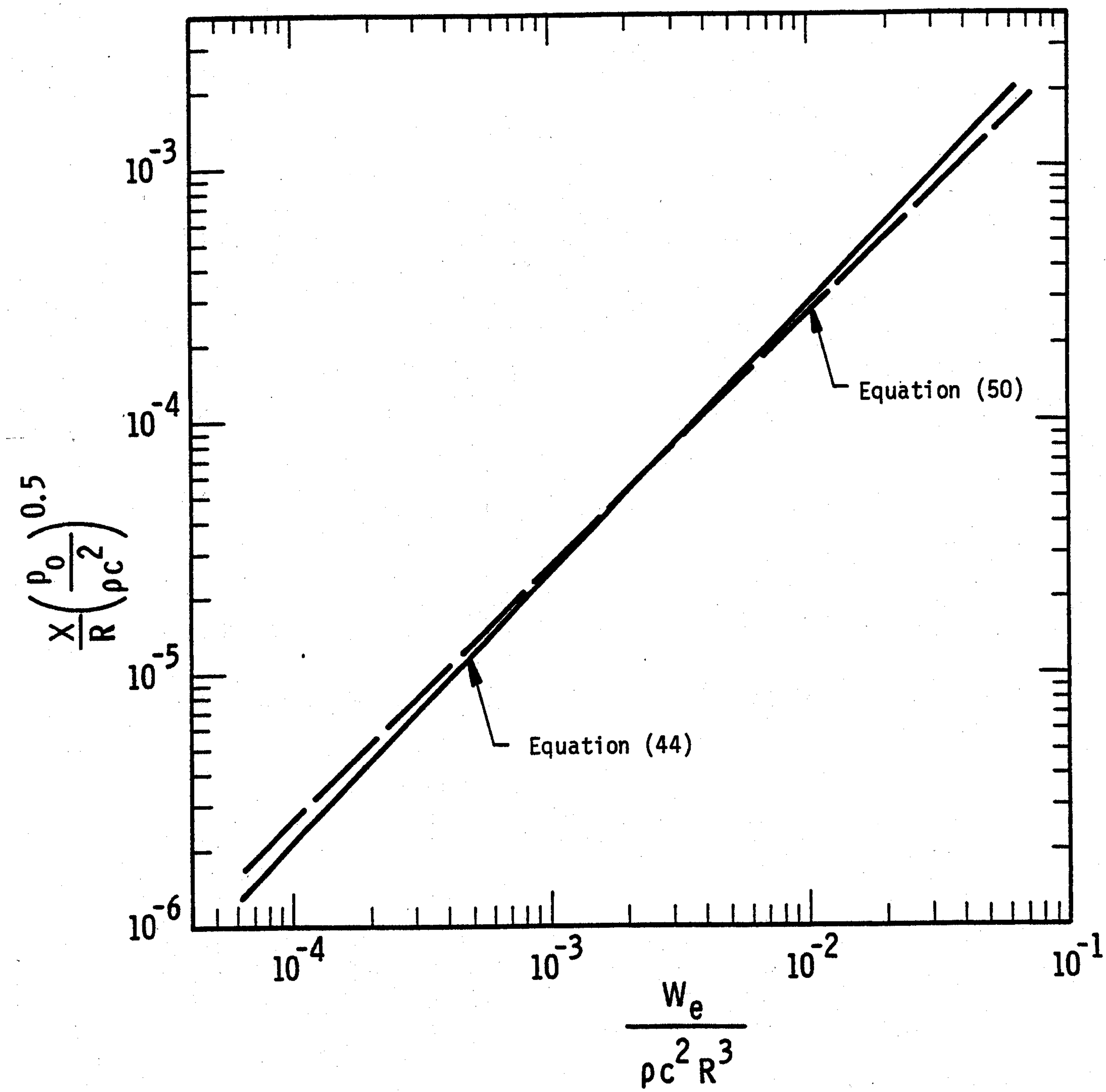

Figure 67. Comparison of Approximate Displacement Solution Curve and Log-Linear Data Fit Curve for Point Explosive Source

brief discussions concerning the explosive energy parameters in the equations and perhaps an illustrative problem. In addition, for a particular test site, the equations can be simplified further (since ρ and c would be essentially constant) and used in direct computation or in graphical form. An example of this will also be presented.

Most chemical explosives have close to the same energy release per unit weight (W_e). This observation implies that if the explosive being used in a blasting situation is not known, the prediction equations can be used by substituting a "typical" value for W_e. Table 12 lists average specific energy release values for a number of commercial explosives.

Table 12. Typical Specific Energy Release of Some Commercial Explosives

Explosive	W_e/lb_m ($ft\text{-}lb_f/lb_m$)
AN Low Density Dynamite	1.50×10^6
ANFO (94/6)	1.52×10^6
Comp B (60/40)	1.70×10^6
Comp C-4	1.70×10^6
HBX-1	1.30×10^6
NG Dynamite (40%)	1.59×10^6
NG Dynamite (60%)	1.70×10^6
Pentolite (50/50)	1.68×10^6
RDX	1.76×10^6
TNT	1.49×10^6

To demonstrate the direct use of the log-linear ground motion equations, Example Problem No. 1 follows:

Example Problem No. 1

Given: A point charge of 2.5lb of 60 percent NG Dynamite will be detonated, buried 4 ft in a soil with a density of 120 lb/ft^3 and a seismic propagation velocity of 1,000 ft/sec.

Find: The horizontal ground motions at a standoff distance of 15 ft.

Solution: (a) Put parameters in Equations (44) and (45) in consistent units

$$W_e = (2.5\ lb_m)\left(1.7 \times 10^6 \frac{ft\text{-}lb_f}{lb_m}\right) = 4.25 \times 10^6\ ft\text{-}lb_f$$

$$\rho = \frac{120\ \text{lb}_m/\text{ft}^3}{32.2\dfrac{\text{lb}_m\text{-ft}}{\text{lb}_f\text{-sec}^2}} = 3.73\frac{\text{lb}_f\text{-sec}^2}{\text{ft}^4}$$

$$c = 1{,}000\ \text{ft/sec}$$

$$R = 15\ \text{ft}$$

$$p_o = \left(14.7\frac{\text{lb}_f}{\text{in}^2}\right)\left(144\frac{\text{in}^2}{\text{ft}^2}\right) = 2{,}117\frac{\text{lb}_f}{\text{ft}^2}$$

(b) Calculate each dimensionless group

$$\left(\frac{p_o}{\rho c^2}\right)^{0.5} = \left[\frac{2117}{(3.73)(1{,}000)^2}\right]^{0.5} = 2.38\times 10^{-2}$$

$$\left(\frac{W_e}{\rho c^2 R^3}\right) = \left[\frac{4.25\times 10^6}{(3.73)(1{,}000)^2(15)^3}\right] = 3.376\times 10^{-4}$$

Note that the value for the scaled charge is within the limits of applicability of the log-linear solutions.

(c) Substitute into Equation (44) and solve for X

$$\frac{X}{15}(2.38\times 10^{-2}) = 0.0373(3.376\times 10^{-4})^{1.060}$$

$$X = 0.00491\ \text{ft}$$

$$\underline{X = 0.059\ \text{in.}}$$

(d) Substitute into Equation (45) and solve for U

$$\frac{U}{1,000}(2.38 \times 10^{-2}) = 0.00489(3.376 \times 10^{-4})^{0.79}$$

$$U = 0.372 \text{ ft/sec}$$

$$\underline{U = 4.46 \text{ in./sec}}$$

A similar example will now be presented for a parallel line source, for which the radial ground motions are in a direction perpendicular to the explosive line. The effective length (L) of the equally spaced line of charges is the number of charges multiplied by the spacing between them. Also, the energy release W_e is that of the total explosive line. The example problem which uses Equations (48) and (49) is as follows:

Example Problem No. 2

Given: Seven 60 percent NG dynamite charges weighing 2.5 lb each and spaced 3 ft apart will be detonated simultaneously. The charges will be buried 4 ft in a soil media. The density of the soil is measured to be 120 lb/ft^3 and the seismic propagation velocity is estimated to be 1,000 ft/sec.

Find: The horizontal radial ground motions at a point 15 ft from the explosive line, and perpendicular to the center of the line.

Solution: (a) Put parameters in Equations (48) and (49) in consistent units

$$W_e = (7)(2.5 \text{ lb}_m)\left(1.7 \times 10^6 \frac{\text{ft-lb}_f}{\text{lb}_m}\right) = 29.75 \times 10^6 \text{ ft-lb}_f$$

$$L = (7)(3 \text{ ft}) = 21 \text{ ft}$$

$$\rho = \frac{120 \text{ lb}_m/\text{ft}^3}{32.2 \text{ lb}_m\text{-ft/lb}_f\text{-sec}^2} = 3.73 \frac{\text{lb}_f\text{-sec}^2}{\text{ft}^4}$$

$$c = 1{,}000 \text{ ft/sec}$$

$$R = 15 \text{ ft}$$

$$p_o = \left(14.7 \frac{lb_f}{in^2}\right)\left(144 \frac{in^2}{ft^2}\right) = 2{,}117 \frac{lb_f}{ft^2}$$

Note that since R < L, the spacing between charges is much less than R, and the charges will be detonated with no delays, the line of explosives can be considered as being continuous and infinite.

(b) Evaluate each dimensionless group

$$\left(\frac{p_o}{\rho c^2}\right)^{0.5} = \left[\frac{2117}{(3.73)(1{,}000)^2}\right]^{1/2} = 2.382 \times 10^{-2}$$

$$\left(\frac{W_e/L}{\rho c^2 R^2}\right) = \left[\frac{29.75 \times 10^6}{(3.73)(1{,}000)^2 (15)^2 (21)}\right] = 1.688 \times 10^{-3}$$

Note that the value for the scaled charge is within the limits of applicability for the log-linear solutions.

(c) Substitute into Equation (48) and solve for X

$$\frac{X}{15}(2.382 \times 10^{-2}) = 0.0746(1.688 \times 10^{-3})^{1.073}$$

$$X = 0.0498 \text{ ft}$$

$$\underline{X = 0.597 \text{ in.}}$$

(d) Substitute in Equation (49) and solve for U

$$\frac{U}{1{,}000}(2.382 \times 10^{-2}) = 0.00465(1.688 \times 10^{-3})^{0.734}$$

$$U = 1.801 \text{ ft/sec}$$

$$\underline{U = 21.6 \text{ in./sec}}$$

If ground motion predictions are repeatedly needed for a specific test site, it might be more convenient to graph the prediction equations rather than use direct calculation. Since *p* and c would be essentially constants, any of the ground motion equations would reduce to a three-parameter space which can easily be plotted. For example, Figure 68 is a plot of Equation (45), the log-linear radial particle velocity equation for a test site in which c = 1,000 ft/sec and *p* = 120 lb/ft^3, as in Example Problem No. 1. The estimate of 4.5 in./sec is quite close to the value calculated earlier using the prediction equations directly.

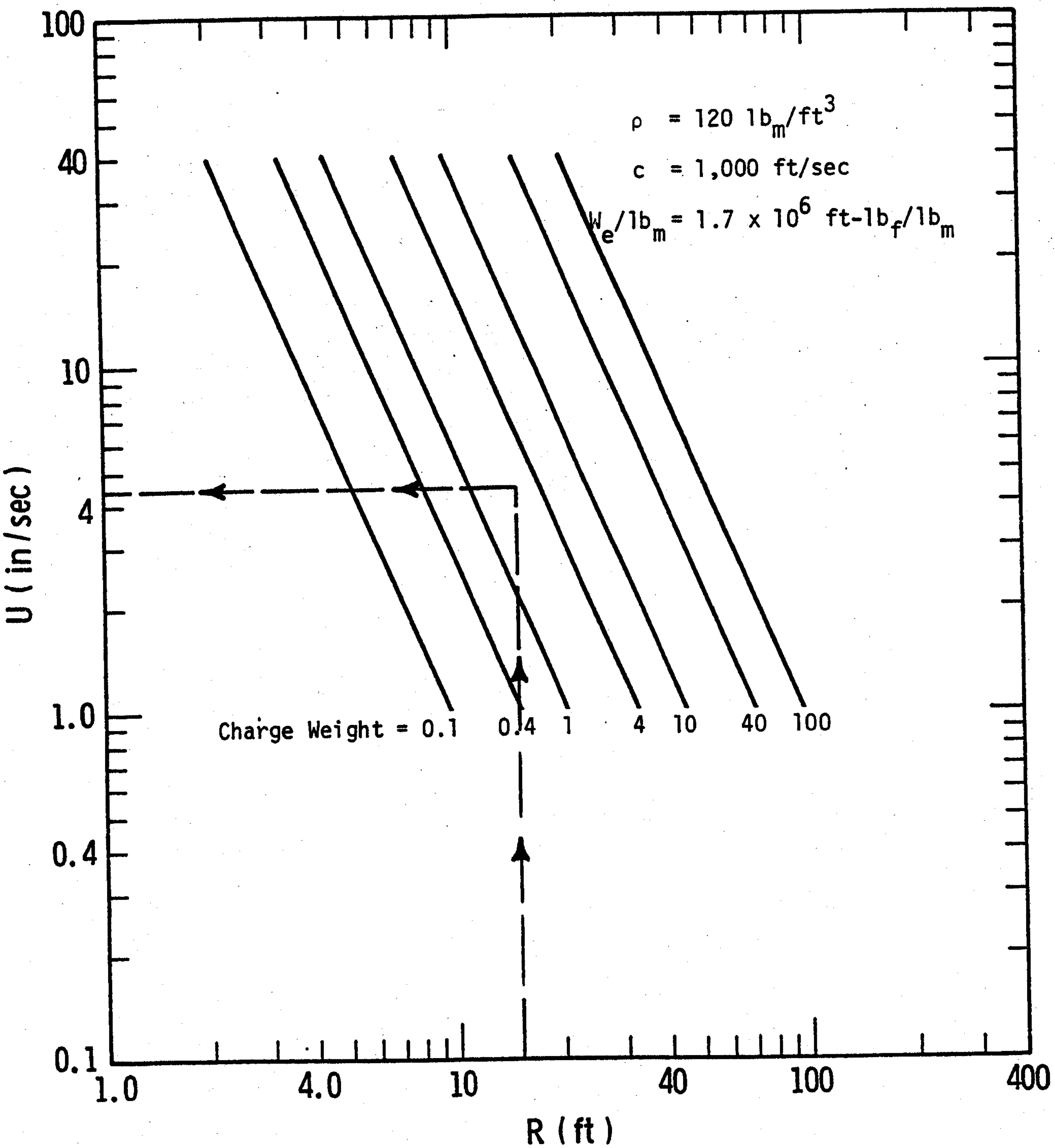

Figure 68. Graphical Solution of Example Problem No. 1

VI. PIPE STRESSES FROM POINT AND PARALLEL LINE SOURCES

Introduction

The ground motions predicted in the previous chapter impart a transient loading to a buried pipe. Basically, this load takes the form of an impulse imparting kinetic energy to a buried pipe. This kinetic energy is dissipated by changing to strain energy. Significant strains were recorded and are reported in Section IV in both circumferential and longitudinal directions. The purpose of this section is to present the derivation of approximate formulas to interrelate maximum pipe strain in both directions to the pipe, soil, and explosive parameters of importance. Only elastic analysis procedures were used because yielding of a pipeline is considered unacceptable. The pipe strain data from tests using point and parallel line explosive sources were then used to define the strain functions and to determine the biaxial stresses to develop a similar empirical stress prediction equation for these explosive configurations.

Predicting impulse Imparted to Pipes

Before structural calculations can be made, the impulse distribution imparted to a pipe from a ground seismic wave must be estimated. This explosively induced load becomes the forcing function needed in structural calculations.

The side-on pressure and subsequent impulse must be determined without a pipe present before the impulse imparted to a pipe can be determined. Fortunately, soil particle velocity and displacement, predicted in Section V, relate directly to free-field or side-on pressures and impulses. To calculate pressure from particle velocity, we use the Rankine-Hugoniot relationships for conservation of mass and momentum. For a stationary coordinate system with a shock front moving at velocity V, these equations are:

$$-\rho_s V = \rho_a (U - V) \tag{52}$$

$$\rho_s V^2 = p_s + \rho_a (U - V)^2 \tag{53}$$

where ρ_a is the density behind the shock front, p_s is the side-on overpressure and U is the soil particle velocity. Multiplying both sides of Equation (52) by (U - V) and then subtracting the new Equation (52) from Equation (53) gives:

$$p_s = \rho_s VU \tag{54}$$

Equation (54) states that peak side-on overpressure is the product of soil density, shock front velocity, and peak particle velocity. In a fairly incompressible medium such as soil with its massive particles, the shock front propagation velocity V very rapidly decays to c, the seismic velocity. Substitution of c for V is a common practice in hydraulic shock studies and would appear to be equally valid in soil. This final substitution yields Equation (55) which will be used to relate side-on overpressure and particle velocity.

$$p_s = \rho_s c U \tag{55}$$

Either Equation (45) in Section V for point sources or Equation (49) in Section V for line sources can be substituted into Equation (55) to determine p_s. To determine the side-on specific impulse i_s, we will treat p_s and c as constants and integrate Equation (55). Because the time integral of pressure is impulse (i_s) and the time integral of velocity is displacement (X), integrating Equation (55) gives:

$$i_s = \rho_s c X \tag{56}$$

Equation (56) can be used for values of X from either point or parallel line charges. Next, the distribution of impulse imparted to a buried pipe by side-on impulses must be estimated. Figure 69 shows a pipe loaded by an assumed distribution of applied impulse. At the top and bottom of the pipe, the applied impulse will be i_s. A lower limit at the front of the pipe for the impulse will equal at least 2 i_s. Between the top and front edge of the pipe, some distribution will exist which is not known. Therefore, a convenient mathematical expression, Equation (57), was selected which reaches the correct limits,

$$i = i_s\left(1 + \frac{2\theta}{\pi}\right) \qquad \text{for } 0 < \theta < \pi/2 \tag{57}$$

The back side of the pipe will also be loaded by the shock wave diffracting around the pipe. At $\theta = -\pi/2$, on the very rear surface of the pipe, the impulse could very easily exceed i,; however, no one knows the exact magnitude. This was solved by assuming that the applied specific impulse equals (1 + m) i_s at the back of the pipe where m is some number between 0 and 1. The distribution of impulse over the back surface of the pipe is similar to that used over the front surface and is

$$i = i_s \left(1 + \frac{2\theta}{\pi}\right) \quad \text{for} \quad 0 < \theta < \frac{\pi}{2}$$

$$i = i_s \left(1 - \frac{2m\theta}{\pi}\right) \quad \text{for} \quad 0 > \theta > -\frac{\pi}{2}$$

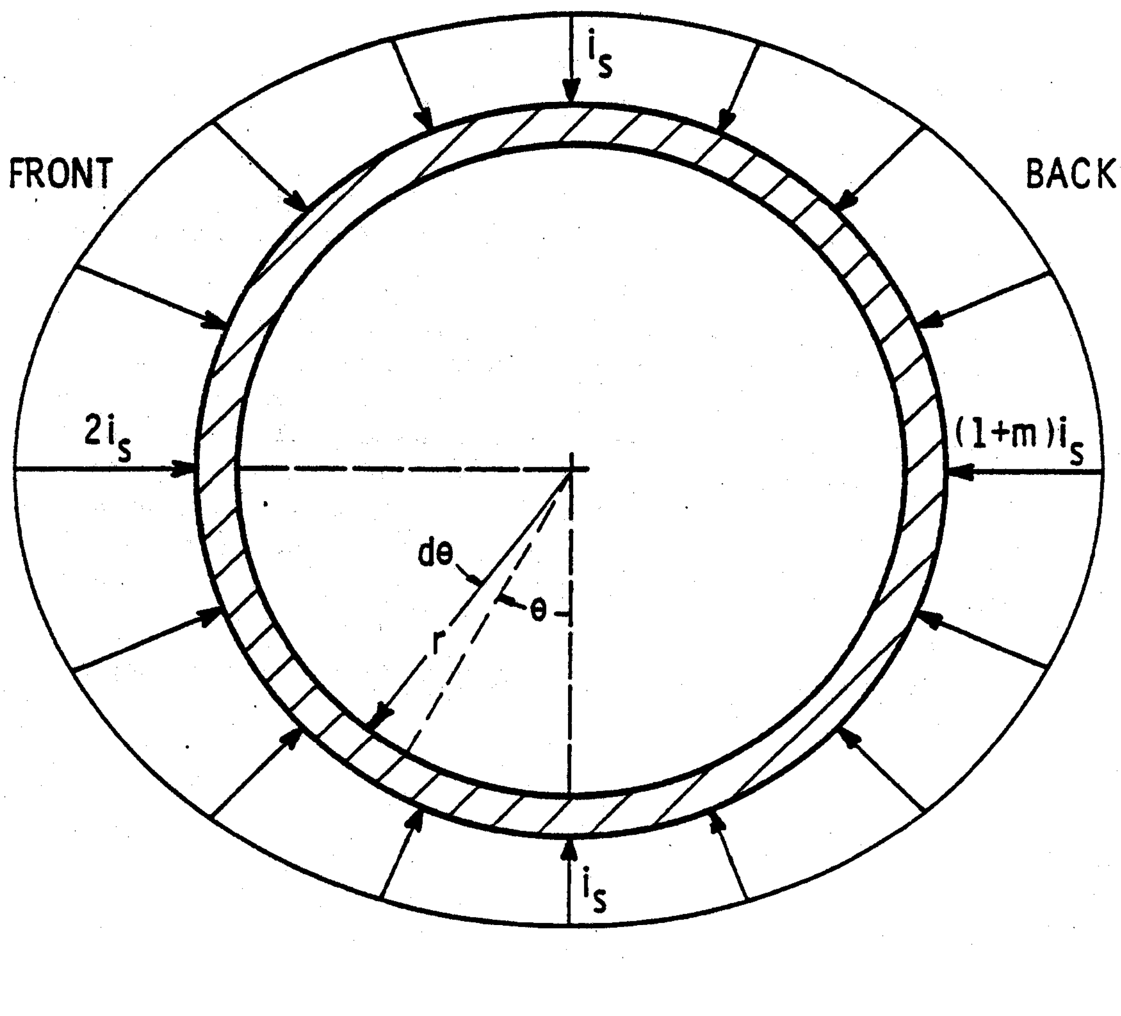

Figure 69. Assumed Distribution of Impulse Imparted to a Pipe

$$i = i_s \left(1 - \frac{2\, m\, \theta}{\pi}\right) \qquad \text{for } 0 > \theta > -\pi/2 \tag{58}$$

A minus sign appears in Equation (58) because the angle θ is measured in a negative direction.

Circumferential Strain Estimate

Now that an impulse distribution function has been derived, the pipe strains can be estimated by assuming a deformed shape and equating the kinetic energy to the strain energy. The kinetic energy imparted initially to the pipe is given by:

$$KE = \sum_{pipe} \frac{1}{2} M V_o^2 = \sum_{pipe} \frac{M}{2} \left(\frac{i_p A_p}{M}\right)^2 = \sum_{pipe} \frac{i^2 A_p^2}{2M} \tag{59}$$

The impulse distribution has already been given in Equations (57) and (58), so the summation can be made by writing the area A, as a differential area of (r $d\theta$ dx) which must be double integrated over the pipe.

The mass term M also requires some thought because it involves both the pipe mass and a large mass of earth that moves with the pipe. Empirical observation made in the first test series on periods of pipe oscillation indicated that this effective mass of earth extends from the center of the charge to the center of the pipe. This large mass of earth moving with the pipe causes the mass of the pipe itself to be insignificant. If we use some of the early point source test results reported in Section IV, the assumption of attaching a large mass of earth to the pipe can he demonstrated to be a good one for the range of standoff distance to pipe diameter ratios used in this program. For much larger ratios this assumption may or may not be as good.

For an ovalling bending mode in a ring, the fundamental natural frequency ω is given by Den Hartog (1947) as:

$$\omega = 2.6833 \sqrt{\frac{EJ}{\mu r^4}} \tag{60}$$

where J = 1/12 (dx) h^3, the second moment of area

μ = the mass per unit length

If one substitutes (ρ_s R dx) for μ in Equation (60), and compute the period τ from the frequency ω 'we obtain:

$$\tau = 8.11\sqrt{\frac{\rho_s R r^4}{E h^3}} \tag{61}$$

where ρ_s is the density of the soil, R is the standoff distance, r is the pipe radius, E is the pipe modulus of elasticity, and h is the pipe thickness.

Calculated periods using Equation (61) agreed well with observed periods in the pipe strain records on early model soil tests, as shown in Table 13. These strain records also showed pipe ovalling, inferring that pipe bending was a correct mode of response for these first few tests. However, for media with a significant elastic constant (perhaps rock), Equation (61) may not apply. Should the strength of the media contribute significantly, the quantity $E\ h^3$ would become an effective $E\ h^3$ that is larger than that of the pipe by itself and the periods would decrease accordingly.

Table 13. Observed and Calculated Periods for Buried Pipe Systems

Test Series	Test No.	Pipe Diameter (in.)	Standoff Distance (ft)	Observed Periods (milliseconds)	Calculated Periods (milliseconds)
1	1	2.95	1.5	16	11.7
1	2	2.95	1.5	11	11.7
1	3	2.95	1.5	13	11.7
1	4	2.95	11.0	25	31.6
1	5	5.95	3.0	35	34.8
1	6	5.95	3.0	36	34.8
1	7	5.95	11.0	71	66.8

In firing a series of explosive charges near a pipeline, questions often arise as to whether the stresses induced on the pipe can be decreased by use of delays. If one assumes that the pipe response is approximately sinusoidal bending in both the circumferential and longitudinal direction, then any series of loading impulses which arrive at the pipe under 1/4 period apart would be considered to load the pipe with no delays. Shock arrivals which are spaced between 1/4 and 2 periods apart are in a regime where the stresses may or may not be reduced depending on how the transient loads interphase and whether the pipe is excited at different modes. Finally, for transient loads which arrive at the pipe more than 2 periods apart, one would expect that the maximum stress would be that induced by any one blast wave and thus no enhancement would occur.

Now that the mass is *seen* to be a large effective mass of earth, the kinetic energy imparted to the pipe in an ovalling mode can be calculated by substituting (ρ_s R dx) for the mass per unit circumferential length. The total impulse (iA_p) in the numerator to Equation (59) is given by (i r $d\theta$ dx). The mass M in Equation (59) is given by (ρ_s R r $d\theta$ dx). By taking advantage of symmetry and integrating over the top half of the pipe, we obtain for Equation (59):

$$KE = 2\int_{-\ell/2}^{+\ell/2}\int_{-\pi/2}^{+\pi/2}\frac{i^2(rd\theta dx)^2}{2(\rho_s Rrd\theta dx)} = \frac{r}{\rho_s R}\int_{-\ell/2}^{+\ell/2}\int_{-\pi/2}^{+\pi/2} i^2 d\theta dx \tag{62}$$

where ℓ is an arbitrary length of the pipe. But i is given by Equations (57) and (58) which means:

$$KE = \frac{ri_s^2}{\rho_s R}\left[\int_{-\ell/2}^{+\ell/2}\int_{0}^{+\pi/2}\left(1+\frac{2\theta}{\pi}\right)^2 d\theta dx + \int_{-\ell/2}^{+\ell/2}\int_{-\pi/2}^{0}\left(1-\frac{2m\theta}{\pi}\right)^2 d\theta dx\right] \tag{63}$$

or:

$$KE = \left[\frac{\pi}{2}\left(3.333 - m + \frac{m^2}{3}\right)\right]\frac{i_s^2 r\ell}{\rho_s R} \tag{64}$$

Next, one needs to compute the strain energy SE so that it can be equated to the kinetic energy to estimate circumferential strains. If we assume that the pipe goes into an ovalling bending mode as was indicated by the recorded strains from point charges and by the calculated and observed durations associated with the vibrating pipes, the strain energy in the circumferential direction is computed from an assumed deformed shape y given by:

$$y = w_o \cos 2\theta \tag{65}$$

where w_o = the maximum deformation.

The elastic bending moment (M_b), as computed from two derivatives of Equation (65) is:

$$M_b = -EJ\frac{d^2y}{r^2 d\theta^2} = \frac{4\ EJ\ w_o}{r^2}\cos 2\theta \tag{66}$$

The strain energy (SE_{cir}) is given by:

$$SE_{cir} = 8\int_0^{\pi/4} \frac{M_b^2 \ r \ d\theta}{2 \ EJ} \tag{67}$$

Which, after substitution of Equation (66) into Equation (67), yields:

$$SE_{cir} = \frac{64 \ EJ \ w_o^2}{r^3} \int_o^{\pi/4} \cos^2(2\theta) d\theta \tag{68}$$

Integration of Equation (68) gives the result:

$$SE_{cir} = \frac{8 \ \pi \ EJ \ w_o^2}{r^3} \tag{69}$$

Substituting into the flexure equation for the circumferential strain (ϵ_{cir})

$$\epsilon_{cir} = \frac{M_{max} h/2}{J \ E} \tag{70}$$

the maximum moment from Equation (66) when cos 2θ equals unity and solving for w_o gives

$$w_o = \frac{\epsilon_{cir} r^2}{2h} \tag{71}$$

The second moment of area J about an axis through the wall of the pipe is given by:

(72)

where ℓ i is an arbitrary length of the pipe. Then, substituting Equations (71) and (72) into Equation (69) gives for the circumferential strain energy:

$$SE_{cir} = \frac{\pi}{6}\epsilon_{cir}^{2}Erh\ell \tag{73}$$

Finally, equating the strain energy SE,, to the kinetic energy KE given by Equation (64) yields the result:

$$\frac{\pi}{6}\epsilon_{cir}^{2}Erh\ell = \left[\frac{\pi}{2}\left(3.333 - m + \frac{m^2}{3}\right)\right]\frac{i_s^2 r\ell}{\rho_s R} \tag{74}$$

or:

$$\epsilon_{cir} = [10 - 3m + m^2]^{1/2}\frac{i_s}{[EhR\rho_s]^{1/2}} \tag{75}$$

But, the side-on impulse i_s is related to displacement by Equation (56). Substituting to eliminate i_s gives:

$$\epsilon_{cir} = [10 - 3m + m^2]^{1/2}\frac{\rho_s^{1/2}cX}{E^{1/2}h^{1/2}R^{1/2}} \tag{76}$$

The quantity $[10 - 3m + m^2]^{0.5}$ is a diffraction coefficient, C_c. The final version of Equation (76) which will be used to develop this solution empirically is then:

$$\epsilon_{cir} = C_c\frac{\rho_s^{1/2}cX}{E^{1/2}h^{1/2}R^{1/2}} \tag{77}$$

The advantage to having Equation (77) in its present format is that the strain is related to ground motion X. Ground motion X can be caused by a point source, line source, or grid source. In this manner, ground motion is studied and characterized separately for different sources, and then the circumferential strain can be predicted.

Next, we will estimate the longitudinal strain associated with longitudinal bending of a pipe segment.

Longitudinal Strain Estimate

The longitudinal bending strains will also be estimated by assuming a deformed shape and equating kinetic energy to strain energy. For a longitudinal bending mode of response, the pipe must be treated as a long beam. Now, we need to compute the total resultant impulse acting on the pipe because of the impulse distributions from the load which diffracts around the pipe. For a dx differential length of pipe, this resultant impulse I is given by:

$$\frac{I}{(dx)} = 2\int_{-\pi/2}^{+\pi/2} i(\sin\theta) r d\theta \tag{78}$$

which, after substituting Equations (57) and (58), is given by:

$$\frac{I}{(dx)} = 2ri_s\left[\int_{-\pi/2}^{0}\left(1-\frac{2m\theta}{\pi}\right)\sin\theta \; d\theta + \int_{0}^{+\pi/2}\left(1+\frac{2\theta}{\pi}\right)\sin\theta \; (\right. \tag{79}$$

Performing the required integration gives:

$$I = \frac{4}{\pi}(1-m)i_s r(dx) \tag{80}$$

Equation (80) is the total impulse imparted to a ring segment. This equation can also be written as:

$$I = C\, i_s A_p \tag{81}$$

where A_p = 2 r (dx), the projected area
C = $(2/\pi)(1-m)$, longitudinal coefficient.

Equation (81) states that the total impulse is the specific impulse times the projected areas times a coefficient.

Now, we are prepared to calculate the kinetic energy associated with a longitudinal bending of the pipe. This kinetic energy (KE) is given by:

$$KE = \sum_{pipe} \frac{1}{2} MV_o^2 = \sum_{pipe} \frac{I^2}{2m} = 2\int_0^{\ell/2} \frac{I^2}{2m} \tag{82}$$

Substituting Equation (81) for I and assuming that an effective mass of earth from the center of the charge to the center of the pipe moves with the pipes gives the result:

$$KE = \int_0^{\ell/2} \frac{C^2 i_s^2 (2r)^2 (dx)^2}{\rho_s (2r)\ R\ (dx)} \tag{83}$$

This assumption of a large effective mass of earth moving with the pipe causes the mass of the pipe itself to be insignificant. It is based upon the same empirical observations that were made for the circumferential strain solutions. After performing the required integration, we obtain:

$$KE = \frac{C^2 i_s^2 r \ell}{\rho_s R} \tag{84}$$

Substituting Equation (56) for i_s in Equation (84) finally yields:

$$KE = \frac{C^2 \rho_s c^2 r \ell X^2}{R} \tag{85}$$

Next, the strain energy SE_{long} must be calculated because of the pipe responding in a longitudinal bending mode. This computation is done by assuming a deformed shape given by:

$$y = w_o\ \cos\left(\frac{\pi x}{\ell}\right) \tag{86}$$

where w_o = maximum pipe deflection
ℓ = total length of the deforming pipe

Differentiating Equation (86) twice and substituting into the elastic moment-curvature relationship gives:

$$M_b = -EJ\frac{d^2y}{dx^2} = \frac{\pi^2 \; EJ \; w_o}{\ell^2} co \tag{87}$$

But the strain energy is given by:

$$SE_{long} = 2\int_o^{\ell/2} \frac{M_b^2 \; dx}{2 \; EJ} \tag{88}$$

Substituting Equation (87) into Equation (88) gives:

$$SE_{long} = \frac{\pi^4 \; EJ \; w_o^2}{\ell^4} \int_o^{\ell/2} \cos^2\left(\frac{\pi x}{\ell}\right) dx \tag{89}$$

Which, after integrating, gives:

$$SE_{long} = \frac{\pi^4 \; EJ \; w_o^2}{4\ell^3} \tag{90}$$

Next, we wish to substitute for J and w_o. The second moment of area J for a pipe is given by:

$$J = \frac{\pi}{4}(r_o^4 - r_i^4) \tag{91}$$

Substituting (r_i + h) for r_o, this becomes:

$$J = \frac{\pi r_i^4}{4}\left[\left(1 + \frac{h}{r_i}\right)^4 - 1\right] \tag{92}$$

Using the binomial expansion and retaining only the first two terms because h/r_i is small gives:

$$J = \frac{\pi r_i^4}{4}\left[1 + 4\left(\frac{h}{r_i}\right) + \ldots\ldots - 1\right] \tag{93}$$

Equation (93) reduces to:

$$J \approx \pi r^3 h \tag{94}$$

The deformation w_o is related to the maximum longitudinal strain ϵ_{long} by substituting into:

$$\epsilon_{long} = \frac{M_{max}(h/2)}{E\ J} \tag{95}$$

But M_{max} occurs when the cos $\pi x/\ell$ equals 1.0 in Equation (87), hence:

$$\epsilon_{long} = \frac{\pi^2\ J\ w_o}{\ell^2}\frac{r}{J} \tag{96}$$

Which gives, when solved for w_o:

$$w_o = \frac{\epsilon_{long}\ell^2}{\pi^2 r} \tag{97}$$

Substituting Equations (94) and (97) into Equation (90) gives the longitudinal strain energy:

$$SE_{long} = \frac{\pi}{4}\epsilon_{long}^2 Erh\ell \tag{98}$$

Finally, equating the strain energy SE_{long} to the kinetic energy KE given by Equation (63) yields the result:

$$\frac{\pi}{4}\epsilon_{long}^2 Erh\ell = \frac{C^2 \rho_s c^2 r\ell X^2}{R} \tag{99}$$

Which, after substituting for C and reducing, becomes:

$$\epsilon_{long} = \left[\frac{4(1-m)}{\pi^{3/2}}\right] \frac{\rho_s^{1/2} cX}{E^{1/2} h^{1/2} R^{1/2}} \tag{100}$$

The quantity $[4(1-m)/\pi^{3/2}]$ is a coefficient C_L similar to C_c in Equation (77) for circumferential stress. This final substitution gives:

$$\epsilon_{long} = C_L \frac{\rho_s^{1/2} cX}{E^{1/2} h^{1/2} R^{1/2}} \tag{101}$$

Notice that Equation (101) for longitudinal strain is the same equation as Equation (77) for circumferential strain except for the proportionality coefficients C_c and C_L . This observation means that a change in some parameter will have the same relative influence on ϵ_{cir} as on ϵ_{long}.

Observe that in both the circumferential strain and longitudinal strain solutions, the radius r and length ℓ of the pipe are not in the equations. This occurs because the quantity $(r\ell)$ on the strain energy side of the energy balance cancels with $(r\ell)$ on the kinetic energy side. Because these parameters are not in the final solution, the strains are independent of both the pipe length ℓ and the pipe radius r . Static analysis procedures do not yield this conclusion, and cannot be used to draw valid conclusions in this dynamic problem. Dynamically, this solution infers that doubling the radius r or size of the pipe doubles the kinetic energy imparted to the pipe; however, this process doubles the amount of material available for absorbing the input energy through strain energy. The net result is that the pipe radius r cancels out of the analysis and the stresses are independent of pipe radius, The experimental data obtained in this program on 3-inch, 6-inch, 16-inch, 24-inch, and 30-inch diameter pipes will be used later in comparisons which uphold this analytical observation.

The other major observation which should be made concerning Equations (77) and (101) is that strain solutions can be obtained by two plots of test data, one for maximum circumferential strain ϵ_{cir} and the other for maximum longitudinal strain ϵ_{long}. This procedure is precisely the one which was followed to develop the final quantitative functional formats for predicting pipe strains from buried detonations. Similarly, since the pipe stresses are functions of these two orthogonal strains, stress prediction equations for point and parallel line sources were derived using the strain data.

Use of Test Data to Complete Solutions

Equations (77) and (101) relate the pipe response to the forcing function, the radial ground displacement X. To derive pipe response formulas which are in terms of the pipe parameters, charge size, and charge location, Equations (50) and (51) were used to eliminate X and the other ground parameters. Then the experimental data were used to define the pipe response functions.

As test data were obtained in the program, curve fits were made to complete the hoop and axial strain prediction equations. Then, these equations were approximately transformed to stress equations by doing a uniaxial conversion, i.e., by simply multiplying both sides of the equation by the modulus of elasticity. In this way the blasting stresses could be combined with other pipe stresses to determine if the allowable pipe stress would be exceeded. As more tests were conducted, the prediction equations were revised.

Later in the program, the Supervisory Committee and SwRI decided that the approximate uniaxial conversion of strains to stresses was not adequate. Therefore, making some conservative assumptions, the peak measured strains for each test were converted to biaxial stresses. This conversion is explained in Section III. With these data, biaxial stress prediction equations were derived for point and parallel line explosive sources.

The relationship derived earlier in this section for the elastic circumferential strain is of the form

$$\epsilon_{cir} = C_c \frac{\rho_s^{1/2} c X}{E^{1/2} h^{1/2} R^{1/2}} \tag{77}$$

A similar dimensionless expression was also developed for the longitudinal strain, Equation (101). Substituting the equation for X for a point source from Equation (50) into Equation (77) results in

$$\epsilon_{cir} = C_1 \left(\frac{W_e}{\sqrt{p_o E h}\ R^{2.5}} \right) \tag{102}$$

Equation (102) is nondimensional. The left side of the equation is the pipe response which is a function of the parameters on the right side. The constant C_1 is a combination of the constants in Equations (50) and (77), including C,, the diffraction coefficient (or function), which will not be evaluated explicitly. Instead, a function for Equation (102) was defined by fitting a log-linear expression to the experimental strain data. But, before the data fit was performed, the parameters in Equation (102) were converted into units which are customarily used in the field. The following substitutions were, made: quantity nW as equivalent pounds of ANFO in place of W_e, the quantity 14.7 psi for p_o, and the proper dimensional conversions so that R would be in feet, E in psi, and h in inches. These substitutions transformed Equation (102) into

$$\epsilon_{cir} = C_2 \left(\frac{nW}{\sqrt{Eh}\ R^{2.5}} \right) \tag{103}$$

Note that in this equation, C_2 includes all the necessary conversion units and factors to keep the right-hand side of the equation dimensionless. Using the strain data presented in Section III, the log-linear function for circumferential (and longitudinal) strain was defined.

Similarly, for a parallel line source, the circumferential and longitudinal strain function were simplified into the form

$$\epsilon = C_3 \left(\frac{nW/L}{\sqrt{Eh}\ R^{1.5}} \right) \tag{104}$$

Again, experimental data were used to define the prediction equations for parallel line sources. Only data from parallel line sources in which the ratio of the standoff distance to the length of the explosive line was less than 0.5 and the ratio of the charge spacing to standoff distance was less than 0.42 were used. The results of the fits to the point and parallel line source strain data showed that all of the circumferential data could be fitted together to produce a predictive equation for both sources. Likewise, all the longitudinal data could be fitted together. The only adjustment necessary was to introduce a different numerical constant to the right side of Equation (104) for the line source data.

The resulting equations for predicting elastic pipe strains from point and parallel line explosive sources are as follows:

$$\epsilon_{cir} = 4.78\ \chi^{0.805} \tag{105}$$

and

$$\epsilon_{long} = 1.98\ \chi^{0.735} \tag{106}$$

The term χ is defined as

$$\chi = \frac{nW}{\sqrt{Eh}\ R^{2.5}} \qquad \text{(point source)} \qquad (107)$$

and

$$\chi = \frac{1.3nW/L}{\sqrt{Eh}\ R^{1.5}} \qquad \text{(parallel line source)} \qquad (108)$$

For these strain prediction equations

ϵ_{cir} = maximum circumferential strain (in./in.)
ϵ_{long} = maximum longitudinal strain (in./in.)
n = equivalent energy release (nondimensional)
W = total charge weight of point or line (lb)
E = modulus of elasticity (psi)
h = wall thickness (in.)
R = distance between pipe and charge (ft)
L = total length of explosive line (ft)

Due to the format of the point and parallel line predictive equations, only two graphs are required to compare the curves defined by the. equations to the test data. The first graph, Figure 70, includes the circumferential strain predictive curve and all of the corresponding point and parallel line explosive source data obtained by SwRI. Figure 71 is a similar graph for the longitudinal strains. The scatter of the data about the two solution lines, as indicated by the estimate of the standard error S, is good for this type of testing. Also, the wide range of the data makes these solutions valid for pipe strains ranging from 10 to 1,500 µin/in. This range should cover most blasting situations near gas pipelines.

As these strain solutions evolved, they were useful in estimating the strains for the experimental portions of the program. They provided realistic prediction values of strain for setting amplifier gains and recording voltage levels. It is for this type of application that Equations (105) through (108) are most useful. However, for a blasting situation near an operational pipeline for which an estimate of the blasting stresses is required, the estimated blast strains need to be converted to stresses so that they can be combined with other stresses on the pipe to determine the total state of stress. This conversion may be dictated by company policy. or be decided upon by the engineer in charge.

As was done early in the program, the stresses can be approximated by converting the maximum predicted strains using the uniaxial conversion formula. Or, one can make the

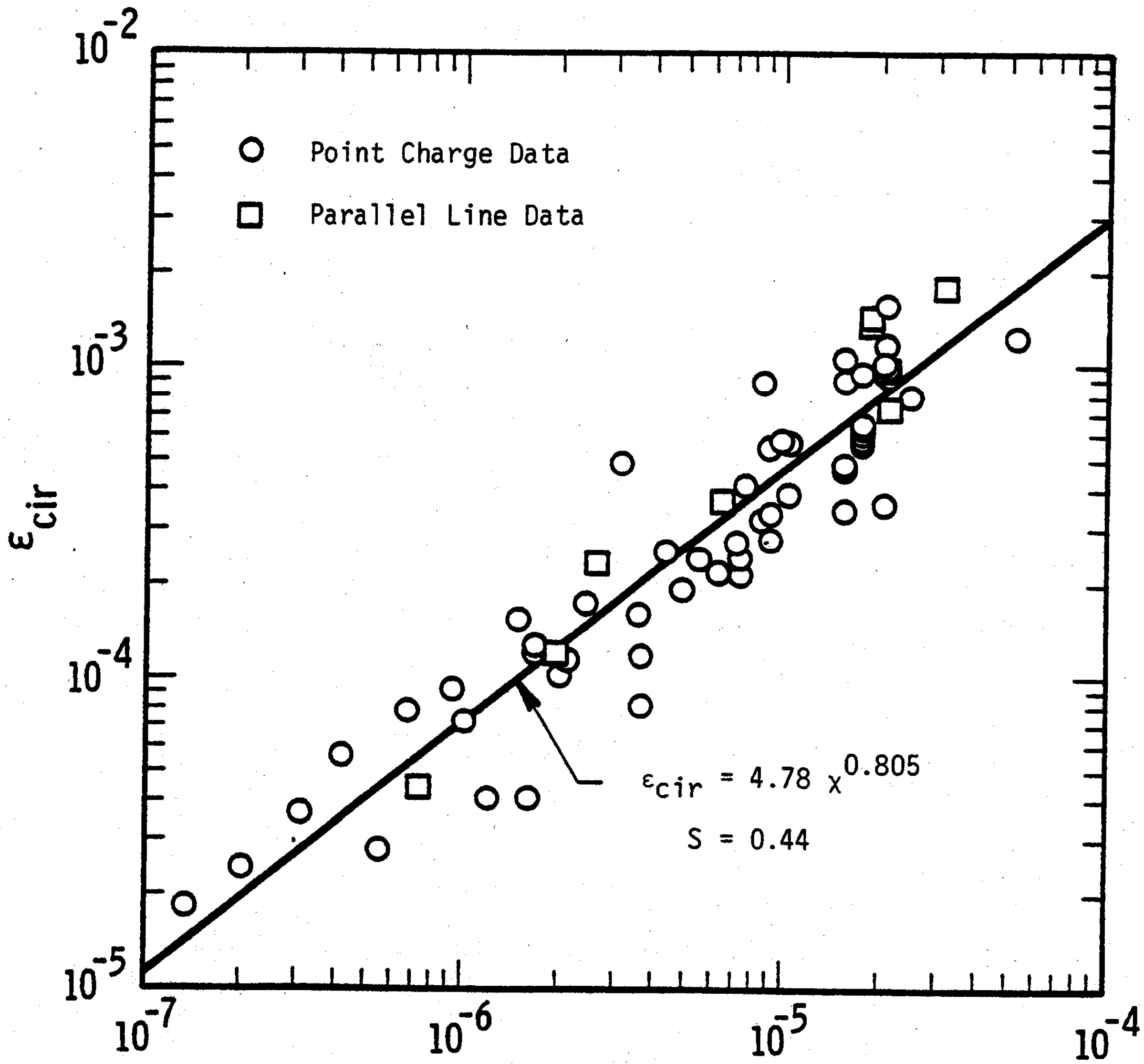

$$\text{POINT CHARGE:}\quad X = \frac{nW}{\sqrt{Eh}\ R^{2.5}} \qquad \left(\frac{lb_m}{psi^{0.5}\ in^{0.5}\ ft^{2.5}}\right)$$

$$\text{PARALLEL LINE:}\quad X = \frac{1.3n\ W/L}{\sqrt{Eh}\ R^{1.5}}$$

Figure 70. Circumferential Strain Solutions for Point and Parallel Line Explosive Charges

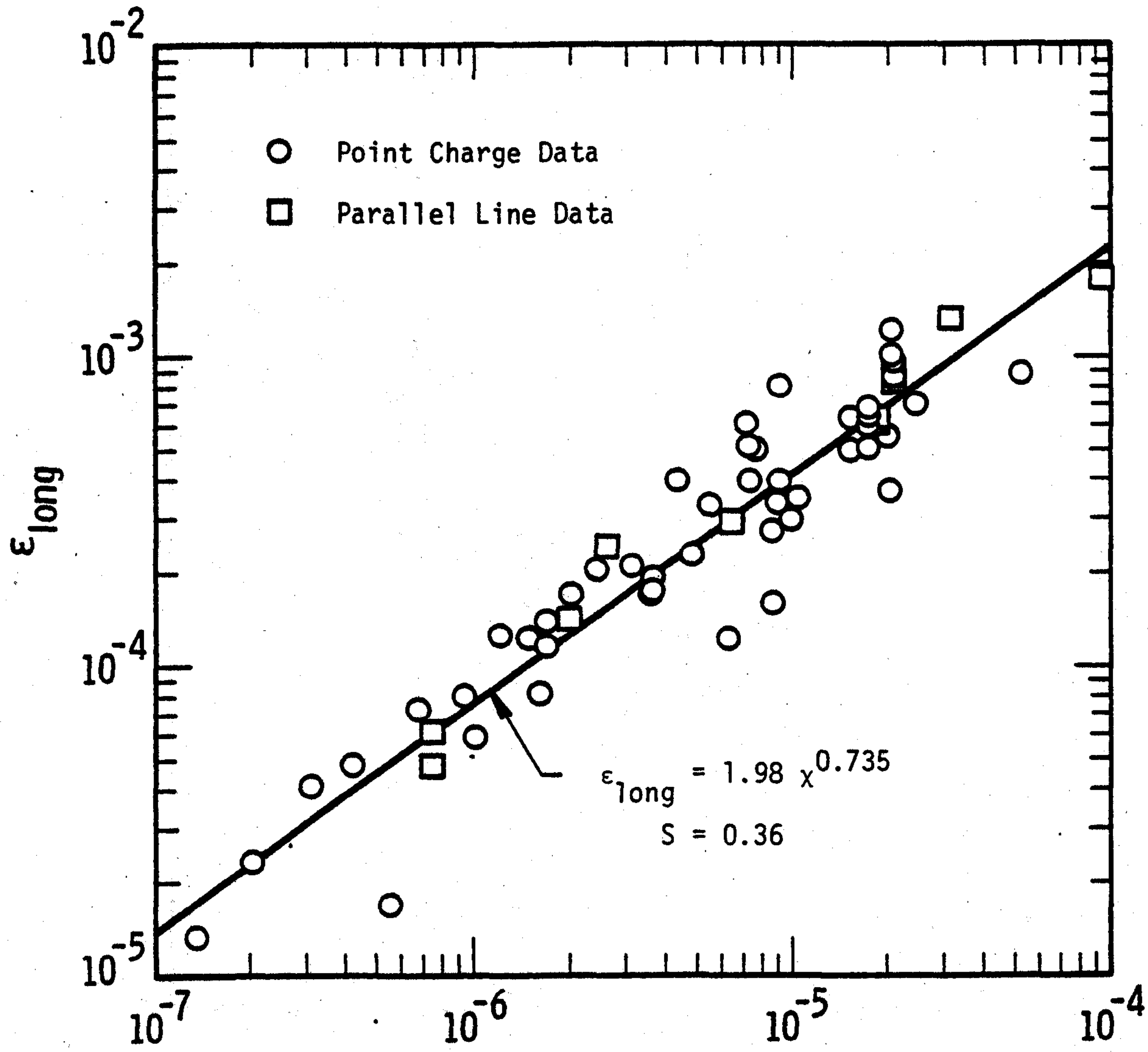

POINT CHARGE: $\chi = \dfrac{nW}{\sqrt{Eh}\ R^{2.5}}$

PARALLEL LINE: $\chi = \dfrac{1.3\, n\, W/L}{\sqrt{Eh}\ R^{1.5}}$

$$\left(\frac{lb_m}{psi^{0.5}\ in^{0.5}\ ft^{2.5}}\right)$$

Figure 71. Longitudinal Strain Solutions for Point and Parallel Line Explosive Charges

same conservative assumptions presented in Section III to compute biaxial stresses using Equations (30) and (31).

$$\sigma_{cir} = \frac{E}{1-\nu^2}(\epsilon_{cir} + \nu\epsilon_{long}) \tag{30}$$

$$\sigma_{long} = \frac{E}{1-\nu^2}(\epsilon_{long} + \nu\epsilon_{cir}) \tag{31}$$

To eliminate the step of converting the strains to stresses, the biaxial stress data presented in Section III were used to derive stress equations using similar data analysis and empirical observations as was done to develop the strain equations for point and parallel line sources. One thing that changes slightly is the size of the data base. For some of the early tests, only hoop measurements were made and were used in the strain data fits. However, the corresponding hoop stresses could not be computed since the longitudinal strain components were not measured on these tests. Thus, fewer circumferential stress data points were available than strain data points.

As indicated by Equations (30) and (31), surface biaxial stresses on a particular pipe are strictly a function of the two orthogonal strains. Therefore, one can combine Equations (105) and (106) with Equations (30) and (31) and obtain a pair of complex stress equations to derive stress prediction equations for a point source. To derive a simpler set of equations, the following approach was used. For a point source, earlier discussions showed that

$$\epsilon_{long} = f_\epsilon\left(\frac{nW}{\sqrt{Eh}\ R^{2.5}}\right) \tag{109}$$

Therefore,

$$\frac{\sigma_{cir}}{E}, \frac{\sigma_{long}}{E} = f_\sigma\left(\frac{nW}{\sqrt{Eh}\ R^{2.5}}\right) \tag{110}$$

Similarly, for a parallel line source

$$\frac{\sigma_{cir}}{E}, \frac{\sigma_{long}}{E} = f_\sigma\left(\frac{nW/L}{\sqrt{Eh}\ R^{1.5}}\right) \tag{111}$$

Using the pipe stress data, the hoop and axial stress functions for point and parallel line sources were curve fit. The resulting equations for circumferential and longitudinal stresses defined prediction curves which almost coincided with each other. Therefore, all of the stress data, regardless of sensing direction, was then used to derive a single function. This makes the predicted stresses equal in both the circumferential and longitudinal direction. To combine both point and parallel line data into a single solution, a numerical constant was again introduced to the right side of Equation (111) for the parallel line data. The best data fit required a constant slightly different than had been used with the strain data. The resulting equation for predicting the maximum pipe stresses for point and parallel line explosive sources is

$$\frac{\sigma}{E} = 4.44 \ \chi^{0.77} \tag{112}$$

where the term x is defined as follows:

$$\chi = \frac{nW}{\sqrt{Eh} \ R^{2.5}} \qquad \text{(point source)} \tag{113}$$

and

$$\chi = \frac{1.4nW/L}{\sqrt{Eh} \ R^{1.5}} \qquad \text{(parallel line source)} \tag{114}$$

The parameters in these equations are defined as follows:

σ = maximum circumferential or longitudinal stress (psi)
n = equivalent energy release (nondimensional)
W = total charge weight of point or line (lb)
E = modulus of elasticity (psi)
h = wall thickness (in.)
R = distance between pipe and charge (ft)
L = total length ofexplosive line (ft)

Note again that the constant in Equation (112) has units which correspond to those of the other parameters and makes the right-hand side of the equation dimensionless.

A comparison of the curve defined by Equation (112) and the stress data used to derive this final solution is made in Figure 72. This equation is applicable for any blasting situation

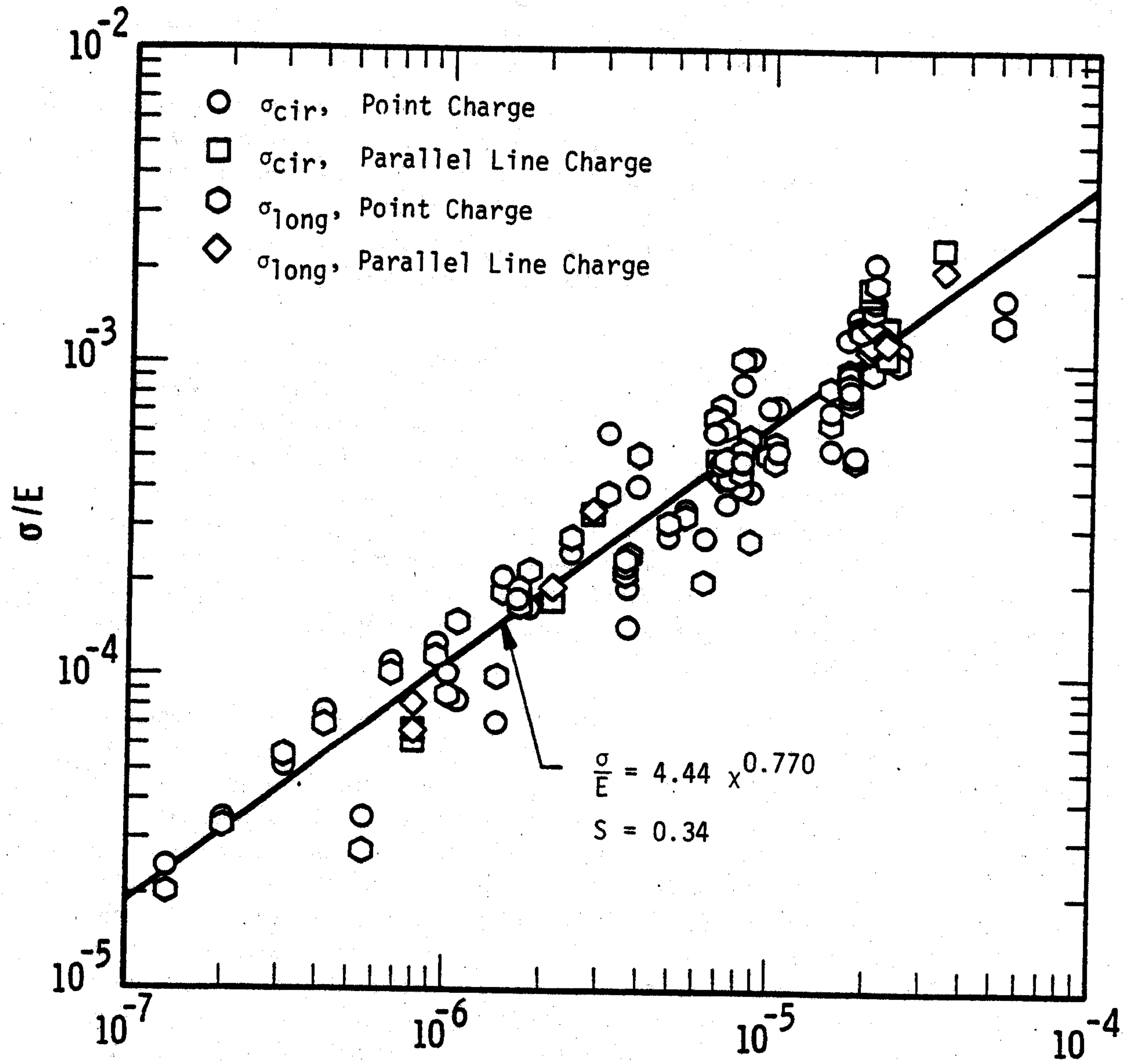

POINT CHARGE : $\chi = \dfrac{nW}{\sqrt{Eh}\ R^{2.5}}$

PARALLEL LINE : $\chi = \dfrac{1.4n\,W/L}{\sqrt{Eh}\ R^{1.5}}$ $\left(\dfrac{lb_m}{psi^{0.5}\ in^{0.5}\ ft^{2.5}}\right)$

Figure 72. Pipe Stress Solution Curve for Point and Parallel Line Explosive Charges and Comparison with Test Data

in which point or parallel line explosive sources are detonated in soil in the vicinity of a pipeline. The maximum stress data in this figure ranged from values in excess of the yield stress of most pipeline steels down to 596 psi. This range is broad enough to make the equation applicable to most soil blasting situations near steel gas pipelines provided standoff distances are greater than 2 pipe diameters.

The estimate of the standard error S of the stress data points about the solution curve in Figure 72 is only 0.34, somewhat better than what was obtained on the strain solutions. Thus, this solution predicts stresses with a slightly better accuracy. Irrespective of the pipe size, test site, or stress orientation, the data points plot above and below the curve in Figure 72. This infers that the scatter is random rather than systematic. Additional discussions about the standard error of the data about the line, sometimes referred to as the standard deviation, are presented in Section XI.

All of the parallel line data used in developing Equation (112) were treated as if obtained from continuous explosive lines because the spacing between charges was smaller than the standoff distance, the standoff distance was smaller than the length of the explosive line, and all the charges making up the line were detonated simultaneously. If the ‘spacing between charges is larger than the standoff distance, each charge should be analyzed as a point source. And, if the standoff distance between the pipe and the explosive line source is greater than the length of the explosive line, the entire explosive array can be approximated by a point source. In this program, four parallel line tests were conducted to obtain data for establishing the transition limit at which a parallel line source should be approximated by a point source.

Looking at Equations (113) and (114), and equating the value of x for a point source to that of a line source, one finds that the transition point is at a value of R/L = 0.714. Data from four experiments in which values of R/L greater than this transition value were used to check this limit. Both pipe stress and ground motion data were used in the analysis. The stress data indicated that for the two tests in which R/L = 0.95, the point source equation predicted stresses closer to the magnitude of those measured than did the parallel line solution. However, the difference was only slight, with the parallel line predictions somewhat higher. On the other hand, the data obtained from the two tests in which R/L>0.95 definitely produced data that compared much better to values predicted with the point source equation. For simplicity in application of the predictive equations, a transition value of R/L = 1.0 is recommended. This value is on the conservative side but sufficiently accurate and easy to remember. Thus, for values of R/L $\leq$ 1.0, a series of equal charges in a straight line parallel to a pipe is treated as a parallel explosive line to estimate the pipe stresses. For values of R/L> 1.0, the explosive line is treated as an equivalent point source to estimate the pipe stresses. Figure 73 summarizes how to estimate pipe stresses from parallel line explosive sources.

To show that the transition value of R/L = 1.0 is a reasonable choice, parallel line source pipe stress data obtained in 1980 are used in Figure 74 to compare to the curves defined by the prediction equations. To further support this choice, peak radial soil displace-

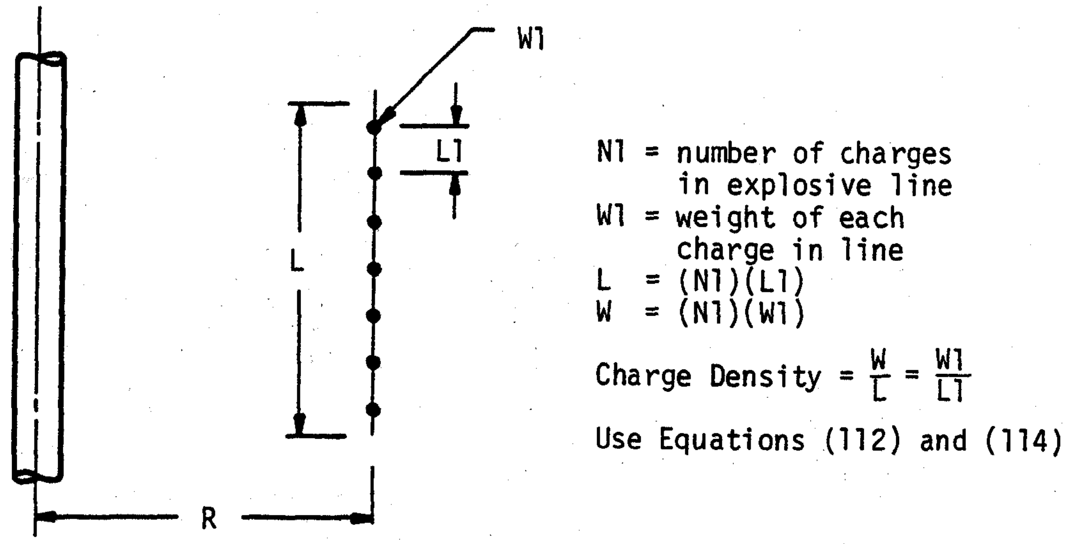

(a) Explosive Line Parallel to Pipeline for R ≤ L

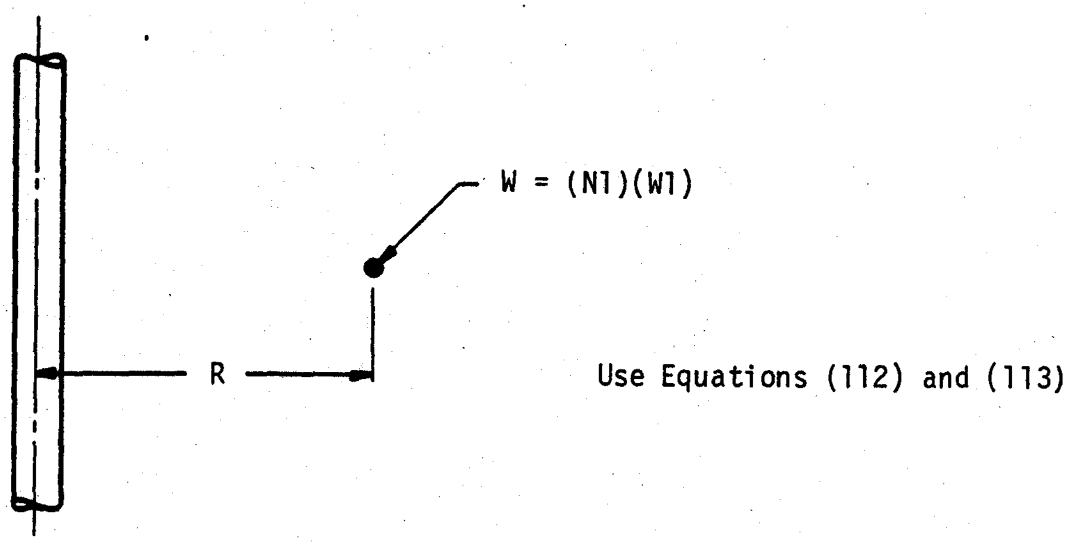

(b) Parallel Line as Equivalent Point Source for R > L

Figure 73. Methodology for Estimating Pipe Stresses from Parallel Line Explosive Sources

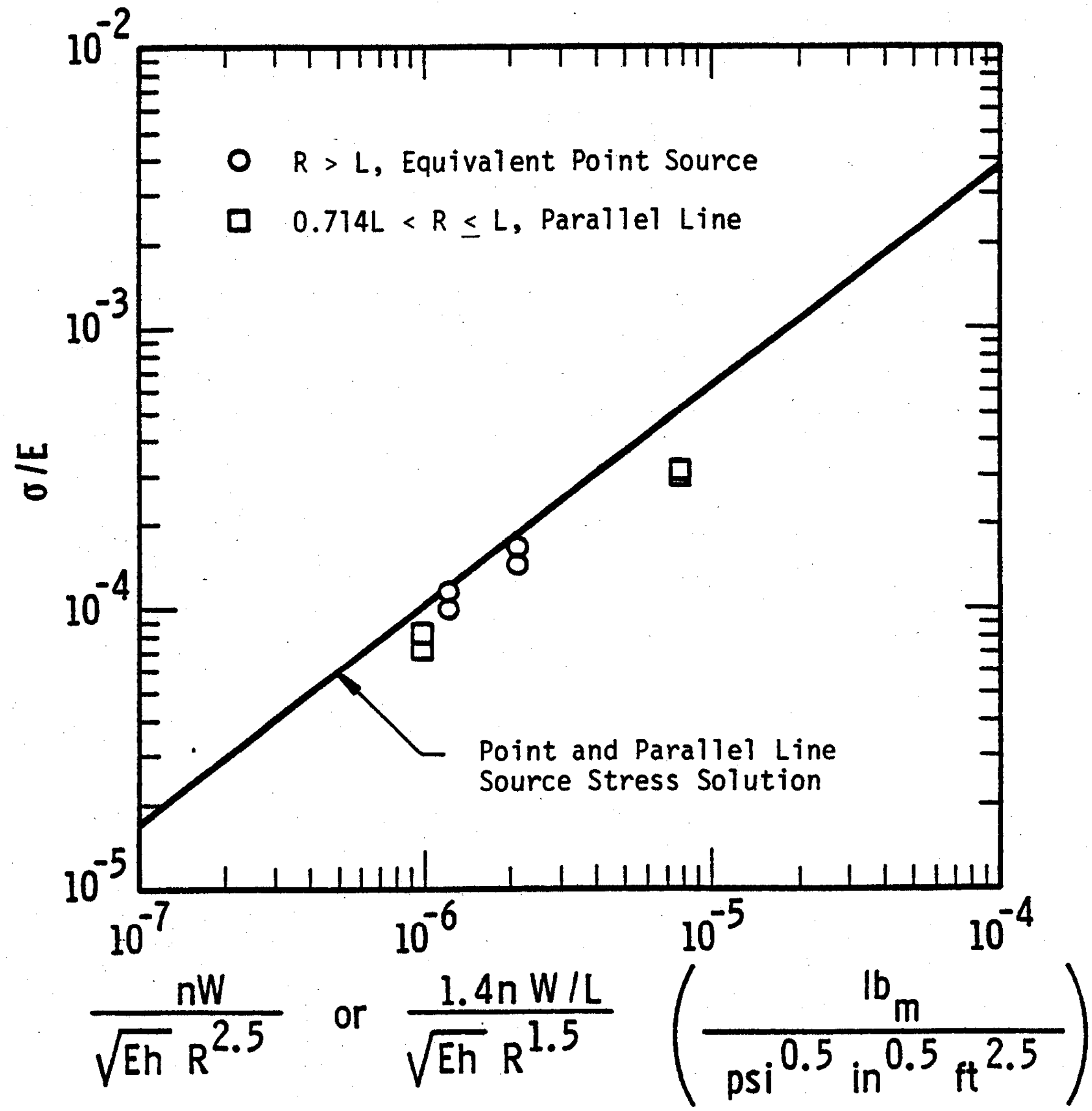

Figure 74. Parallel Line Stress Data Treated as an Equivalent Point Source or Parallel Line Source and Compared to Point and Parallel Line Stress Solution Curve

ment data obtained from all the parallel line tests are used in Figure 75 to make similar comparisons. In part (a) of this figure, data from transducers located such that 0.714 L < R $\leq$ 1.0 L are treated as being induced by parallel explosive lines. In part (b) of this figure, data from transducers located at R > L are treated as coming from equivalent point sources. Another comparison is made in Figure 76 for the soil particle velocity data. Therefore, a transition value of R > L at which a parallel line source is treated as an equivalent point source is a good choice as justified by these data comparisons.

Assumptions and Limitations

In applying the stress prediction equations developed above for point and parallel line explosive sources, it must be remembered certain idealizations were made in defining the problem and developing functional relationships. Then, assumptions were necessary to perform experiments and obtain data for defining the functions. The stress data used in completing the solutions are that presented in this report. These data points were obtained from a limited number of blasting situations. No test program of this type will ever include every possible permutation of significant parameters. Therefore, the solutions become applicable primarily within the range of the data. This limitation must be recognized in applying the results to other blasting situations.

The primary idealizations and assumptions made in defining the point and parallel line blasting problem are as follows:

- The charge and pipeline are buried in a homogeneous and isotropic ground media.
- A point source has no shape or finite size.
- A line source is a continuous explosive line parallel to a pipeline.
- All explosive sources detonate instantly.
- The pipeline is straight and infinite in length without any discontinuities.
- The pipe is in direct contact with the ground media.
- Reflections of the seismic waves from the surface are insignificant.
- A constant percentage of the explosive energy goes into cratering and other related phenomena.
- Only elastic stress contributions from blasting were considered. Inelastic behavior was not included.

Some of these idealizations could only be approximated in the actual tests. The general test conditions were as follows:

- The charge and pipeline were buried in relatively homogeneous soils.

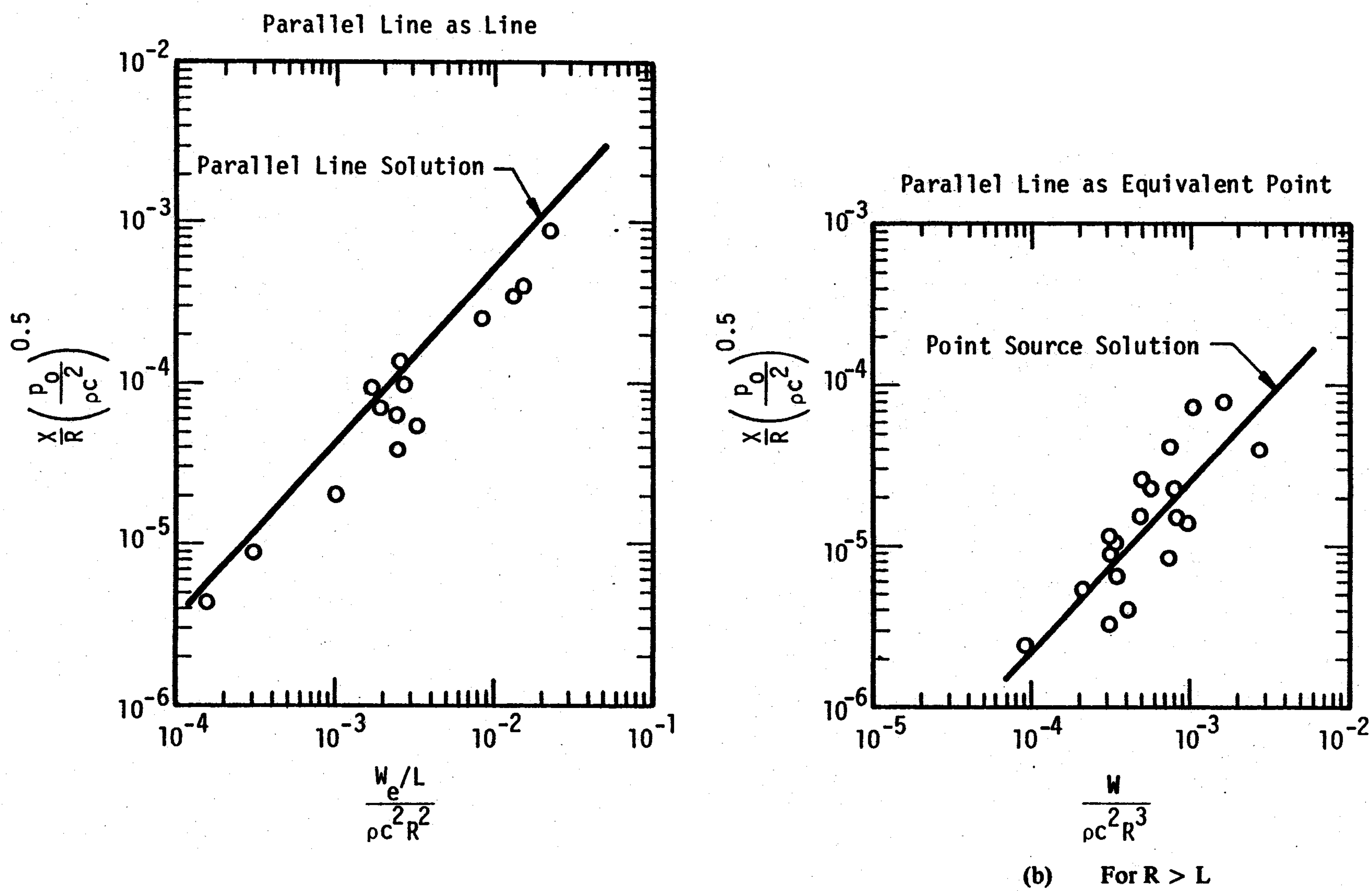

Figure 75. Comparison of Radial Soil Displacements From Parallel Explosive Lines Treated as Parallel Lines or Point Sources

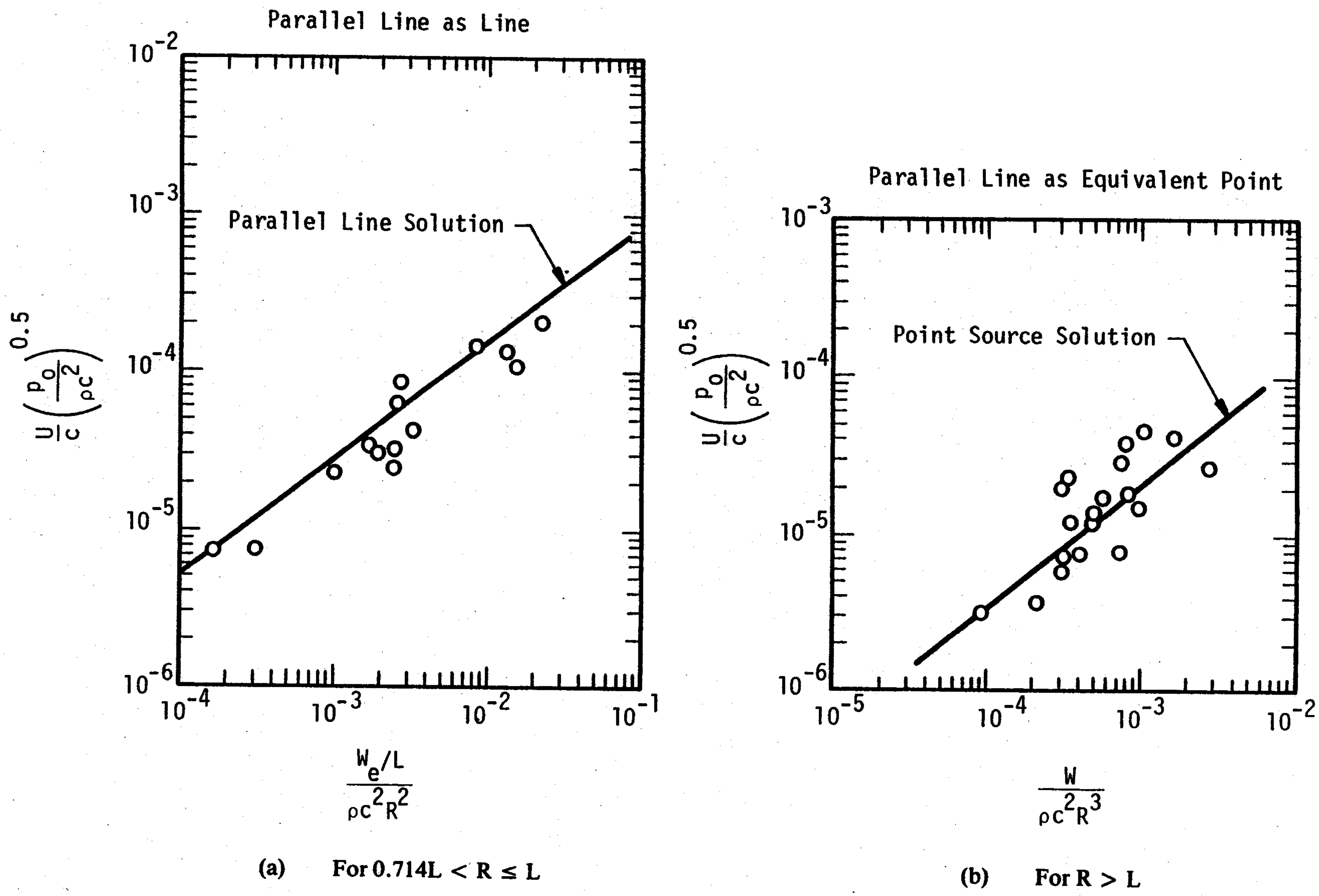

Figure 76. Comparison of Radial Soil Velocities from Parallel Lines Treated as Parallel Lines or Point Sources

- The pipes tested were buried to a depth equal to about two pipe diameters to their centerline.

- In most cases, the explosive source was buried to the same depth as the center of the pipe.

- A point source was approximated with a sphere of explosive material.

- A parallel line source was approximated mostly by a series of seven point charges of equal weight and spaced equidistant from each other.

- For a parallel line source, the ratio of the standoff distance to the length of the explosive line was less than 0.5.

- All the model pipes were buried in direct contact with the soil. Full scale pipelines had coating on them.

- For a line source, the ratio of the charge spacing to the standoff distance was less-than 0.42.

- Except for 6 grid tests which used delays of 3 and 6 milliseconds, the explosive sources were detonated within 50 microseconds.

- The length of the pipe tested was at least two times longer than the standoff distance (in most cases, it was longer).

The range of the significant dimensional and nondimensional parameters varied in the SwRI tests and were as follows:

- Point charge weights were varied from 0.03 to 15 lb.

- Line charge explosive densities varied from 0.015 to 0.267 lb/ft.

- All pipes tested were carbon steel pipes with a handbook modulus of elasticity of 29.5×10^6 psi and a Poisson's ratio of 0.3.

- Pipe thickness varied from 0.059 to 0.515 in.

- The maximum biaxial stresses computed from the measured strains varied from 596 to 69,400 psi.

- The estimate of the standard error of the stress data about the solution curve was 34%.

- The dimensionless ratio of σ/E varied from 2.02×10^{-5} to 2.08×10^{-3} for point sources, and 6.2×10^{-5} to 2.35×10^{-3} for parallel line sources.

- The quantity x varied from 1.35×10^{-7} to 5.23×10^{-5} for point sources, and 7.96×10^{-7} to 3.38×10^{-5} for parallel line sources.

In order to apply the point and parallel line solutions, the blasting situation in question should be such that it falls primarily within the range of *x* of the solutions, and the test conditions are close to the same as those listed above. The model analysis of Section II tells us that satisfaction of the pi terms (or combinations thereof) is most important, not the individual physical parameters. For instance, the fact that the largest explosive weight used in this program was 15 lb does not limit use of the equations to charges smaller than this value. Instead, the charge size in combination with its location and pipe description dictate the limits of the experimental data and the solutions derived from them.

Furthermore, the fact that only some particular pipe sizes were used does not limit the solutions to those specific pipes. Again, the replica model law tells us that a 6-inch diameter, 0.093-inch wall thickness pipe models any other pipe of proportional dimensions. Thus, the response of a 12-inch diameter, 0.186-inch wall thickness pipe can be predicted with the data of the smaller pipe as long as the blasting situations are analogous. Obviously, the less similarity there is between a blasting situation in question and those of this test program, the less valid will be the point and parallel line source equations.

Illustrative Examples

Two simple problems will now be solved to illustrate the use of the point and parallel line solutions. in deriving these equations, substitutions were made to have the various parameters in the units most used in the field. Thus, the energy release (W,) which had been used in the ground motions discussions was replaced by nW. The quantity n is a measure of the relative energy among the explosives and consequently is dimensionless. Using the energy release of ANFO (94/6) as the base, all explosive energies can be normalized to determine the value of n. Thus, for ANFO (94/6), n equals 1.00. Those explosives more energetic have a value of n greater than 1.00 and those less energetic have a value of n less than 1.00. Using the same explosives listed in Table 12, a list of equivalent energy releases is presented in Table 14.

Table 14. Equivalent Energy Release

Explosive	n
ANFO (94/6)	1.00
AN Low Density Dynamite	0.99
Comp B (60/40)	1.12
Comp C-4	1.12
HBX-1	0.83
NG Dynamite (40%)	1.05
NG Dynamite (60%)	1.12
Pentolite (50/50)	1.11
RDX	1.16
TNT	0.98

To demonstrate the use of Equations (112) and (113) to predict stresses from a point source, Example Problem No. 3 follows:

Example Problem No. 3

Given: A 2.5-lb point charge of 60 percent NG dynamite will be detonated buried 4 ft in soil adjacent to a 24-inch O. D. by 0.312 W. T., API-5L, Grade "B" pipeline. In this area, the pipeline has a 3-ft cover of soil.

Find: Estimate the blast-induced circumferential and longitudinal pipe stresses if the charge is 15 ft from the pipe.

Solution: (a) List parameters required in Equation (113) in proper units

E = 29.5×10^6 psi
h = 0.312in.
n = 1.12
W = 2.5 lb
R = 15ft

(b) Evaluate *x* using Equation (113)

$$\chi = \frac{(1.12)(2.5)}{\sqrt{(29.5 \times 10^6)(0.312)}\ (15)^{2.5}}$$

$$\underline{\chi = 1.059 \times 10^{-6}}$$

This value is within the range of the solution data.

(c) Substitute into Equation (112) and solve for σ

$$\frac{\sigma}{(29.5 \times 10^6)} = 4.44(1.059 \times 10^{-6})^{0.77}$$

σ = 3,284 psi

$$\underline{\sigma_{cir} = \sigma_{long} = 3{,}284 \text{ psi}} \qquad (S = \pm 1{,}117 \text{ psi})$$

The estimate of the standard error S of the stress data points about the solution curve defined by Equation (112) was ±0.34. Therefore, the quantity in parentheses by the answer to Example Problem No. 3 represents the standard error applicable to this problem.

To show how Equations (112) and (114) are used to estimate blast induced stresses from a parallel line source, Example Problem No. 4 is provided.

Example Problem No. 4

Given: Seven 60 percent NG dynamite point charges weighing 2.5 lb each and spaced 3 ft apart are buried 4 ft in a soil media. The line of charges is parallel to a 24-inch O. D. by 0.312 W. T., API-5L, Grade- "B" pipeline which has 3 ft of soil cover.

Find: The estimated blast-induced pipe stresses if the line of charges is 15 ft from the pipe.

Solution: (a) List parameters required in Equation (114) in proper units

E = 29.5×10^6 psi
h = 0.312 in.
n = 1.12
N1 = 7 charges
L1 = 3 ft
L = (7)(3) = 21 ft
W1 = 2.5 lb
W = (7)(2.5) = 17.5 lb
R = 15 ft

(b) Since R < L, evaluate x using Equation (114)

$$\chi = \frac{(1.4)(1.12)(17.5)}{\sqrt{(29.5 \times 10^6)\ (0.312)}\ (15)^{1.5}\ (21)}$$

$$\chi = 7.414 \times 10^{-6}$$

(c) Substitute into Equation (112) and solve for σ

$$\frac{\sigma}{(29.5 \times 10^6)} = 4.44(7.414 \times 10^6)^{0.77}$$

$$\sigma = 14{,}690 \text{ psi}$$

$$\underline{\sigma_{cir} = \sigma_{long} = 14{,}690 \text{ psi}} \qquad (S = \pm 4{,}995 \text{ psi})$$

These two examples illustrate the direct use of Equations (112) through (114) for estimating pipe stresses from buried point and parallel line explosive sources. In the next section of this report, different methods and forms of presenting these equations are presented. One or more of these alternative forms of presenting these solutions may be selected and used for solving these types of blast problems in office or field manuals.

VII. ALTERNATIVE FORMS FOR POINT AND PARALLEL LINE STRESS EQUATIONS

The solutions for estimating pipe stresses developed in the preceding section can be applied in the field. This report is not a field manual; however, some alternative ways of using the pipe stress solutions are presented, illustrated and discussed. All of the procedures which will be illustrated use the same relationships to compute stress. Each approach is nothing more than a different method for arriving at the same answers. Thus, all the limitations must be kept in mind regardless of which form the solution takes. Five procedures are presented.

Direct Use of Equations

This is, of course, the most obvious way of using the prediction equations. At the end of Section VI, two examples illustrated the direct use of the equations to predict the pipe stresses. However, another point source problem will be used here to predict the pipe stresses and to determine the largest charge that would be allowed in a particular situation.

As derived earlier, the point source prediction equation can be written simply as

(115)

To illustrate the use of this equation, Example Problem No. 5, which follows, will be used throughout this section. Assume that an ANFO (94/6) explosive charge weighing 20 lb is buried 25 ft from a 24-inch O. D. by 0.25 W. T. steel pipe with a modulus of elasticity of 29.5×10^6 psi. Both pipe and charge are buried to about the same depth in a soil medium. Estimate the maximum stresses, σ_{cir} and σ_{long}, caused by the blast wave propagated through the soil.

The equivalent charge weight for the given explosive is first obtained from Table 14. In this case n = 1.0. Substituting all the parameters into Equation (115) and solving for σ gives:

$$\sigma = (4.44)(29.5 \times 10^6)\left[\frac{(1.0)\ (20)}{\sqrt{(29.5 \times 10^6)\ (0.25)}\ (25)^{2.5}}\right]^{0.77}$$

$$= (4.44)\ (29.5 \times 10^6)\ (2.357 \times 10^{-6})^{0.77}$$

$$\underline{\sigma_{cir} = \sigma_{long} = 6{,}080 \text{ psi}} \qquad (S = \pm 2{,}067 \text{ psi})$$

These stresses are the elastic contributions due to blast loading. To determine the total state of stress in the pipe, the stresses due to pressurization, temperature changes, pipe settlement, and other causes must be superimposed and some biaxial yield theory used to determine if the pipe yields.

Assume in this problem that the maximum allowable blast stress is only 3,000 psi. What charge weight would produce this stress? Solving Equation (115) for W and substituting the numerical values for the other parameters gives

$$W = \frac{\sqrt{Eh}\ R^{2.5}}{n}\left(\frac{\sigma}{4.44E}\right)^{1/0.77}$$

$$W = \frac{\sqrt{(29.5\times 10^{6})(0.25)}\ (25)^{2.5}}{(1.0)}\left[\frac{3,000}{(4.44)(29.5\times 10^{6})}\right]^{1.2987}$$

$$\underline{W = 7.99\ \text{lb}}$$

The direct use of the prediction equations is fairly straightforward in estimating either the stress or any of the other parameters. However, it does require the use of a scientific calculator or other means to evaluate quantities to a power. Furthermore, to compute any of the other parameters, besides stress, requires algebraic manipulation.

Computer or Calculator Program

With the extensive availability of desk-top microcomputers and programmable pocket calculators, it is quite easy to generate a simple program to solve the point and parallel line stress prediction equations. An example of a logic diagram which was used to develop such a program by SwRI is shown in Figure 77. With a program, the solution of blasting situations involving point and parallel line sources becomes quite routine. The use of a continuous memory programmable calculator also allows these calculations to be made easily at remote sites.

To solve for any parameter besides stress, the same basic program is useful, but requires some iteration to obtain an answer. Or one can simply develop a separate program for each parameter of interest. The solution of the first part of Example Problem No. 5 obtained using an HP 9830 computer program is shown in Figure 78. The answer is the same as previously given for the direct use of the equations. The value of *x* is also included in the printout to insure the problem falls within the limits of the solution.

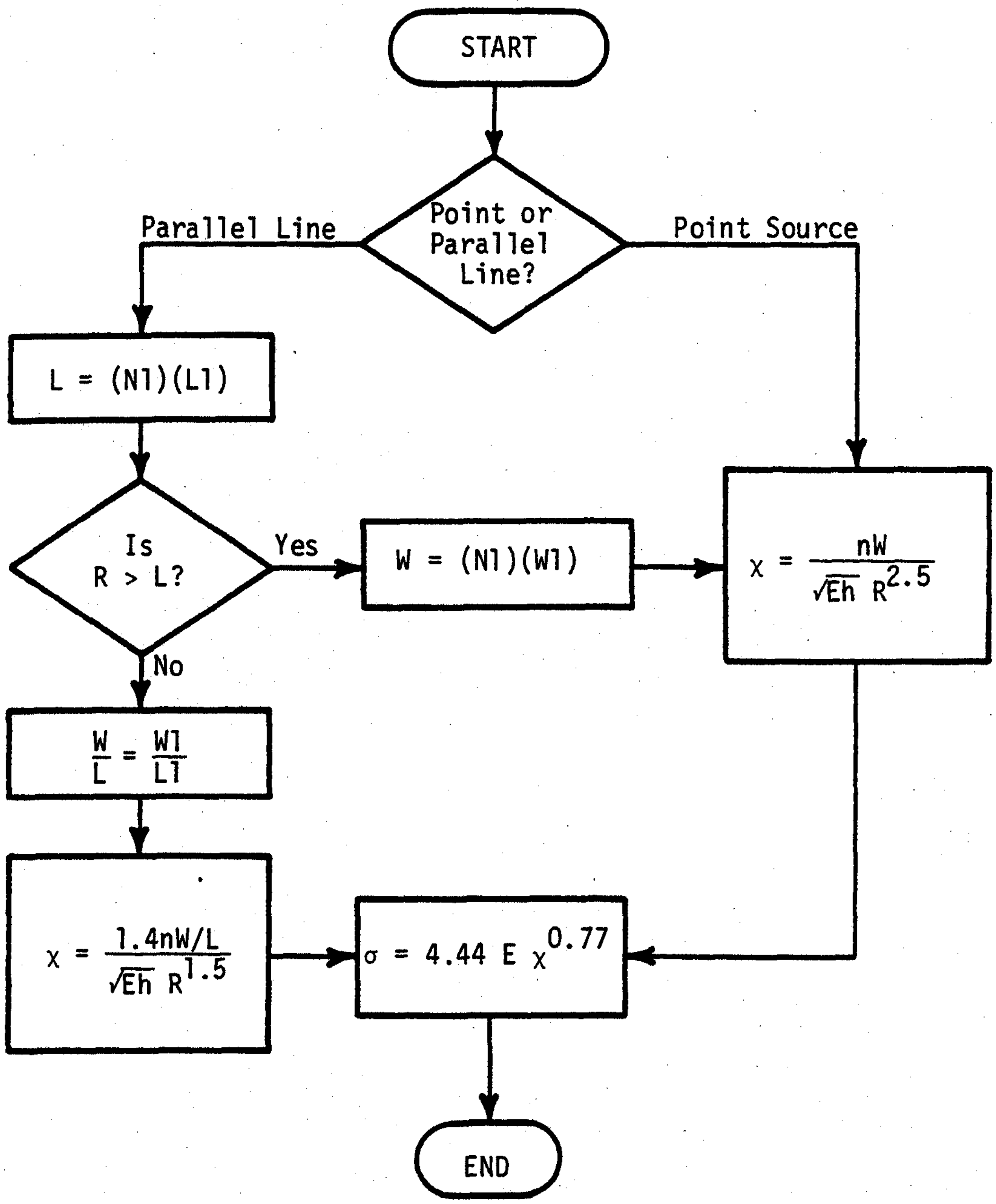

Figure 77. Logic Diagram Using Point and Parallel Line Source Pipe Stress Prediction Equations

```
BLAST EFFECTS FROM POINT SOURCE FOR   0.250  INCH PIPE
ESTIMATED CIRCUMFERENTIAL AND LONGITUDINAL STRESSES

E =  29.5 MILLION PSI      N =  1.00

CHARGE    DIST         X          CIR OR LONG STRESS
 (LB)     (FT)                          (PSI)

20.000   25.00      2.357E-06           6080
```

Figure 78. Solution of Example Problem No. 5a Using Computer Program

Tabulations

Using the type of program just discussed, it is possible to generate tables in which a range of conditions are precalculated for various pipes. This format could be very useful for particular company applications in which a number of blasting situations will take place near a particular pipe or pipes. Table 15 presents parts of a printout for a point source in the vicinity of a steel pipe with a 0.25 wall thickness.

Using Table 15 to solve Example Problem No. 5 (nW = 20lb, R = 25 ft), interpolation is required between the limits bracketing the standoff distance as follows:

$$\sigma \text{ @ } R = 24 \text{ ft} = 6{,}577 \text{ psi}$$

$$\sigma \text{ @ } R = 26 \text{ ft} = 5{,}637 \text{ psi}$$

and

$$\sigma \text{ @ } 25 \text{ ft} \simeq 6577 - \frac{(6577 - 5637)}{(26 - 24)}(26 - 25)$$

$$\underline{\sigma \text{ @ } 25 \text{ ft} \simeq 6{,}107 \text{ psi}}$$

This answer is close to, but not exactly the same as, that obtained by direct calculation. Furthermore, if interpolation had also been required between two charge weights, the difference might be greater. Of course, the tables can be produced with smaller incremental steps to get more accuracy and perhaps eliminate the need for interpolations. However, this will greatly increase the length of the table. Note that the corresponding values of *x* have also been included in this particular table to show that they are within the limits of the solution.

Table 15. Computer Tabulation of Point Source Pipe Stress Equation

BLAST EFFECTS FROM POINT SOURCE

ESTIMATED CIRCUMFERENTIAL AND LONGITUDINAL STRESSES

E = 29.5 MILLION PSI   H = 0.250

NW (LB)	R (FT)	X	CIR OR LONG STRESS (PSI)
8.000	10.00	9.316E-06	17518
8.000	12.00	5.905E-06	12333
8.000	14.00	4.017E-06	9166
8.000	16.00	2.877E-06	7089
8.000	18.00	2.143E-06	5651
8.000	20.00	1.647E-06	4613
8.000	22.00	1.298E-06	3840
* 8.000	24.00	1.044E-06	3248
* 8.000	26.00	8.546E-07	2784
8.000	28.00	7.101E-07	2414
8.000	30.00	5.976E-07	2114
8.000	32.00	5.086E-07	1867
8.000	34.00	4.370E-07	1661
8.000	36.00	3.788E-07	1488
8.000	38.00	3.309E-07	1341
8.000	40.00	2.911E-07	1215
10.000	10.00	1.164E-05	20803
10.000	12.00	7.382E-06	14645
10.000	14.00	5.021E-06	10885
10.000	16.00	3.596E-06	8418
10.000	18.00	2.679E-06	6710
10.000	20.00	2.058E-06	5478
10.000	22.00	1.622E-06	4560
10.000	24.00	1.305E-06	3857
10.000	26.00	1.068E-06	3306
10.000	28.00	8.876E-07	2866
10.000	30.00	7.470E-07	2510
10.000	32.00	6.357E-07	2217
10.000	34.00	5.463E-07	1973
10.000	36.00	4.735E-07	1767
10.000	38.00	4.137E-07	1592
10.000	40.00	3.639E-07	1443
12.000	10.00	1.397E-05	23938
12.000	12.00	8.858E-06	16852
12.000	14.00	6.025E-06	12525
12.000	16.00	4.315E-06	9686
12.000	18.00	3.215E-06	7721
12.000	20.00	2.470E-06	6304
12.000	22.00	1.946E-06	5247
12.000	24.00	1.566E-06	4438
12.000	26.00	1.282E-06	3804
12.000	28.00	1.065E-06	3298
12.000	30.00	8.964E-07	2888
12.000	32.00	7.628E-07	2551
12.000	34.00	6.555E-07	2270
12.000	36.00	5.683E-07	2033
12.000	38.00	4.964E-07	1832
12.000	40.00	4.367E-07	1660

Table 15. Computer Tabulation of Point Source Pipe Stress Equation (Cont'd)

BLAST EFFECTS FROM POINT SOURCE

ESTIMATED CIRCUMFERENTIAL AND LONGITUDINAL STRESSES

E = 29.5 MILLION PSI H = 0.250

NW (LB)	R (FT)	X	CIR OR LONG S (PSI)
20.000	10.00	2.329E-05	35474
20.000	12.00	1.476E-05	24974
20.000	14.00	1.004E-05	18562
20.000	16.00	7.192E-06	14354
20.000	18.00	5.358E-06	11442
20.000	20.00	4.117E-06	9342
20.000	22.00	3.244E-06	7776
* 20.000	24.00	2.610E-06	6577
* 20.000	26.00	2.137E-06	5637
20.000	28.00	1.775E-06	4888
20.000	30.00	1.494E-06	4280
20.000	32.00	1.271E-06	3780
20.000	34.00	1.093E-06	3364
20.000	36.00	9.471E-07	3013
20.000	38.00	8.274E-07	2715
20.000	40.00	7.278E-07	2460
22.000	10.00	2.562E-05	38175
22.000	12.00	1.624E-05	26876
22.000	14.00	1.105E-05	19975
22.000	16.00	7.911E-06	15447
22.000	18.00	5.893E-06	12314
22.000	20.00	4.529E-06	10053
22.000	22.00	3.568E-06	8368
22.000	24.00	2.871E-06	7077
22.000	26.00	2.350E-06	6067
22.000	28.00	1.953E-06	5260
22.000	30.00	1.643E-06	4606
22.000	32.00	1.399E-06	4068
22.000	34.00	1.202E-06	3620
22.000	36.00	1.042E-06	3243
22.000	38.00	9.101E-07	2922
22.000	40.00	8.006E-07	2647
24.000	10.00	2.795E-05	40821
24.000	12.00	1.772E-05	28738
24.000	14.00	1.205E-05	21359
24.000	16.00	8.630E-06	16518
24.000	18.00	6.429E-06	13167
24.000	20.00	4.940E-06	10750
24.000	22.00	3.893E-06	8948
24.000	24.00	3.132E-06	7568
24.000	26.00	2.564E-06	6487
24.000	28.00	2.130E-06	5625
24.000	30.00	1.793E-06	4925
24.000	32.00	1.526E-06	4350
24.000	34.00	1.311E-06	3871
24.000	36.00	1.137E-06	3467
24.000	38.00	9.928E-07	3125
24.000	40.00	8.733E-07	2831

With this table, it is also possible to solve the second part of Example Problem No. 5 (determine what charge weight located at R = 25 ft will limit the blast stress to 3,000 psi). Since the standoff distance of 25 ft is not specifically listed, interpolation is again necessary. Looking for a stress value of 3,000 psi between R's of 24 and 26 ft, we find that for an nW = 8 lb

$$\sigma @ R = 24 ft = 3,248 psi$$

$$\sigma @ R = 26 ft = 2,784 psi$$

Therefore,

$$\sigma @ R = 25 ft = 3,016 psi$$

and

$$\underline{W \simeq 8 \text{ lb}}$$

The process gets' slightly more complicated if interpolation had also been required between two charge weights.

Good approximate answers can be obtained without too much manipulation using this type of table. If the tables are brief, and the number of interpolations increases, the answers become less accurate. If the tables are made such that very small increments of nW and R are used to decrease the interpolation process and obtain better approximate answers, then their length increases considerably. In addition, the number of tables can become very bulky if many pipe sizes, and parallel line as well as point sources are to be considered.

Graphs

All of the information contained in Table 15 can be displayed in a single graph plotting σ versus (nW) and R for constant values of h and E. The abscissa can either by values of (nW) or R. The other parameter would then plot as a series of lines of constant values. Figure 79 is one of these plots drawn for a pipe modulus of elasticity of 29.5 x 10^6 psi and a pipe wall thickness of 0.25 inch. In this case, R was selected as the abscissa and the series of isoclines drawn are for constant values of equivalent charge weights (nW).

The solution of the first part of Example Problem No. 5 (nW = 20 lb, R= 25 ft) is shown in Figure 79. The pipe stress is determined to be

$$\sigma_{cir} = \sigma_{long} \simeq 6,100 \text{ psi}$$

The second part of this example can also be solved by finding the intersect of the orthogonal lines derived by σ = 3,000 psi and R = 25 ft. By visually interpolating between lines of (nW) we find

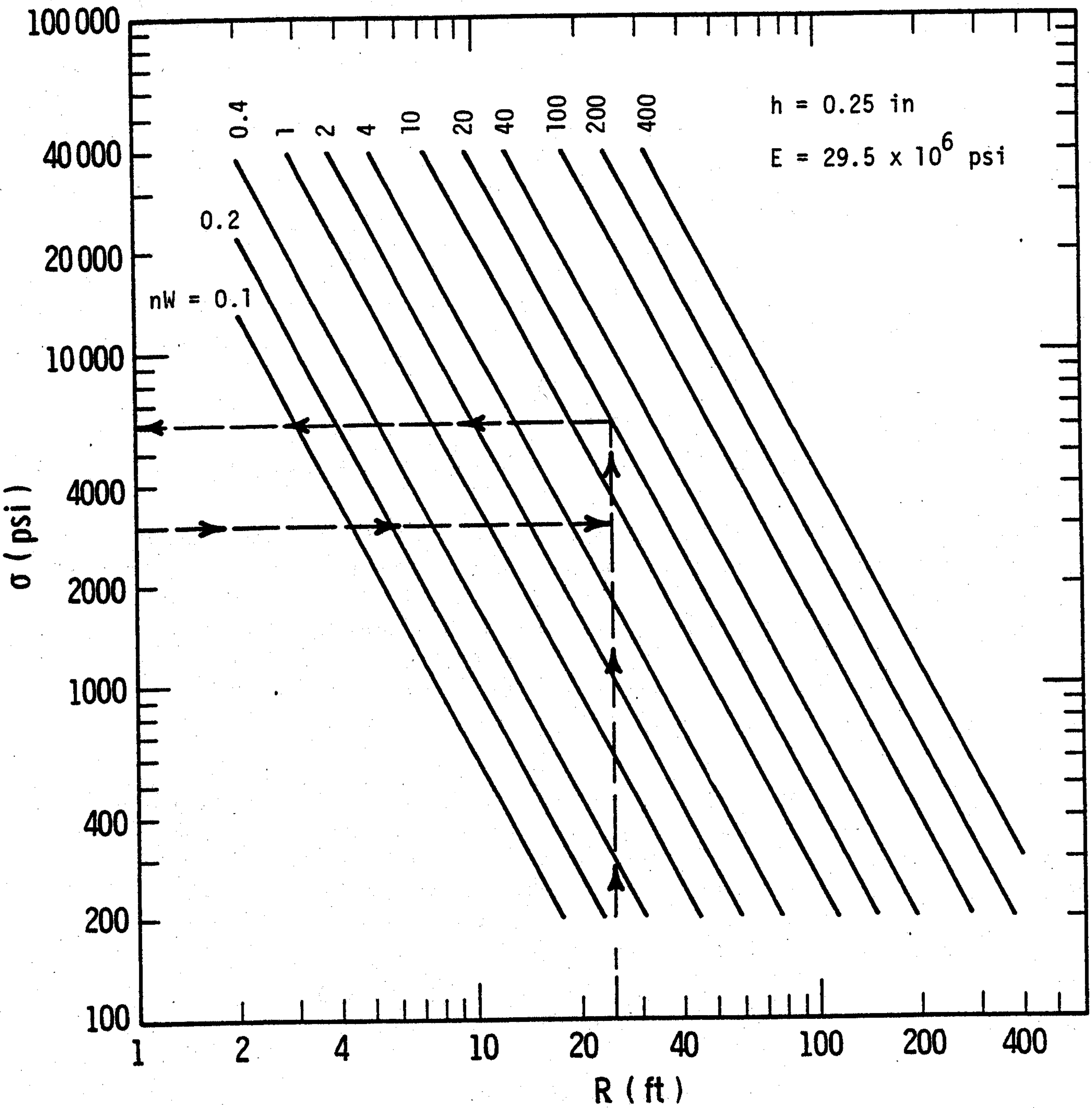

Figure 79. Graphical Solution of Point Source Equation

$$W \simeq 8 \text{ lb}$$

This form of the point source solution has the advantage of requiring no computations. Interpolation is required but it is visual. However, one graph is required for every pipe thickness or pipe material, and a similar set of graphs would be necessary for the parallel line source equation. The major disadvantage of this form of the solution is that the user must be proficient in using graphs and understanding logarithmic scales.

Nomographs

It is possible to develop a graphical solution for each equation with all the-parameters shown separately because of the nature of the point and parallel line source equations. One nomograph would represent the complete solution of the point source equations and a second would represent the solution of the parallel line source equations. Figures 80 and 81 are these nomographs. In these figures, logarithms are being added and subtracted until the pipe stress is obtained. For instance, for a point source, Figure 80 represents Equation (115) in the form of

[logo] = 0.615 [log E] -0.385 [log h] + 0.77 [log nW] -1.925 [log R] + [log 4.44] (116)

A similar expression can be written for a parallel line source.

To use one of these nomographs, one begins by finding the modulus of elasticity for the pipe material on the vertical axis. A horizontal line is then projected from this modulus over to the appropriate pipe thickness in the contours in the lower left quadrant of the nomographs. From the pipe thickness, a vertical line is projected up to the appropriate equivalent charge weight (lbs of ANFO) in the contours in the upper left quadrant. From the charge weight, a horizontal line is projected over to the appropriate standoff distance in the contours in the upper right quadrant of the figures. Finally, the pipe stress from blasting is read by projecting a vertical line from the standoff distance to the pipe stress axis.

To illustrate the use of one of these nomographs, the solution of the first part of Example Problem No. 5 is shown in Figure 80. For this problem, the parameters are

E = 29.5 X 10^6 psi
h = 0.25 in.
nW = 20 lb
R = 25 ft

The maximum pipe stresses as read from this figure are

$$\sigma_{cir} = \sigma_{long} \simeq 6{,}000 \text{ psi}$$

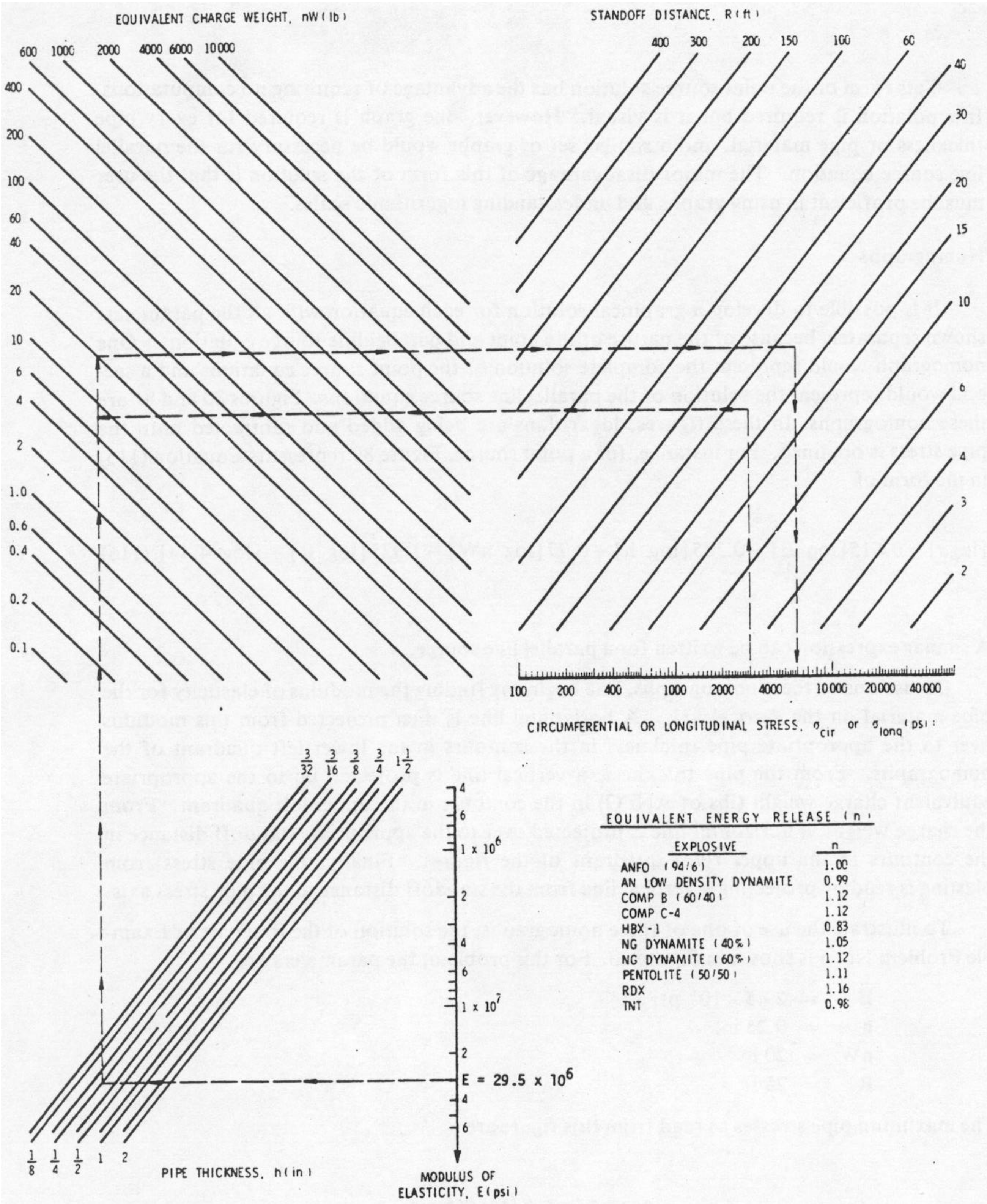

EXPLOSIVE	n
ANFO (94/6)	1.00
AN LOW DENSITY DYNAMITE	0.99
COMP B (60/40)	1.12
COMP C-4	1.12
HBX-1	0.83
NG DYNAMITE (40%)	1.05
NG DYNAMITE (60%)	1.12
PENTOLITE (50/50)	1.11
RDX	1.16
TNT	0.98

Figure 80. Pipe Stress Nomograph for Point Sources

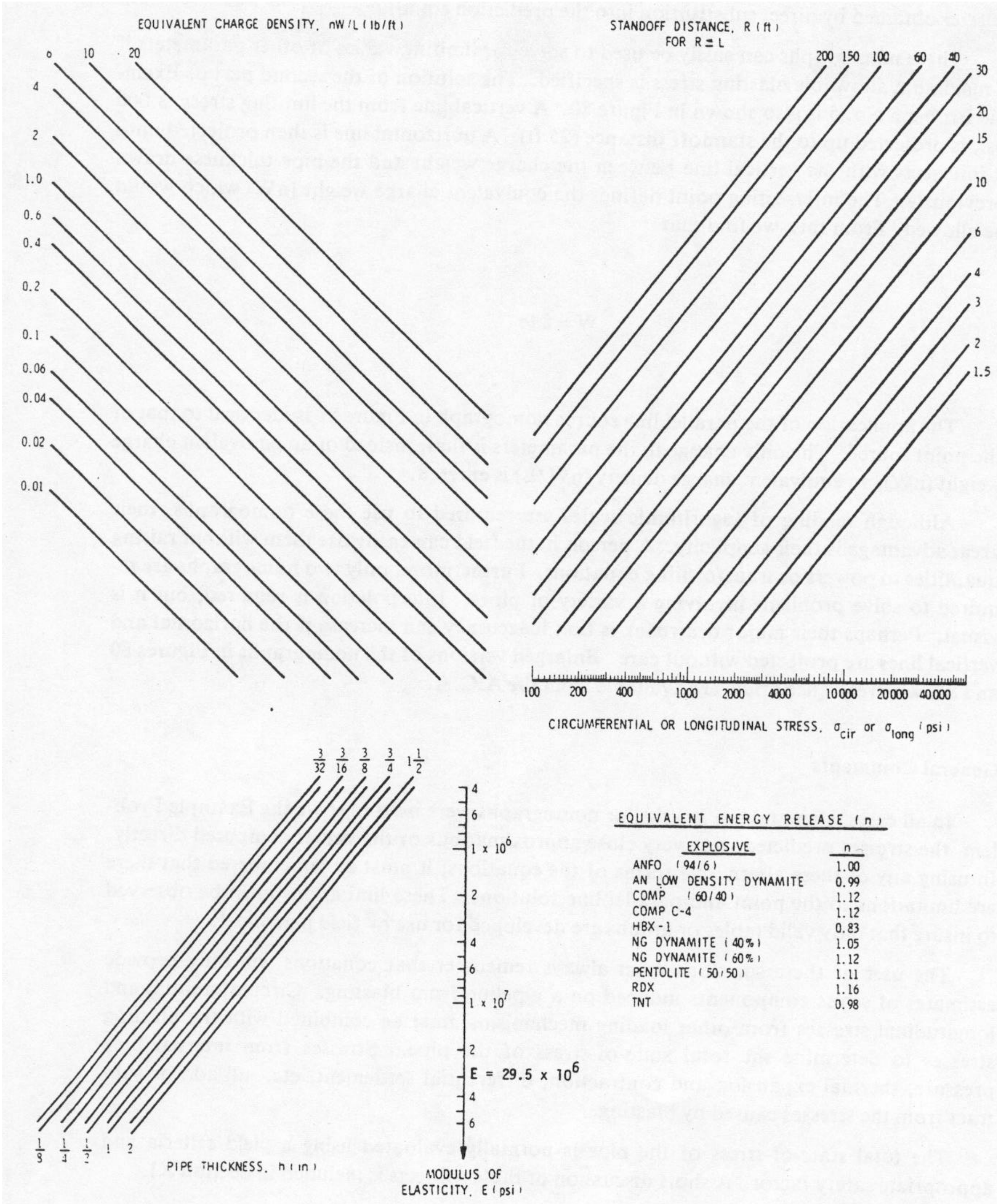

Figure 81. Pipe Stress Nomograph for Parallel Line Sources

Once again graphical inaccuracies prevent the solution from having the precision of an answer obtained by direct substitution into the prediction equation.

These nomographs can easily be used to solve for limiting values of other parameters if a maximum allowable blasting stress is specified. The solution of the second part of Example Problem No. 5 is also shown in Figure 80. A vertical line from the limiting stress, 3,000 psi, is projected up to the standoff distance (25 ft). A horizontal line is then projected until it intersects with the vertical line between the charge weight and the pipe thickness drawn previously. The intersecting point defines the equivalent charge weight (nW) which would be allowed. From this, we find that

$$W \simeq 8 \text{ lb}$$

The application of the parallel line source nomograph in Figure 81 is identical to that of the point source. The only change in the parameters is that, instead of an equivalent charge weight (nW), an equivalent charge density (nW/L) is entered.

Although reading of logarithmic scales are required to use these nomographs, their great advantage is their simplicity. A person in the field can easily use them without raising quantities to powers or transforming equations. Furthermore, only two nomographs are required to solve problems involving a variety of pipes. Interpolation is required, but it is visual. Perhaps their major drawback is that inaccuracy can increase if the horizontal and vertical lines are projected without care. Enlarged versions of the nomographs in Figures 80 and 81, with reference grids, are available from the A.G.A.

General Comments

In all cases where tables, graphs, or nomographs were used to solve the Example Problem, the stresses predicted were very close approximations of the values computed directly. In using any of these alternative forms of the equations, it must be remembered that there are limitations to the point and parallel line solutions. These limitations must be observed to insure that only valid tables or graphs are developed for use by field personnel.

The user of these solutions must always remember that equations will only provide estimates of stress components induced on a pipeline from blasting. Circumferential and longitudinal stresses from other loading mechanisms must be combined with the blasting stresses to determine the total state-of-stress of the pipe. Stresses from internal pipe pressure, thermal expansion and contraction, differential settlement, etc., all add or subtract from the stresses caused by blasting.

The total state-of-stress of the pipe is normally evaluated using a yield criteria and appropriate safety factor. A short discussion of these subjects is included in Section XI.

VIII. METHODOLOGY FOR SIMPLIFYING COMPLEX EXPLOSIVE GEOMETRIES

General

In the two preceding sections, the solutions for estimating pipe stresses from point and parallel line explosive sources detonated in soil were derived and discussed in detail. In addition to these two sources, three other more complex explosive geometries detonated in soil were studied experimentally in this program using model pipes. These studies were not as extensive as for the point sources. Therefore, the approach followed in analyzing the test data was to develop consistent methods by which these complex geometries could be simplified into equivalent parallel line or point sources, and thus be used with the corresponding prediction equations to obtain reasonable estimates of the pipe stresses.

Three complex explosive geometries were used:

- Explosive lines buried at an angle to a pipeline
- A rectangular grid of explosive charges buried parallel to a pipeline
- A grid of explosive charges at an angle to a pipeline.

In all cases, the individual charges making up the arrays were buried in soil to the same depth as the center of the model pipe. In the paragraphs that follow, the simplifying methods will be presented by explosive geometry, with the simplest first. Comparisons of the test data from these explosive geometries and the point and parallel line solution curves will also be made.

Angled-Line Explosive Source

The pipe stress and ground motion data from the ten angled-line tests listed in Tables 8 and 9 (Section IV) were analyzed extensively to obtain a method that would yield reasonable stress estimates by simplifying this source into an equivalent parallel line or point source. In discussing the results of these analyses, it is first necessary to define the following parameters which are applicable to angled-line, as well as grid, sources:

A = distance of nearest charge making up the explosive line
B = angle between pipeline and explosive line
R_{gel} = distance between the geometric center of the explosive line and the longitudinal center of a pipeline

The value of R_{gel} for any explosive line can be computed as follows:

$$R_{gcl} = A + \frac{(N1 - 1)L1 \ \sin B}{2} \tag{117}$$

where $N1$ = number of charges in the explosive line
$L1$ = spacing of charges in the explosive line

In general, the distance between the pipeline and the explosive line relative to the length of the explosive line determines whether an angled-line source is treated as an equivalent parallel line or point source. At close distances (as defined later), the angled-line source can be treated as a parallel line source of the same effective length L and charge density W/L as that of the angled-line. However, the location or standoff distance of the equivalent parallel line becomes

$$R = R_{gel}/\cos B \qquad \text{(line)} \tag{118}$$

The effective length L and charge density W/L of an angled-line source are the same as were defined for a parallel line source. To reiterate

$$L = (N1)(L1) \tag{119}$$

and

$$\frac{W}{L} = \frac{(N1)(W1)}{(N1)(L1)} = \frac{W1}{L1} \tag{120}$$

where W1 is the explosive weight of one of the point charges making up a line source. These two equations apply for explosive lines made up of equally spaced charges of the same weight. This geometry was true of all the field tests conducted in this blasting research project. With the equivalent values of R and W/L as defined above, the pipe stresses can be estimated using the parallel line equation which is

$$\frac{\sigma}{E} = 4.44\left(\frac{1.4nW/L}{\sqrt{Eh}\ R^{1.5}}\right)^{0.77} \tag{121}$$

Further away from a pipeline, an angled-line source would be expected to behave like a point source. The analyses of the angled-line test data indicated that this transition occurs at a standoff distance R, as defined by Equation (118), approximately equal to the length of the explosive line L. A good comparison between the test data (both stress and ground motion) and the point and parallel line solution curves was possible when the transition value of R/L was made unity. This value is the same as was obtained for parallel line sources in Section VI.

Therefore, at values of R [defined in Equation (118)] greater than L [defined in Equation (119)], the angled-line source is collapsed into an equivalent point source located at the geometric center of the line with a charge weight equal to the total explosive weight in the line. When an angled-line explosive source is made into an equivalent point source, R and W are defined as follows:

$$R = R_{gel} \qquad \text{(point)} \tag{122}$$

and

$$W = (N1)(W1) \tag{123}$$

With these values of R and W, the blast-induced pipe stresses can be estimated using the point source equation which is

$$\frac{\sigma}{E} = 4.44\left(\frac{nW}{\sqrt{Eh}\;R^{2.5}}\right)^{0.77} \tag{124}$$

The methodology for simplifying the angled-line sources used in this program into an equivalent parallel line or point source is illustrated in Figure 82.

Parallel Grid Explosive Source

To estimate pipe stresses induced by a rectangular grid of explosives buried in soil to the same depth as the adjacent pipe, an empirical method was developed using data from 15 model tests described in Section III of this report. Analyses of these data (Tables 10 and 11, Section VI) indicated that reasonable agreement could be obtained between experimental and estimated stresses if the grid is treated as a parallel line equivalent in location, length and charge density as the first explosive row making up the array. This being the case, the standoff distance R, length of the equivalent parallel line source L, and equivalent charge density W/L are simply defined as

$$R = A \qquad \text{(line)} \tag{125}$$

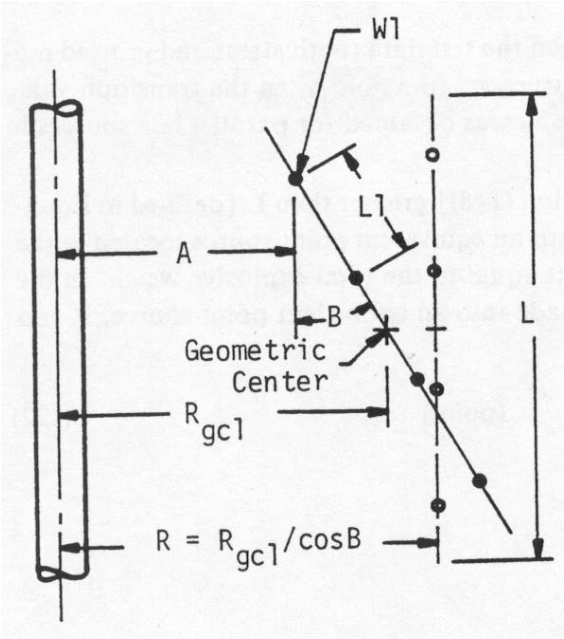

A = distance to nearest charge
N1 = number of charges in explosive line
W1 = weight of each charge in line
L = (N1)(L1)
w = (N1)(w1)
B = angle between pipe and explosive line

Charge Density = $\frac{W}{L} = \frac{W1}{L1}$

Use Equation (121)

(a) Angled-Line as Equivalent Parallel Line for $R \leq L$

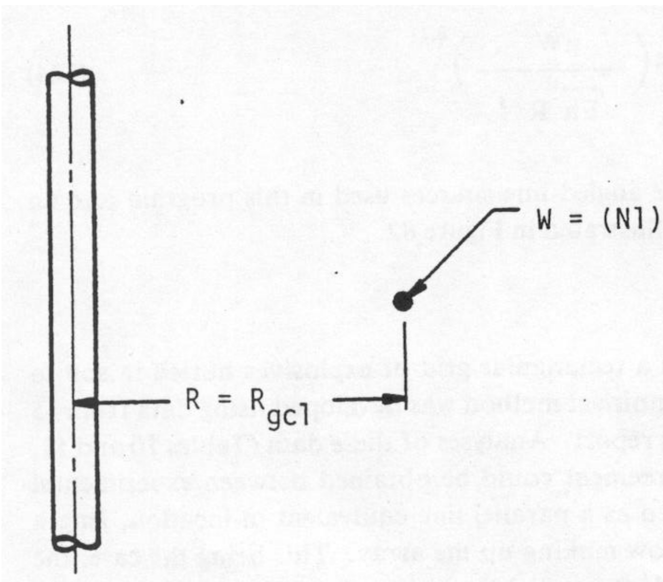

Use Equation (124)

(b) Angled-Line as Equivalent Point Source for $R > L$

Figure 82. Methodology for Estimating Pipe Stresses from an Angled-Line Explosive Source

$$L = (N1)(L1) \tag{126}$$

$$\frac{W}{L} = \frac{W1}{L1} \tag{127}$$

where A = distance of nearest row making up the grid (ft)
N1 = number of equally spaced charges in the front row
L 1 = spacing of charges in the front row (ft)
W 1 = explosive weight of one charge in grid (lb)

Analyses of the data indicated that as long as $R \leq 1.5L$, good agreement occurred with the parallel line source solution, Therefore, for these values of R, Equation (121) is used to estimate the pipe stresses from a grid source simplified into an equivalent parallel line source.

As shown in Figure 83b, at values of R_{gcg} greater than 1.5L, the experimental data indicated that a better comparison with a prediction equation was possible if the grid was approximated by a single charge equal in weight to that in the entire array and located at the geometric center of the grid, a distance R away from the centerline of the pipe. In other words, when the front row of the grid was located at distance greater than 1.5L, R and W were defined as follows:

$$R = R_{gcg}, = A + \frac{(N2-1)L2}{2} \tag{128}$$

$$W = (N1)(N2)(W1) \tag{129}$$

where N2 is the number of equally spaced rows making up a grid. With these values for the standoff distance and charge weight, Equation (124) is used to estimate the pipe stresses from a grid explosive source simplified into an equivalent point charge. The simplifying procedures for a grid charge array parallel to a pipeline are summarized in Figure 83.

Angled-Grid Explosive Source

The method developed for simplifying rectangular explosive arrays located at an angle to a pipeline combines the procedures for the parallel grid and angled-line sources. Data obtained in 13 angled-grid tests were used in this analysis. As indicated in Figure 84a, the front row of the angled-grid first becomes an equivalent angled-line. This equivalent angled-line, with its geometric center located a distance R_{gc1} away from the pipe centerline, is further simplified into an equivalent parallel line if. $R=R_{gc1}/\cos B$ is less than or equal to 1.5 times the length L of the equivalent angled-line (the first row making up the grid). As was the case

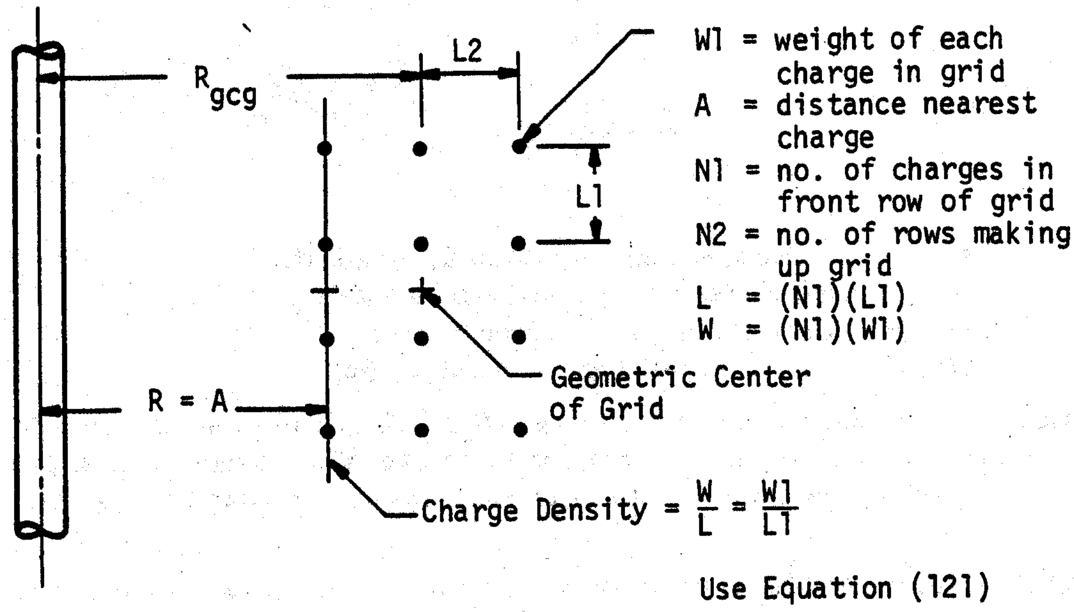

(a) Parallel Grid as Equivalent Parallel Line for R $\leq$ 1.5 L

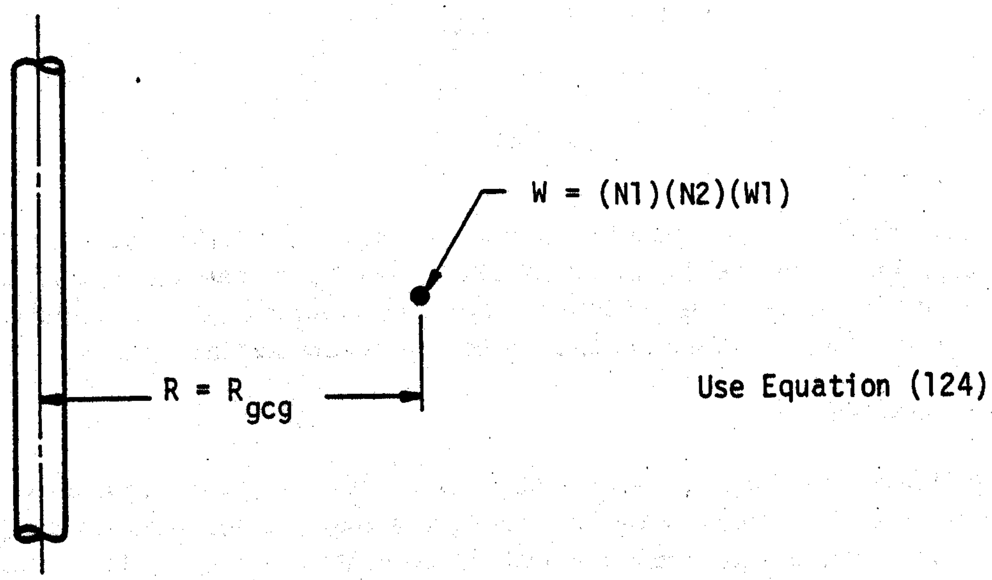

(b) Parallel Grid as Equivalent Point Source for R > 1.5 L

Figure 83. Methodology for Estimating Pipe Stresses from a Parallel Grid Explosive Source

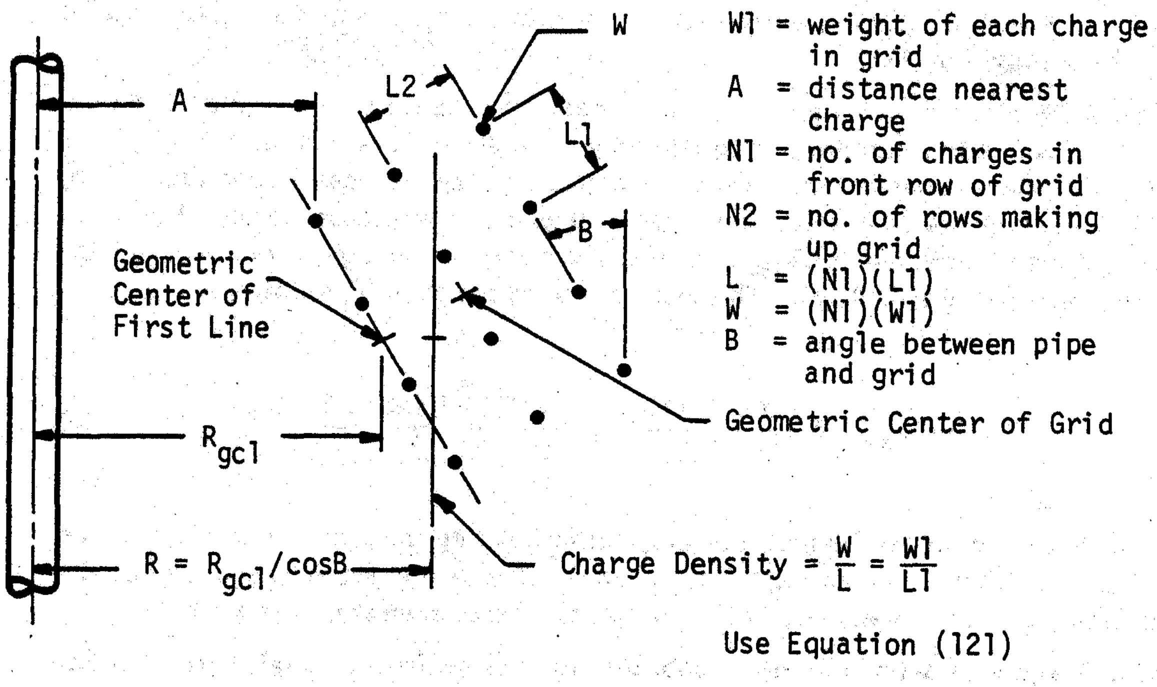

(a) Angled-Grid as Equivalent Parallel Line for R ≤ 1.5 L

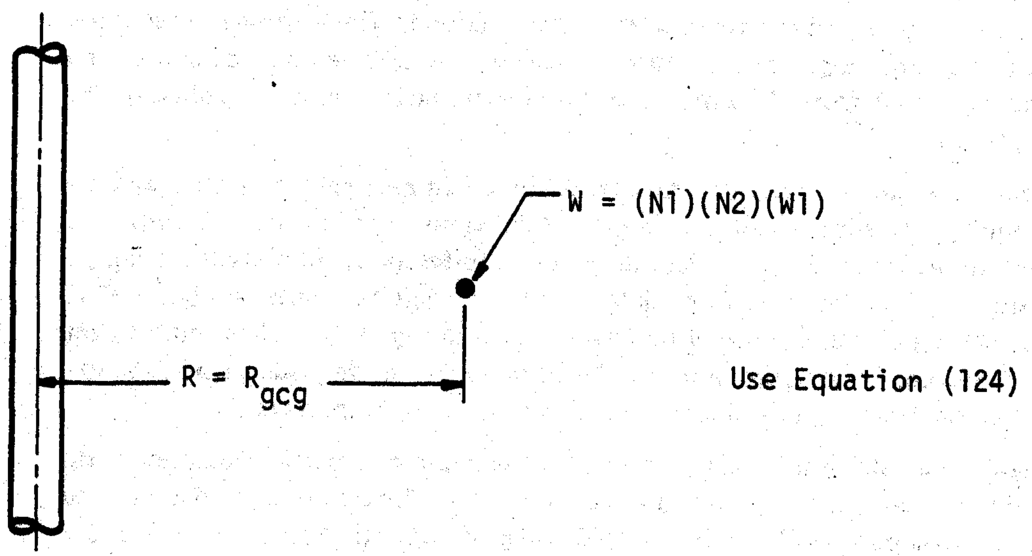

(b) Angled-Grid as Equivalent Point Source for R > 1.5 L

Figure 84. Methodology for Estimating Pipe Stresses from an Angled-Grid Explosive Source

with a parallel grid; the charge density W/L becomes that of the first row of the grid. With R and W/L defined, the pipe stresses for an angled-grid can be estimated using the parallel line solutions, Equation (121).

As was the case for the parallel grid, if the standoff distance [as defined by Equation (118)] of the equivalent parallel line representing an angled-grid is such that R = R_{gcl} /cos B> 1.5 L, the grid is collapsed into an equivalent point source. As indicated in Figure 84b, the equivalent point charge W would equal the total explosive weight of the angled-grid and its standoff distance would be R_{gcg} the distance between the pipe centerline and the geometric center of the angled-grid. This distance can be computed as follows:

$$R = R_{gcg} = A + \frac{(N1-1)L1\ \sin B + (N2-1)L2\ \cos B}{2} \tag{130}$$

Note that this equation can be used not only for calculating the standoff distance of the equivalent point charge for an angled-grid, but it is also the general equation for the equivalent point source for any grid or line source, parallel or at an angle to a pipe.

With W and R as defined in Figure 84b, the pipe stresses from an angled-grid that has been simplified into an equivalent point source can be estimated using Equation (124).

Comparisons with Test Data

In the three preceding subsections, methods for estimating pipe stresses from angled-line, parallel grid, and angled-grid explosive sources were defined. These empirical methods simplify the complex explosive geometries into equivalent parallel line or point sources so. that the prediction equations from the simpler explosive geometries could be applied to the more complex geometries.

Figure 85 compares the experimental data from these complex geometry tests against the parallel line and point source solution curve. This figure shows that the empirical methods presented do provide reasonable estimates of circumferential and longitudinal pipe stresses. The scatter of the complex source data about the prediction lines in Figure 85 is within the scatter of the point and parallel line data shown in Figure 72. This comparison shows that the methodology for approximating the complex explosive grids used in the experiments performed on this project yields reasonable estimates of pipe stress.

To show further that the simplifying methods for the complex explosive geometries do provide reasonable predictions, the ground motion data from these tests were also used to compare to the point and parallel line solutions. These ground motion data provided more evidence for determining the transition distance at which the complex source is to be treated as a point instead of a parallel line source, particularly since only nine of the total of 38 tests were set up such that the pipe happened to be distant enough for the explosive geometry to be treated as a point source. Figure 86a compares the parallel line solution curve, Equation

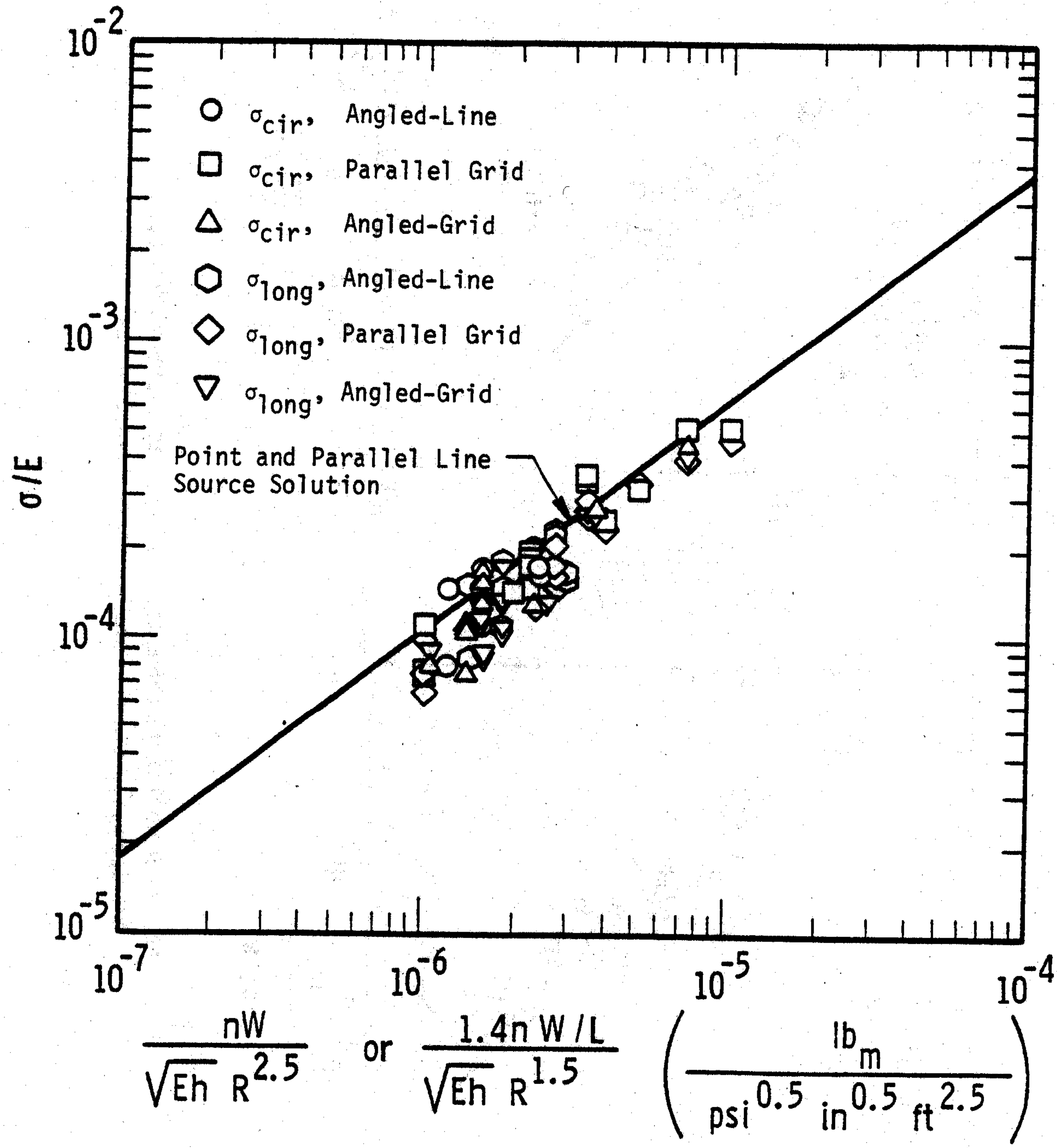

Figure 85. Comparison Between Pipe Stress Data from Complex Explosive Sources and Point and Parallel Line Source Solution

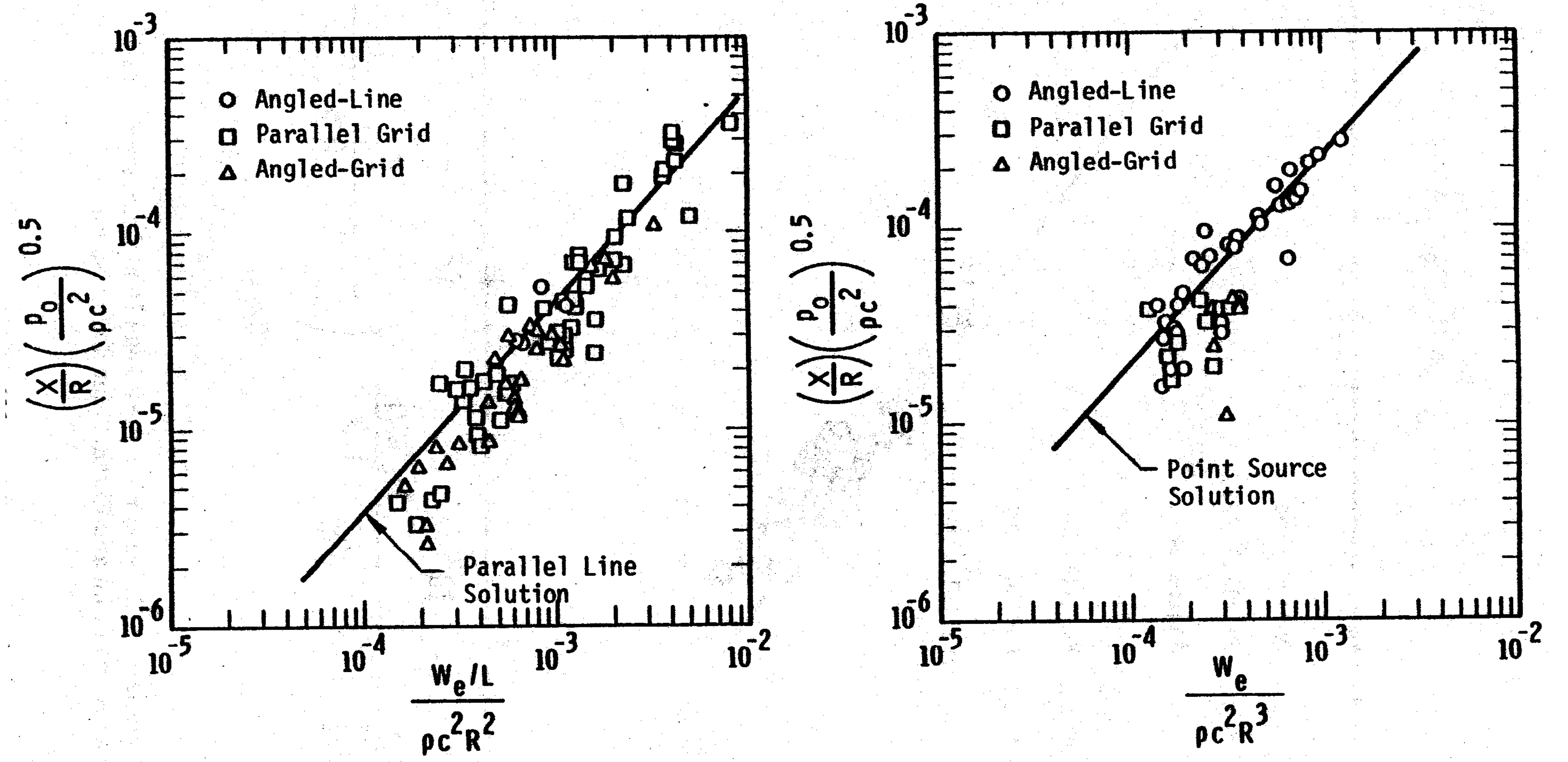

Figure 86. Radial Displacements from Complex Explosive Sources Treated as Equivalent Parallel Line or Point Sources

(48), and all of the displacement data which could be categorized as being from an equivalent parallel line source. Figure 86b compares the rest of the displacement data obtained from transducers located such that the complex geometry could be treated as a point source to the point source data fit, Equation (44). The complex geometry data compare well to the solution lines in both of these graphs. Similarly, Figure 87 shows plots of the soil particle data compared to the parallel line and point source solutions, Equations (49) and (45) which were derived in Section V. Again, good agreement was found between the complex explosive source data, and the parallel line and point source particle velocity equations.

The reader must not forget the assumptions and limitations which apply to the point and parallel line solutions in applying the simplifying methods discussed in this section to estimate pipe stresses from buried explosive sources. Furthermore, the test data from the complex explosive geometries presented in the figures of this section are somewhat limited and not every blasting problem encountered will be geometrically similar and within the parameter range of these data. For example, comparing Figure 72 from Section VI and Figure 85 in this section, one can observe that the range of the stress data are considerably less for the complex sources. The range of the measured stresses was from about 2,200 psi to almost 15,000 psi, and x ranged only from 1.01×10^{-6} to 1.02×10^{-5}. Consequently, these methods must always be used judiciously.

The next section of this report will present some exceptions to the methods developed here and will summarize the prediction methods by use of a logic diagram which will simplify their application. In addition, the use of this diagram will be illustrated with an example problem.

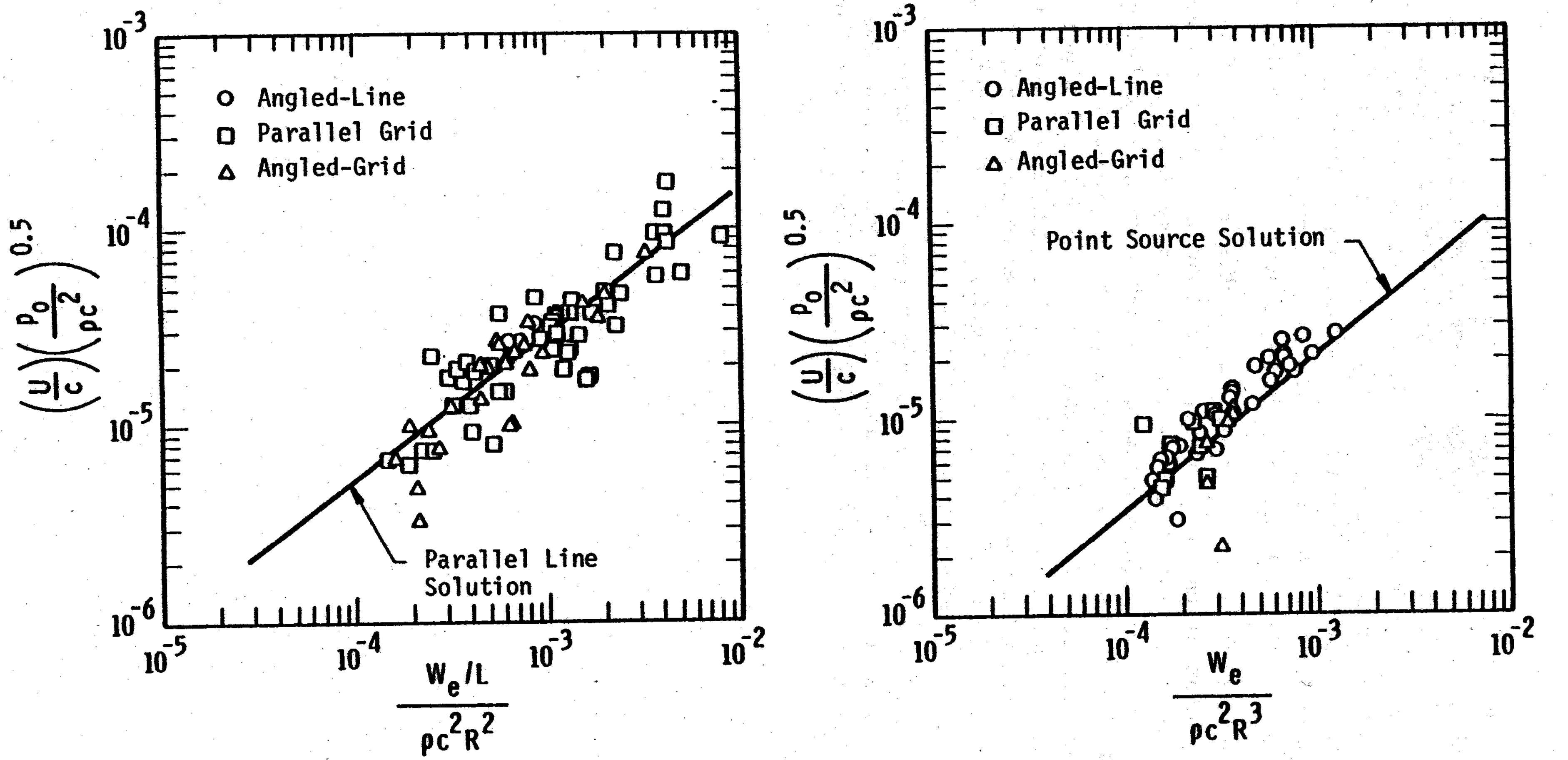

Figure 87. Soil Particle Velocities from Complex Explosive Sources Treated as Equivalent Parallel Line or Point Sources

IX. SUMMARY OF PIPE STRESS PREDICTION METHODS

In Sections VI and VIII, prediction equations- and methods were presented for estimating blast-induced pipe stresses from five explosive configurations detonated in soil. These explosive geometries were:

- point
- parallel line
- angled-line
- parallel grid
- angled-grid

For the first two geometries, prediction equations were derived using theoretical and experimental analyses and they can be used directly to compute the circumferential and longitudinal stresses. For the other three, more complex geometries, the concept used was to simplify the explosive geometry in such a way as to be able to represent it as an equivalent parallel line or point source. In this way, the stresses could again be estimated by direct computation using the relatively simple equations derived for the parallel line and point sources.

For the complex geometries, the prediction procedures were derived empirically using experimental data from tests in which some of the pertinent parameters were limited to small variations. Obviously, enough experiments cannot feasibly be conducted to model every possible variation to include all field cases using the different explosive geometries. However, the prediction methods developed are general enough to provide reasonable stress estimates over a fairly wide range of scaled parameters. Nevertheless, some exceptions to the general procedures will exist as a result of particular explosive geometric configurations.

Exceptions to General Methods

Two significant exceptions to the general rules of handling explosive line and grid sources, identified in analyzing the model test data, will be presented here. The first one concerns angled-line sources. The largest angle possible between an explosive line and a pipeline is 90°. At this angle, it is obvious that such a line source could not be represented by an equivalent parallel line source. Therefore, such a line source would always be treated as a point source with a charge weight equal to the total weight in the line and located at its geometric center. None of the explosive angled-lines used on the A.G.A. tests were positioned at 90° to the pipe. However, ground motion transducers were located to represent such an angle. These data were included in Figures 86 and 87 and compared well with the ground motion point source equations.

The second exception to the general procedures is in reality an additional step that should be included whenever stress estimates are made on explosive line and grid sources.

One of these complex geometries can have a charge spacing and location relative to a pipeline such that the nearest individual charge making up the line or grid when analyzed by itself as a point source would result in higher stress predictions than if the total array is analyzed as a line or grid. Of the 53 line and grid model tests conducted by SwRI, only three had the line or grid positioned with the nearest charge predicting slightly higher stresses than the general methods for handling the complex charge geometries. For these three tests, all angled-grids, the general methods still gave better stress estimates when compared to the, measured values. However, in the process of estimating pipe stresses for a particular field situation in which an explosive line or grid is to be used, the stress magnitudes should be checked for the closest single charge. If the single charge stresses are higher than those from the total geometry, those higher stress estimates should be used in deciding whether a blasting situation will be permitted without modifications to charge weights or standoff distances.

Logic Diagram

To summarize the prediction methods (including the two exceptions above) and simplify their application, a logic diagram has been devised to assist the reader. This flow chart is a simplification of a more detailed one developed by SwRI and used in coding a BASIC computer program for an HP 9830 desk top computer. A similar program was also developed for a hand-held, ‘programmable calculator and used in testing, analysis and solution development for this program. The logic diagram is presented in Figure 88.

The definitions for the symbols used in this figure have been given in the earlier sections and some of the figures. Reference is also made to a number of equations presented in the preceding section of this report. For clarity, the parameter x is differentiated by adding subscripts as follows:

$$\chi_{pt} = \frac{nW}{\sqrt{Eh}\ R^{2.5}} \quad \text{(point source)} \tag{131}$$

$$\chi_{l} = \frac{1.4nW/L}{\sqrt{Eh}\ R^{1.5}} \quad \text{(parallel line source)} \tag{132}$$

$$\chi_{npt} = \frac{n\ W1}{\sqrt{Eh}\ A^{2.5}} \quad \text{(nearest point source)} \tag{133}$$

The stress prediction equation can then be put in the form of

$$\sigma = 4.44\, E\, \chi^{0.77} \tag{134}$$

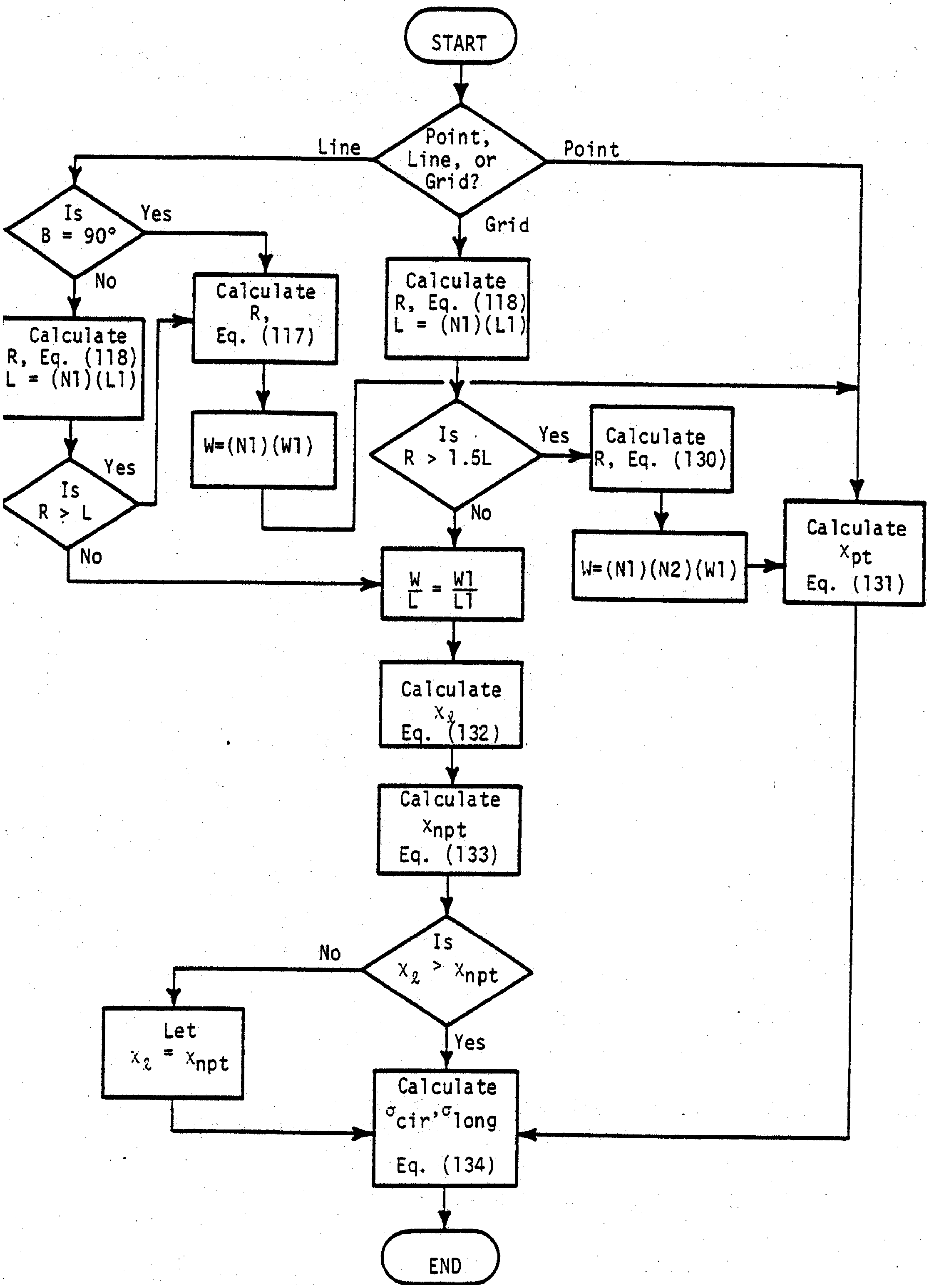

Figure 88. Logic Diagram for Estimating Pipe Stresses from Point, Line, and Grid Explosive Sources

The appropriate value for *x* is used in Equation (134) to compute the estimated values for the circumferential and longitudinal pipe stresses for the blasting situation being analyzed.

Illustration Problems

To illustrate the use of Figure 88, the following example problems will be solved:

Example Problem No. 6

Given: The explosive grid defined in the figure will be used to loosen the soil overburden.

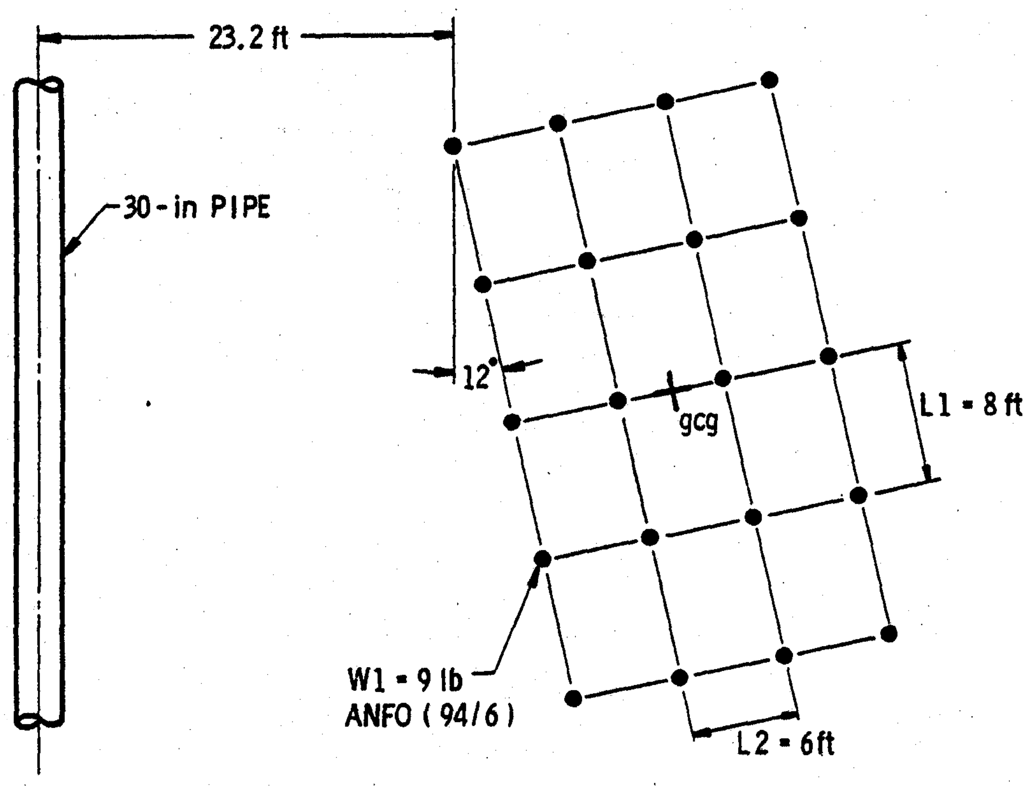

A 30-inch O. D. by 0.344 W. T. pipeline is adjacent to the grid as shown in the figure. The centerline of the pipe and the charges are 5 ft below the surface of the ground.

Find: Estimate of the blast-induced stresses.

Solution: (a) List all parameters in proper units

E = 29.5×10^6 psi
h = 0.344in.
n = 1.0
N1 = 5
L1 = 8 ft
W1 = 9 lb
B = 12°
A = 23.2ft
N2 = 4
L2 = 6ft

b) Solve the problem using Figure 88

(1) $$R = R_{gcl}/\cos B$$

$$R = \frac{\left[A + \frac{(N1-1)L1 \sin B}{2}\right]}{\cos B}$$

$$= \frac{\left[23.2 + \frac{(4)\ (8)\ \sin 12}{2}\right]}{\cos 12}$$

<u>R=27.12ft</u>

(2) L = (N1)(L1) = (5)(8)

<u>L=40ft</u>

(3) Is R > 1.5 L? No, therefore, parallel line solution applies.

(4) $$\frac{W}{L} = \frac{W1}{L1} = \frac{9}{8}$$

$$\underline{\frac{W}{L} = 1.13 \text{ lb/ft}}$$

(5) $$\chi_1 = \frac{1.4n\ W/L}{\sqrt{Eh}\ R^{1.5}}$$

$$= \frac{(1.4)\ (1.0)\ (1.13)}{\sqrt{(29.5 \times 10^6)\ (0.344)}\ (27.12)^{1.5}}$$

$$\underline{\chi_1 = 3.5 \times 10^{-6}}$$

(6) Check nearest point

$$\chi_{npt} = \frac{n\ W1}{\sqrt{Eh}\ A^{2.5}}$$

$$= \frac{(1.0)\ (9)}{\sqrt{(29.5 \times 10^6)\ (0.344)}\ (23.2)^{2.5}}$$

$$\underline{\chi_{npt} = 1.09 \times 10^{-6}}$$

(7) Using the larger value of *x*

$$\sigma = 4.44\ E\ (3.5 \times 10^{-6})^{0.77}$$

$$\underline{\sigma_{cir} = \sigma_{long} = 8{,}240\ psi} \qquad (S = \pm 2{,}802\ psi)$$

Note that the nomographs in Figures 80 and 81 can also be used to solve this problem once values for R and W/L are obtained for the equivalent parallel line source and using R = A and W = W1 for the nearest point. Then, the larger value of σ that results becomes the estimate for σ_{cir} and σ_{long}.

Example Problem No. 7

Given: The same explosive grid and pipeline given in the preceding problem except, in this case, the charge nearest the pipe is 65 ft away.

Find: Estimate of the blast-induced stresses.

Solution: (a) List all parameters

$$\begin{aligned}
E &= 29.5 \times 10^6 \text{ psi} \\
h &= 0.344 \text{ in.} \\
n &= 1.0 \\
N1 &= 5 \text{ ft} \\
L1 &= 8 \text{ ft} \\
W1 &= 9 \text{ lb} \\
B &= 12^\circ \\
A &= 65 \text{ ft} \\
N2 &= 4 \\
L2 &= 6 \text{ ft}
\end{aligned}$$

(b) Solve the problem using Figure 88

(1)
$$R = \frac{\left[A + \dfrac{(N1-1)\ L1\ \sin B}{2}\right]}{\cos B}$$

$$= \frac{\left[65 + \dfrac{(4)\ (8)\ \sin 12}{2}\right]}{\cos 12}$$

$$\underline{R = 69.9 \text{ ft}}$$

(2) $L = (N1)(L1) = (5)(8)$

$$\underline{L = 40 \text{ ft}}$$

(3) $1.5\,L = 60$ ft

Is $R > 1.5\,L$? Yes, therefore, point solution applies.

(4) As a point source

$$R = R_{gcg} = A + \frac{(N1-1)\ L1\ \sin B + (N2-1)\ L2\ \cos B}{2}$$

$$R = 65 + \frac{(4)\ (8)\ \sin\ 12 + (3)\ (6)\ \cos\ 12}{2}$$

$$\underline{R = 77.1\ \text{ft}}$$

(5) $$W = (N1)(N2)(W1)$$

$$= (5)(4)(9)$$

$$\underline{W = 180\ \text{lb}}$$

(6) $$\chi_{pt} = \frac{n\ W}{\sqrt{Eh}\ R^{2.5}}$$

$$= \frac{(1.0)(180)}{\sqrt{(29.5 \times 10^6)\ (0.344)}\ (77.1)^{2.5}}$$

$$\underline{\chi_{pt} = 1.08 \times 10^{-6}}$$

In this case, it is obvious that $x_{pt} > x_{npt}$.

(7) $$\sigma = 4.44\ E\ (\chi_{pt})^{0.77}$$

$$= (4.44)(29.5 \times 10^6)(1.08 \times 10^{-6})^{0.77}$$

$$\underline{\sigma_{cir} = \sigma_{long} = 3{,}330\ \text{psi}} \qquad (S = \pm 1{,}132\ \text{psi})$$

Once it was determined that the grid could be simplified into an equivalent point source, the nomographs or any of the other alternative forms of the solution could have been used to estimate the maximum stresses for this problem. The solutions of Example Problem Nos. 6 and 7 are also illustrated in Figure 89 by the use of a microcomputer program developed using the logic diagram in Figure 88.

SWRI PROJECT NO. 02-5567, 3/ 20/ 81

BLAST EFFECTS FROM GRID SOURCE FOR 0.344 INCH PIPE

ESTIMATED CIRCUMFERENTIAL AND LONGITUDINAL STRESSES

E = 29.5 MILLION PSI N = 1.00

GRID DESCRIPTION:

5 CHARGES IN FRONT ROW SPACED 8.00 FT APART

4 ROWS MAKING IJP GRID SPACED 6.00 FT APART

23.20 FT TO CLOSEST POINT CHARGE OF GRID

GRID ANGLE = 12 DEG WT OF EACH CHARGE = 9.00 LB

CHARGE (LB/FT)	DIST (FT)	X	CIR OR LONG; STRESS (PSI)
1.125	27. 12	3.501E-06	8246

(a) Solution of Example Problem No. 6

SWRI PROJECT NO. 02-5567, 3/ 20/81

BLAST EFFECTS FROM GRID SOURCE FOR 0.344 INCH PIPE

ESTIMATED CIRCUMFERENTIAL AND LONGITUDINAL STRESSES

E = 29.5 MILLION PSI N = 1.00

GRID DESCRIPTION:

5 CHARGES IN FRONT ROW SPACED 8.00 FT APART

4 ROWS MAKING UP GRID SPACED 6.00 FT APART

65.00 FT TO CLOSEST POINT CHARGE OF GRID

GRID ANGLE = 12 DEG WT OF EACH CHARGE = 9.00 LB

CHARGE (LB)	DIST (FT)	X	CIR OR LONG STRESS (PSI)
180.000	77.13	1.081E-06	3337

(b) Solution of Example Problem No. 7

Figure 89. Solution of Explosive Grid Problems Using Computer Program

X. OTHER BLAST STUDIES

In addition to the extensive research efforts which are covered in all the previous sections of this report to determine the response of pipelines to nearby detonations in soil from point, line and grid explosive sources buried to essentially the same depth as the pipe, other much more limited studies were conducted by SwRI as part of the PRC-A.G.A. blasting research program. The first of these studies concerned the response of pipelines which are relatively near a free surface such that the blast-induced stresses would be enhanced. The second study concerned a review of the literature and analysis of some data on the effects of shielding a pipeline by the use of a trench between the charge and the pipe. Finally, the third study was an experimental and analytical effort to determine the feasibility of using concrete/ soil tests to model the effects of placing the charge in a harder media, e.g., rock, than that surrounding the pipe. The results of these limited studies are contained in this section and are not presented as all inclusive solutions to these related blasting problems. Rather, the results provide limited guidelines on how to handle these types of situations until future research can provide more inclusive and general solutions.

Pipeline Near a Free Surface

The limited study concerning pipelines which are relatively near a free surface began as a result of data recorded by SwRI for the DOW Chemical Company in four very deep point source firings.. In all of the A.G.A. program tests, the point charges used were either at the same depth as the center of the pipe or deeper than the pipe such that the charge-to-pipe centerline was at a 45° angle to the horizontal. For these few deeper A.G.A. experiments, the largest vertical distance to the charge was 4.2 times greater than the depth of the pipe. The data obtained, however, compared quite well with the same depth data when the slant distances between the pipe and the charge are used as the standoff distance. In fact, these deeper data have been used to develop the stress prediction relationships developed in Section VI.

The unpublished stress data released by the DOW Chemical Company for use in this part of the program are listed in Table 16. In the four very deep point source firings monitored by SwRI, one circumferential strain gage was mounted near the bottom of the pipe, and one longitudinal strain gage was mounted near the top of the pipe. These gages were of the weldable type manufactured by AILTECH and were installed by DOW personnel on a 16-inch O. D. by 0.25 W. T. steel pipe. The point charges were buried approximately 15 times deeper than the center of the pipeline and the slant distances ranged from 70 to 212 ft. In addition, the shortest slant distances in these tests were considerably longer, even when scaled down from the 16-inch diameter pipe to a 6-inch diameter, than those used in the A.G.A. tests. If these slant distances are used in the point source prediction equation, one would underestimate considerably the stresses when compared to the actual measurements, particularly in the longitudinal direction,. Therefore, a correction factor was introduced to modify the predictive equations. This resulted in better comparisons between the measured and estimated stresses.

Table 16. DOW Very Deep Point Source Data

Test No.	h (in.)	n	W (lb)	R (ft)	ϵ_{cir} (μin./in.)	ϵ_{long} (μin./in.)	σ_{cir} (psi)	σ_{long} (psi)
D1	0.25	1.12	20	212	6	9	282	350
D2	0.25	1.12	20	122	14	35	794	1271
D3	0.25	1.12	25	86	27	70	1556	2532
D4	0.25	1.12	20	70	45	93	2363	3452

The basis for this correction factor is that an effective mass of earth was assumed to move with the pipe during loading in the derivation of the stress formulae. Since the original analysis assumed that the charge and the pipe were at the same depth, this soil mass would extend in front and in back of the pipe an equal distance, approximately that between the pipe and the charge. If a pipeline is quite close to a free surface relative to the standoff distance, the soil mass backing the pipe will be considerably smaller such that the pipe would then experience greater strain and consequently higher stresses. This increase in pipe stress will occur when the charge is considerably deeper than the pipeline or when the pipe is very near a free face (such as a vertical face of a cliff as in Figure 90) even if the charge is at the same depth as the pipe. (Note that in the case of the charge being near the free face instead of the pipe, the results that follow do not apply and also a reduction in pipe stress should not be expected.) To account for the decrease in inertial resistance, the point source solution is modified by introducing the following expression:

$$F = \left[\frac{H}{R} + \frac{\rho_p h}{\rho_s R} \right] \tag{135}$$

where
- H = effective thickness of soil backing up the pipeline (ft), see Figure 90
- R = shortest distance between centers of pipe and charge (ft)
- h = pipe wall thickness (ft)
- ρ_s = soil mass density (lb-sec^2/ft^4)
- 5 = pipe material density (lb-sec^2/ft^4)

Equation (135) is dimensionless and any self-consistent set of units, such as the one defined with the parameters above, is required to compute a numerical value for F.

Obviously, since the A.G.A. deeper charge data compared well with the same depth data, Equation (135) must be applicable only when the depth of the charge is greater than 4.2 times the depth of the pipe. Since no other data are available between charge-to-pipe depth ratios of 4.2 and 15, it is not possible to decide empirically (or theoretically) at what

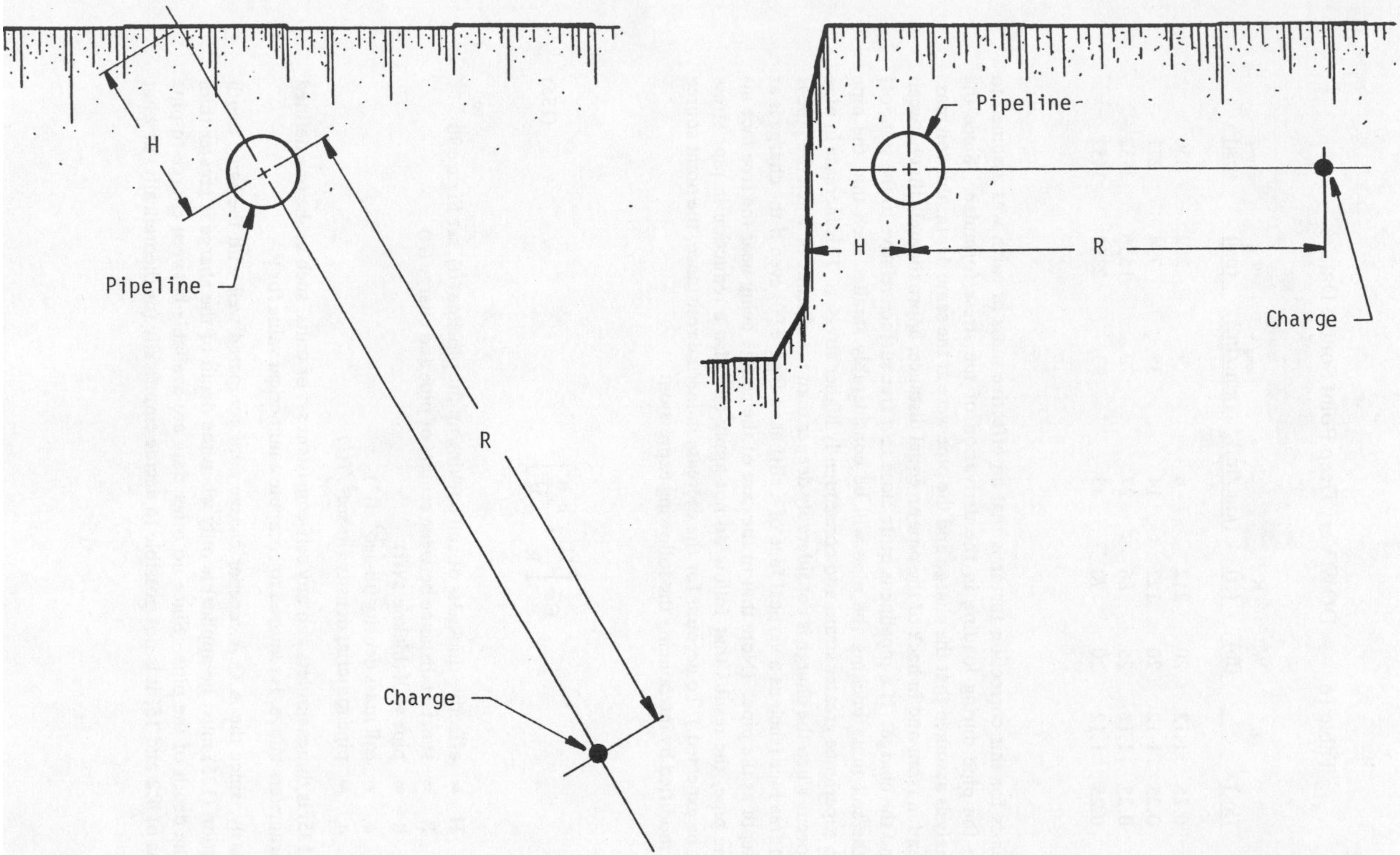

Figure 90. Examples of a Pipeline Near a Free Surface

ratio Equation (135) should modify the point source solution. Therefore, it is suggested that a conservative choice be made such as a depth ratio of 5. From the geometry of the problem, a depth ratio of 5 would make H/R = 4. Thus, it is recommended that for situations in which very deep charges are used or the pipeline is relatively close to a free face, the point source solutions be modified by the correction factor F as follows:

$$\frac{\sigma}{E} = 4.44\left(\frac{nW}{\sqrt{EhF}\ R^{2.5}}\right)^{0.77} \tag{136}$$

where F = 1 for R/H ≤ 4

F = Equation (135) for R/H > 4

A similar modification can probably be made to the parallel line solution for the limits of R/H given. Note that the correction factor was derived empirically from only a few data points and should be used with caution and engineering judgement. The results of applying Equation (136) to the DOW data, the only data available for which R/H>4, are presented in Figure 91. In these plots, reasonable agreement between the predicted and measured values is shown. The solution line overpredicts slightly the four circumferential data points while the opposite occurs with the longitudinal data points. In both cases, however, all the test dam points are well within the scatter of the data used to fit the solution lines (see Figure 72). Note that the solution line was developed with data that ranged down to a value of $x = 1.4 \times 10^{-7}$. Thus, some extrapolation has been necessary to compare with one of the very deep data points which has a value of $x = 4.7 \times 10^{-8}$. A more important observation about this comparison is that the hugest stress measured on the DOW tests was 3,452 psi in the longitudinal direction. Therefore, Equations (135) and (136) were derived with data at the low end of the range of the solution line. Consequently, these equations should be used with even more caution at stress values greater than the values corresponding to a value of $x = 1 \times 10^{-6}$.

Pipeline Shielding Study

Sometimes, the placement of either sheet piling or trench barriers between a vibration source and the receiver can reduce the severity of ground motions. Barkan (1962), in the U.S.S.R., has done more than anyone in evaluating the effectiveness of all types of barriers. R. D. Woods (1968), in the U.S.A., has tested the effectiveness of some trench designs.

One would expect that because solid and fluid barriers transmit some wave energy, a void would be the most effective barrier. Tests reported in the literature tend to demonstrate that some barrriers can be expected to reduce displacement or particle velocity amplitudes. Figures 92 and 93 show some vertical displacement amplitude reduction contours of Woods (1968) in which the amplitude reduction factor is defined as the amplitude with a barrier present divided by the amplitude without a barrier. Figure 92 shows the

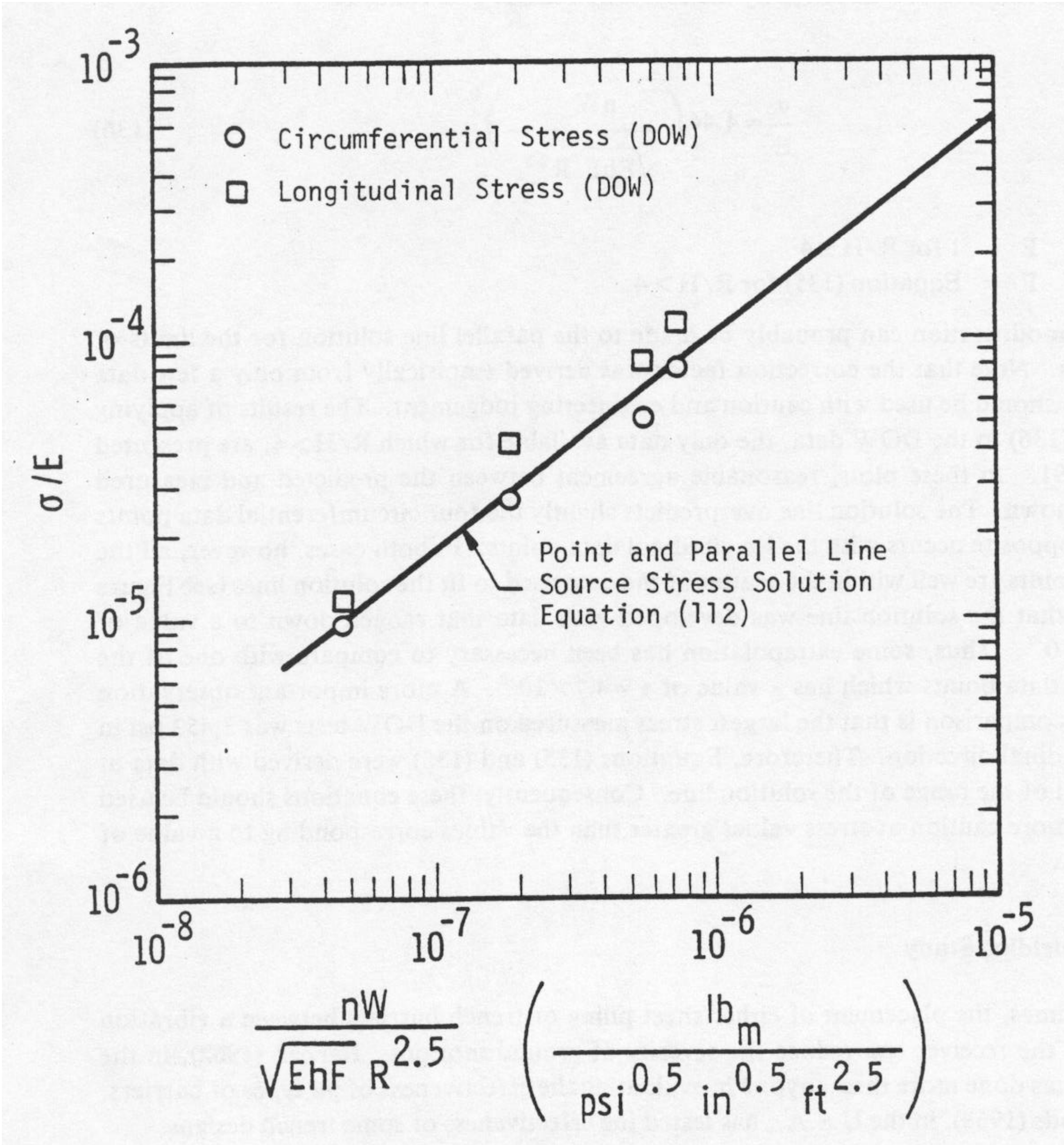

Figure 91. Comparison Between Very Deep Point Charge Test Data and Point and Parallel Line Source Stress Solution Curve

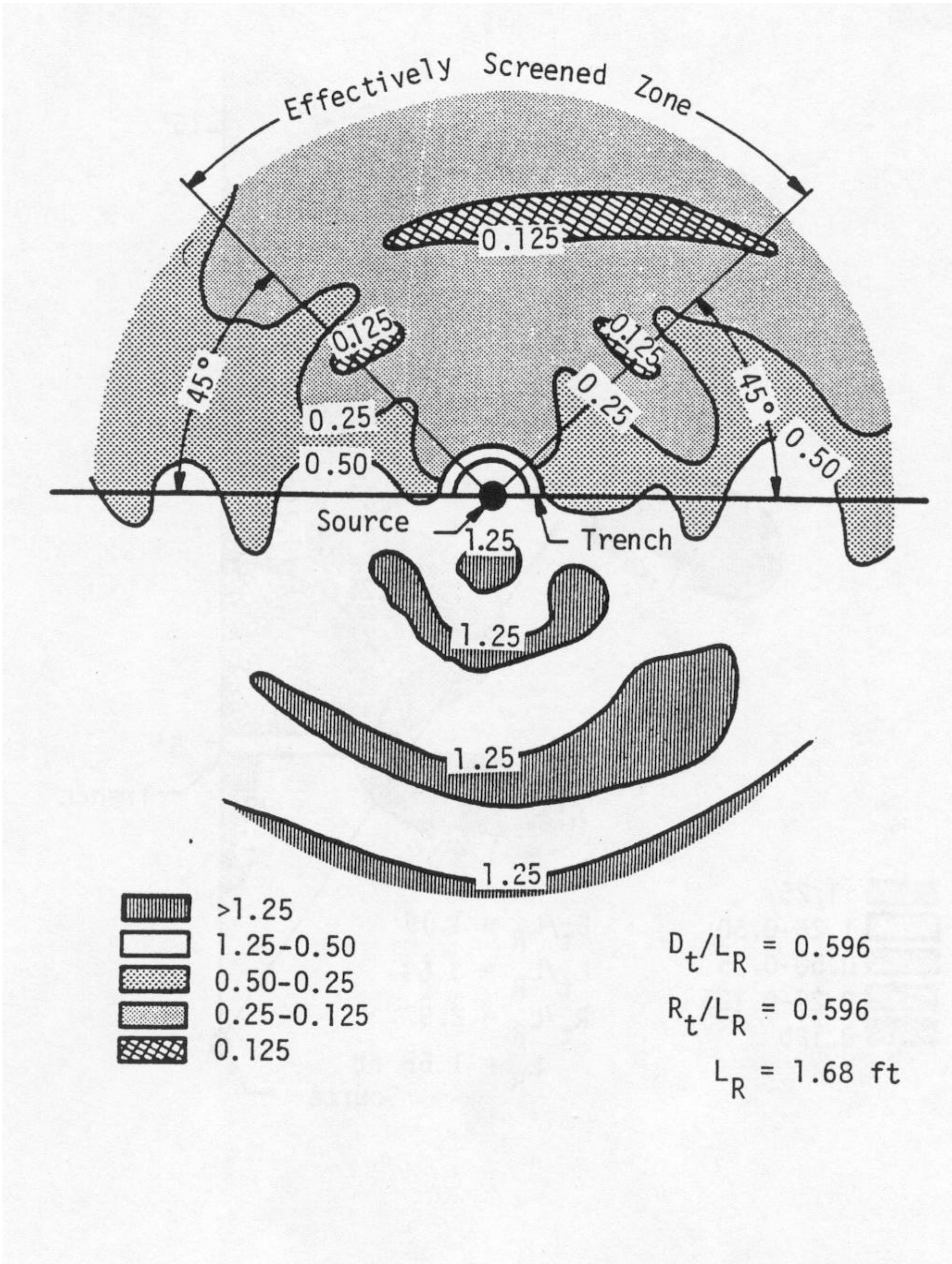

Figure 92. Amplitude Reduction Contours for an Active Trench - Woods (1968)

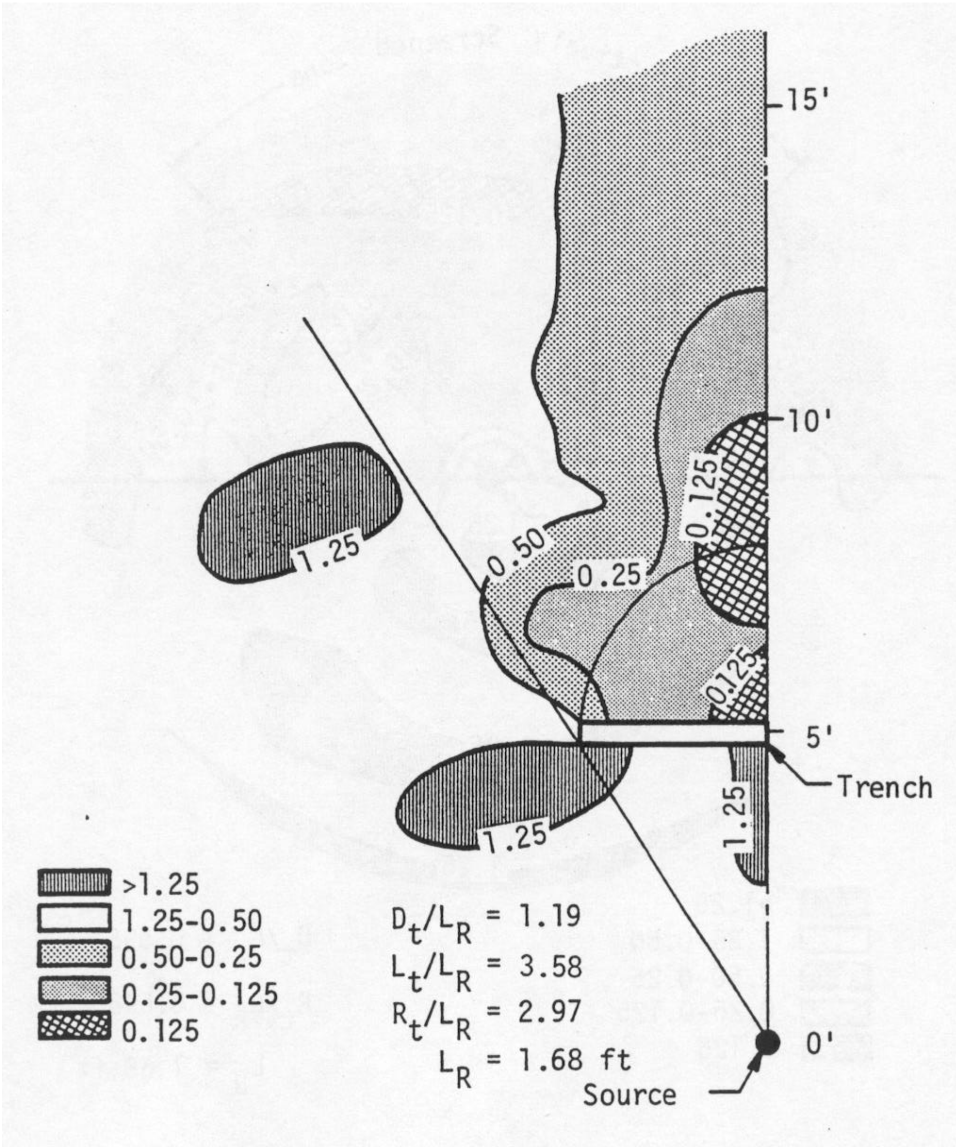

Figure 93. Amplitude Reduction Contours for a Passive Trench - Woods (1968)

results of one particular test using an active trench (a barrier close to the source) with a 180-degree arc at a scaled distance R_t/L_R of 0.596 Rayleigh wavelengths from the source and with a scaled depth D_t/L_R of 0.596 Rayleigh wavelengths. As can be seen, the maximum reduction in amplitude is a factor of approximately 1/8. Notice that at other locations, amplitudes are increased because of reflections and focusing. In this figure, D_t is the depth of the trench, L_R is the wavelength of the Rayleigh wave [see Equation (138)], and R, is the distance between the trench and the source. The results shown in Figure 92 can only be used for a similar active trench with the same values for D_t/L_R and R_t/L_R.

In the case where separate detonations are made progressively closer to the pipe, passive trenches (barriers near the ground being shielded) are more likely to be beneficial than active ones. Figure 93 from Woods (1968) is one example of a vertical surface vibration amplitude reduction contours for a passive trench with a scaled trench depth D_t/L_R of 1.19 wavelengths, scaled trench length L_t/L_R of 1.79 wavelengths, and scaled standoff distance R_t/L_R of 2.97 wavelengths. This figure also shows that a trench can reduce peak amplitudes to values as low as 1/8 the amplitude without a trench, and that amplitudes can also be increased, especially forward and to the side of the barrier. Barkan (1962) has additional trenching results plotted in graphs of amplitude versus distance behind trenches for different trench depths and frequency of vibration. He concluded that a trench may be effective for high frequency vibrations with short wavelengths, and that it is essentially impossible to build trenches deep enough to screen low frequency waves with long wavelengths.

Barkan claims that deep barriers are generally required if low frequency waves are to be screened. Figure 94 is one of Barkan's examples of active sheet piling screening effectiveness for different frequencies of vibration. Plotted in Figure 94 is amplitude of vertical displacements before and after the screen is erected as a function of distance from the source of the vibrations. The sheet piling in Figure 94 had a depth of 14.8 ft and was in the shape of a square 11.2 ft on each side. Three different plots are presented in Figure 94, because the results are for three different frequencies of vibration N.

In addition to studying the effectiveness of screening on vertical vibration components, Barkan also observed the effects of screening on horizontal vibration components. Figure 95 shows both horizontal and vertical vibration components for different frequencies of excitation. The profiles presented in Figure 95 are parallel to the sheet piling and located either directly behind or directly in front of the barrier. Using these test results is very dangerous, because Barkan fails to report the propagation velocity, and the depth of the barriers in Figure 95 is uncertain. Obviously, very complex laws govern vibration changes in the immediate vicinity of barriers; hence, these results should only be used qualitatively. The largest change in amplitude ratios is always along the two central quarters of the barrier's length.

Most of the reported ineffective vibration screens are for attempts to decrease the effects of very low frequency vibrations -- vibrations less than 10 Hz which imply long wavelengths. Unfortunately, explosive sources usually have very long wavelengths, and,

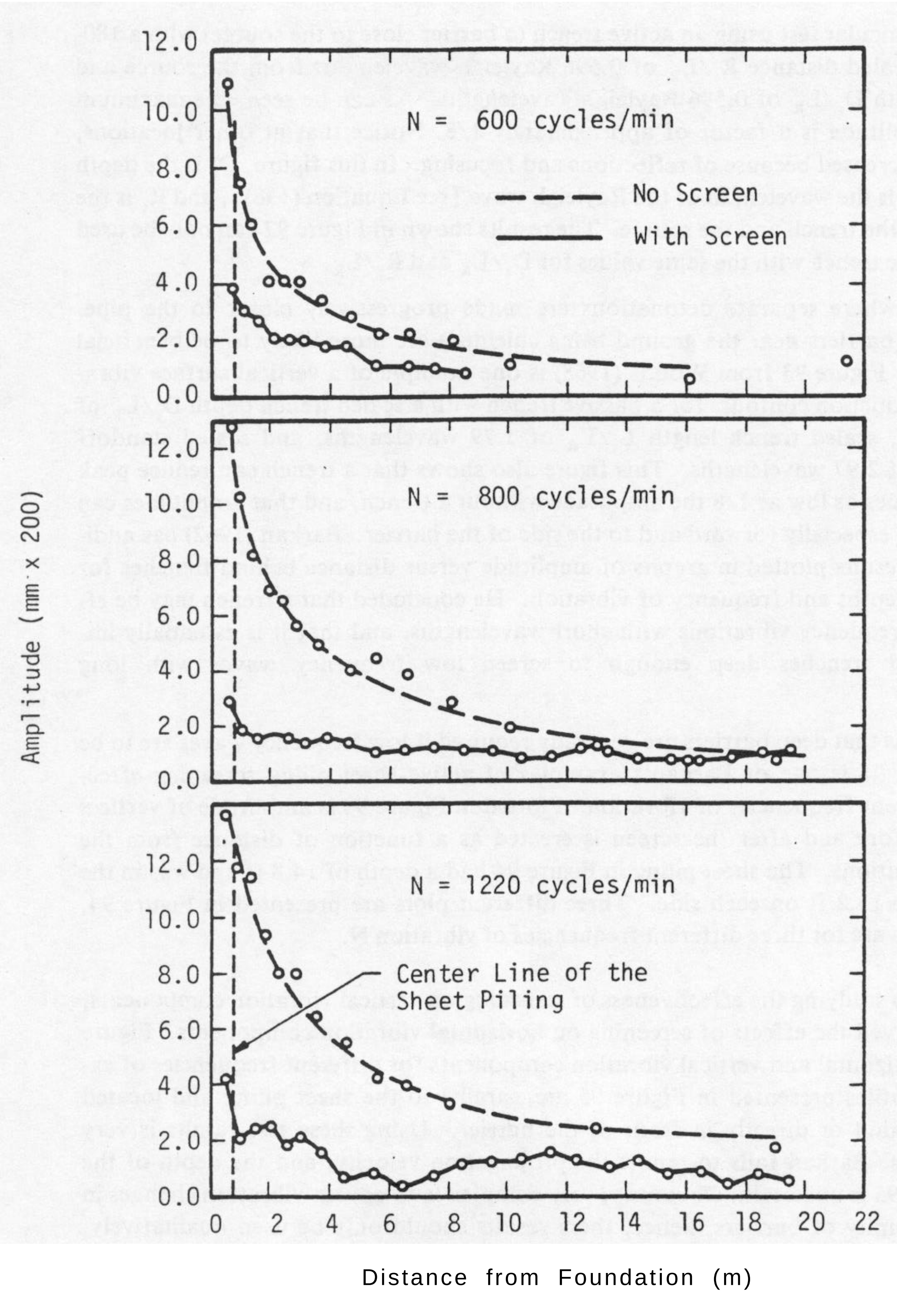

Figure 94. Effectiveness of an Active Sheet Pile Screen - Barkan (1962)

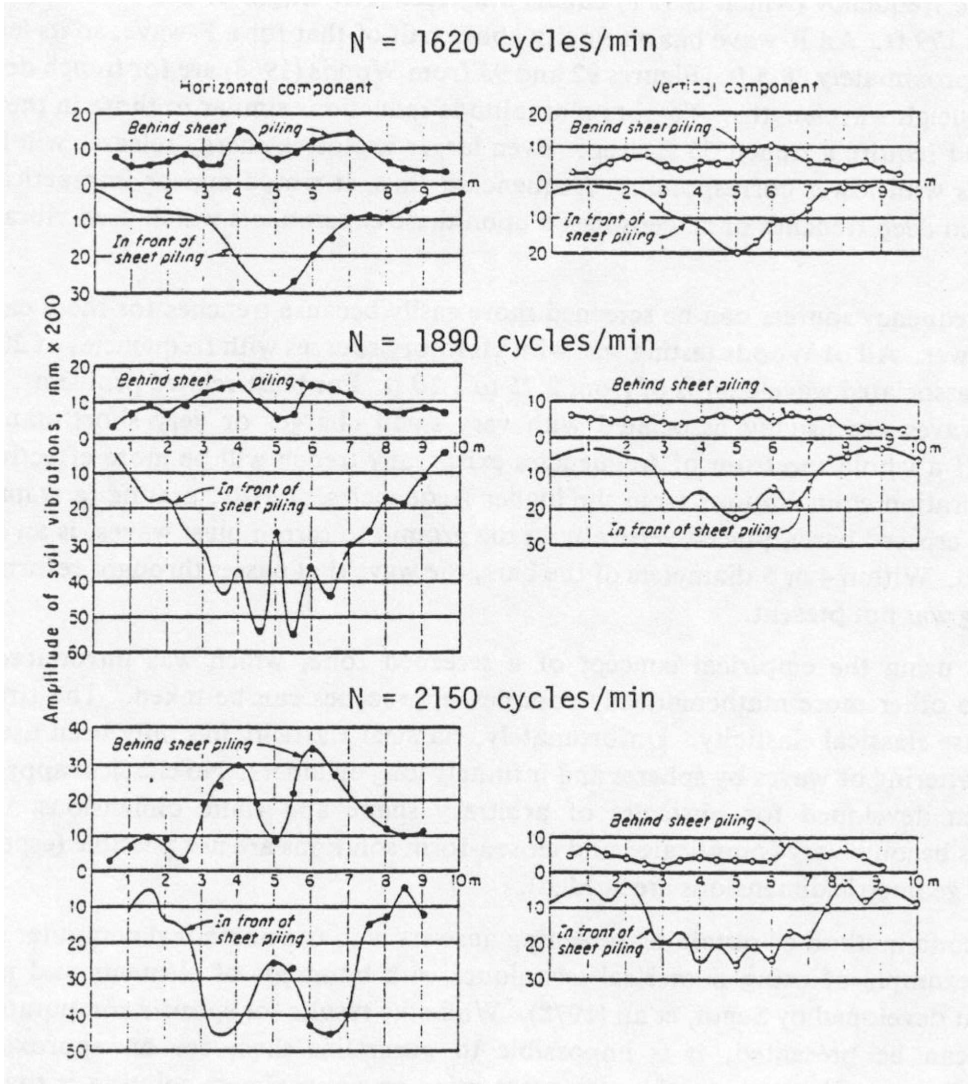

Figure 95. Sheet Piling Screening Profiles Immediately Behind and In Front of Barriers - Barkan (1962)

therefore, very low frequencies, associated with them. For example, a 20 lb high-explosive charge buried 30 ft from an object in a soil with a P-wave velocity of 940 ft/sec and a density of 102 lb/ft^3, will induce a radial soil displacement of 0.138 in. and a radial particle velocity of 4.55 in/sec [using Equations (44) and (45)]. Assuming simple harmonic motion, the period T equals $2\pi X/U$, and for this example, T=0.191 seconds. Consequently, the harmonic frequency (which is l/T) equals 5.25 Hz. The length of the P-wave (which equals cT) is 179 ft. An R-wave has a velocity about half of that for a P-wave, so its length would be approximately 88.5 ft. Figures 92 and 93 from Woods (1968) are for trench depths of 0.596 Rayleigh wavelengths. To obtain amplitude reductions similar to those in the two figures would require a trench 53 ft deep. Even larger explosive energy releases will have longer waves with lower corresponding frequencies; thus, it would appear impractical to fabricate such deep trenches or screens based upon these experiments which used vibratory sources.

High frequency sources can be screened more easily because trenches for these can be much shallower. All of Woods testing was with vibratory sources with frequencies of 200 to 350 Hz and associated wavelengths of from 2.25 to 1.10 ft. For blast-related problems, high frequency waves are usually associated with very small charges or very short standoff distances. If a whole spectrum of frequencies exists, any trench will be more effective in reducing vibration contributions from the higher frequencies. Lastly, grating (a frame of parallel and crossed bars), placed vertically in the ground to screen blast waves, is an ineffective shield. Within 4 or 5 diameters of the bars, the wave that passes through, reforms as if the grating was not present.

Besides using the empirical concept of a screened zone, which was introduced by Barkan, two other more mathematically complex approaches can be taken. The first of these is to use classical elasticity. Unfortunately, classical elasticity has only been used to study the scattering of waves by spheres and infinitely long cylinders. No classical approach has yet been developed for obstacles of arbitrary shape and finite dimensions. The mathematics become very complicated and closed-form solutions are not possible (especially when two geometric dimensions are needed).

The second method of obtaining screening answers is to use numerical computer solutions. An example of using numerical techniques with hundreds of elements and nodal points is that developed by Segol, et al. (1978). While the results for specific computational conditions can be presented, it is impossible to generalize them for an approximate graphical solution. The main problem in attempting an approximate solution is that the space to be represented is too large. If, as an example, one were predicting maximum ground motion behind a vertical trench for a weak wave (a wave propagating near the velocity of sound in the ground), the solution would require at least the following parameters:

$$\left(\frac{X_t}{X}\right) = f\left(\frac{D_t}{L_R}, \frac{X}{L_R}, \frac{Y}{L_R}, \frac{Z}{L_R}, \frac{L_t}{L_R}\right) \tag{137}$$

where X_t = ground motion with a trench
X = ground motion predicted without a trench
L_R = wavelength of R-wave
D_t = depth of trench
Y = horizontal coordinate to locate point of interest behind the trench
Z = vertical coordinate to locate point of interest behind the trench
L_t = length of trench

An analysis was made in this study to see what could be done with Equation (137) by using unpublished test results compiled by J. K. Means of Michigan Wisconsin Pipe Line Company for sewer and water line blasting in Winnabago County, Wisconsin. Both circumferential and longitudinal strains were measured on parallel 16-inch and IO-inch diameter pipes. These pipes were approximately 25 ft apart. Because charges were placed on both sides of the parallel pipelines, trenches were dug on both sides of the pipes. However, during blasting operations, only one side was blasted at a time and a trench was open only on the side being blasted. The trench dug near the 16-inch line was 50 ft long. The trench dug near the IO-inch line was 62 ft long. In both cases the trench was 9 ft deep and 5 ft away from the pipe nearest the charge.

Thirteen experiments used single 2.5-lb charges detonated at various standoff distances of from 10 to 56 ft from the trenched pipe. Five other tests used arrays of charges sufficiently far away from the pipe and trench that the entire array could be treated as a single charge at the geometric center. These five experiments allowed us to estimate response for 5-, 12.5-, 20-, and 22.5-lb charges at various standoff distances. The strain data measured by Michigan Wisconsin is presented in Table 17.

To use these experimental test results, the Rayleigh wave wavelength L_R for each test was estimated by using the expression:

$$L_R \approx \pi \frac{c\ X}{U} \tag{138}$$

where c = seismic velocity (a value of 950 ft/sec was assumed)
X = radial soil displacement (ft)
U = soil particle velocity (ft/sec

The ground motions were computed using Equations (44) and (45) assuming ρ = 102 lb/ft^3 . Since pipe strain depends on the ground displacement, Equation (137) can be expressed as a strain ratio as follows:

$$\left(\frac{\epsilon_{meas}}{\epsilon_{cal}}\right) = f\left(\frac{R}{L_R}, \frac{D_t}{L_R}, \epsilon_{cal}, \frac{Y}{L_R}, \frac{Z}{L_R}, \frac{L_t}{L_R}\right) \tag{139}$$

Table 17. Michigan Wisconsin Trench Strain Data

Shot No.	W (lb)	Pipe Dia.	R (ft)	ϵ_{cir} Meas.	ϵ_{long} Meas.
31-2	2.5	16"	31	8.8	11.6
		10"	56	12.8	8.8
31-4	2.5	16"	18	26.0	38.0
		10"	43	21.0	24.0
31-5	2.5	16"	16	11.6	15.6
		10"	41	10.0	9.6
31-6	2.5	16"	14	11.6	16.8
		10"	39	8.0	9.6
31-7	2.5	16"	12	19.2	26.8
		10"	37	10.4	10.8
31-8	2.5	16"	10	14.8	20.8
		10"	35	10.0	9.2
4-5	2.5	10"	25	7.6	12.8
		16"	50	7.6	11.6
4-6	2.5	10"	24	11.6	12.8
		16"	49	4.0	10.0
4-7	2.5	10"	21	14.0	9.6
		16"	46	9.8	8.8
4-8	2.5	10"	21	10.8	18.0
		16"	46	4.8	12.8
4-9	2.5	10"	19	16.0	22.0
		16"	44	19.6	11.2
4-10	2.5	10"	19	19.2	18.8
		16"	44	12.0	13.2
4-11	2.5	10"	16	10.8	16.0
		16"	41	9.6	10.8
31-3	5.0	16"	21.5	11.6	12.8
		10"	46.5	9.2	9.4
4-1*	22.5	10"	45.5	--	16.4
		16"	70.5	11.2	12.8
4-2*	20.0	10"	42.25	9.6	13.2
		16"	67.25	8.4	10.0
4-3*	12.5	10"	36.80	12.8	15.6
		16"	61.80	12.0	12.0
4-4*	20.0	10"	29.25	27.2	24.8
		16"	54.25	14.4	20.8

$E = 30 \times 10^6$ psi
$n = 1.05$
*$n = 1.12$
$p = 102$ lb/ft^3

This permitted all of the quantities R/L_R, D_t/L_R, Y/L_R, Z/L_R, and L_t/L_R to be calculated. The quantity ϵ_{meas} means the strain value with a trench and ϵ_{cal} means the estimated value of either circumferential or longitudinal strain where no trench is present. At this test site, Michigan Wisconsin also made some no trench measurements on 10-inch, 16-inch and 24-inch pipes using primarily explosive arrays. When no trench was present, the recorded strains were of similar magnitude as those predicted using our analysis procedures; hence, no reduction seems to have been caused by any special site conditions.

At first glance, Equation (139) would appear to have too many nondimensional terms to develop a solution unless some of the terms proved to be of secondary importance. Analysis of the test data showed that the strain ratio $\epsilon_{meas}/\epsilon_{cal}$ and the scaled standoff distance from the pipe R/L, are the most important parameters in this case. Figure 96 is a plot of $\epsilon_{meas}/\epsilon_{cal}$ versus R/L_R for the Michigan Wisconsin test data. The other parameters did vary and may be a cause of some scatter; nevertheless, for this set of data the major parameters appear to be $\epsilon_{meas}/\epsilon_{cal}$ and R/L_R. Both circumferential and longitudinal strain ratios are plotted in Figure 96.

The parameter ϵ_{cal} varied from a low of 5 μin./in. (10^{-6} in./in.) to a high of 174 μin./in. Because the results in Figure 96 are independent of ϵ_{cal}, this result infers independence from strength of the shock. However, for really strong shocks inducing strain of thousands of μin./in.'s, this observation may no longer hold. The scaled depth of the trench D_t/L_R, distance from the trench to the pipe Y/L_R, the depth of the pipe Z/L_R, and length of the trench L_t/L_R varied by only limited amounts. D_t/L_R varied from a low of 0.08 to a high of 0.22, Y/L_R had a greater variation of from 0.05 to 0.60, Z/L_R varied approximately from 0.05 to 0.12, and L_t/L_R varied from 0.28 to 1.41. Provided another field situation had conditions which fell within the bounds given for ϵ_{cal}, D_t/L_R, Y/L_R, Z/L_R, L_t/L_R, and R/L_R, the results in Figure 96 could be used at other sites. One standard deviation S for the results about the line in Figure 96 is 0.34 or essentially the same as for the solution of ϵ_{cir} and ϵ_{long} when no trench is present.

For R/L_R less than 0.83, the wave may not be fully formed and will contain higher frequency contributions. Figure 96 shows that a trench can reduce peak strains when R/L_R is less than 0.83. However, when R/L, becomes large, waves become fully developed and trenching may not be as effective unless L_t/L_R is large.

At values of R/L, greater than 0.83 $\epsilon_{meas}/\epsilon_{cal}$ appears to be greater than 1.0. This observation may be true as some focusing can occur, but the straight line through the data points should not be extended. At values of R/L_R greater than 0.83, we recommend using $\epsilon_{meas}/\epsilon_{cal}$ equal to 1.0. The test data in Figure 96 are also limited in the near field to values of R/L_R greater than 0.25. At R/L_R equal to 0.25, the strain reduction ratio is very close to Barkan's and Wood's maximum effectiveness trenching ratio of 1/8. At closer standoff distances (R/L_R less than 0.25), we would not necessarily expect $\epsilon_{meas}/\epsilon_{cal}$ to be less than 1/8. Thus, the straight line has been passed through the data in Figure 96 between R/L of 0.25 and 0.83. The equation of this curve fit is given by:

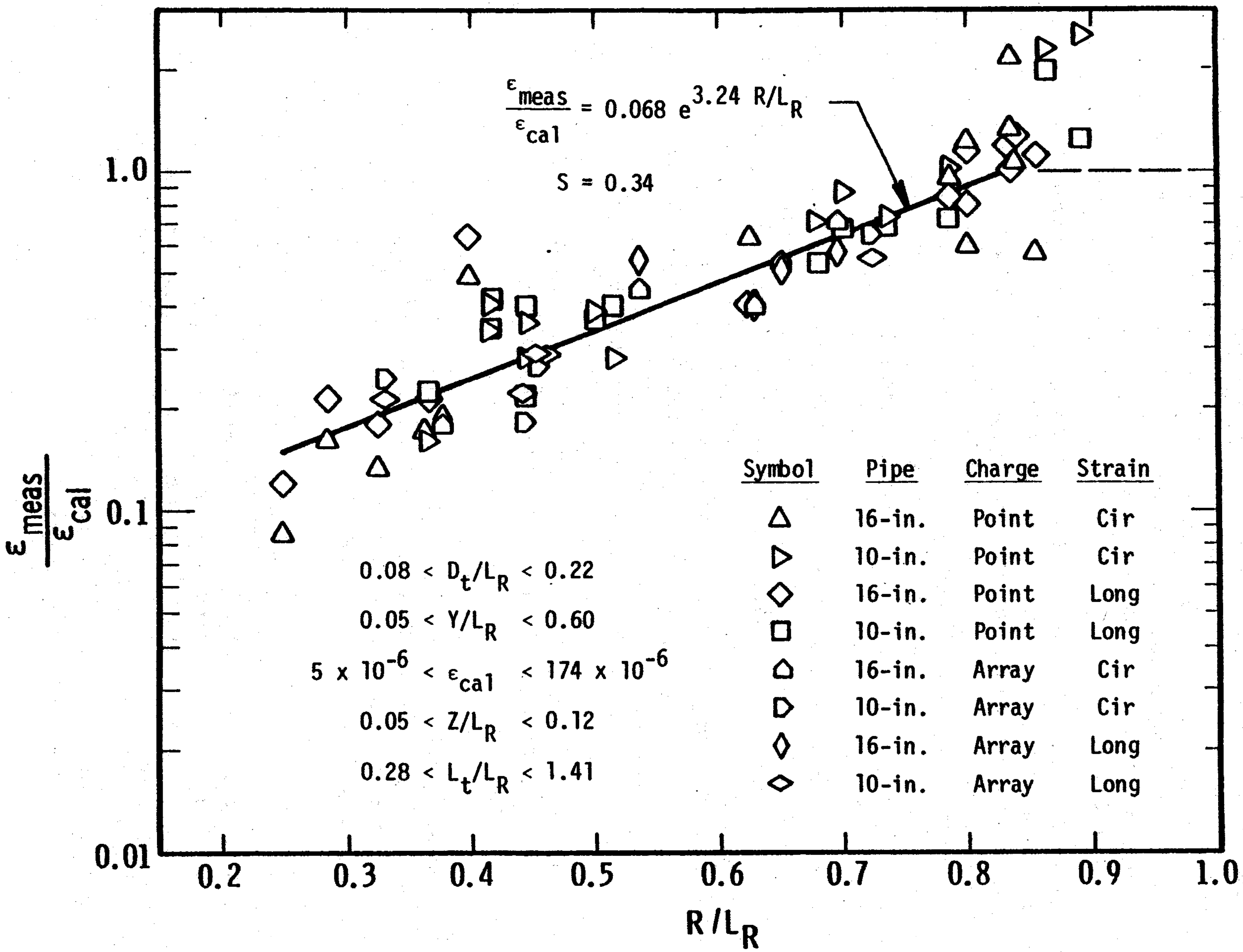

Figure 96. Estimate of Pipe Strain Reduction for a Passive Trench

$$\frac{\epsilon_{meas}}{\epsilon_{cal}} = 0.068 \; e^{3.24R/L_R} \tag{140}$$

for

$$0.25 < \frac{R}{L_R} < 0.83$$

This equation can be used provided all the restrictions are observed on R/L_R, D_t/L_R, ϵ_{cal}, Y/L_R, Z/L_R, and L_t/L_R. In addition, these results are only for open trenches, so it does not follow that these results can be extended for' use when sheet metal, piles and other screening barriers are used.

Two-Media Feasibility Tests

All of the experimental data presented in earlier sections of this report on pipe response to nearby detonations were obtained from tests in which both the pipeline and the explosive charges were buried in soil. Analyses of these soil data, from both model and full-scale tests, have produced the numerous prediction equations and methods presented in this report. However, blasting in a rock mass near steel pipelines which are buried in soil is a fairly common occurrence for which no experimental data were available to obtain a feel for the magnitude of stresses induced on the pipe.

To generate sufficient data using full-scale tests at an actual rocky site adjacent to an operational pipeline would be very expensive. Therefore, in one of the tasks conducted in 1980 for the A.G.A. blasting research program, SwRI conducted an experimental study to determine the feasibility of using a concrete block/soil model to simulate the problem of blasting in a rock mass in the vicinity of a pipeline buried in soil.

The original plan was to simulate a rock mass by placing a concrete block in the soil next to the instrumented 6-inch model pipe described earlier in this report. Provisions were made for three point charge locations, and thus, three experiments provided the level of damage inflicted on the concrete block by each detonation Was not extremely severe. The limited pipe response and ground motion data were to be analyzed to observe the results of a charge detonated in a hard media loading a pipe buried in a softer medium.

The test layout for the concrete/soil experiments is shown in Figure 97. A 10 x 10 x 3 ft slab was poured adjacent to the pipe using 6,000 psi concrete. Four tests, one more than originally planned, were conducted. Test Nos. 25 through 27 were fired using the holes that were molded in the concrete slab when it was poured. The charge hole for Test No. 28 was drilled after the other three experiments had been completed. In all four tests, the hand-molded, C-4 plastic-explosive charge was surrounded with soil, and the hole backfilled with gravel up to the surface. To prevent venting of the explosion, a steel plate was then placed over the charge hole and three, 2 X 2 X 4 ft concrete blocks were pyramid over the plate to weigh it down. Figure 98 shows the type of damage observed on the surface of the block from these tests.

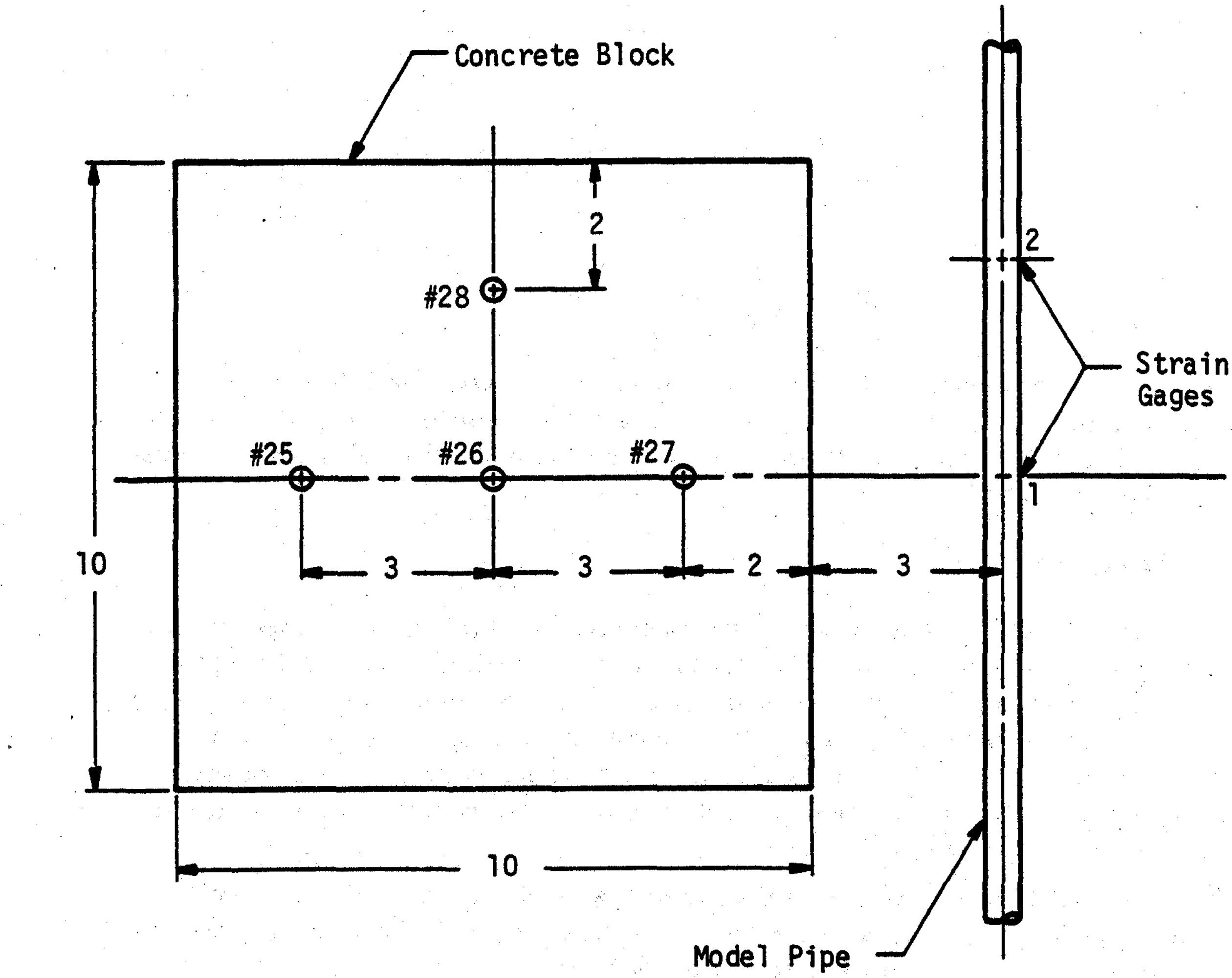

Plan View

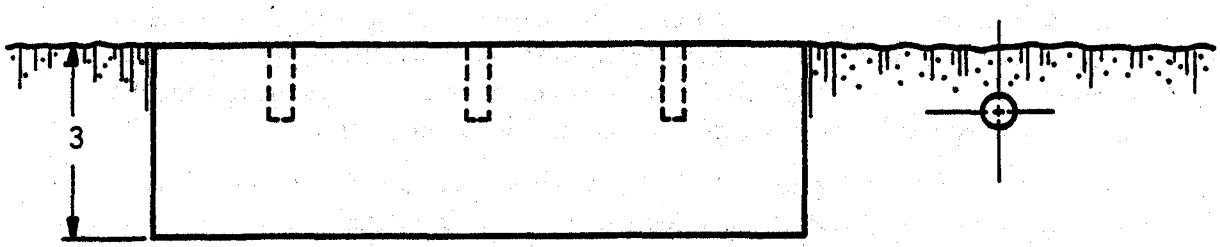

Elevation View

Figure 97. Field Layout for Concrete/Soil Tests

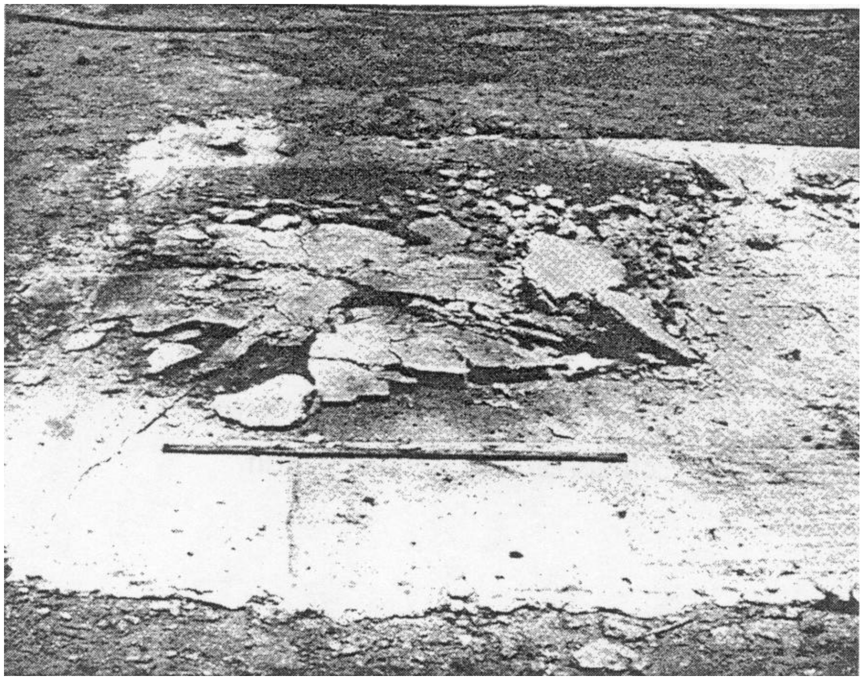

Figure 98. Damage to Concrete Block

Strain measurements were made primarily on the front, top and back of the pipe at a location opposite the charges. Examples of data traces from Test No. 25 are shown in Figures 99 and 100. Soil particle velocity measurements were also made. The maximum stresses computed from the strains measured for each concrete/soil test, part of Test Series No. 5, are presented in Table 18. In addition, the location of the velocity transducers and the corresponding ground motion dam are included in this table. The total standoff distance R is given in the table along with the portion of that distance that was in the con-Crete and the portion that was in soil for each measurement.

If these tests had been conducted in soil and the distance R, as well as the corres-ponding charge weight and seismic velocity are used in the point source equations presented in earlier sections of this report, one would predict lower stresses and ground motions than were measured in these concrete/soil tests. Thus, the effect of the concrete mass appeared to be one of making the charge seem closer to the pipe than it would have been if only soil had been used in these tests. With this observation in mind, approximate relationships were developed using previous derivations and the experimental data for this effective distance. The soil point source solutions were then used to estimate the pipe stresses for blasting situa-tions similar to the ones performed.

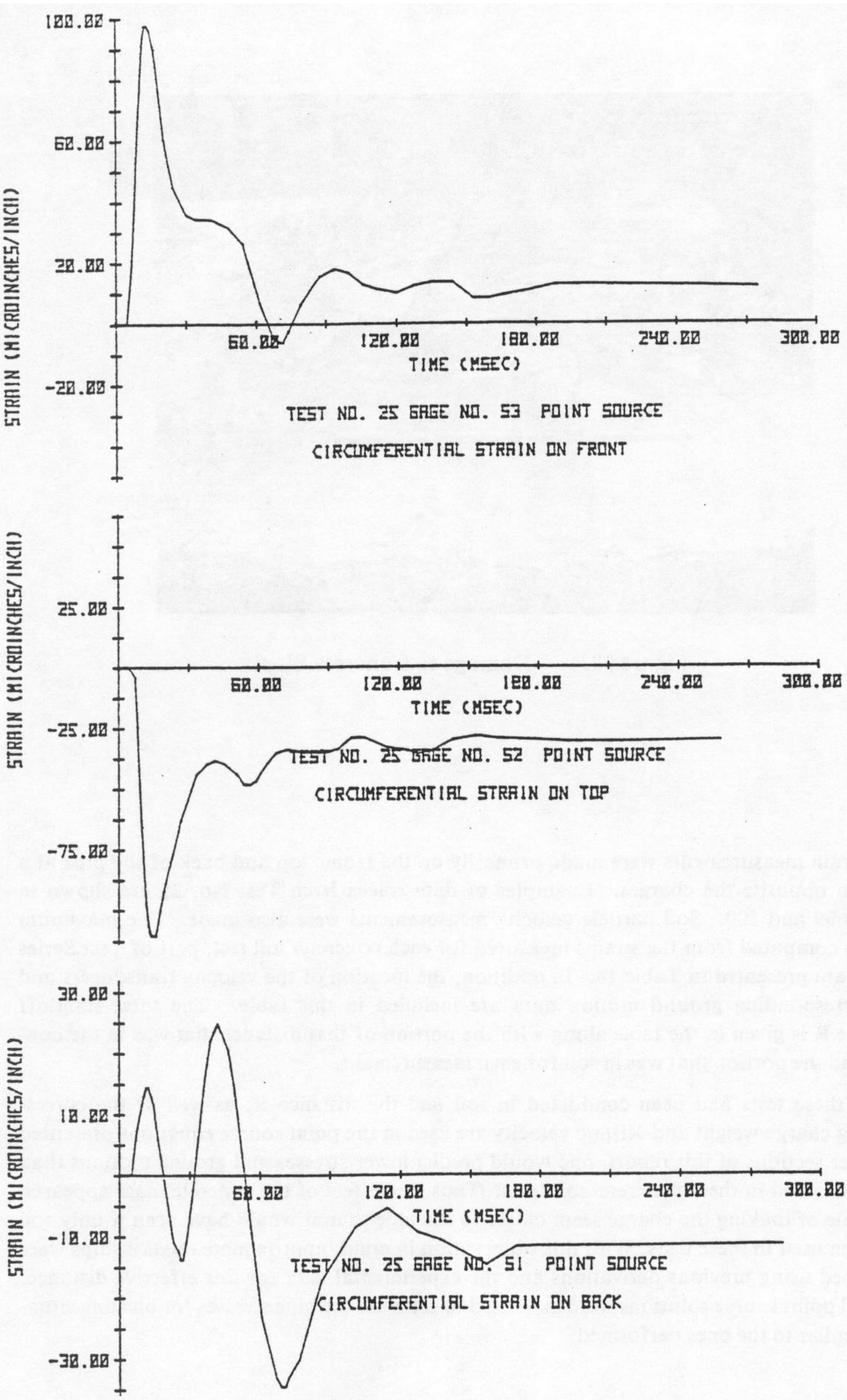

Figure 99. Circumferential Strains for Concrete/Soil Test

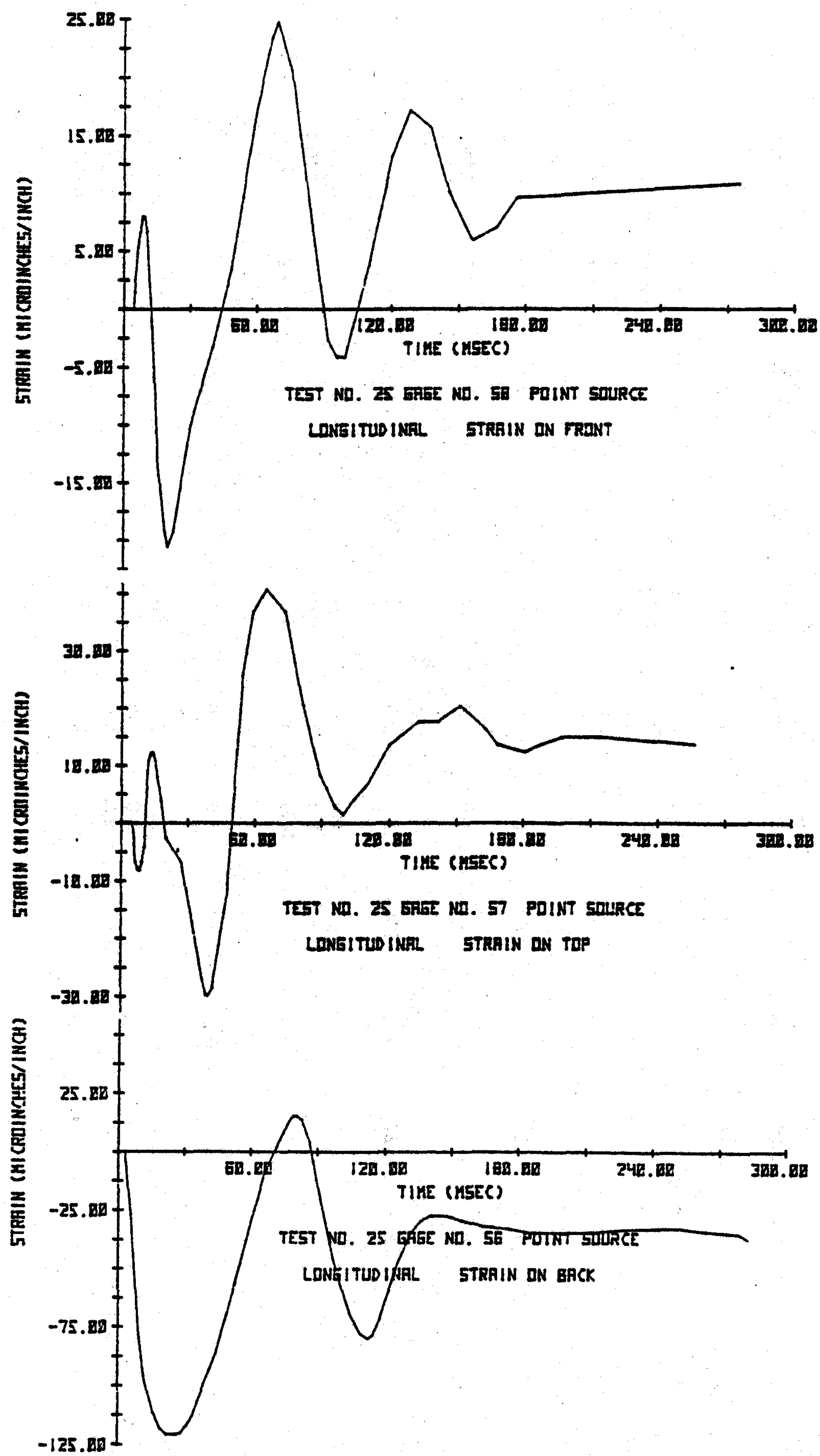

Figure 100. Longitudinal Strains for Concrete/Soil Test

Table 18. Results of Concrete/Soil Point Source Tests

Test Series	Test No.	W (lb)	c (fps)	R (ft)	R_{conc} (ft)	R_{soil} (ft)	σ_{cir} (psi)	σ_{long} (psi)	U (ips)	X (in.)
5	25	0.40	766	11.0	8.0	3.0	5,000	5,220		
				5.0	2.0	3.0			34.7	0.403
				8.0	2.0	6.0			24.4	0.229
				11.0	2.0	9.0			9.1	0.090
				8.0	5.0	3.0			12.7	0.181
5	26	0.25	792	8.0	5.0	3.0	--	--		
				8.0	5.0	3.0			4.7	0.077
5	27	0.25	726	5.0	2.0	3.0	9,570	10,500		
				8.0	5.0	3.0			12.9	0.164
				8.0	5.0	3.0			11.3	0.110
				14.0	5.0	9.0			3.8	0.049
5	28	0.25	944	8.0	5.0	3.0	11,150	8,220		
				5.0	2.0	3.0			17.5	0.131
				8.0	5.0	3.0			15.8	0.145
				8.0	2.0	6.0			7.8	0.068
				11.0	2.0	9.0			5.0	0.045

In Section V, the general equation for estimating the maximum radial particle velocity in a continuum was defined as

$$\frac{U}{c}\left(\frac{P_o}{\rho c^2}\right)^{0.5} = \frac{0.00617\left(\dfrac{W_e}{\rho c^2 R^3}\right)^{0.852}}{\tanh\left[26.0\left(\dfrac{W_e}{\rho c^2 R^3}\right)^{0.3}\right]} \tag{141}$$

Because shock pressure P in a continuum relates to particle velocity U through the relationship,

$$P = \rho c U \tag{142}$$

the particle velocity U can be eliminated from Equation (141) so that

$$\left(\frac{P}{\rho c^2}\right)\left(\frac{P_o}{\rho c^2}\right)^{0.5} = \frac{0.00617\left(\dfrac{W_e}{\rho c^2 R^3}\right)^{0.852}}{\tanh\left[26.0\left(\dfrac{W_e}{\rho c^2 R^3}\right)^{0.3}\right]} \tag{143}$$

If the subscript t is used to define the media into which a shock is transmitted, and the subscript i to define the incident media, then the transmitted shock is related to the incident shock through the relationship:

$$\frac{P_t}{P_i} = \frac{2}{1 + \dfrac{\rho_i c_i}{\rho_t c_t}} \tag{144}$$

In this case, the incident medium is concrete and the transmitting medium is soil. Because $\rho_c c_c$ for concrete is very much greater than $\rho_s c_s$ for soil, Equation (144) can be approximated by:

$$\frac{P_s}{P_c} = 2\left(\frac{c_c}{c_s}\right)\left(\frac{\rho_s c_s^2}{\rho_c c_c^2}\right) \tag{145}$$

In the concrete/soil tests, the seismic velocity ratio c_c/c_s was almost always a constant so Equation (145) can be written as

$$\frac{P_s}{P_c} = K\left(\frac{\rho_s c_s^2}{\rho_c c_c^2}\right) \tag{146}$$

where K is a constant.

Next, Equation (143) for shock transmission is used to determine the pressure P in con-Crete near, the concrete/soil interface. Then Equation (146) is used to transmit the shock from the concrete to the soil. The result of combining these equations is Equation (147) for pressure in the soil near the concrete/soil interface.

$$P_s = K\left(\frac{\rho_s c_s^2}{\rho_c c_c^2}\right) \frac{0.00617(\rho_c c_c^2)\left(\frac{W_e}{\rho_c c_c^2 R_c^3}\right)^{0.852}}{\left(\frac{p_o}{\rho_c c_c^2}\right)^{1/2} \tanh\left[26.0\left(\frac{W_e}{\rho_c c_c^2 R_c^3}\right)^{0.3}\right]} \tag{147}$$

Using the concept of an equivalent standoff distance for the same size charge detonated in a homogeneous soil, then P_s at the edge of the concrete would be:

$$P_s = \frac{0.00617(\rho_s c_s^2)\left(\frac{W_e}{\rho_s c_s^2 R_{eff}^3}\right)^{0.852}}{\left(\frac{p_o}{\rho_s c_s^2}\right)^{1/2} \tanh\left[26.0\left(\frac{W_e}{\rho_s c_s^2 R_{eff}^3}\right)^{0.3}\right]} \tag{148}$$

Combining Equations (147) and (148) and reducing terms gives:

$$K\left(\frac{\rho_s c_s^2}{\rho_c c_c^2}\right)^{0.352} = \frac{\left(\frac{R_c}{R_{eff}}\right)^{2.556} \tanh\left[26.03\left(\frac{\rho_s c_s^2}{\rho_c c_c^2}\right)^{0.3}\left(\frac{W_e}{\rho_s c_s^2 R_c^3}\right)^{0.3}\right]}{\tanh\left[26.03\left(\frac{R_c}{R_{eff}}\right)^{0.3}\left(\frac{W_e}{\rho_s c_s^2 R_c^3}\right)^{0.3}\right]} \tag{149}$$

The solution was completed by creating a log-linear approximation to Equation (149). Over different segments of an argument, the tanh may be approximated by:

$$\tanh\theta = \theta^{\beta} \tag{150}$$

For large values of the argument θ. the exponent β equals zero, and for very small values of the argument, β equals 1.0. There are different arguments in the two tanh functions in Equation (149); however, if anapproximation as in Equation (150) can be used, the three different nondimensional quantities

$$\left[\frac{R_{eff}}{R_c}, \frac{\rho_c c_c^2}{\rho_s c_s^2}, \text{ and } \frac{W_e}{\rho_s c_s^2 R_c^3}\right]$$

can be related through a log-linear equation as follows:

$$\frac{R_{eff}}{R_c} = C\left(\frac{\rho_c c_c^2}{\rho_s c_s^2}\right)^{\beta_c}\left(\frac{W_e}{\rho_s c_s^2 R_c^3}\right)^{\beta_w} \tag{151}$$

Equation (151) was curve fitted to the test data by taking logarithms and solving for the constant C, β_c, and β_w.

$$(\log C) + (\beta_c) \log\left(\frac{\rho_c c_c^2}{\rho_s c_s^2}\right) + (\beta_w) \log\left(\frac{W_e}{\rho_s c_s^2 R_c^3}\right) = \log\left(\frac{R_{eff}}{R_c}\right) \tag{152}$$

In matrix format, Equation (152) can be written:

$$\left[1.0,\ \log\frac{\rho_c c_c^2}{\rho_s c_s^2},\ \log\frac{W_e}{\rho_s c_s^2 R_c^3}\right]\begin{bmatrix}\log C\\ \beta_c\\ \beta_W\end{bmatrix} = \left[\log\frac{R_{eff}}{R_c}\right] \tag{153}$$

Using an abbreviated notation, Equation (153) can be expressed as:

$$[W][C] = [R] \tag{154}$$

And the coefficients in the C matrix follow from:

$$[C] = [W^T W]^{-1}[W^T][R] \tag{155}$$

The resulting equation for estimating the effective standoff distances for the concrete/soil tests is:

$$\frac{R_{eff}}{R} = 0.746\left(\frac{W_e}{\rho_s c_s^2 R_c^3}\right)^{0.028}\left(\frac{\rho_s c_s^2}{\rho_c c_c^2}\right)^{0.014} \tag{156}$$

where
- R_{eff} = effective standoff distance in soil (ft)
- R = standoff distance (ft)
- R_c = part of R in concrete (ft)
- W_e = explosive energy release (ft-lb)
- ρ_s = mass density of soil (lb-sec^2/ft^4)
- c_s = seismic p-wave velocity in soil (ft/sec)
- ρ_c = mass density of concrete (lb-sec^2/ft^4)
- c_c = seismic p-wave velocity in concrete (ft/sec)

The energy W_e in an explosive charge is computed by multiplying the specific energy release of the explosive by the weight of the charge. For these tests, C-4 plastic explosive was used and its specific energy release is 1.7 x 10^6 ft-lb_f/lb_m. The mass density and seismic velocity of the concrete were measured values for the block used in the experiments. The values used in fitting the data were p_c =4.745 lb-sec^2/ft^4 and c_c, = 13,000 ft/sec. The density of the soil was p_s -3.17lb-sec^2/ft^4.

Note that in Equation (156), both exponents are quite small thus making R_{eff}/R weak functions of dimensionless groups in the parenthesis. An average value for $W_e/\rho_s c_s^2 R_c^3$ in these tests was about 0.016 making the term

$$\left(\frac{W_e}{\rho_s c_s^2 R_c^3}\right)^{0.028} = 0.89 \tag{157}$$

Likewise, an average value for the impedance ratio of soil to concrete was about 0.003, thus

$$\left(\frac{\rho_s c_s^2}{\rho_c c_c^2}\right)^{0.014} = 0.92 \tag{158}$$

Therefore, for these specific tests a good approximation for Equation (156) is

$$\frac{R_{eff}}{R} = 0.61 \tag{159}$$

By using Equation (156) to compute values of R_{eff} corresponding to the pipe strain measurements for each setup, predicted stresses can be compared with measured values for the soil/concrete tests. This comparison is made in Figure 101. In this figure, the point and parallel line solution curve is shown along with the concrete/soil stress data. Notice that R_{eff} does provide a good way of predicting stresses for two media experiments similar to those conducted in this program. This figure also shows that the range of the stresses measured is quite narrow.

Similarly, Equation (156) was used to compute values of R_{eff} for each soil particle velocity transducer used in these experiments. With this computed effective standoff distance for one medium, each measured displacement and velocity listed in Table 18 for the two media tests can be compared to the one medium, point source equations. In Figure 102, the concrete/ soil ground motion data are compared to the point source curves. This comparison is additional evidence that the computed R_{eff} for each situation will yield reasonable estimates for two media situations similar to those used in the concrete/soil tests of this program.

In Figure 102 the range of the ground motion data is wider than that of the stress data. However, as can be seen in Table 18, the range of the various standoff distances in soil and concrete was limited, particularly for the stress data. Consequently, strict use of Equation (156) should be limited to situations which are geometrically similar to those in this study. For other layouts, some test data are first necessary to determine its applicability. One final observation concerning Equation (156) is that within the range of the experimental data, the estimate of the standard error in computing an R_{eff} was only 0.19. However, because the effective standoff distance is then used in the point source equations (which raises this parameter to a power of 2.5 or 3) to predict pipe stress or ground motion, any error in R_{eff} is magnified significantly.

Ideally, considerable more data arc needed before this solution can be considered as general as the ones for one medium (soil) because of the larger parameter space. Because no data arc available from rock/soil tests, it is not possible at this time to determine if Equation (156) can be applied directly to rock/soil blasting situations. However, for other two media situations geometrically similar to those in this study, this equation should provide rough estimates of the effective standoff distance using the corresponding parameter values for the rock in question. For other geometries, tests at the actual site with smaller charges are recommended for placing Equation (156) on a firmer basis.

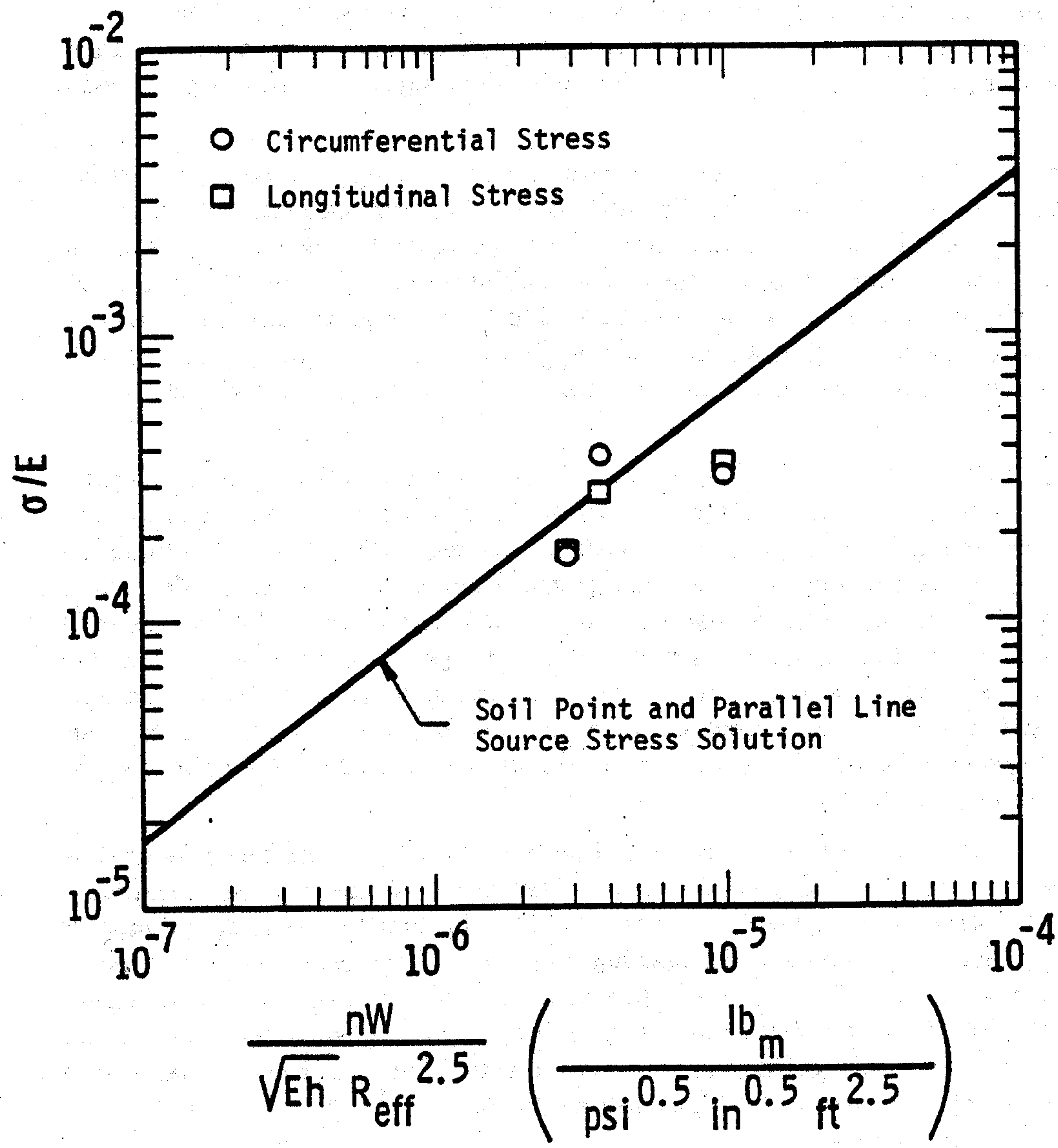

where

$$R_{eff} = 0.746\ R \left(\frac{W_e}{\rho_s c_s^2 R_c^3} \right)^{0.028} \left(\frac{\rho_s c_s^2}{\rho_c c_c^2} \right)^{0.014}$$

Figure 101. Comparison Between Concrete/Soil Pipe Stresses and Soil Point and Parallel Line Solution Using R_{eff}

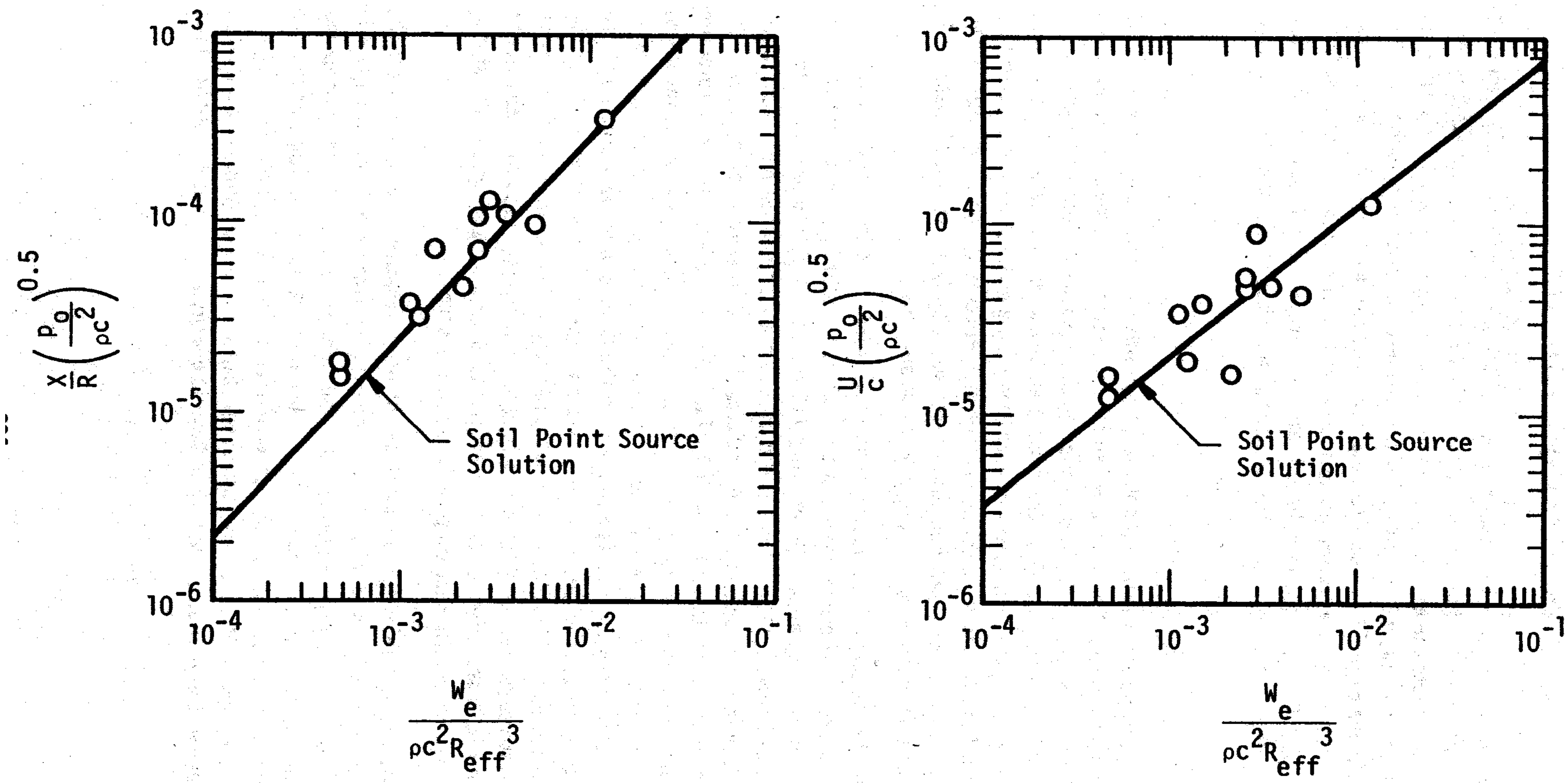

Figure 102. Comparison of Ground Motion Data from Concrete/Soil Tests to Soil Point Source Solutions Using R_{eff}

XI. ANALYSIS OF STRESS EQUATIONS

In addition to the limitations for the stress prediction equations and methods discussed in earlier sections of this report, the reader should be aware of how changes in each parameter in the solution affects the estimated stresses. In this section, a sensitivity analysis is used to show this effect. Then, a brief discussion is presented concerning other stresses loading the pipe and the use of yield theories to determine if the maximum allowable stress on the pipe has been exceeded. Some comments are then made concerning factors of safety. Finally, a discussion of other procedures based on past work and found in blasting regulatory codes is included in this section to put the stress solutions derived in this research effort in perspective.

Sensitivity Analysis

One of the best ways to determine how a solution responds to a change in some variable is to perform a sensitivity analysis, The variables which determine the circumferential stress (a,) and the longitudinal stress (σ_{long}) from blasting are the equivalent charge weight (nW), the modulus of elasticity for the pipe (E), the pipe wall thickness (h), and the standoff distance (R). For a line source, the equivalent charge (nW) for a point source is replaced by a charge weight per unit length (nW/L). Although the influence of E and h, as well as nW or nW/L, remain the same in both point and line source solutions, the standoff distance R has a different influence on pipe stresses for point and line sources.

Table 1.9 presents the results of a sensitivity analysis when blasting stresses from the point and parallel line sources are considered. In this table σ_{cir} and σ_{long} represent the sensitivity. The strain prediction equations [Equations (105) and (106)] arc used to compute the peak strains which arc then combined using the biaxial elasticity equations [Equations (30) and (31)] to produce the corresponding circumferential and longitudinal stresses. The parameter σ is the sensitivity when the stress curve fit [Equation (112)] is used to predict the maximum stresses which are made equal in both directions. For all practical purposes, either approach gives essentially the same result. In Table 19, each parameter E, h, nW, nW/L, and R is doubled independently. The number in the table shows how much σ_{cir} and σ_{long}, or alternatively σ, increases or decreases because one parameter was doubled. If the number is greater than 1.0 as for E and nW, the stress increases. If the number is less than 1.0 as for h and R, the stress decreases. Table 19 indicates that stresses are most sensitive to standoff distance R and least sensitive to the pipe properties E and h, Changes in the standoff distance also have a greater influence on point than line sources.

The list of parameters in Table 19 may seem small; however, these parameters are the main ones which determine the change in stress in a buried pipe from blasting. Particularly obvious by their omission are the pipe diameter, the soil density, and the seismic propagation velocity in the soil. These parameters are absent because the stress solution as derived in this report is independent of them. In the case of larger diameter pipes, more kinetic energy is imparted to the pipe as its diameter increases, but more strain energy can also be stored in pipes with larger diameters. Because the kinetic energy and strain energy are both

Table 19. Effects on Predicted Stresses When Each Parameter is Doubled Independently

Stress Component	Pipe Properties E	Pipe Properties h	Point Sources nW	Point Sources R	Line Sources nW/L	Line Sources R
σ_{cir}	1.52	0.76	1.74	0.25	1.74	0.44
σ_{long}	1.54	0.77	1.70	0.27	1.70	0.45
σ	1.53	0.77	1.71	0.26	1.71.	0.45

first power functions of the pipe diameter, the pipe diameters cancel when these quantities are equated, and the resulting response becomes independent of pipe diameter. Experiments on 3-, 6-, 16-,24-, and 30-inch pipes all yielded results that show this observation is a correct one.

In a similar manner, the approximation concerning the radial ground displacement equations in which $(X/R)(p_o/\rho c^2)^{0.5}$ was made proportional to either $(nW/\rho c^2R^3)$ or $(nW/L/\rho c^2R^2)$ eventually leads to p and c being eliminated from the pipe response analysis. If the more complex relationships for the ground displacement are used, the circumferential stress and the longitudinal stress become weak functions of p and c. The simpler format was used because adequate engineering answers result without appreciable benefit from added complexity.

All of the conclusions in the sensitivity analysis assume no contribution to σ_{cir} and σ_{long} from pipe pressurization or other loading mechanisms. Table 19 represents only a change in the circumferential or longitudinal stress components associated with blasting.

Other stress states

A knowledge of the state of stress caused by blasting is only one of the stress parameters necessary to determine if a buried pipe will yield. Other loading mechanisms also cause a pipe to be stressed. Because of symmetry, circumferential and longitudinal stresses from blasting and other effects are principle stresses. This observation means that an accurate estimate of the elastic state of stress can be made by superposition through addition of stresses with their signs considered. The purpose of this program does not include a discussion of states of stress from other causes. These stresses can be very significant, so readers should consider including longitudinal and circumferential stresses from such causes as:

1) Internal pipe pressurization
2) Thermal expansion or contraction
3) Surcharge or overburden
4) Residual stresses from welding and other installation processes

After the resultant longitudinal and circumferential stresses have been obtained, a yield theory will have to be selected to determine if the pipe yields. In this discussion, we will only mention some of the theories which might be chosen. Actual selection of an appropriate theory must be left up to engineers in each company. Sometimes state law, company policy, and other considerations beyond our control dictate the choice or selection of a particular criteria for determining yield. We will illustrate some of the theories which might be selected.

A biaxial state of stress may be plotted on a graph with one stress such as the circumferential on the x-axis and the other such as the longitudinal on the y-axis. Figure 103 is such a plot, with the circumferential and longitudinal stresses normalized by dividing by a uniaxial yield stress σ_y. Four different quadrants exist in the solution shown in Figure 103 because these are the different combinations of tension and compression which could exist for the two orthogonal resultant stresses. Different yield theories have been applied by various investigators to determine what combinations of these resultant stresses constitute the onset of yield. Five of these theories arc illustrated in Figure 103, To determine if the pipe yields because of the combination of the blasting and other applied stresses, the reader most likely will have to select one of these yield theories.

The five theories shown in Figure 103 are: 1) the maximum stress theory, 2) the maximum strain theory, 3) the maximum shear theory, 4) the maximum energy theory, and 5) the distortion energy theory. Additional details and discussions of these theories can be found in Section X of Timoshenko (1956). All of the lines in Figure 103 represent the threshold of yield. If any biaxial combination of stresses falls within the envelopes, no yield occurs, but if stresses fall outside the envelopes, yielding is assumed to have occurred. Notice that all theories agree on the yield criteria for a uniaxial state of stress; however, they differ for biaxial states of stress and also have different envelopes whenever the algebraic signs are the same and when the signs differ.

For all of these theories, the worse conditions occur in quadrants II and IV where the signs of the resultant stresses differ. Often regulations and specifications simplify yield criteria by taking absolute values of the resultant stresses, and use a yield criteria for a worse state quadrant such as quadrant II. Figure 104 is the plot for the five yield theories in this quadrant.

Many state codes use the maximum shear theory, sometimes called Tresca's Theory, because it is the most conservative. The equation for this theory is very simple because it is a straight line. The threshold yield equation for the maximum shear theory is given by:

$$\left|\frac{\sigma_{cir}}{\sigma_y}\right| + \left|\frac{\sigma_{long}}{\sigma_y}\right| = 1.0 \qquad (160)$$

In this equation, the normalized stresses are the absolute values.

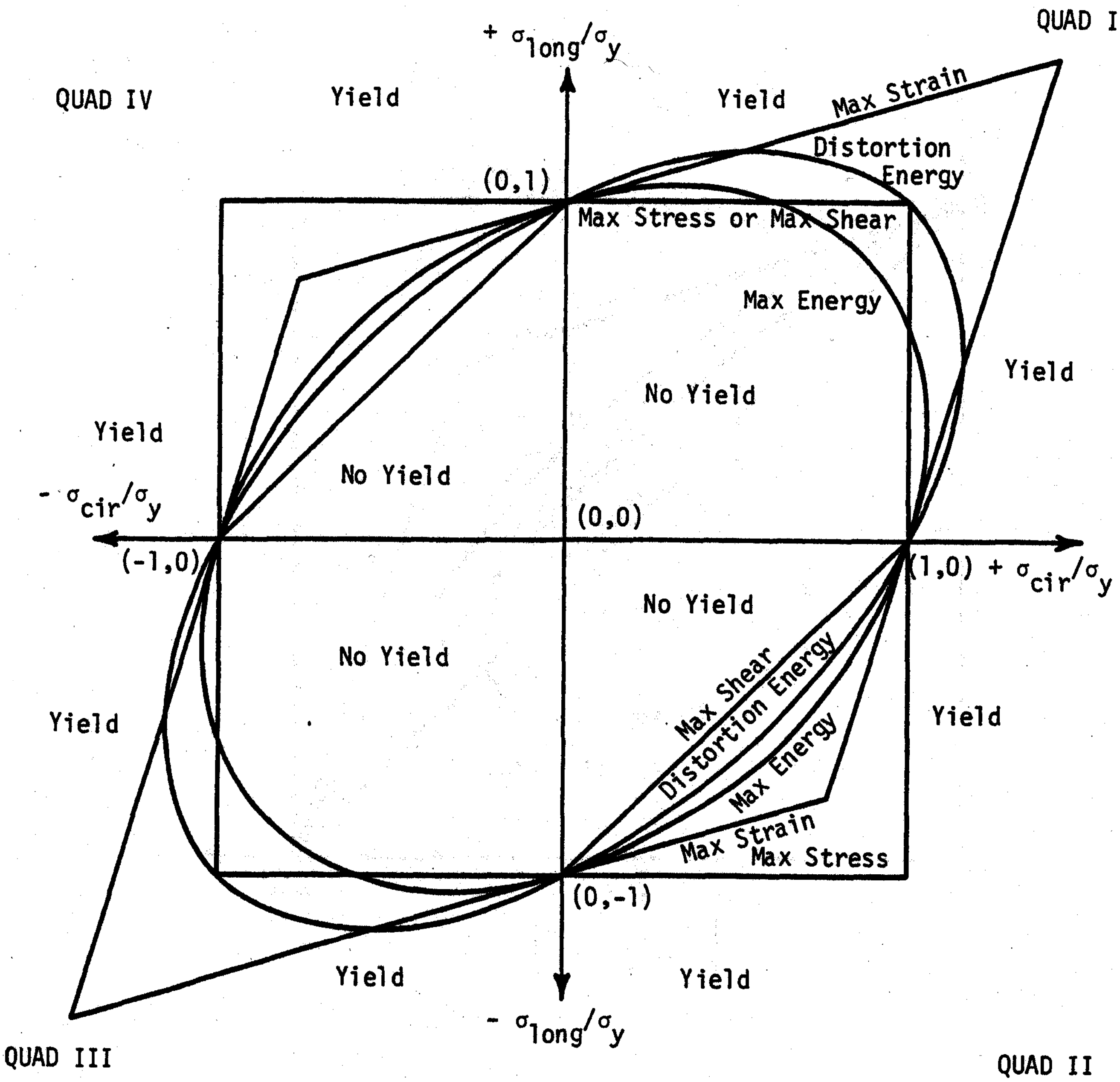

Figure 103. Stress States for Different Yield Theories

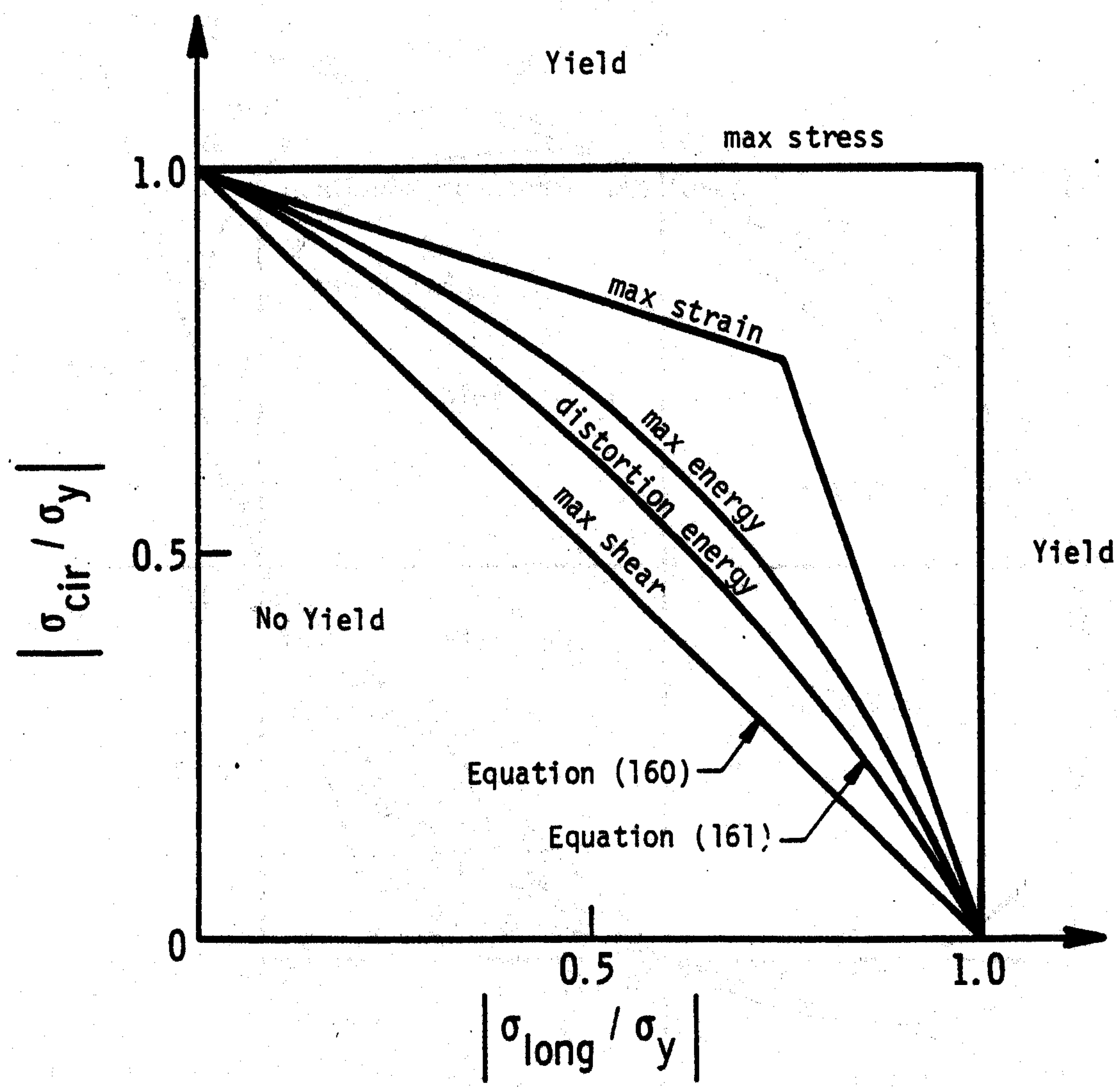

Figure 104. Simplified Yield Theories

Many engineers tend to use the distortion energy criteria, sometimes called the Huber-Hencky-Mises Theory, as they believe it is the most accurate. The equation relating the threshold for yield using distortion energy is given by:

$$\left(\frac{\sigma_{cir}}{\sigma_y}\right)^2 + \left|\left(\frac{\sigma_{cir}}{\sigma_y}\right)\right|\left|\left(\frac{\sigma_{long}}{\sigma_y}\right)\right| + \left(\frac{\sigma_{long}}{\sigma_y}\right)^2 = 1.0 \qquad (161)$$

The other three theories (maximum energy, maximum strain, and maximum stress) are seldom used anymore, so equations for these will not be given. In using any yield theory, the reader has to add other stresses, such as those from pipe pressurization, to the blasting stresses and then choose one of the yield theories, Company philosophy, approach, regulations, and policy can all influence the selection of a yield theory. We present this discussion of yield theories to aid in the selection of an approach and to show a comparison of the different theories. Actual selection of any one approach is beyond the limits placed on this work by the Blasting Research Supervisory Committee. Different organizations in various sections of the country may be using different yield criteria for different corporate reasons.

Factor of Safety

In addition to combining the blasting and other stresses loading a pipe and selecting a yield criteriato evaluate a particular situation, a safety factor must be included in the stress analysis, What factor is used will depend on a number of considerations, and the user must decide for himself the actual value used. In some cases, company policy may dictate minimum- values for safety factors in terms of maximum allowable stresses, In the discussion that follows, some guidance is provided for selecting safety factors.

No one number should be used as a factor of safety because many interactions are involved. Most newer pipes are manufactured from ductile materials, but some older pipes were manufactured from brittle materials. A, ductile material can strain well beyond yield and still exhibit very little deformation. On the other hand, a brittle pipe material cannot exceed yield at all or the pipe will crack. Obviously, the consequence of yielding is much more severe in a brittle than in a ductile pipeline. Therefore, much larger safety factors should be used in brittle as opposed to ductile pipelines.

One standard deviation or estimate of the standard error for predicting both circumferential and longitudinal stresses from blasting equals approximately 34 percent of the predicted value. This statement infers that, were the same blasting conditions repeated a large number of times, approximately 68.3 percent of the results would fall between 1 ± 0.34 times the predicted value, and 95.4 percent of the results would fall between 1 ± 0.68 times the predicted value. This prediction of scatter assumes a normal distribution of test results which may not be quite true, and it applies only to those stress components caused by blasting.

Knowing the probable error in estimating the blasting components of stress helps, but it alone cannot determine the safety factor. Another key consideration is the magnitude of the blasting stresses relative to the total stresses. For example, in a pipeline with a yield stress of 60 ksi, a blasting stress of 10 ksi means one standard deviation is ± 3.4 ksi; whereas, a blasting stress of 40 ksi means one standard deviation is ± 13.6 ksi. Obviously, a probable error in the blasting stress estimate of 3.4 ksi is less significant relative to a 60 ksi yield point than one of 13.6 ksi. The magnitude of the blasting stress relative to the total state of stress must be considered in selecting an appropriate safety factor.

One final consideration in the selection of a safety factor is some concept of the consequences of failure. Loss of service in a major pipeline serving an entire region of the United States has to be more serious than loss of service in an artery into some building development. This observation implies that a factor of safety might be presented as a function of pipe diameter because the larger lines are usually the most important ones.

As should be apparent by this discussion, what factor of safety is used on a blasting situation is not a one answer question. We must leave this consideration up to each individual company as regulations and company policy can also differ in various sections of the country.

Other Analysis Methods

Two methods in particular have found some usage for setting limits on blasting near pipelines, and should be discussed to place their misuse in proper perspective, The first of these is a series of maximum velocity criteria and, sometimes, maximum acceleration criteria, which came into use in the 1940's. Unfortunately, these efforts were concerned with very narrow bounds that pertain to some particular problem such as cracks in building and machinery misalignment. On occasion, the results would even conflict. These limiting ground motion criteria which have found their way into some state codes have been applied to pipelines and can be placed into perspective by looking at the following qualitative model:

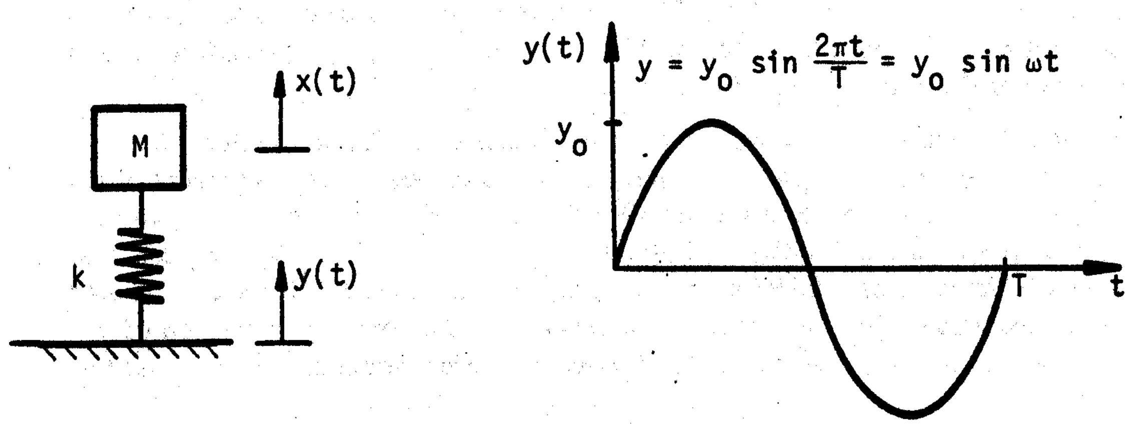

Figure 105. Qualitative Ground Shock Model

In this model, a sinusoidal ground shock pulse of amplitude y_o and period T excites a linear elastic oscillator of mass M and spring constant k. If the maximum relative motion $(x-y)_{max}$ exceeds a certain magnitude, we assume that a building will crack, machinery will be misaligned, etc. By limiting the relative motion $(x-y)_{max}$, we are also limiting the force applied to the mass because the strength of the structure k times this motion is this maximum force. The equation of motion for this model is:

$$M\frac{d^2x}{dt^2} + k\ x = k\ y(t) = k\ y_o\ \sin\ \omega t \tag{162}$$

If the structure is initially at rest, the initial conditions at time t = 0 are X = 0 and dx/dt = 0, and the solution to Equation (162) is:

$$\frac{x-y}{y_o} = \underbrace{\frac{(\omega/\sqrt{k/M})^2}{1-(\omega/\sqrt{k/M})^2}\sin\ \omega t}_{\text{Complementary Solution}} - \underbrace{\frac{(\omega/\sqrt{k/M})}{1-(\omega/\sqrt{k/M})^2}\sin\sqrt{k/M}\ t}_{\text{Particular Solution}} \tag{163}$$

Equation (163) has two parts to it the complementary solution and the particular solution. Dependent upon whether $(\omega/\sqrt{k/M})$ is much less than 1.0 or much greater than 1.0, one part or the other will predominate. If $(\omega/\sqrt{k/M}) << 1.0$, the solution becomes:

$$\frac{(x-y)}{y_o} = \left(\frac{\omega}{\sqrt{k/M}}\right)^2 \sin\omega t - \left(\frac{\omega}{\sqrt{k/M}}\right)\sin\sqrt{k/M}\,t \tag{164}$$

Under this circumstance, the major term is the particular solution, and the complementary solution is a small amount of noise superimposed on the dominant term. Because the maximum occurs when the sin $\sqrt{k/M}\ t$ equals -1.0, the maximum relative displacement is given by:

$$\left(\begin{array}{c}\omega/\sqrt{k/M} << 1.0 \\ \textbf{Particular Solution}\end{array}\right) \tag{165}$$

But: $(y_0\omega)$ is the maximum soil velocity which says that under these conditions, a constant limiting specified velocity is the correct criterion for a specific structure.

On the other hand, if $(\omega/\sqrt{k/M}) >> 1.0$, the solution becomes:

$$\frac{(x-y)}{y_0} = -\sin\ \omega t + \frac{1}{\omega/\sqrt{k/M}} \sin\sqrt{k/M}\ t \tag{166}$$

The dominant term now becomes the complementary solution, which is a maximum when displacement is:

$$\left(\omega/\sqrt{k/M} >> 1.0 \right) \tag{167}$$

Complementary Solution

Under these conditions, a constant specified limiting soil displacement is the correct criterion for a specific structure.

A third domain also exists especially when: 1) the particular solution can be suppressed by heavy damping, or 2) the complementary solution made to dominate as when steady state continuous vibratory sources are present. Under these conditions for $(\omega/\sqrt{k/M}) << 1.0$, the solution is:

$$(x-y) = \left(\frac{\omega}{\sqrt{k/M}} \right)^2 \sin\ \omega t \tag{168}$$

Which has a maximum given by:

$$\left(\omega/\sqrt{k/M} << 1.0 \right) \tag{169}$$

Complementary Solution

This solution is a constant acceleration criteria. Which criteria are important thus depends upon: 1) whether a single pulse or steady state vibrations are involved, and 2) whether $(\omega/\sqrt{k/M})$ is large or small relative to 1.0.

In 1942, Theonen and Windes conducted experiments for the Bureau of Mines because of damage and litigation arising from the detonation of buried explosive charges. Because the Bureau had difficulty locating structures which could be blast loaded to damage, 13 experiments were conducted using a mechanical vibrator with an unbalanced motor, a steady-state vibration source. Force and frequency were adjusted with upper limits of 1000 pounds and 40 Hz, respectively. The report based upon these tests recommended an acceleration criterion with no damage at less than 0.1 g's, minor damage between 0.1 and 1.0 g's and, minor damage at greater than 1.0g's. Whenever constant acceleration criteria are specified, it is usually based on this study. Notice that although they were interested in blasting, a vibratory excitation was used. We have just shown that when $\omega/\sqrt{k/M}$ is small and steady&ate vibrations are involved, an acceleration criterion is possible. A criterion such as this one has nothing to do with blast, however.

In 1949, Crandell prepared a constant velocity ($\omega/\sqrt{k/M}$ is small) criterion for protecting above-ground' structures from buried detonations. His lower limit for caution corresponds to a peak ground velocity of 3.3 in./sec. Crandell used test results to relate this velocity (he calls it an energy ratio) to standoff distance, charge weight, and a ground transmission coefficient. Many state blasting codes are based upon this study.

In Sweden, Langefors, Kihlström, and Westerberg (1958) accumulated a large data base during a reconstruction project requiring blasting near buildings. Because large blasts were desired for economy of operation, a policy was adopted whereby minor damage to adjacent structures, which could be replaced at moderate cost, was acceptable. Thus, these investigators recorded and analyzed a large amount, of data on actual damage to buildings from more than 100 blasting tests. By and large, these Swedish tests had frequencies higher than those recorded elsewhere, 50 to 500 Hz. Once again, particle velocity became the best damage criterion for failure of plaster. Velocities of 2.8 in./sec resulted in no noticeable damage, 4.3 in./sec in fine cracking, 6.3 in./sec in cracking, and 9.1 in./sec in serious cracking.

When the St. Lawrence Seaway Project was being built, Edwards and Northwood (1960) conducted controlled. blasting tests on six residences slated for removal. Acceleration, particle velocity, and displacement were all measured on the residences for charges ranging from 47 to 750 lb buried at depths of 15 to 30 ft and at various standoff distances from these buildings. Frequencies ranged from 3 to 30 Hz. They too concluded that building damage was more closely related to velocity than displacement or acceleration, and that 4 to 5 in./sec was likely to cause damage. A safe velocity limit of 2.0 in./sec was recommended based on this study.

One final study in Czechoslovakia by Dvorak (1962) was for buried explosive charges of 2 to 40 lb placed 16 to 100 ft from one and two-story brick buildings. In this study, the measured frequencies were in the range of 1.5 to 15 Hz. Dvorak concluded that threshold damage occurred at soil particle velocities between 0.4 to 1.2 in./sec, minor damage at 1.2 to 2.4 in./sec and major damage above 2.4 in./sec.

A very good summary of low-frequency blasting criteria was put together by Nicholls, et al. (1971) for the Bureau of Mines. Basically, Nicholls took data from the sources which we have just described and made a composite plot of displacement amplitude versus frequency data. Three degrees of structural damage severity was considered: no damage, minor damage such as new crack formation or opening of old cracks, and major damage such as serious cracking and fall of plaster. Figure 106 shows this displacement versus frequency plot of Nicholls. Notice that after conducting a regression analysis, the slope of the lines for the different degrees of damage to buildings are all constant velocity curves - 7.6 in./sec for major damage, 5.4 in./sec for the threshold of minor damage. The 2.0 in./sec as a safe blasting threshold which is shown was not based upon any curve fit to the data.

Many state codes use 2.0 in./sec as a safe blasting criterion for surface structures. A large amount of data are behind this criterion, but remember the 2.0 in./sec criterion has nothing to do with pipelines which are strong buried structures. Analytically, a velocity criterion is appropriate whenever $(\omega/\sqrt{k/M})$ is small, Equation (165). But whenever $(\omega/\sqrt{k/M})$ large, a displacement criterion is analytically more appropriate, Equation (167). In buried pipelines, a large mass of earth acts along with the pipe, This large mass of earth makes a larger M which, in turn, makes $(\omega/\sqrt{k/M})$ much larger. The results obtained in this blasting study on buried pipelines have a displacement criterion. This result is not inconsistent with all of the velocity criteria results obtained on above ground structures. These results only infer that $(\omega/\sqrt{k/M})$ places all of our pipeline and the various building test results in different domains.

The velocity criteria arc valid for buildings, but not at all for buried pipes. If one computes the radial soil particle velocity for many of our experiments, the unstressed pipe has very acceptable stress levels for particle velocities greater than 2.0 in./sec. Those velocity criteria are in state laws because no data on pipelines existed, and no one had any concept of what else could be easily used.

A second criterion, which is sometimes used, was derived by McGlure, et al. (1964) at Battelle Memorial Institute. It uses the Morris (1950) equation for ground motion, and assumes that the pipeline movements equal those of the surrounding soil. Those assumptions lead to a quasi-static analysis and permits no diffraction of the shock front around the pipe. The equation for circumferential stress is given by:

$$\sigma_{cir} = 4.26 \frac{K\ E h\ \sqrt{W}}{R\ D^2} \tag{170}$$

where
K = site factor to account for soil conditions
E = pipe modulus (psi)
W = charge weight (lb)
R = standoff distance (ft)
D = pipe diameter (in,)
h = pipe thickness (in.)
σ_{cir} = circumferential stress (psi),

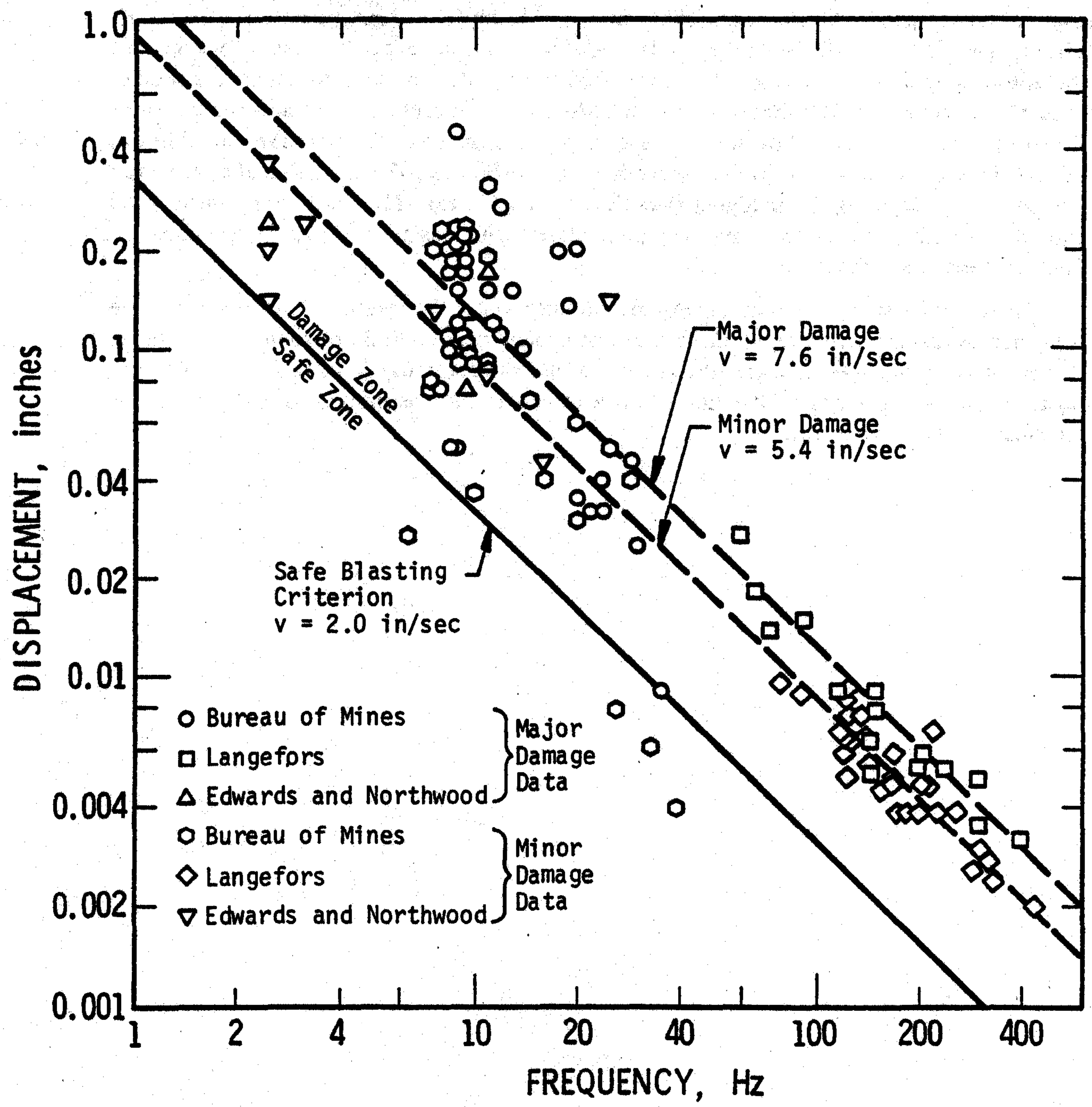

Figure 106. Displacement versus Frequency, Combined Data with Recommended Safe Blasting Criterion (Nichols)

Figure 107 shows a plot of point source test data recorded by SwRI in the A.G.A. blasting research program versus this equation. To be perfectly fair, this evaluation is not a proper one because McClure, et al. (1964) state that Equation (170) is not valid for standoff distances less than 100 ft. Nevertheless, this comparison is made because users have ignored the author's qualifying statement and have used the equation at standoff distances smaller than 100 ft. As Figure 107 shows, Equation (170) is not as accurate as the new relationships developed in this report and the data for each pipe size forms a different curve.. In addition, misuse does not necessarily give conservative results (Figure 107 shows that the measured stresses on the larger pipes are higher than the predicted ones). The Battelle circumferential equation also implies that doubling the pipe thickness while keeping everything else constant doubles the stress in the pipe.

Finally, we wish to say that a company's ability to use the results in this report may be restricted by governmental regulations based on ground motion limitations or other criteria. When these circumstances arise, the reader should probably use both this report and the regulations. In this manner, blasting conditions can at least be limited to whichever gives the most conservative result.

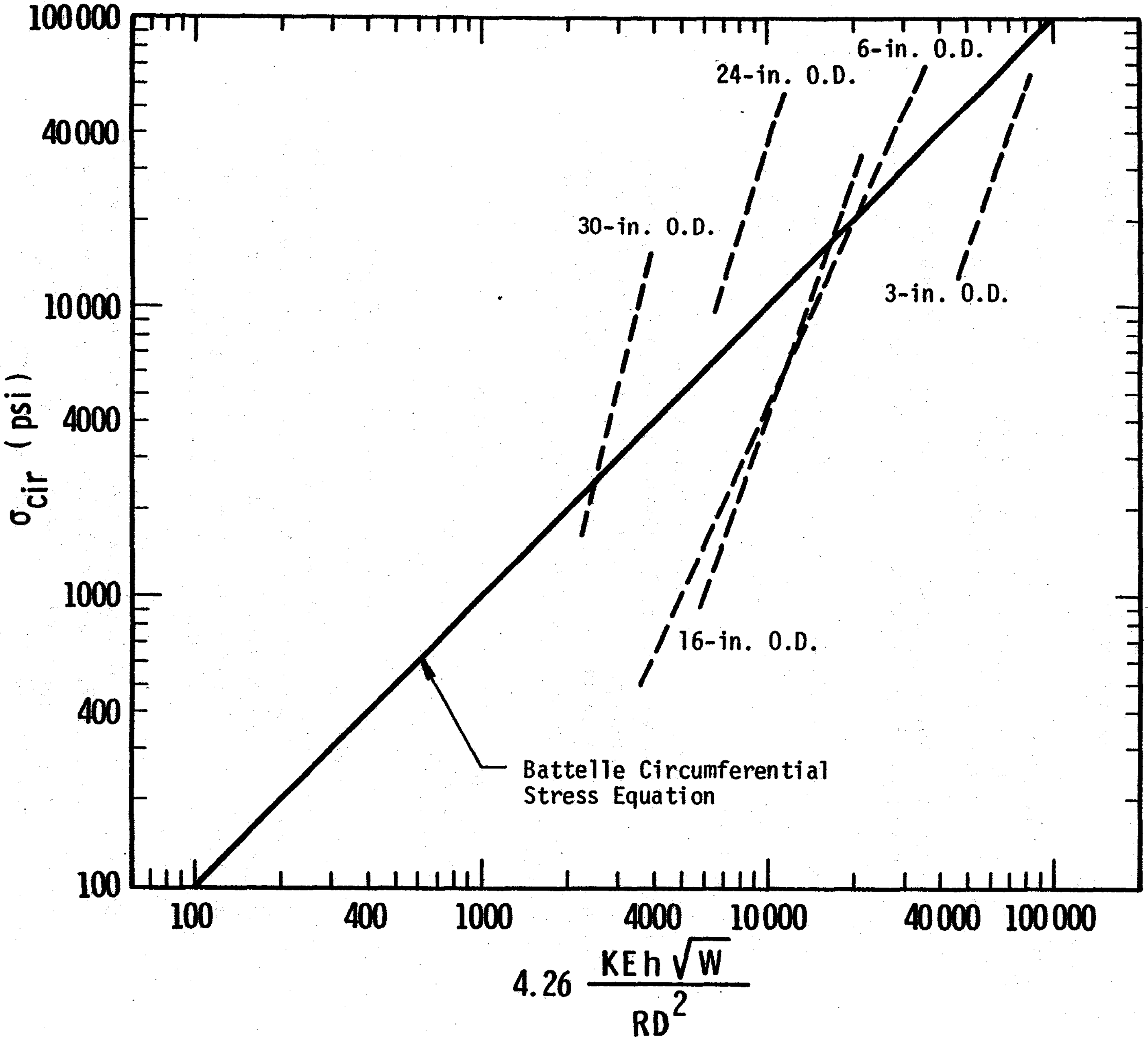

Figure 107. Battelle Circumferential Stress Formula Compared to Measured Pipe Stresses from Nearby Point Source Tests

XII. FINDINGS AND CONCLUSIONS

The blasting research program conducted by Southwest Research Institute for the Pipeline Research Committee of the American Gas Association produced a number of significant findings and conclusions relevant to blasting in the vicinity of pipelines. These findings, which have advanced the state-of-the-art for predicting blast effects on pipelines, include the following:

- From the model analysis, functional expressions were developed which related ground motion and pipe stresses to the significant parameters which define underground blasting conditions from point and parallel line sources.

- These functional relationships produced a replica model law which defines the relationship between the various parameters in model. and full-scale experiments.

- The test data presented in this report show that ground motions and pipe response parameters from blast-induced seismic pulses can be scaled or modeled. The data were obtained at three different test sites using five different size pipes.

- Using the extensive quantity of ground motion data obtained in this program plus data from the literature, the functional relationships for radial ground displacement and radial particle velocity were defined. The general equations derived for point sources in a homogeneous and isotropic media are applicable over a wider range of scaled distances than any empirical equation derived previously.

- Simplified log-linear equations for the radial ground motions from buried point sources were derived empirically over the range of the data most applicable to pipeline problems.

- For parallel line explosive sources, test data (primarily obtained in this program) were also used to define empirically the functional expressions for radial soil displacement and radial soil particle velocity. These parallel line ground motion equations arc based on data whose range is not as broad as that of the general point source solutions. Furthermore, all parallel line tests were done in soil and, thus, these equations should be given only tentative acceptance and used with certain amount of judgement when applied to other ground media.

- Prediction equations for estimating the maximum strains and stresses induced on a buried pipeline by point and parallel line explosive sources detonated in soil were derived using approximate analyses for the kinetic energy imparted to the pipe by the impulse distribution from the seismic wave and for the elastic strain energy which defines the pipe response. Pipe strain and stress data obtained on model and full-scale tests conducted in this program were used to define simple log-linear equations for estimating the circumferential and longitudinal strains and stresses resulting from buried point and parallel line source explosive detonations.

These closed form prediction equations depend only on the explosive weight or density, pipe modulus of elasticity and thickness, and the standoff distance. They are independent of pipeline length and diameter. Static analysis procedures do not yield this conclusion, and cannot be used to solve this transient dynamic problem. Because of the linear approximation made to the displacement equations, the stresses are also independent of the soil density and seismic velocity. Had the more complex relationships for radial soil displacement been used, the circumferential and longitudinal stresses would become weak functions of the soil parameters. The simplified format was used because adequate engineering answers were obtained without appreciable benefit from added complexity.

The stress prediction equations developed are limited in application to point and parallel line explosive sources detonated in soil where the pipe and the charge are buried to about the same depth. The range of the stress data used to complete the solutions was such that the equations should be applicable for most soil blasting situations near gas pipelines to distances as-close as two-pipe diameters.

Assuming a normal distribution of the experimental data about the point and parallel line solution curve, the estimate of the standard error was only $\pm$ 0.34. This statistic infers, that for a similar blasting situation in soil there is a 97.7 percent probability that the maximum stress will not exceed 1.68 times the predicted value.

A sensitivity analysis of the point and parallel line stress prediction equations indicated that pipe stresses are most sensitive to the standoff distance and least sensitive to pipe properties (i.e., modulus of elasticity and pipe thickness). Changes in the standoff distance also have a greater influence on the stress for a point source than a parallel line source.

Experimental data from multiple charge arrays such as explosive lines and grids oriented parallel and at an angle to a pipeline were used to develop empirical methods for estimating pipe stresses. The approach used for these more complex explosive geometries was to simplify them into equivalent parallel line and point sources and then use the prediction equations for these simpler sources.

- In applying the stress prediction methods for the complex explosive geometries, the reader must observe the limitations in charge geometry and parameter range of the complex explosive source data. In addition, the limitations for the point and parallel line source equations also apply in estimating pipe response for a complex explosive source.

- Exceptions to the general methods for simplifying line and grid sources exist in the case of line sources oriented perpendicular to the pipeline and in cases where the nearest charge making up an explosive array would result in higher stress predictions than those of the entire charge pattern.

- The blasting stress prediction equations and methods can easily be formulated into a logic diagram and coded into a calculator or computer program for application purposes.

- A knowledge of the state of stress caused by blasting is necessary but not sufficient information to determine if the maximum allowable stress has been exceeded. Other stresses such as those caused by internal pipe pressurization, overburden, etc., can be very significant. This program did not include studies into stresses from other causes, However, an accurate estimate of the elastic state of stress can be made by superposition through additions of stresses with their signs considered, After the resultant longitudinal and circumferential stresses have been obtained, safety factors and a yield theory are necessary to determine if the pipe yields or exceeds its allowable stress.

- Other analytical methods have and are. being used to determine quantity-distance limits for underground detonations near pipelines. Two methods in particular have found some usage. The first of these is a series of maximum soil velocity criteria, and sometimes acceleration criteria. The second is 'use of the Battelle equations, which are based on Morris' equation for ground motion. The first criteria have some validity for surface structures such as buildings, but none at all for buried pipes. It is often misused because people find it easy to apply in spite of, its limited applicability. The Battelle equations were limited to standoff distances of more than 100 ft. However, users have ignored this limitation and have applied the results for much closer standoff distances, with the possibility of significantly underpredicting, pipe stresses as indicated by some of those measured in this program.

- The use of the results from this report may be restricted by government regulations or company policy based on othercriteria. When this circumstance arises, the reader should use both, this report and the other criteria so blasting conditions can at least be limited to whichever gives the most conservative results.

- For a pipeline near a free surface, such as for charges considerably deeper than the pipe or *a* pipeline very close to a free face, the stresses from a point source are enhanced. Based on the strain data from four tests, a correction factor for the point source equation was developed empirically. This factor is based on low amplitude blasting stress data and it should be applied with caution and engineering judgement .

- From the literature study on the effect of an open trench between a charge and a pipeline, it was concluded that a trench can reduce the blast effects on a pipe. For vibratory sources using low frequency vibrations, a trench would have to be very' deep to be very effective. However, test data from a limited number of small charge blasting experiments indicated significant reductions in pipe strains under certain conditions. An approximate equation to, predict the reduction of pipe strain level as a function of a scaled distance was developed from these data. This equation can be used provided all the restrictions are observed on the dimensionless parameters which define the problem.

- From a limited series of concrete/soil feasibility tests, a physical model was developed for use in specific two-media blasting situations. Approximate equations can be developed for computing an equivalent, homogeneous media, standoff distance. This allows use of the soil point or parallel line source prediction equations to estimate stresses and ground motions in a two-media blasting problem.

- All previous formal or interim reports published during the conduct of this blasting research program are replaced by this two volume document.

All of the new equations and methods for estimating pipe stresses from point, parallel line, angled-line, parallel grid, and angled-grid explosive sources provide a better criteria than anything presently in use for limiting blasting near pipelines, within the stated limitations. These new equations and methods are valid over a fairly wide range of stress and other pertinent parameters. However, for some situations, these equations may not be directly applicable. Furthermore, their application may also be restricted by regulatory codes.

The equations presented in this report for the correction factor when a pipeline is near a free surface, for the strain reduction due to a trench, and for the two-media effective distance are much more limited in application and should be used with caution.

For a field application outside the valid limits of any of the equations presented in this report, we recommended that the results be used very judiciously and primarily as a guide to evaluate the magnitude of the problem. If possible, on-site diagnostic measurements are recommended to monitor the blasting effects using lower charge weights or greater standoff distances prior to setting up the actual situation. As an alternative to on-site measurements, a blasting situation whose configuration falls outside the limits of the present solutions can be conducted in model scale either in a “laboratory” environment or at the actual test site.

XIII. REFERENCES

W. M. Adams, R. G. Preston, P. L. Flanders, D. C. Sachs, and W. R. Perret, Summary *Report of Strong-Motion Measurements, Underground Nuclear Detonations,* **Journal of Geophysical Research,** Vol. 66, No. 3, March 1961, pp. 903ff.

Anon., Project Dribble Salmon, *Analysis of Ground Motion and Containment,* Roland F. Beers, Inc. report to Atomic Energy Commission on Tests in Tatum Salt Dome, Mississippi, Final Report VUF-1026, November 30, 1965.

W. E. Baker, P. S. Westine, and F. T. Dodge, **Similarity Methods In Engineering Dynamics,** Spartan Division of Hayden Books, Rochelle Park, New Jersey, 1973.

D. D. Barkan, **Dynamics of Bases and Foundations,** McGraw Hill Book Company, New York, 1962.

P. W. Bridgman, **Dimensional Analysis,** Yale University Press, New Haven, 1931.

D. *S.* Carder and W. *K.* 'Cloud, *Surface Motion from Large Underground Explosions,* **Journal of Geophysical Research,** Vol. 64, No. 10, October 1959, pp. 1471-1487.

F. J. Crandell, *Ground Vibrations Due to Blasting and Its Effect* Upon *Structures,* **Journal Boston Soc. Civil Engineers,** Vol. 36, 1949, pp. 245.

F. J. Crandell, *Transmission Coefficient for Ground Vibrations Due to Blasting,* ***Journal*** **of Boston Soc. Civil Engineers,** Vol. 47, No. 2, April 1960, pp. 142-168.

C. Cranz, **Lehrbuch der Ballistik,** Vol. 2, Berlin, 1926.

J. P. DenHartog, **Mechanical Vibrations,** 3rd Edition, McGraw Hill Book Company, New York, 1947.

A. Dvorak, *Seismic Effects of Blasting on Brick Houses,* ***Proce*** **Geofyrikeniha Ustance Ceskoslavenski Akademic,** Vol. 169, Geofysikalni Sbornik, 1962, pp. 189-202.

A. *T.* Edwards and T. D. Northwood, *Experimental Studies of the Effects of Blasting on Structures,* **The Engineer,** Vol. 210, September 30, 1960, pp. 538-546.

G. M. Habberjam and J. T, Whetton, *On the Relationship Between Seismic Amplitude and Charge of Explosive Fired to Routine Blasting Operations,* Geophysics, Vol. 17, No. 1, January 1952, pp. 116-128.

B. Hopkinson, British Ordnance Board Minutes 13565, 1915.

D. E. Hudson, J. L. Alford, and W. D. Iwan, *Ground Accelerations Caused by Large Quarry Blasts,* **Bulletin of the Seismic Society of America,** Vol. 51, No. 2, April 1961, pp. 191-202.

Ichiro Ito, *On the Relationship Between Seismic Ground Amplitude and the Quantity of Explosives in Blasting,* **Reprint from Memoirs of the Faculty of Engineering,** Kyoto University, Vol. 15, No. 11, April 1953, pp. 579-587.

U. Langefors, B. Kihlstrom, and H. Westerberg, *Ground Vibrations in Blasting,* **Water Power,** February 1958, pp. 335-338,390-395, and 421-424.

G. M. McClure, T. V. Atterbury, and N. A. Frazier, *Analysis of Blast Effects on Pipelines,* **Journal of the Pipelines Division, Proceeding of ‘the American Society of Civil Engineers,** November 1964.

G. Morris, *The Reduction of Ground Vibrations from Blasting Operations,* **Engineering,** April 21, 1950, pp. 430-433.

B. F. Murphey, *Particle Motions Near Explosions in Halite,* **Journal of Geophysical Research,** Vol; 66, No. 3, March 1961, pp. 947ff.

A. W. Nicholls, C. F. Johnson, and W, I. Duvall, *Blasting Vibrations and Their Effects on Structures,* Bureau of Mines Bulletin 656, 1971.

N. Ricker, *The Form and Nature of Seismic Waves and the Structure of Seismograms,* **Geophysics,** Vol. 5, No. 4, October 1940, pp. 348-366.

G. Segol, P. *C. Y.* Lee, and J. F. Abel, *Amplitude Reduction of Surface Waves by, Trenches,* **Journal of Engineering Mechanics Division,** American Society of Civil Engineers, June 1978, pp. 621-641.

G. A. Teichmann and R. Westwater, *Blasting and Associated Vibrations,* **Engineering,** April 12, 1957, pp. 460-465.

J. R. Thoenen and S. L. Windes, *Seismic Effects of Quarry Blasting,* Bureau of Mints Bulletin 442, 1942.

S. Timoshenko, **Strength of Materials, Part II: Advanced Theory and Problems,** 3rd Edition, Van Nostrand Company, Princeton, New Jersey, March 1956.

D. E. Willis and J. T. Wilson, *Maximum Vertical Ground Displacement of Seismic Waves Generated by explosive Blasts,* **Bulletin of the Seismic Society of America,** Vol. 50, No. 3, July 1960, pp. 455-459.

R. D. Woods, *Screening of Surface Waves in Soils,* **Journal of Soil Mechanics and Foundations Division,** American Society of Civil Engineers, Vol. 94, No. SMS, July 1968, pp. 951-979.

XIV. LIST OF PARAMETERS AND SYMBOLS

English Symbols

$\mathbf{A}$	Distance of nearest charge. For point and parallel line sources, A = R (ft)
$\mathbf{A_p}$	Differential area around the pipe; projected differential area
$\mathbf{A_1, A_2, \ldots}$	Acceleration
$\mathbf{B}$	Angle between pipeline and explosive source
C's	Constants
$\mathbf{C_C, C_L}$	Diffraction coefficients
$\mathbf{c, c_s}$	Seismic compression P-wave velocity in soil or 'rock (ft/sec)
$\mathbf{c_c}$	Seismic P-wave velocity in concrete (ft/sec)
$\mathbf{D}$	Pipe diameter (in.)
$\mathbf{D_t}$	Depth of a trench (ft)
$\stackrel{d}{=}$	"Dimensionally equal to"'
$\mathbf{dx}$	Differential length of pipe
$\mathbf{E}$	Modulus of elasticity for the pipe material (psi)
$\mathbf{F}$	Correction factor for pipeline near a free surface (nondimensional)
$\mathbf{F, L, T}$	Fundamental units of measure; force, length and time, respectively
$\mathbf{f, f1, f_\epsilon, \ldots}$	Symbol for function of
$\mathbf{G}$	Ground motion, either peak velocity or displacement
$\mathbf{g}$	Acceleration of gravity (32.16 ft/sec^2)
$\mathbf{H}$	Effective thickness of soil backing a pipeline (ft)
$\mathbf{h}$	Pipe wall thickness (in.)
$\mathbf{I}$	Total applied impulse (lb-see)
$\mathbf{i}$	Any applied specific impulse (lb-sec/ft^2)
$\mathbf{i_s}$	Side-on specific impulse (lb-sec/ft^2)
$\mathbf{J}$	Second moment of area (in.^{4})
$\mathbf{K}$	Site factor for soil condition; a constant
$\mathbf{KE}$	Kinetic energy
$\mathbf{k}$	Spring constant in the qualitative structural response model
$\mathbf{L}$	Length of an explosive line (for uniform charges spaced equal distances apart, this length is the spacing between charges times the number of charges), L = (N1)(L1) (ft)
$\mathbf{L_R}$	Wavelength of a Rayleigh wave (ft)
$\mathbf{L_t}$	Length of a trench (ft)
$\mathbf{L1}$	Spacing of charges in an explosive lint or the front row of a grid (ft)
$\mathbf{L2}$	Spacing of rows making up a grid (ft)
ℓ	Arbitrary effective length of deforming pipe
$\mathbf{M}$	Effective mass or mass in the qualitative structural response mode of a pipe (lb$_m$)
$\mathbf{M_b}$	Elastic bending moment (in.-lb)

M_{max}	Maximum elastic bending moment (in.-lb)
m	Ratio of impulse or pressure on the back of the pipe relative to impulse or pressure at the front of the pipe
N	Frequency of vibration (cycles/min); a number
N1	Number of equally spaced charges in an explosive line or the front row of a grid
N2	Number of equally spaced rows making up a grid
n	Equivalent explosive energy release constant (nondimensional)
nW	Charge weight equivalent in lb_m of ANFO (lb)
P	Shock pressure in a continuum
p_o	Atmospheric pressure
p_s	Side-on pressure
P-wave	Compression wave generated by a disturbance in the ground
$q_1, q_2, \ldots$	Physical parameters
R, R_{eff}	Standoff distance (actual or effective) from the center of the pipe or ground motion transducer to the center, of the charge (ft)
R_{gcl}	Distance between geometric center of explosive line and a pipe (ft)
R'_{gcg}	Distance between geometric center of explosive grid and a pipe (ft)
R_c	Part of R in concrete (ft)
R-wave	Surface Raleigh wave generated by a disturbance near the surface of the ground
R_t	Distance between a charge and a trench (ft)
r	Pipe radius (in.)
S	Estimate of the standard error of experimental data about fitted curve
SE_{cir}	Circumferential strain energy
SE_{long}	Longitudinal strain energy
t	Time
T	Time constant or period associated with duration of the load
U	Peak radial soil particle velocity (ft/sec)
U/c	Nondimensionalized velocity
V	Velocity of shock front
V_o	initial velocity imparted on pipe by a shock front
W	Total charge weight of explosive source (lb)
W_e	Explosive energy released (ft-lb)
W_e/L	Energy released per unit length in an explosive line source (ft-lb/ft)
W/L	Explosive density, charge weight per unit length of an explosive line (lb/ft)
W1	Explosive weight of individual point charges making up a line or grid source (lb)
w_o	Maximum elastic deflection of pipe in either circumferential or longitudinal mode (in.)
X	Peak radial soil displacement (ft)

X/R	Nondimensionalized displacement
x	Displacement in the qualitative structural response model
$x-y$	Relative motion
Y	Horizontal coordinate to locate point of interest behind a trench (ft)
y	Assumed deformed shape of pipe; displacement of ground surface in qualitative model
y_o	Ground motion amplitude; threshold of damage
Z	Vertical coordinate to locate point of interest behind a trench (ft)

Greek Symbols

α's	Exponents on parameters in the equation of dimensional homogeneity
β's	Constant exponents
ϵ	Strain (in/in.)
ϵ_{cir}	Maximum circumferential pipe strain (in/in.)
ϵ_{long}	Maximum longitudinal pipe strain (in./in.)
ϵ_{cal}	Strain calculated from strain equations (in./in.)
ϵ_{meas}	Measured pipe strain with a trench (in./in.)
η	Density times the heat of fusion
θ	Angled
λ	Geometric scale factor
μ	Mass per unit length
$\mu\epsilon$	Microstrain (10^{-6}in./in.)
ν	Poisson's ratio
π term	Dimensionless group
ρ	Mass density of soil or rock (lb-sec^2/ft^4)
ρ_s	Mass density of soil (lb-sec^2/ft^4)
ρ_a	Density behind the shock front
ρc^2	Compressibility of the soil (lb/ft^2)
$\rho c_p \theta$	Heat capacity times temperature increase
ρ_c	Mass density of concrete (lb-sec^2/ft^4)
ρ_p	Mass density of pipe (lb-set^2/ft^4)
σ, σ_{max}	Maximum pipe stress; may be either the longitudinal or circumferential direction (psi)
σ_{cal}	Pipe stress calculated from prediction equations (psi)
σ_{cir}	Maximum circumferential pipe stress (psi)
σ_{long}	Maximum longitudinal pipe stress (psi)
σ_{meas}	Pipe stress derived from measured strains (psi)
σ_y	Yield stress for the pipe material (psi)
τ	Period of pipe response (sec)
ω	Fundamental natural frequency (rad/sec)
χ	Symbol used to represent the various parameters that affect the pipe strain and stress (lb$_m$ /psi$^{0.5}$ -in.$^{0.5}$ -ft$^{2.5}$)